

University of Alberta

Giant Quartz Veins of the Great Bear Magmatic Zone, Northwest
Territories, Canada

by

Suzanne J. Byron

A thesis submitted to the Faculty of Graduate Studies and Research
in partial fulfillment of the requirements for the degree of

Master of Science

Earth and Atmospheric Sciences Department

©Suzanne J. Byron
Fall 2010
Edmonton, Alberta

Permission is hereby granted to the University of Alberta Libraries to reproduce single copies of this thesis and to lend or sell such copies for private, scholarly or scientific research purposes only. Where the thesis is converted to, or otherwise made available in digital form, the University of Alberta will advise potential users of the thesis of these terms.

The author reserves all other publication and other rights in association with the copyright in the thesis and, except as herein before provided, neither the thesis nor any substantial portion thereof may be printed or otherwise reproduced in any material form whatsoever without the author's prior written permission.

Examining Committee

Sarah A. Gleeson, Earth and Atmospheric Sciences

Jeremy P. Richards, Earth and Atmospheric Sciences

Thomas H. Etsell, Chemical and Materials Engineering

Abstract

The Great Bear magmatic zone, Northwest Territories, hosts numerous giant quartz veins and stockwork zones. These zones can be up to 100m wide and up to 10km long, with two or more generations of quartz. A few of the giant quartz vein zones host base-metal ± uranium mineralization, and some are proximal to mineralization, although most are barren. Cathodoluminescence imaging shows the quartz veins have complex growth zones and a trace element study suggests that these zones are the result of Al and Li substitution in the quartz lattice. Oxygen isotope ($\delta^{18}\text{O}_{\text{qtz}}$) values of quartz generally fall between +8 to +14.6‰ (VSMOW). Fluid inclusion homogenization temperatures range from 100 to 375°C, and the fluids have variable salinities. The fluids that created the giant quartz veins are epithermal in nature with a meteoric water ± brine signature, and formed as a result of multiple fluid pulses and re-fracturing events.

Acknowledgements

This project was made possible by the Northwest Territories Geoscience Office (NTGO) funding, in the field and the laboratory. I am very appreciative of this, and thank them for their support. I would also like to thank Fortune Minerals Limited and Hunter Bay Minerals Incorporated for allowing me to sample on their property and release these results. Laboratory work and conference funding were made possible by a National Sciences and Engineering Research Council of Canada (NSERC) Discovery grant awarded to Dr. Sarah Gleeson. Additional travel funding was provided by a student travel award from the Mineralogical Association of Canada, and the Bruce Nesbitt Memorial graduate student award, distributed by the Faculty of Graduate Studies and Research. I also wish to recognize NSERC for awarding me a post-graduate scholarship.

I would like to thank the following individuals of the Earth and Atmospheric Science department at the University of Alberta for their help in various laboratory components of this study: Dr. Sergei Matveev for the helpful suggestions during my time on the electron microprobe, Diane Caird for the swift XRD analyses, and Don Resultay and Mark Labbe for the high quality thin/thick sections. Thanks go to Dr. Jeremy Richards for training and use of his fluid inclusion laboratory. Thanks go to Dr. Karlis Muehlenbachs and Olga Levner for the use of his laboratory, and for running my carbon and oxygen isotope analyses. I would also like to acknowledge Dr. Iain Samson from the University of Windsor, and the laboratory technicians Sharon Lackie and Zhaoping Yang for their guidance and help in the SEM-CL and LA-ICP-MS trace element studies.

I would like to extend my gratitude in working with Valerie Jackson, Project Geologist for the NTGO, initially, for teaching me much more about mapping than a classroom can, especially the necessity of drawing contacts and picking a good tent spot! I would also like to thank Luke Ootes, Metallogenist for the NTGO, for the conception of this MSc project, and his unwavering support, ideas, and questions, which have helped throughout the development of this thesis. Last, but in no ways least, I would like to thank Dr. Sarah Gleeson. She has been a wonderful instructor and mentor, and this project has been fun, challenging and rewarding, often, all at the same time. I have learned much from her in the field, the classroom, and the laboratory, not to mention the hydrothermal wine tastings and, even, sharing tents.

I would like to thank my fellow graduate students in the Earth and Atmospheric Department; the lunch-hour or coffee-break was frequently a highlight of my day. You taught me a lot about myself and have influenced me in many good, as well as liver-damaging, ways. I appreciate and love every one of my LLP's and hope we continue our friendships for many years to come!

My family has been very supportive in my education and I appreciate all of their kindness, humour, interest and love.

Table of Contents

1. Introduction
 - 1.1 Regional Geology and Tectonic Setting
 - 1.1.1 Hottah Terrane
 - 1.1.2 Caldarian Accretionary Wedge
 - 1.1.3 Great Bear Magmatic Zone
 - 1.1.4 Mineralization in the GBmz
 - 1.1.5 Giant Quartz Vein Zones
 - 1.2 Local Geology
 - 1.2.1 Giant Quartz Vein Zones Located near Base-Metal Mineralization
 - 1.2.2 Uranium Associated Giant Quartz Vein Zones
 - 1.2.3 Giant Quartz Vein Zones Isolated from Mineralization
2. Analytical Methods
 - 2.1 Electron Microprobe
 - 2.2 Scanning Electron Microscope – Cathodoluminescence
 - 2.3 Laser Ablation Inductively Coupled Mass Spectrometry
 - 2.4 X-ray Diffraction
 - 2.5 Microthermometry
 - 2.6 Stable Isotopes
 - 2.6.1 Oxygen Isotopes in Quartz
 - 2.6.2 Carbon and Oxygen Isotopes in Calcite
3. Analytical Results
 - 3.1 Petrography, Cathodoluminescence and Trace Element Results
 - 3.1.1 Giant Quartz Vein Zones Located near Base-Metal Mineralization
 - 3.1.2 Uranium Associated Giant Quartz Vein Zones
 - 3.1.3 Giant Vein Zones Isolated from Mineralization
 - 3.2 Fluid Inclusions from Giant Vein Zones
 - 3.2.1 Giant Quartz Vein Zones Located near Base-Metal Mineralization
 - 3.2.2 Uranium Associated Giant Quartz Vein Zones
 - 3.2.3 Giant Quartz Vein Zones Isolated from Mineralization
 - 3.2.4 Fluid Inclusion Summary
 - 3.3 Stable Isotopes from Giant Quartz Vein Zones
 - 3.3.1 Giant Quartz Vein Zones Located near Base-Metal Mineralization
 - 3.3.2 Uranium Associated Giant Quartz Vein Zones
 - 3.3.3 Giant Quartz Vein Zones Isolated from Mineralization
4. Discussion
 - 4.1 Giant Quartz Vein Zones in the GBmz
 - 4.1.1 Tectonic Control and Age of Giant Quartz Vein Zone Formation
 - 4.1.2 Quartz Textures and Mineralogy

- 4.1.3 Pressure Estimates of Vein Formation and Isochores
- 4.2 Fluid Origin
 - 4.2.1 Giant Quartz Vein Zones Spatially Associated with Mineralization
 - 4.2.1.1 Relationship to Mineralization in the GBmz
 - 4.2.2 Giant Quartz Vein Zones Isolated from Mineralization
- 4.3 Epithermal Systems
- 5. Conclusions
- 6. Future Research and Implications for Exploration
- 7. References
- 8. Appendices
 - A. Sample location and analytical techniques
 - B. Mineral chemistry data from NICO
 - C. Detection limits of LA-ICP-MS trace element study
 - D. Combined SEM-CL image with LA-ICP-MS study
 - E. Fluid inclusion microthermometry data
 - F. Isochores
 - G. Calculated fluid oxygen isotopic values

List of Tables

Table 1. Summary of fluid inclusion data for all vein zones.....75-76
Table 2. Summary of stable isotope data for all vein zones.....82

List of Figures

Figure 1. Giant quartz vein zones and geology of the GBmz.....11
Figure 2. The Wopmay orogen, Northwest Territories.....12
Figure 3. Giant quartz vein zone and local geology at NICO.....19
Figure 4. Giant quartz vein zone and local geology at Sue-Dianne.....22
Figure 5. Giant quartz vein zone and local geology at Sloan, Sloan Extension,
Northern Sloan Extension and Boadway.....24
Figure 6. Giant quartz vein zone and local geology at Beaverlodge Lake.....28
Figure 7. Giant quartz vein zone and local geology at Fab Lake.....29
Figure 8. Giant quartz vein zone and local geology at the Northern Wopmay
fault.....30
Figure 9. Giant quartz vein zone and local geology at “Arm Lake”.....32
Figure 10. Giant quartz vein zone and local geology at Hardisty Lake.....33
Figure 11. Giant quartz vein zone and local geology at Margaret Lake.....35
Figure 12. Microthermometry data from giant quartz vein zone near NICO.....55
Figure 13. Microthermometry data from giant quartz vein zone within NICO
drill-core.....56
Figure 14. Microthermometry data from Q1 veins near Sue-Dianne.....57
Figure 15. Microthermometry data from (sample SBS017) Q2 vein near
Sue-Dianne.....58
Figure 16. Microthermometry data from (sample SBS019) Q2 vein near
Sue-Dianne.....59
Figure 17. Microthermometry data from (sample SBS020-F) Q2 vein near
Sue-Dianne.....59
Figure 18. Microthermometry data from a Q3 vein near Sue-Dianne.....60
Figure 19. Microthermometry data from Q1 veins at Beaverlodge Lake.....61
Figure 20. Microthermometry data from Q2 veins at Beaverlodge Lake.....62
Figure 21. Microthermometry data from Q1 veins at Fab Lake.....63
Figure 22. Microthermometry data from Q2 veins at Fab Lake.....54
Figure 23. Microthermometry data from Q1 veins at Northern Wopmay fault...65
Figure 24. Microthermometry data from Q2 vein at Northern Wopmay fault.....65
Figure 25. Microthermometry data from (sample SBA034-2) Q2 vein at “Arm”
Lake.....66
Figure 26. Microthermometry data from (sample SBA035) Q2 vein at “Arm”
Lake.....67
Figure 27. Microthermometry data from Q1 veins at Hardisty Lake.....68
Figure 28. Microthermometry data from a Q2 vein at Hardisty Lake.....68
Figure 29. Microthermometry data from a Q3 vein at Hardisty Lake.....69

<i>Figure 30.</i> Microthermometry data from Q1 veins at Margaret Lake.....	70
<i>Figure 31.</i> Microthermometry data from a Q2 vein at Margaret Lake.....	71
<i>Figure 32.</i> Microthermometry summary for giant quartz vein zones near base-metal mineralization.....	72
<i>Figure 33.</i> Microthermometry summary for giant quartz vein zones associated with uranium mineralization.....	73
<i>Figure 34.</i> Microthermometry summary for giant quartz vein zones isolated from mineralization.....	74
<i>Figure 35.</i> Oxygen isotope values from giant quartz vein zone near NICO.....	77
<i>Figure 36.</i> Oxygen isotope values from giant quartz vein zone within NICO drill-core.....	78
<i>Figure 37.</i> Oxygen isotope values from a Q2 vein from NICO.....	78
<i>Figure 38.</i> Oxygen isotope values from giant quartz vein zone at Fab Lake.....	79
<i>Figure 39.</i> Oxygen isotope values from giant quartz vein zone at Northern Wopmay fault.....	80
<i>Figure 40.</i> Oxygen isotope values from giant quartz vein zone at “Arm” Lake..	81
<i>Figure 41.</i> Oxygen isotope values from giant quartz vein zone at Hardisty Lake.....	81
<i>Figure 42.</i> Paragenesis of giant quartz vein zones near base-metal mineralization.....	88
<i>Figure 43.</i> Paragenesis of giant quartz vein zones associated with uranium mineralization.....	88
<i>Figure 44.</i> Paragenesis of giant quartz vein zones isolated from mineralization..	92

List of Plates

<i>Plate 1.</i> Giant Quartz Vein Zone photos.....	17
<i>Plate 2.</i> Giant Quartz Vein Zone field photos.....	21
<i>Plate 3.</i> Microscope/electron microscope images of giant quartz vein zone near NICO.....	40
<i>Plate 4.</i> Microscope/SEM-CL images of the giant quartz vein zone near Sue-Dianne.....	44
<i>Plate 5.</i> Microscope/SEM-CL images of the Northern Sloan Extension giant quartz vein zone.....	46
<i>Plate 6.</i> Electron microscope images of giant quartz vein zone at Beaverlodge Lake.....	48
<i>Plate 7.</i> Microscope/SEM-CL images of various giant quartz vein zones.....	49
<i>Plate 8.</i> Type I and Type I fluid inclusion photos.....	53
<i>Plate 9.</i> Fluid inclusions from giant quartz vein zone near NICO.....	54
<i>Plate 10.</i> Fluid inclusions from giant quartz vein zone near Sue-Dianne.....	57
<i>Plate 11.</i> Fluid inclusion from giant quartz vein zone at the Northern Wopmay fault.....	64

List of Abbreviations

Units

wt. % NaCl eq.	weight percent NaCl equivalent
‰	per mille (per thousand)
bar	bar of pressure (100 kilopascals)
°C	degrees Celsius
cps	counts per second
δ	delta
Ga	Giga annum (billion years)
kV	kilovolts
Ma	Mega annum (million years)
mL	millilitres
1σ	1 standard deviation
t	tonne (imperial)
lbs	pounds
µm	microns (micrometres)

Mineral Short Forms

bn	bornite
cal	calcite
cc	chalcocite
cpy	chalcopyrite
fsp	feldspar
ga	galena
hm	hematite
mz	monazite
py	pyrite
qtz	quartz
sph	sphalerite

Other

GBmz	Great Bear magmatic zone
IOCG	Iron oxide copper gold
VSMOW	Vienna Standard Mean Ocean Water
SMOW	Standard Mean Ocean Water
VPDB	Vienna Pee Dee Belemnite

1 Introduction

Throughout the Great Bear magmatic zone (GBmz) numerous giant quartz vein zones exist. These zones and their relationship to mineralization within the GBmz have remained a subject of controversy in the Northwest Territories for many years. Most giant quartz vein zones are barren and are not near areas of mineralization; however, copper-sulfide and uranium mineralization locally occur near giant quartz vein zones. Some giant quartz vein zones are located proximal to areas of mineralization and Normin showings, a database of mineral showings and commodities, within the Northwest Territories (Fig. 1; Normin 2009). NICO, a Co-Au-Bi deposit, and Sue-Dianne, a Cu-Ag deposit, are two examples of mineralization, both with giant quartz vein zones less than 250m from their high grade zones. As well, two past-producing uranium mines are located within the GBmz; the first, Rayrock mine is a 150t U deposit located within a giant vein zone, and second, Beaverlodge Lake is a small uranium deposit located at the contact between the host rock and a giant quartz vein zone (Gandhi et al. 2000). Although many small mines, such as Echo Bay and Camsell River Districts, Beaverlodge Lake, and Rayrock, are now the focus of reclamation projects, mineral exploration continues within the GBmz, due to recent discoveries at NICO and Sue-Dianne. It has been suggested that the giant quartz vein zones are a low-temperature end-member of a larger hydrothermal continuum in the GBmz (Mumin et al. 2008). This study aspires to demonstrate that giant quartz vein zones are unrelated to the mineralization within the GBmz; and although the giant quartz vein zones contain only trace amounts of mineralization themselves, may assist mining companies in defining grassroots exploration targets within the GBmz from remobilized mineralization within late-stage veins.

The rocks of the Great Bear magmatic zone were affected by a set of major transcurrent faults and their subsidiary fractures, which are the structural hosts of numerous giant quartz vein zones (Gandhi 1994). The giant quartz vein zones of the GBmz were first described in 1935 by Furnival, which was followed by a PhD dissertation on pitchblende in a giant quartz vein, at Beaverlodge Lake, Northwest Territories by Jolliffe (1935), but since then little work has been carried out on these features. The vein zones were reported to obtain maximum widths of “up to one thousand feet” and strike for “distances up to fifty miles” (Furnival 1935). Nine giant quartz vein zones are included in this study; a few of the giant quartz vein zones are located proximal to base-metal ± uranium mineralization, although most are barren (Fig. 1). This study evaluates the origin of the fluid(s), the conditions present during the formation of the giant quartz veins, and critically examines their relationship, if any, to adjacent mineralization in the GBmz.

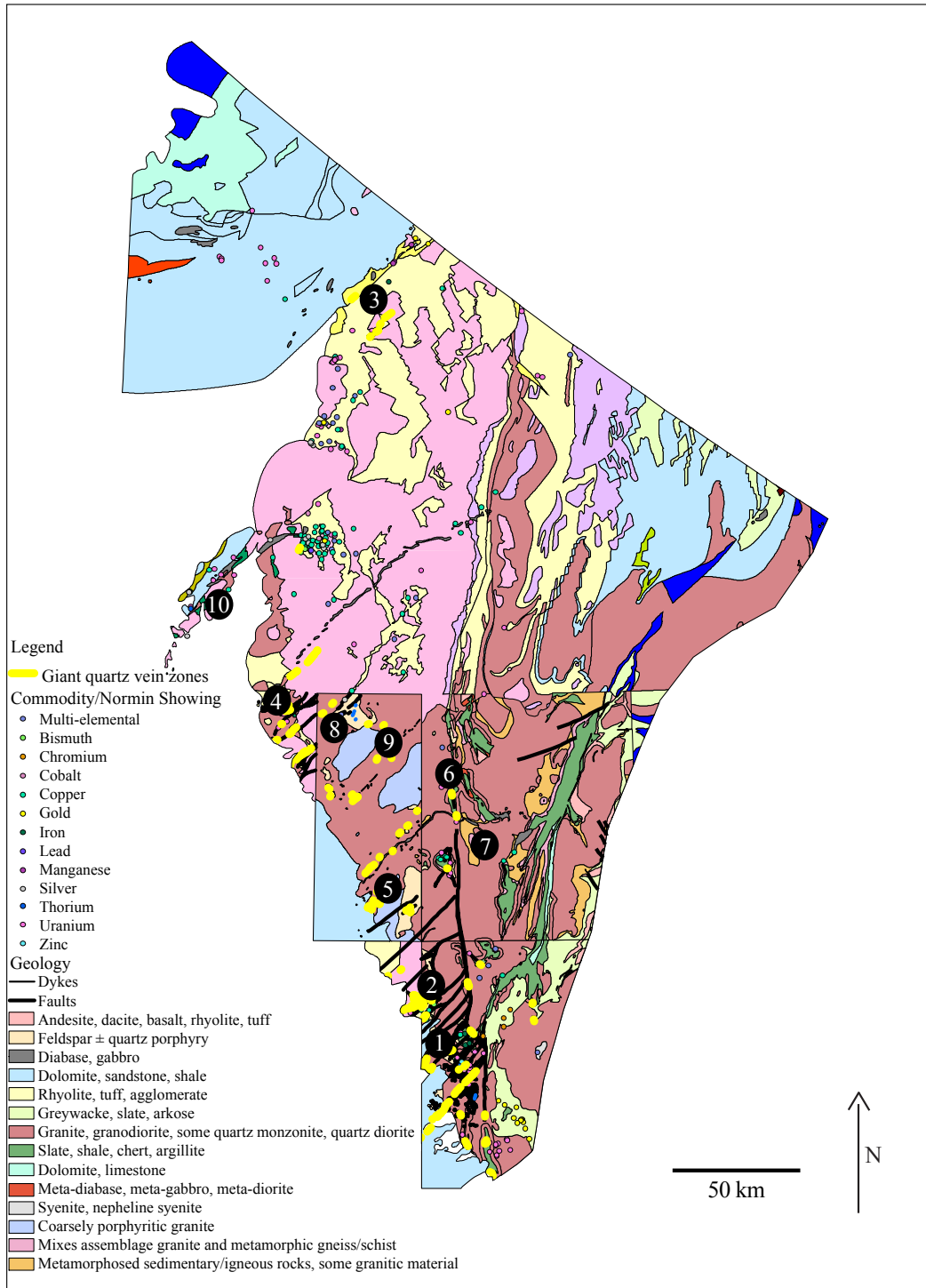


Figure 1. Giant quartz vein zones and geology of the Great Bear magmatic zone, Northwest Territories, Canada (geology by Pierce and Turner 2004; showings from Normin 2009). Numbers indicated giant quartz vein zones studied: 1 NICO, 2 Sue-Dianne, 3 Sloan/Sloan Extension/Northern Sloan Extension/Boadway, 4 Beaverlodge Lake, 5 Fab Lake, 6 Wopmay fault zone, 7 “Arm” Lake, 8 Hardisty Lake, 9 Margaret Lake, 10 Echo Bay/Camsell River mining districts.

1.1 Regional Geology and Tectonic Setting

The Great Bear magmatic zone (GBMz), also referred to as the Great Bear continental arc, comprises Paleoproterozoic volcanic and plutonic rocks exposed over 450km from Great Bear Lake to Great Slave Lake and is the central tectonic element of the north-trending Wopmay orogen (Fig. 2; Hildebrand et al. 1987; Gandhi et al. 2000). The Wopmay orogen was developed on the western side of the Archean Slave craton between 2.1 and 1.8 Ga (Hoffman 1973; Hoffman 1980). It is presently considered to represent stages in an evolving Cordilleran-type plate developed above an east-dipping subduction zone (Hildebrand et al. 1987). The exposed northern part of the orogen is divided into three major tectonic elements, from west to east: the Hottah terrane, the Great Bear magmatic zone, and the Calderian accretionary wedge (Fig. 2; Hildebrand et al. 1987; Gandhi et al. 2001).

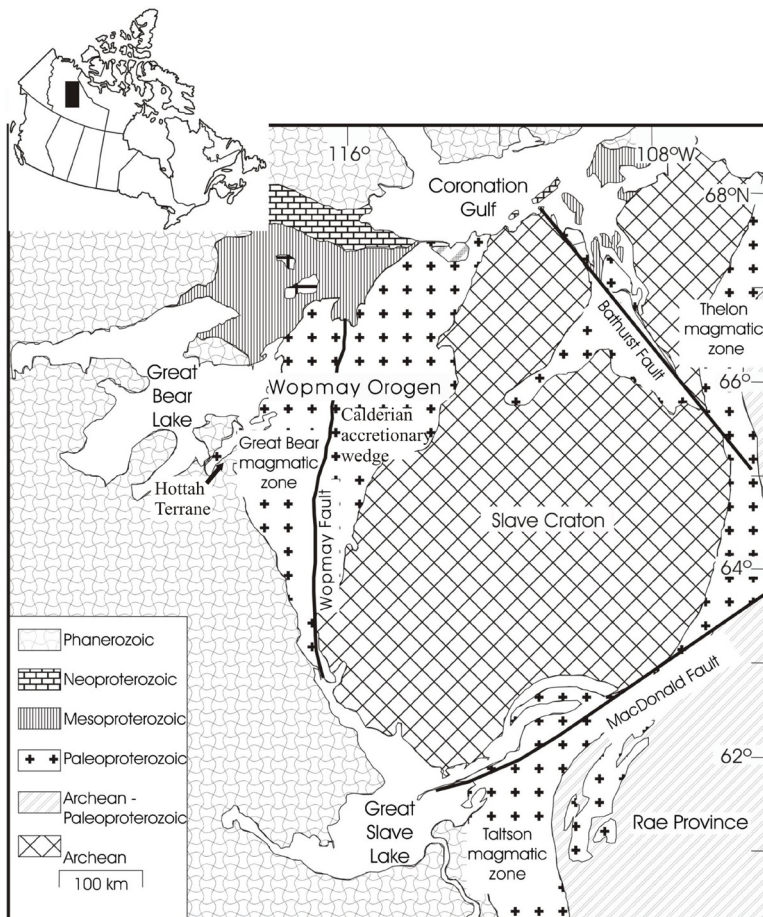


Figure 2. The Wopmay orogen, Northwest Territories, Canada (reproduced from Gandhi et al. 2001).

1.1.1 Hottah Terrane

The Hottah terrane is the westernmost tectonic element of the Wopmay orogen and contains the oldest magmatic suite (Hildebrand et al. 1987). The terrane is comprised of amphibolite facies sedimentary and intermediate metavolcanic rocks, intruded by two distinct suites of plutons. The rocks of the Hottah can be divided into three main groups, based on lithology and degree of deformation. The oldest suite consists of psammites, pelitic schists, volcanic and fine grained andesites, which show variable strain but locally are not deformed (Hildebrand and Roots 1985). Commonly the rocks are metamorphosed to amphibolite facies and sedimentary bedding in many places is completely transposed (Hildebrand and Roots 1985). The second suite of rocks comprising the Hottah Terrane consists of deformed granitoid plutons of dioritic, quartz dioritic, granodioritic and monzogranitic compositions (McGlynn 1979; Hildebrand 1983; Hildebrand and Bowring 1984). The U-Pb ages from zircons of these calc-alkaline plutons range from 1.94 – 1.90 Ga (Hildebrand 1983). Lastly, there are several undeformed plutons, comprised of leucocratic syenogranites, porphyritic syenogranites, and monzogranites, typically with less than 5% ferromagnesian minerals, and these are dated at 1.914 - 1.875 Ga (Hildebrand and Roots 1985).

A major north-south trending fault, the Wopmay fault, is regarded as the boundary between the Slave craton and the Hottah terrane (Hildebrand et al. 1990). The Hottah terrane is believed to extend eastward as the basement for much of the Great Bear magmatic zone and outcrops for a few tens of kilometres on the southeastern border of Great Bear Lake (McGlynn 1979; Hildebrand 1983).

1.1.2 Calderian Accretionary Wedge

The Calderian accretionary wedge makes up the eastern side of the Wopmay orogen. It is composed of sedimentary and volcanic rocks believed to have formed in a volcanic-sedimentary basin, 5 – 10 m.y. after the collision of the Hottah terrane with the western edge of the Slave craton (Easton 1981; Tirrul 1983; Gandhi et al. 2000). The Calderian accretionary wedge consists of volcanic rocks overlain by continental margin clastic and carbonate sedimentary sequences (Mumin et al. 2007). The sedimentary rocks of the Calderian accretionary wedge are part of the Coronation Supergroup, which forms a depositional prism of continental margin shelf and slope sediments. The Coronation Supergroup can be divided into the Snare, Akaitcho, and Epworth Groups (Hoffman 1973, 1980). The Snare Group consists of metasedimentary rocks such as arkosic turbidites, pelites and volcanoclastic sediments (Easton 1981). The Akaitcho Group consists of gabbros, basalts, and rhyolite volcanic complexes and rhyolite sills in association with continent-derived sediments (Easton 1981). The Epworth Group consists of sedimentary marine shelf facies and dolomites.

A compositionally diverse suite of peraluminous to metaluminous granitoid plutons (the Hepburn intrusive suite) intruded the Coronation Supergroup during compression and regional shortening between 1.90 and 1.88 Ga (Mumin et al. 2007). This deformation culminated in folding, imbrication,

and eastward thrusting of the accretionary wedge (both the Calderian supracrustal rocks plus the Hepburn intrusions) onto the Slave craton, forming the internal metamorphic zone of the Wopmay orogen (Mumin et al. 2007). This internal metamorphic zone, east of the Wopmay fault, is often referred to as the Coronation Margin.

1.1.3 Great Bear magmatic zone

The calc-alkaline GBmz in the Wopmay Orogen developed after a collision ca. 1890 Ma of the Archean Slave craton with the Paleoproterozoic Hottah terrane to the west, and exists west of the Wopmay fault to the eastern edge of Great Bear Lake (Fig. 1; Gandhi et al. 2001). The GBmz unconformably overlies the suture that joins the western Calderian accretionary wedge with the eastern Hottah terrane (Hildebrand and Bowring 1984; Gandhi et al. 2000). The rocks of the GBmz are exposed over 100km east to west and 450km north to south, between Great Bear Lake and Great Slave Lake, although regional gravity and magnetic surveys suggest the GBmz extends 850 – 950km N-S beneath a thin veneer of flat-lying Paleozoic rocks (Hildebrand and Bowring 1984; Cook et al. 1999; Gandhi et al. 2000). The sequence of events that formed the Great Bear magmatic zone has been interpreted as the result of eastward subduction of oceanic lithosphere beneath the Archean Slave craton (Hildebrand et al. 1987; Hoffman 1988).

Early stages of Great Bear magmatic activity were dominated by volcanism and related sub-volcanic intrusions, and consist of felsic calc-alkaline rocks (Hoffman 1988; Gandhi et al. 2000). The oldest rocks of the western GBmz consist of intermediate ash-flow tuffs and other volcanic rocks, which unconformably overlie pillow basalts of the earlier marginal basin (Hildebrand et al. 1987). These extrusive rocks are interpreted to originate from large calderas, lavas from post-collapse caldera-fills and large stratovolcanoes (Hildebrand 1981; Hildebrand 1983). The rocks along the eastern margin of the GBmz are similar to those along the western margin, with considerably more ash-flow tuffs and lavas in the east (Hildebrand et al. 1987).

Late stages of magmatic activity resulted in the emplacement of large granitic batholiths (Hildebrand et al. 1987; Hoffman 1988). Two suites of plutonic rocks make up the GBmz intrusive rocks. The first, an early intermediate intrusive suite, is a pre-folding supersuite (1875 – 1860 Ma) temporally and compositionally related to the volcanic rocks. The early intermediate intrusive suite consists of plutons that are associated with andesite stratovolcanoes along the western part of the GBmz. The monzonite, monzodiorite, and diorite plutons are medium-grained sheets and laccoliths, 5 – 25km in diameter, and 1 – 2km thick (Hildebrand et al. 1987). The second plutonic suite consists of a granodiorite-monzogranite suite. This granodiorite-monzogranite suite is post-folding (1858 – 1843 Ma) and is associated with north to northeast trending granitoid dikes (Hildebrand et al. 1987). This suite consists of large medium-grained bodies of granodiorite and monzogranite, while syenogranite and quartz diorite are less abundant (Hildebrand et al. 1987).

All of the volcanic rocks in the GBmz are metamorphosed to some degree, but the style and intensity vary tremendously. Mainly, the magmatic zone consists of subgreenschist facies metamorphism of volcanic and sedimentary rocks, with the most intense metamorphism recognized adjacent to intrusive bodies (Hoffman and McGlynn 1977; Hildebrand 1986; Hildebrand et al. 1987). Although there is abundant evidence for local water-rock interaction, there is little evidence for regional metamorphism and virtually all volcanic textures, including delicate vitroclastic textures, are well preserved (Hildebrand et al. 1987). Potassic metasomatism occurs locally, characterized by dramatic increases in K_2O by 8-10%, with Na_2O loss to values of less than 1% (Hildebrand 1981). These changes are related to destruction of glass by relatively low-temperature brines in evaporitic basins (Hildebrand 1981), which may be linked to the Proterozoic evaporites of the Great Slave Supergroup, located along the East Arm graben of Great Slave Lake (Badham and Stanworth 1977).

Deformation produced macroscopic gently northwest plunging folds between 1860 – 1850 Ma (Hildebrand et al. 1987). Because the folds generally trend obliquely to the zone and are en-echelon, Hoffman (1980) and Hildebrand (1981) argued that they are dextral transpressional features related to oblique plate convergence (Fitch 1972). Great Bear magmatic activity was followed by brittle faulting, resulting in a prominent set of northeast-trending (west of the Wopmay fault) and northwest-trending (east of the Wopmay fault) transcurrent steeply dipping faults, with up to several kilometres of strike-slip displacement (Furnival 1935; Hildebrand 1987; Gandhi et al. 2000) that truncate at the N-S trending Wopmay fault zone (Hoffman 1980; Gandhi et al. 2001). Almost without exception, the northeast-trending faults are dextral and the northwest trending are sinistral (Hoffman 1980). Similar regional conjugate transcurrent faults are found throughout the Wopmay orogen (Hoffman 1980). The faulting is a reflection of east-west compression and north-south extensional plane strain on a regional scale (Hoffman 1980).

1.1.4 Mineralization in the GBmz

Vein-type mineralization within the GBmz accounts for at least ten past-producing mines, two of which were hosted by giant quartz vein zones (Mumin et al. 2007). Past-producing vein-hosted deposits within the GBmz are near the Camsell River district: Terra and Norex Ag mines, and the Echo Bay district: Eldorado, Echo Bay, Contact Lake, and Bonanza U-Ag-Cu ± Co-Ni-Bi mines (Changkakoti et al. 1986; Mumin et al. 2007). The Echo-Bay district contains more than 5100t Cu and greater than 15 million lbs U_3O_8 (Normin 2009). Vein-hosted mineralization consists of native silver associated with Ni-, Co-, and Fe-arsenides, Cu-, Fe-, Ni-, and Co-sulfides, and pitchblende in localized regions along the Camsell River and Echo Bay area (Changkakoti et al. 1986). These deposits are structurally controlled, high-level, quartz or quartz-carbonate vein systems associated with varying degrees of iron-oxide and alkali metasomatism (Mumin et al. 2007), and both the Camsell and Echo Bay districts have giant quartz vein zones proximal to mineralization (Changkakoti et al. 1986).

1.1.5 Giant Quartz Vein Zones

The giant quartz veins zones of the GBmz were initially mapped by the Geological Survey of Canada in 1932 by D.F. Kidd. Locally, the veins are prominent topographic features, and rise as large white ridges with minimal plant growth, although they are host to a variety of green and black crustose lichen species. Most giant vein zones are emplaced along the northeast-trending transcurrent faults, although some giant quartz vein zones parallel the Wopmay fault and, a small number of veins east of the Wopmay fault trend northwest along northwest trending faults (Fig. 1; Ghandi et al. 2000). These zones were described to attain maximum widths, including stockworks, of 300m and strike lengths up to 80km (Plate. 1A/B; Furnival 1935). The giant quartz vein zones are made up of multidirectional stockworks and numerous veins that are, for the most part, a few cm to 2m in width.

The giant quartz vein zones cross cut all the magmatic and metamorphic rocks of the GBmz, but unfortunately there are very poor timing constraints on their formation. The giant quartz veins follow the orientation of the faults, and this may suggest the vein zones formed at a similar time across the GBmz. The regional transcurrent faulting is estimated to have occurred between 1843 – 1810 Ma (Hildebrand et al. 1987). Two giant vein zones have 1 - 2m fault gouges, which may indicate they formed synchronously with the transcurrent regional faults. A maximum time constraint, post-dating magmatism and metamorphism within the GBmz, would make the vein zones younger than 1843 Ma (Hildebrand et al. 1987). Two giant quartz vein zones are cross cut by gabbroic dykes, termed “Hottah sheets” that are dated at 780 Ma (Park et al. 1995; Gandhi et al. 2001; Harlan et al. 2003); this is the only constraint to the minimum age limit of the giant vein zone formation.

The giant quartz vein zones consist of two or more generations of quartz veining and are classified into three categories throughout this study. The first category consists of vein zones associated with base-metal mineralization, based on the zones’ proximity to mineralization or Normin showings; this includes the NICO, Sue-Dianne and Northern Sloan Extension giant quartz vein zones. The second category consists of vein zones associated with radioactive anomalies or uranium-mineralization; this includes the Beaverlodge Lake, Fab Lake and Northern Wopmay fault giant quartz vein zones. Non-mineralized vein zones do not contain mineralization and are not associated with Normin showings and make up the third classification of giant vein zones; “Arm” Lake, Hardisty Lake and Margaret Lake comprise the barren giant quartz vein zones.

It has been suggested that the giant quartz veins are a low-temperature end-member of a larger hydrothermal continuum (which includes IOCG and porphyry Cu-like systems) in the GBmz (Mumin et al. 2007; Mumin et al. 2008). Although large IOCG-like systems, besides NICO and Sue-Dianne, have yet to be discovered, this study will attempt to show the giant vein zones’ genetic relationship, or lack thereof, to the adjacent mineralization within the GBmz.

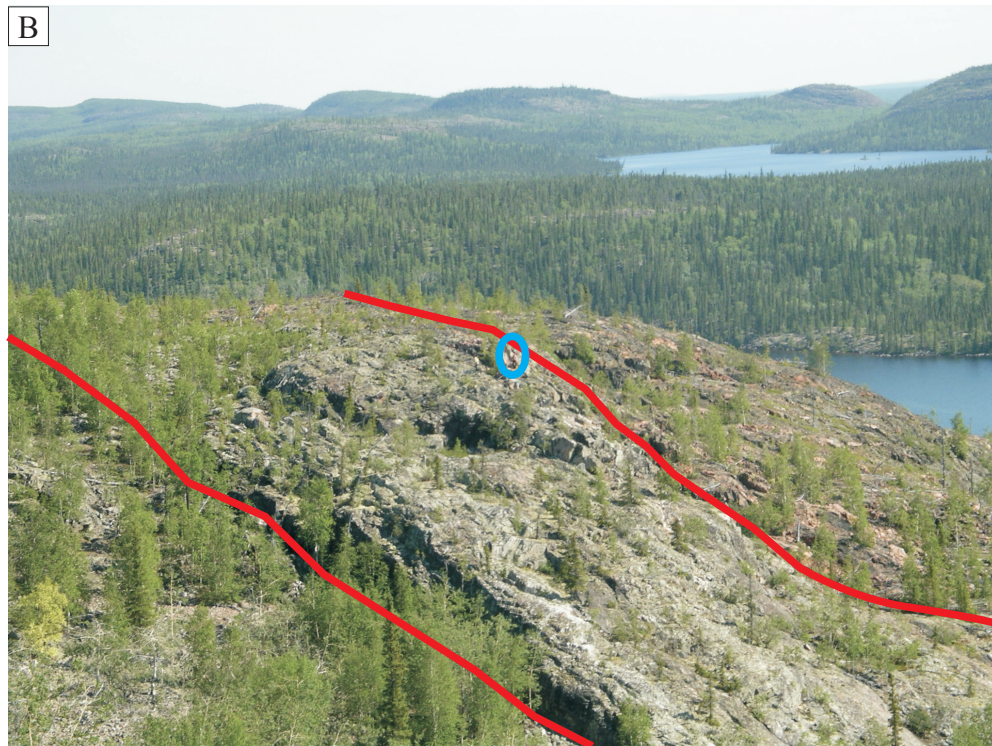


Plate 1. A) Giant quartz vein zone at Hardisty Lake, taken facing northeast. Vein zone indicated by red lines, note fault gouge on left side of the vein zone. B) Giant quartz vein zone at Fab Lake giant quartz vein zone, photo taken facing east. Vein zone indicated by red lines, blue circle indicates a geologist on the vein zone for scale.

1.2 Local Geology

Nine giant quartz vein zones were sampled during the course of this study. These samples have been taken from giant quartz vein zones associated with base metal mineralization: NICO, Sue-Dianne, Northern Sloan Extension; vein zones associated with uranium or radioactive anomalies: Beaverlodge Lake, Fab Lake, Northern Wopmay fault; and vein zones that are isolated from mineralization or lack proximal Normin base or precious metal showings or deposits: “Arm” Lake, Hardisty Lake, and Margaret Lake. At each locale veins from the giant vein zone were sampled, as well as drill-core at NICO that intersected the giant vein zone. Structural measurements and descriptions of the zones were made in the field and samples of the host rock and different quartz vein phases were collected. Strike and dip measurements are recorded in right hand rule orientation. The location and analyses performed for each vein sample are located in Appendix A.

1.1.1 Giant Quartz Vein Zones Located near Base-Metal Mineralization

Giant Quartz Vein Zone located near the NICO deposit

NICO is a polymetallic deposit located on claims surrounding Lou Lake, approximately 160km northwest of the City of Yellowknife, Northwest Territories (Fig. 3; Goad et al. 2000a). NICO contains 30.9 million tonnes (Mt) of proven and probable mineral reserves with grades of 0.12% cobalt, 0.91g/t gold, 0.16% bismuth and 0.04% copper (Puritch and Brown 2010), and it has been suggested it is one of a few known Canadian examples of Proterozoic iron oxide-hosted polymetallic deposits (Goad et al. 2000a). It has been referred to as a “Sabolo type” IOCG deposit, based on the polymetallic mineral assemblage hosted in iron- and potassium-altered, brecciated basement sedimentary rocks (Goad et al. 2000a).

The oldest rocks on the property are laminar siltstones overlain by thick-bedded to massive subarkosic wacke and arenite of the Proterozoic Snare and Treasure Lake Group sediments (Fig. 3; Goad et al. 2000a). At low metamorphic grade, the Snare Group consists of sandstone to mudstones, quartz pebble conglomerates, limestones and locally stromatolitic dolomite, whereas Treasure Lake Group consists of limestones and dolomites with calcareous argillites and calc-silicate beds that are locally metamorphosed to marbles (Jackson 2007).

Unconformably overlying the Snare and Treasure Lake Group sedimentary rocks is a 1.5km thick sequence of bedded rhyolite to rhyodacite tuffs (Goad et al. 2000a). The potassium feldspar-altered rhyolite yields an imprecise age of 1851 Ma \pm 18/-16 from U-Pb dating of zircons (Gandhi et al. 1996). The NICO property has been intruded by quartz-feldspar porphyritic dykes, parallel to the strike of the Faber Group, and diapiric monzonite and syeno-granites intrude the rocks northeast and southwest of the deposit (Gandhi et al. 1996; Goad et al. 2000a). A variety of hydrothermal diatreme and maar-facies breccias within the Snare Group are spatially related to zones of polymetallic sulfide mineralization.

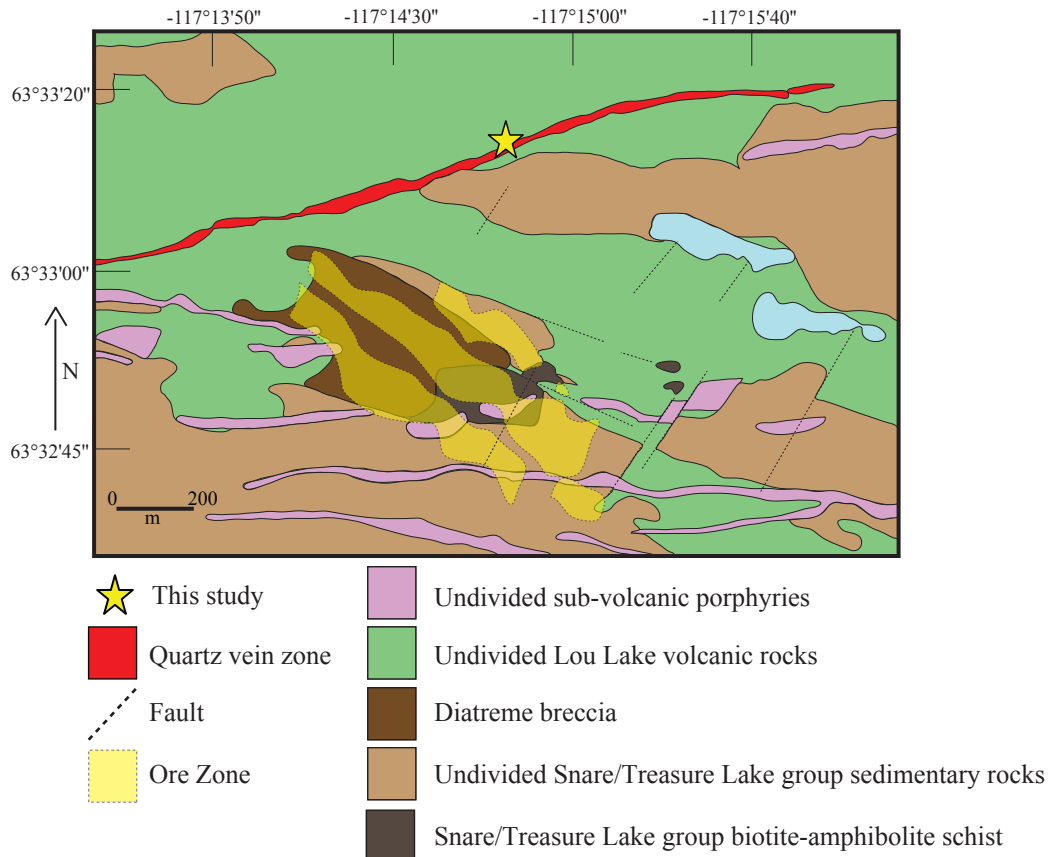


Figure 3. Giant quartz vein zone and local geology at NICO, Northwest Territories (modified from Goad et al. 2000a).

Mineralization at NICO is hosted in intense iron- and potassium feldspar-altered, brecciated basement sedimentary rocks of the Snare Group which underlie the volcanic rocks of the Faber Group (Goad et al. 2000a; Goad et al. 2000b). The high grade ore zone at NICO is constrained to subarkosic wacke and laminar siltstone (Goad et al. 2000a). Mineralization occurs in several closely stacked, stratabound, sulfide-bearing lenses of ironstone parallel to the strike of the subarkosic wacke host in a northwest orientation (Fig. 3; Goad et al. 2000a). These mineralized lenses vary in width between 250 and 700m and up to 70m thick and are variably enriched in cobalt, gold, bismuth, copper and, locally, tungsten. The base and precious metals occur in concordant and discordant sulfide-rich fractures and disseminations typically comprising between 5 and 10 % of the rock (Goad et al. 2000a). Early minerals are chalcopyrite, pyrite, and pyrrhotite, evolving to gold, native bismuth and bismuth tellurides, and sulphosalts, followed by bismuthinite, arsenopyrite and scheelite and finally arsenopyrite (Walker 1999 within Goad et al. 2000a).

The giant quartz vein zone at NICO is located 1km east of the southern edge of Lou Lake at UTM NAD83 11W 7047478N and 0512151E (± 5 m), and is approximately 200m north of the high grade ore zone (Fig. 3). The vein zone is 50m wide and 4km long, with a trend of 050° . The giant vein zone consists of

two main phases of quartz stockwork formation. Late northeast-striking (040°) transverse faults, and major regional faults striking 070° with predominantly vertical displacement, transect Snare, Treasure Lake and Faber Group rocks and adjacent granitoid intrusions forming horst and graben structures (Goad et al. 2000a). There are no cross cutting relationships between the giant vein zone and the mineralized ironstone lenses at NICO; as well, the 050° orientation of the giant quartz vein zone is discordant to the northwest trending ore bodies and porphyritic dykes at NICO (Fig. 3).

Early quartz stockworks are found in many giant vein zones, and are hereafter referred to as Q1 veins and stockworks. At NICO these are cloudy white to grey in colour and brecciate the altered host rock (Plate 2A). The host rock hematitic and K-feldspar alteration likely occurred during mineralization of the NICO deposit (Mumin et al. 2007) and the giant quartz vein zone appears to cross cut this earlier alteration. Near the contact of the vein zone with the host rock, the early stockworks have a blue-green colour, due to entrained host rock. At NICO, this phase of quartz contains chlorite, hematite and muscovite/sericite at the host-rock quartz vein contact.

Cross cutting the Q1 quartz stockworks are Q2 veins, which make up the majority of veins in the giant quartz vein zone. These veins are milky-white in colour, have banding and mosaic textures, and most frequently consist of coxcomb quartz (Plate 2B). These later veins are sporadically mineralized with hematite, pyrite, chalcopyrite, sphalerite and galena (Goad et al. 2000a). Two drill holes at NICO intersected a 10m thick section of quartz veining. The quartz veining within the drill core contained euhedral bladed growth, cloudy stockworks (Q1) and milky white cross cutting quartz veins (Q2). The Q2 drill core veins were locally mineralized, mainly with chalcopyrite, bornite or hematite (Plate 2C).

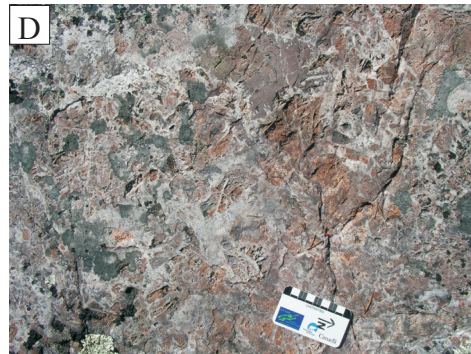


Plate 2. A) Altered rhyolite host rock brecciated by stockwork quartz at NICO. The scale is in centimetres. B) NICO Q2 veins with banding texture. The scale is in centimetres. C) NICO Q2 drill-core vein with chalcopyrite mineralization. Vein from drill-hole 98-122 at 86.13m depth. The scale is in centimetres. D) Sue-Dianne Q1 cloudy stockwork veining through altered rhyodacite. The scale is in centimetres. E) Q2 white quartz veining that split into thinner stockworks at the Northern Sloan Extension vein zone. Hammer for scale.

Giant Quartz Vein Zone located near the Sue-Dianne Deposit

The Sue-Dianne Cu-Ag deposit is located on a lease surrounding the central portion of Dianne Lake, 20km north of the NICO claims (Fig. 4; Goad et al. 2000a; Goad et al. 2000b; Gandhi et al. 2001). Sue-Dianne contains indicated mineral reserves of 8.4Mt at grades of 0.80% copper, 3.2g/t silver and 0.07g/t gold (Puritch and Hennessey 2010). Sue-Dianne has been alleged to share characteristics of Olympic Dam-type ores, with mineralization hosted in a well-zoned diatreme breccia complex (Goad et al. 2000a). The Sue-Dianne deposit is located near the intersection of north-south-trending Mar Lake Fault, and the northeast-trending (070°) Dianne Lake Fault (Goad et al. 2000a); the latter displacing the former by 400m dextrally and separating relatively unaltered rhyodacite ignimbrite to the south from strongly potassium feldspar altered ignimbrite to the north (Goad et al. 2000b).

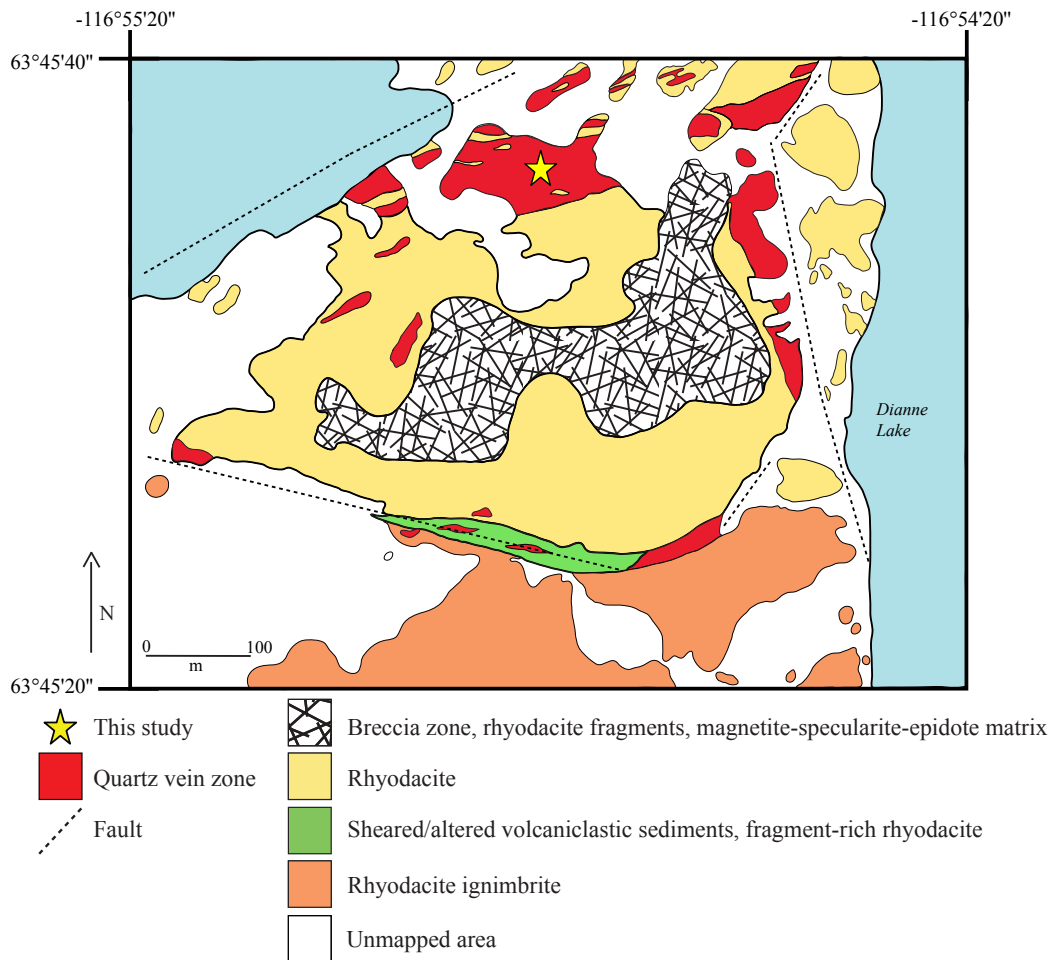


Figure 4. Giant quartz vein zone and local geology of Sue-Dianne (modified from Goad et al. 2000a).

Similarly to NICO, the host rocks at Sue-Dianne include well-preserved Snare Group sedimentary rocks overlain by rhyodacite ash-flow tuffs (ignimbrite) of the Faber Group (Goad et al. 2000a). The zircons found within these tuffs yield U-Pb ages of $1862 \pm 8.7/-1.3$ to $1869 \pm 1.3/-1.2$ Ma (Goad et al. 2000a; Gandhi et al. 2001). In many places, the rhyodacite tuff consists of strong K-feldspar and hematite alteration.

Sue-Dianne is variously enriched in copper, silver, and locally gold within disseminations and sulfide veins (Goad et al. 2000a). Sulfide mineralization is hosted within an elliptical-shaped diatreme breccia complex, approximately 600m long, 500m wide, and extending to a depth of 350m (Goad et al. 2000b); this complex is hosted within an altered ash flow tuff above the volcanic unconformity (Goad et al. 2000a). Copper primarily occurs in chalcopyrite either within the breccia matrix or intergrown with or replacing iron-bearing silicates and oxides, particularly magnetite (Goad et al. 2000a). Bornite, glaucodot and djurleite are also found in localized zones (Goad et al. 2000a). Silver is associated with the bornite zones, and is not observed as a separate silver-bearing mineral (Goad et al. 2000a). Gold occurs locally within a distinct zone on the northern edge of the deposit, where it grades to 2g/t for a few metres (Goad et al. 2000a). Other minerals of interest found are microcrystalline molybdenite, minor pitchblende, bismuthinite, and REE-bearing minerals (Goad et al. 2000a)

The giant quartz vein zone at Sue-Dianne is located at UTM NAD83 11W 0504145 E 7070497 N (± 6 m), less than 100m from the main zone of mineralization (Goad et al. 2000a). The main trend of the quartz vein zone is 280° and it has a maximum thickness of 13m with an average thickness of 7m. The giant quartz vein zone is made up of veins, stockworks, breccias, and locally as pervasive pods of silicification with occasional epidotization. The giant quartz vein at Sue-Dianne consists of fine grained, clear to pinky-clear Q1 stockwork veins (Plate 2D). At the edges of the vein zone, Q1 becomes gray to pink in colour. Q1 veins are cross cut by Q2, which are coarse grained and on average trend 280° and range in size from 1 to 50cm thick. These veins have a pink colour in 3 to 15cm sized patches as a result of entrained fragments of the granitic host rock. Near the giant quartz vein zone are large podiform veins, 2.5m by 4m each, which increase in frequency toward the giant vein zone. Most veins in this area are not laterally extensive, and have a maximum width of 15cm and length of 1.5m.

Quartz veins that occur in Sue-Dianne drill core were also sampled; the core contains minor amounts of veining. These veins are 0.2 to 1.4cm thick and comprised of cloudy gray quartz; however, these veins do not show cross cutting relationships with the giant quartz vein zone. The veins in core are commonly brecciated, and large amounts of epidote, hematite, and magnetite make up the majority of veins and host rock.

Sloan Vein

The southern end of the Sloan vein zone is located at UTM NAD83 11W 0476741E 7369810N ($\pm 7\text{m}$). Trenches blasted within the Sloan giant quartz vein contain copper stainings and other features that differ from the other veins described. Previously, the giant vein zones are located proximal to areas of base-metal mineralization; however, at Sloan, the giant vein zone was the target of the mineral exploration. Here, the 30m wide quartz vein zone was emplaced at the contact between a feldspar porphyry to the east, previously mapped by Kidd (1933) as a well-welded ash flow tuff, and a granite to the west (Fig. 5). Both rock types are altered proximal to the vein. The weathered face of the feldspar porphyry has a greenish-yellow colour, and is strongly epidotized. The granite is a rosy-pink to orange colour, and remains that way for tens of metres away from the vein.

The veining at Sloan is quite complex. An old blue-gray quartz \pm K-feldspar \pm host rock brecciation phase is found within the centre of the vein

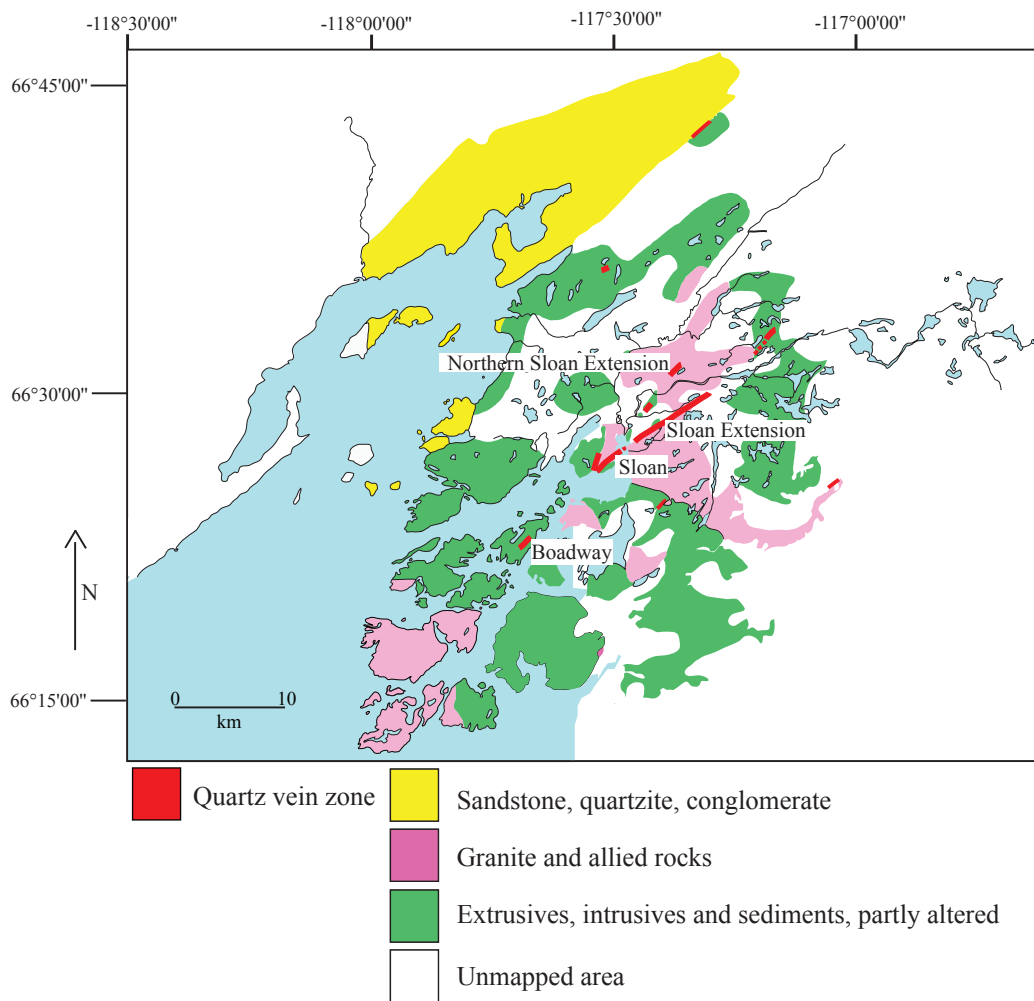


Figure 5. Giant quartz vein zones Sloan, Sloan Extension and Northern Sloan Extension and the surrounding local geology along the east arm of Great Bear Lake (modified from Map 296A by Kidd, 1933).

zone. This is cross cut by a main generation of quartz stockworks (Q1) that are analogous to the Q1 veins of other giant vein zones. Most of the individual Q1 veins are <5cm wide but their thicknesses vary along strike as the veins pinch and swell. Similar to other vein zones, the Q1 stockworks are cross cut by milky white quartz veins (Q2) that trend 040° on average, but can vary from 040 to 055°. These veins contain coxcomb and euhedral quartz textures. To a smaller degree, K-feldspar veining also seems to brecciate or rim some of the white quartz veins.

A unique feature of the Sloan vein is that a large number of the quartz veins are cross cut or brecciated by a later hematite-precipitating fluid event. The hematite rich veins brecciate earlier quartz veins into 0.2-1.5cm angular fragments. The fractures and hematite rich fluids are found throughout the core of the vein, extend to the western flanks, and are locally found on the eastern flank of the vein.

Copper mineralization at Sloan consists of low grades of bornite, chalcopyrite, and malachite. These appear in three distinct ways. The main zone of mineralization is at the contact between the granite and the giant quartz vein, this mineralized zone trends 040° and is 3m wide. This appears at surface as a strip of yellow-weathered quartz, which contains small weathered holes at surface. The fresh rock is white and contains copper-sulfides and disseminated malachite. This zone is a highly altered and silicified host rock proximal to the quartz vein. Secondly, mineralization is found on the eastern flank of the Sloan vein; and malachite staining is pervasive near Q1 stockworks which brecciate the altered greenish-yellow host rock. Here, the surface expression is a series of gossans that appear intermittently along a 045° trend, and are usually 1 - 2m wide and contain chalcopyrite. The youngest type of mineralization is found in fractures within the giant quartz vein itself. Three major joint sets are common to the Sloan vein, the first at 040°, the next at 110°, and the last at 350°. Joint sets at 040° parallel the length of the Sloan vein and do not appear to be mineralized. Jointing at 110° contains hematite staining and veining. The joint sets at 350° contain bornite and malachite. This fracture set is quite late, since in one area it is observed to cross cut the younger Q2 white euhedral coxcomb quartz veining.

Sloan Extension

The Sloan Extension (Fig. 5) is along the same orientation to the Sloan Vein, and is likely part of a separate fault system. The Sloan Extension is located at UTM NAD83 11W 0479352E 7371811N (±9m) and the zone is 47m wide. The Sloan Extension contains early Q1 stockwork veining and a separate generation of massive, blocky quartz.

Most of the Sloan Extension consists of a moderate amount of Q1 stockwork veining within the host rock. These cloudy quartz veins are commonly less than 5cm wide. Some of these veins trend 055°/65° but many of the stockworks are in a variety of orientations. This Q1 stockwork is cross cut by rare thin (<10cm) quartz veins rimmed by K-feldspar. Some of these veins also have greenish selvages, from fine grained actinolite or chlorite.

The stockwork veins and quartz-K-feldspar veins predate an area of

massive white quartz associated with silicified host rock that makes up a major topographic high in the centre of the giant quartz vein. The zone of massive white Q2 quartz is more than 25m in width and on the surface appears to have no internal structure. Upon breaking the rock, coarse-grained euhedral quartz crystals and minor amounts of hematite are found. Vuggy porosity is commonly present in this unit. With the exception of the hematite no other minerals were found in this part of the vein.

The mineralization within the Sloan Extension is identified by the development of gossans. The western flank of the Sloan Extension contains numerous gossans that outcrop in an area of a few metres squared. Quartz veins are associated with these gossans and the veins commonly contain fragments of hematite altered host rock. The quartz veins that contain sulfides have a yellowish colour on the surface. These veins are oriented 055°/65°, and are variable in size, with a maximum width of 15cm. Mineralization is dominated by chalcopyrite, arsenopyrite and pyrite and occurs within the veins themselves, and also within the altered host rock fragments in the veins.

Northern Sloan Extension

The Northern Sloan Extension vein zone is the most northerly giant quartz vein on Hunter Bay Resources' property. The southern end of the vein is located at UTM NAD83 11W 0481035E 7375088N ($\pm 8\text{m}$) (Fig. 5). The vein creates a prominent topographic ridge, approximately 70m wide, and is made up of two main phases of quartz mineralization: a Q1 stockwork with a yellowish weathered appearance, and younger Q2 veins that make up the centre of the vein. At the contact of the giant quartz vein zone the highly altered host rock is silicified, hematitic and epidotized. On the west side of the vein the host rock fragments are altered to a yellow-green colour, whereas on the east side the fragments are orange-pink. This is unlikely to be due to a compositional change in the host rock, since previous mapping shows the same feldspar porphyry on both sides of the vein, but may be the result of variations in the fluid chemistry laterally across the vein.

There is some mineralization associated with the Q1 stockwork veining. The mineralization seems to be focused along the sides of the ridge. Bornite and chalcopyrite can be found in these veins, as well as within the host rock brecciated within the veins. The surface expression of this mineralization is malachite staining on the veins.

The second, Q2, younger phase of white quartz veining consists of individual veins that are generally less than 15cm thick, but split into thinner stockworks, where the veins are only a few millimetres thick (Plate 2E). The veining contains two main orientations, the first at 040°/80-90° and the second at 070°-080°/85°. These thin veins can cross cut each other suggesting that multiple episodes of veining occurred. This youngest set of quartz veins contains vugs and the quartz crystals are euhedral and commonly have prismatic and growth banded crystal terminations. The quantity and appearance of host rock fragments within the younger quartz veins is variable.

The larger Q2 veins trend 040-055°, dip steeply and usually are a few mm

to 3cm thick. They weather to a yellowish colour. On a fresh surface, however, the veins are made of white quartz; and consist mainly of banded quartz and coxcomb textures. There are variable amounts of host rock entrained in the veins, ranging from fragments that are a few millimetres thick in the colloform banded quartz to fragments up to 15cm wide; these fragments are altered to chlorite and clays.

There are a few trenches along the Northern Sloan Extension vein zone that contain mineralization within the Q2 generation of quartz. The vugs contain chalcopyrite, bornite and malachite. Where mineralized the veins are commonly pink to red in colour. This is in part due to the presence of hematite in the veins, but also is the result of Fe staining produced by the breakdown of chalcopyrite. The young coxcomb veins likely represent a late remobilization of copper mineralization in the area. Malachite is commonly found a few millimetres thick along late fractures in this area. These fractures trend $045^{\circ}/85^{\circ}$ and $290^{\circ}/10^{\circ}$.

The Northern Sloan Extension vein zone is cut by two mafic dykes: the southern dyke is 10m wide and cuts the vein at $075^{\circ}/85^{\circ}$; the northern dyke is slightly larger, at 15-18m wide. Both dykes are strongly magnetic and consist of clinopyroxene and albite with a small amount of magnetite, orthoclase, chlorite and sphalerite.

1.1.2 Uranium Associated Giant Quartz Vein Zones

Beaverlodge Lake

Beaverlodge Mine is a former uranium mine that had various owners between 1943 and 1957 (INAC 2009). Geiger measurements recorded high radioactivity along the vein host rock contact. Previously, the area has been a focus for exploration, further mining, and fuel storage; it is now part of a reclamation project since being reverted to Crown land in 1977 (INAC 2009).

The giant quartz vein at Beaverlodge Lake is 25m in width and over a kilometre in length and is located at UTM NAD83 11W 443574 7179358 (± 5 m) (Fig. 6). However, uranium mineralization at Beaverlodge Lake is restricted to the host rock quartz feldspar porphyry that can contain up to 2% pitchblende in localized areas and is beige to yellow in colour. The giant quartz vein is hosted by a coarse grained, white, quartzite and green siltstone package which is approximately 30m thick. Beaverlodge Lake contains minor cloudy Q1 stockwork veining and the vein zone is, for the most part, comprised of milky white veins (Q2) that are coarse grained and include subhedral to euhedral, growth zoned quartz with individual quartz grains, usually between 0.1 to 1.5mm, in veins 10 to 20cm thick. Pyrrhotite and pyrite can be found in 0.1mm small anhedral crystals within some Q2 veins. The Fe-sulfides occur along late fractures and are associated with chlorite, muscovite and anhedral monazites.

Lastly, hematite is deposited along 110° trending joint surfaces. These hematite fractures are up to 15cm in diameter and brecciate the milky white veins into angular to subangular fragments.

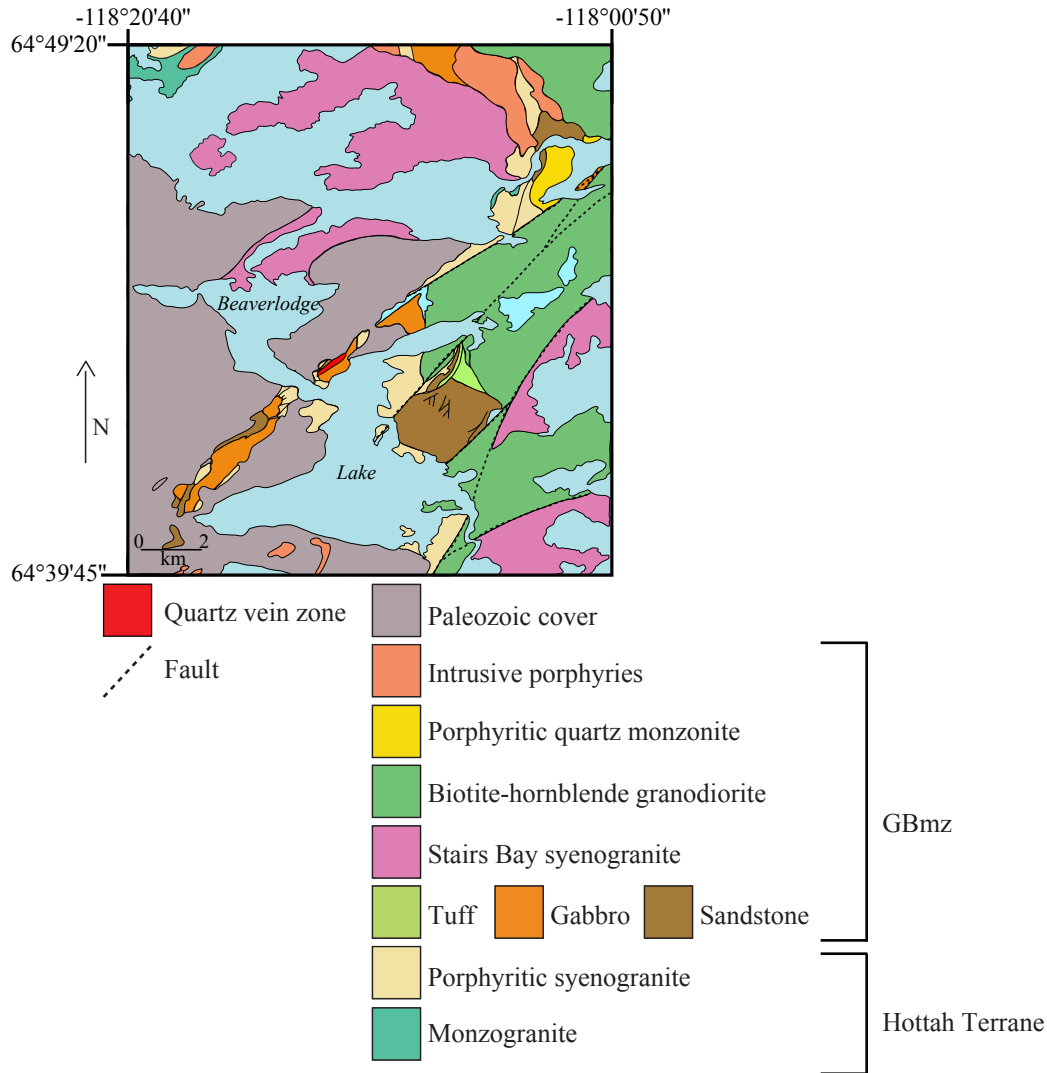


Figure 6. Giant quartz vein zone of Beaverlodge Lake and the surrounding local geology along the east arm of Great Bear Lake (modified from Hildebrand and Roots, 1985).

Fab Lake

Fab Lake is located west of the Wopmay fault and northeast of the larger Faber Lake (Fig. 7; Gandhi 1988). Fab Lake is named for the “FAB” U ± Cu mineral claims along the central east side of the lake.

The host rocks at Fab Lake comprise Great Bear magmatic and Faber Group intrusive and extrusive rocks. West of Fab Lake, the Mazenod Lake volcanic assemblage of the Faber Group consists of rhyodacites and rhyolites, which have been dated at 1868 Ma (Gandhi et al. 2001). These rocks are calc-alkaline, with considerable variation in alkali elements, especially near mineralized zones (Gandhi 1994). East of Fab Lake the main units found include undifferentiated granite – granodiorite, quartz monzonite – monzodiorite (dated to 1867 Ma), and feldspar ± quartz porphyries (also dated to 1867 Ma) (Gandhi et al. 2001). Approaching the northeast trending fault, the pinky fractured quartz-

feldspar porphyry host rock becomes increasingly red, and the rocks contain a subvertical joint set at 060°. Subvertical fractures within the host rock are coated with hematite.

The giant quartz vein at Fab Lake is located at UTM NAD83 11W 0492893E 7110921N ($\pm 7\text{m}$); it is 60m wide and emplaced along a northeast (060°/subvertical) trending fault on the west side of Fab Lake. The NE trending fault transects both sides of Fab Lake and is approximately 12km long. The FAB U \pm Cu claims are focused along the east side of Fab Lake, and uranium mineralization is absent from the giant quartz vein zone. The rhyolitic host rock is heavily epidotized, silicified and fractured proximal to the quartz vein.

The abundant quartz veins consist of clear to cloudy Q1 stockwork quartz, which has bluish-green hue as the result of entrained host rock fragments. The veins range in width from 2mm to 10cm in width and are multidirectional. This generation of veins is mostly found at the contact of the giant quartz vein zone with the host rock.

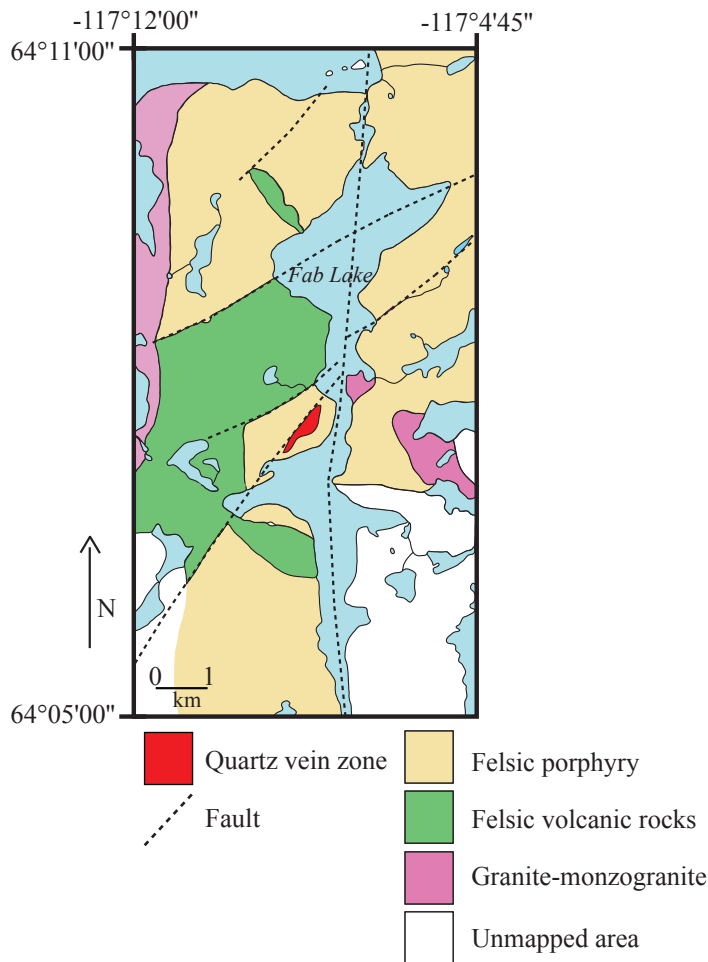


Figure 7. Giant quartz vein zone and local geology at Fab Lake (modified from Jackson 2007).

The younger, Q2, milky white quartz is commonly multidirectional, and individual veins are usually 1-10cm wide but the largest vein observed was 5m wide and traceable for many tens of meters. Many of these veins branch into thin mm sized stockwork veins. Even within a single vein, multiple generations of quartz growth can be recognized; commonly, the veins contain clear, fine grained, quartz at the contact with the host rock with coxcomb textured, fine grained milky white quartz in the centre of the vein. There is a second generation of milky white veins that trend 300°, cross cutting earlier milky white veins, and offsetting them a few centimetres sinistrally and dextrally, this quartz is referred to as Q3.

Northern Wopmay Fault

The Wopmay fault is a regional linear north-south zone found along the length of the GBmz; it consists of sheared volcanics and metasediments, and mylonites. The host rocks to the vein consist of a gabbro to the west, next to a large package (~20m thick) of foliated greywacke and a mylonitic granodiorite. The greywacke is green on fresh face and has an orange-red rusty weathered surface. The pink-orange, mylonitic, granodiorite hosts the giant quartz vein. Historically, this area is reported to contain U mineralization and radioactive anomalies (Normin 2009); however, no anomalies were discovered with a Geiger counter at this location.

The Northern Wopmay fault giant quartz vein zone is located at UTM NAD83 11W 515412E 7153625N (±6m) and is north-south trending (Fig. 8). The giant quartz vein and stockwork zone here is 20m in width but the stockwork zone is discontinuous for approximately 500m, with a length of approximately

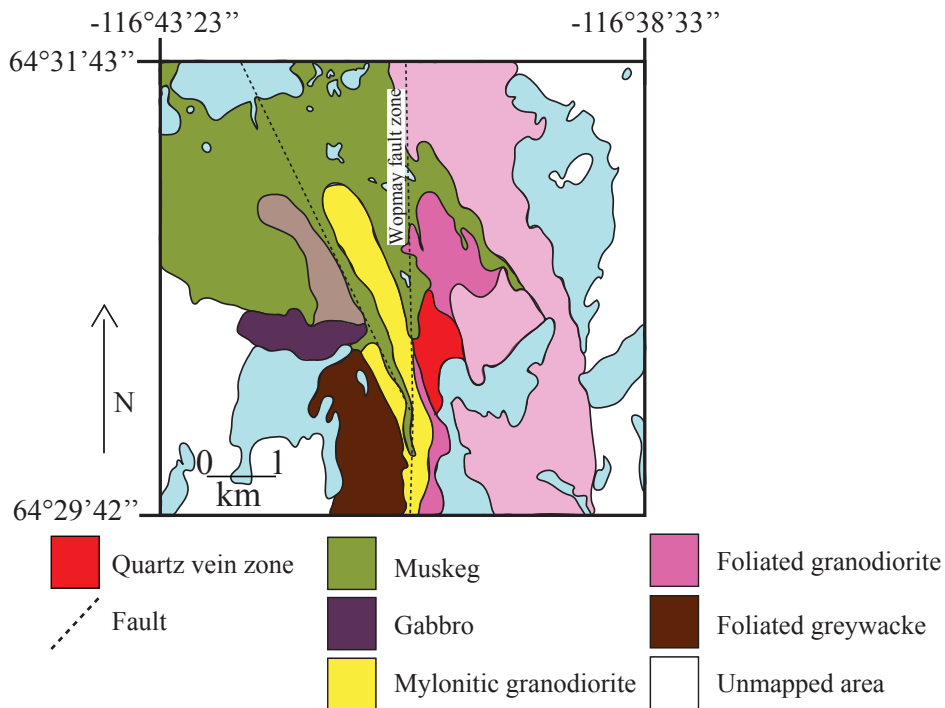


Figure 8. North trending giant quartz vein and local geology from field notes at the Wopmay fault zone (traced from an aerial photo).

1km, although some veins pinch out after 50-100m. The quartz veining within the Wopmay fault zone is not as established as some other vein zones, and, locally, veins are boudinaged or sheared; these sheared veins are cloudy and contain textures similar to Q1 of other vein zones. The foliation and Q2 veining has a main orientation of $000^{\circ}/85-90^{\circ}$, and Q2 veins consist of euhedral prismatic milky white crystals.

1.1.3 Giant Quartz Vein Zones Isolated from Mineralization

“Arm” Lake

“Arm” Lake is an unnamed lake located on the east side of the Wopmay fault within the Coronation Margin (Fig. 9). This unofficial name “Arm” Lake comes from the numerous branches or channels along the lake’s edge. The host rock here consists of pink granite, with localized orange-rusty colours at the contact with the quartz veins; no mineralization is apparent in the host rock or the veins.

The giant quartz vein at “Arm” Lake is found at UTM NAD83 11W 0521791E 7131869N ($\pm 6\text{m}$) and is northwest trending. It is 25m in width on the west side of “Arm” Lake (Fig. 9).

Multiple phases of quartz precipitation and brecciation result in older gray-cloudy quartz veins (Q1) that are brecciated and cemented by younger milky white quartz veins (Q2). The Q1, gray-cloudy quartz veins, are generally 0.5 – 5cm in width and have no preferred orientation.

Most of the Q1 and Q2 veins at “Arm” Lake are oriented $150^{\circ}/65^{\circ}$ to $170^{\circ}/65^{\circ}$. The Q2 veins are generally 0.5 to 15cm in diameter, but a few are 2m thick, the veins commonly split into smaller veins and rejoin. The granite is brecciated by the veining in subrounded 1 x 1cm up to 15 x 30cm clasts, and late fractures are filled with hematite.

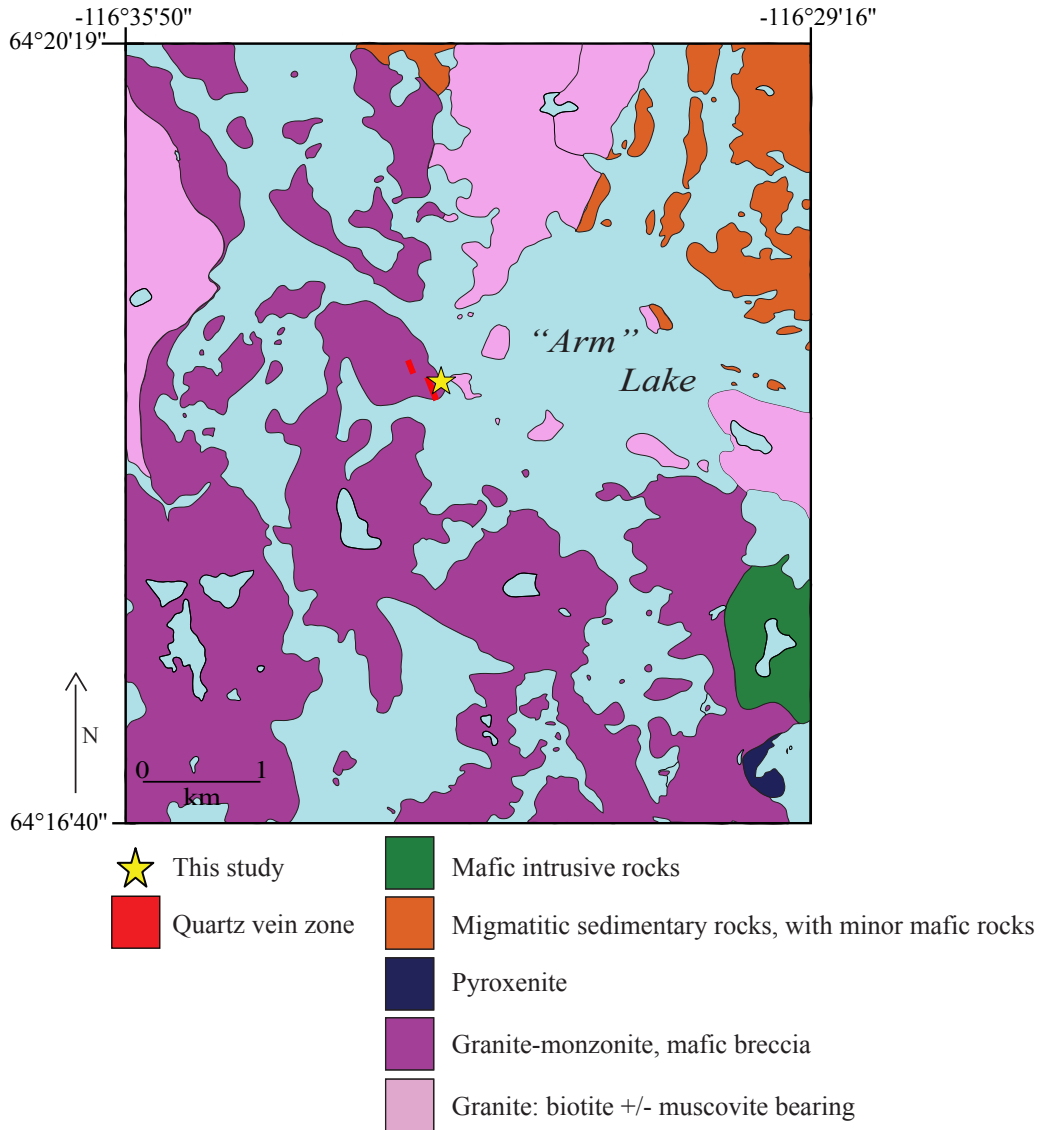


Figure 9. Northwest trending giant quartz vein and local geology at "Arm" Lake (modified from Jackson 2007).

Hardisty Lake

Hardisty Lake is a large lake near the western edge of the Great Bear magmatic zone, near the contact of the GBmz with the Phanerozoic cover. The host rock is a coarse grained pink monzogranite. Proximal to the contact with the giant quartz vein zone, the monzogranite becomes silicified and has a greenish gray colour due to increased chlorite content. At the host rock and quartz vein contact some of the altered host rock contains minor amounts of malachite; this is west of the major vein zone. Proximal to the giant vein zone, the monzogranite is silicified and contains a large amount of chlorite.

At the north end of Hardisty Lake the giant quartz vein zone begins at UTM NAD83 11W 0469127E 7160093N ($\pm 6\text{m}$), is 13m wide and over 1km long (Fig. 10). Regional maps show that although this vein appears to pinch and die

out, it can in fact be traced over many tens of kilometres along the same 060°/subvertical fault. Although the vein follows the fault, a 2.5m wide fault gouge is observed southeast of the majority of quartz veining. This fault gouge may indicate reactivation of the fault post quartz vein deposition.

The oldest veins, Q1, are cloudy to white, fine grained, stockworks that have no preferred vein orientation. Most of the stockwork veins are 0.5 to 5cm in width and the host rock near the veining is extremely silicified and has a pink to greenish-blue colour.

Younger Q2 veins are 5 to 30cm in width, but can be up to 2m, made up of euhedral quartz. These also can be multidirectional, and are locally cross cut by thin (~2mm thick) hematite veinlets. Larger Q2 veins cross cut the very fine grained cloudy stockworks.

Southwest of Hardisty Lake the giant quartz vein zone outcrops again. This extension of the Hardisty Lake quartz vein is located at UTM NAD83 11W 0468166E 7159806N (±6m). Here the quartz vein zone is only 9m wide and 80m long. It runs parallel to a 25cm mafic dyke through the granitic host rock and the orientation is 060°/subvertical. The majority of veining is comprised of Q1 stockworks but some Q2 veins cross cut the stockworks.

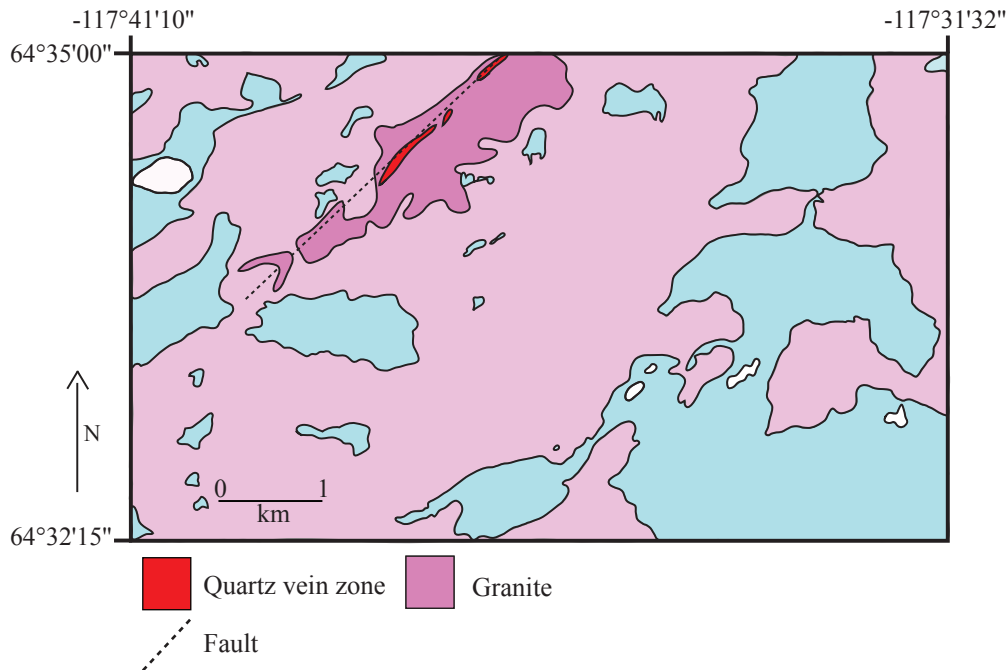


Figure 10. Northwest trending giant quartz vein and local geology at Hardisty Lake (from aerial photos). Note: lightly shaded colour is inferred geology.

Margaret Lake

Margaret Lake is located east of Hardisty Lake and west of the Wopmay fault. The main lithology at Margaret Lake is orange weathering granite and there are no mineral showings at this location. Silicification of the granite is apparent near the quartz vein zone. Scintillometer readings taken at Margaret Lake resulted in only background levels, with values lower than the host rock background over milky white quartz veins.

This giant quartz vein zone can be followed along strike from the North edge of Taka Lake to the southern edge of Margaret Lake (Fig. 11). The location of the north end of the giant quartz vein zone is UTM NAD83 11W 0490354E 7145853N (± 6 m). The quartz vein zone is 22m wide and trends $060^{\circ}/85^{\circ}$.

The older Q1 stockworks are formed from gray, cloudy and fine grained quartz. Although individual veins have no preferred orientation, many do share an orientation of $320^{\circ}/85^{\circ}$. Q1 stockworks brecciate the granitic host rock into subangular centimetre sized clasts. Most quartz stockworks consist of veins that are 1 to 3cm wide.

Milky white quartz veins (Q2) consisting of euhedral, large grains, cross cut the early stockworks. Q2 veins are oriented from 050° - 060° strike and have a 75° - 80° dip. Hematite fills late fractures within the milky white veins. Joints, each approximately 12cm wide, cross cut the veins at $335^{\circ}/60^{\circ}$, and hematite is also concentrated on these surfaces.

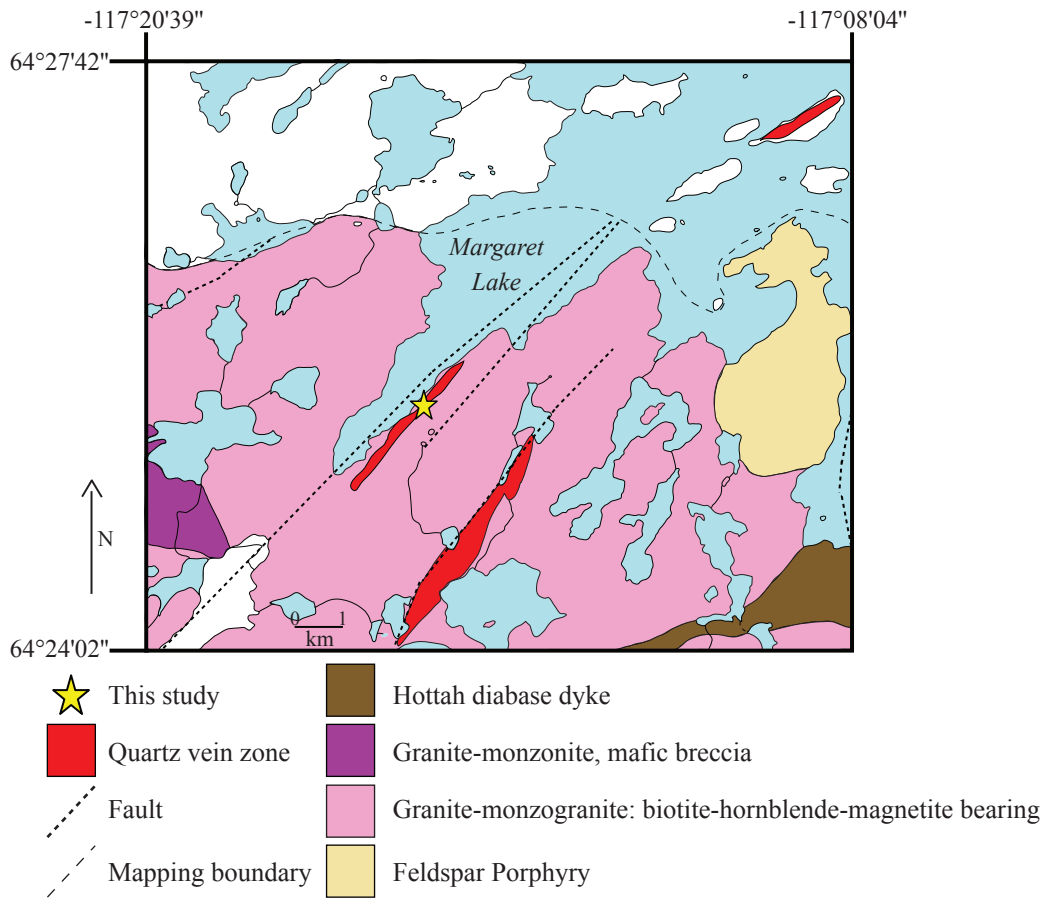


Figure 11. Giant quartz veins and local geology at Margaret Lake (modified from Jackson 2007).

2 Analytical Methods

2.1 Electron Microprobe

Microprobe work was completed at the University of Alberta using a JEOL 8900 electron microprobe and electron probe microanalyser (EPMA) with five wavelength dispersive spectrometers. Samples from Beaverlodge Lake and NICO were analysed for quantitative mineral chemistry and qualitative elemental mapping. One sample from NICO (06SBN001) was mapped using a monochromatic cathodoluminescence detector, with unsatisfactory results. Prior to microprobe work, polished thin sections were coated with a thin film (20nm) of carbon and the microprobe was calibrated with uranium and sulfide standards. The beam was operated at an accelerating voltage of 20.0kV and a diameter of 1µm.

NICO vein and drill-core consisted of altered host rock; a selection of these alteration and host rock samples were qualitatively mapped for Al, Ca, Fe, K, Mg, Mn, Na, P, Si and Ti. Mineral chemistry data from the NICO samples are located in Appendix B. Beaverlodge Lake samples contained uranium-bearing minerals, and these sections were qualitatively mapped for Bi, Pb, Si, Se, Ti, U, and Zr.

2.2 Scanning Electron Microscope – Cathodoluminescence

A cathodoluminescence (CL) study was performed in the environmental scanning electron microscope (SEM) facility at the Great Lakes Institute for Environmental Research (GLIER) laboratories at the University of Windsor, Ontario. The FEI Quanta 200 field emission gun with variable pressure SEM is equipped with a Centaurus CL, which contains a photomultiplier solid state back-scattered detector. SEM-CL was operated in high vacuum mode on carbon coated polished thin sections (30 to 35µm thick), and settings that adjust the electron voltage and spot size are recorded on SEM-CL digital photographs. Samples from NICO vein and drill-core, Sue-Dianne, “Arm” Lake, Northern Sloan Extension, and Beaverlodge Lake were analysed.

2.3 Laser-Ablation Inductively Coupled Mass Spectrometry

Trace elements within the quartz veins were analysed with a high resolution laser-ablation Thermo Instruments X-7 Inductively Coupled Plasma Mass Spectrometer (LA-ICP-MS), at the GLIER laboratories at the University of Windsor, to assess if there was a correlation between trace element concentration and petrographic textures found in SEM-CL images. The trace element study was carried out on thick sections (100 to 150µm) from quartz veins from Beaverlodge Lake, NICO vein zone, NICO drill-core, Sue-Dianne, and Northern Wopmay fault zone. Sixteen elements were analysed: Si, Li, Al, K, Ti, Ge, La, Fe, P, Mn, Be, Na, Rb, Co, Y, and Ca, using a femtosecond laser at a wavelength of 785nm (Shaheen et al. 2008).

The analysis was standardized by the National Institute of Standards and Technology (NIST) 610, and gas blanks were run before and after each

experiment and agree well with certified, reference, and information values within a mean relative difference of $\pm 4\%$ (Shaheen et al. 2008). Detection limits are calculated based on the NIST 610 standard, and vary slightly from one experiment to the other (Shaheen et al. 2008). To minimize this variability, the ICP-MS was run for 1 minute before the laser was engaged to ensure that the sample cell and tubing have been flushed clean of element contamination from preceding samples (Yang pers. comm. 2009). Detection limits were determined individually for each sample, with tables for minimum and maximum element concentrations for each LA-ICP-MS track (Appendix C). Trace element results are reported in parts per million.

Trace element data was processed using Thermo Plasma Lab software, version 2.5.3.280© Thermo Electron 2003. This software was used to control the ICP-MS and collect or manipulate the data for reporting. Plasma Lab results were then input into a LA-ICP-MS data reduction table in Excel. This processes laser experiment data over integrated regions selected by Plasma Lab software, based on algorithm worksheets set up by Dr. J. Gagnon, University of Windsor, and LA-ICP-MS analyte concentration calculation method by H.P. Longerich et al. (1996).

2.4 X-ray Diffraction

This study attempted to date the veins indirectly by Ar-Ar dating of hydrothermal sericite. Although uncommon in the veins, sericite and a small amount of muscovite, formed at the same time that the quartz veins were emplaced. The samples were crushed by jaw or silica crushers, as well as by hand. Separation was attempted through a variety of sieving, paper-shaking and water floatation techniques (Lee pers. comm. 2009; Richards pers. comm. 2009).

X-ray diffraction on separated samples was carried out by Diane Caird, at the University of Alberta. The Rigaku Geigerflex Power Diffractometer with a Co tube and graphite monochromator analysed separated samples that were placed on a quartz plate, for zero background interference. X-ray diffraction on the separated samples showed that the samples consistently contained sericite as well as chloritoid \pm quartz \pm kaolinite and sanidine; the separates were contaminated with several K-bearing minerals, and for that reason, attempts at dating the hydrothermal sericite were abandoned.

2.5 Microthermometry

Fluid inclusion sections are doubly polished and 100 to 150 μm thick; petrography was completed using an Olympus BX60 petrographic microscope with digital photomicrograph capabilities. Microthermometry analysis was carried out in Dr. Richards' fluid inclusion laboratory at the University of Alberta using a Linkam THMS G600 heating/freezing stage mounted on an Olympus BX50 microscope, with a 40X SLCPlan long-working distance fluorite objective lens. The accuracy of temperature is controlled to within 0.1 $^{\circ}\text{C}$ by a TP93 programmable controller. Calibration of the heating/freezing stage was carried out prior to measurements and at the end of microthermometry experiments. Synthetic two-phase fluid

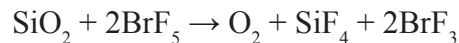
inclusions from SynFline were used, and no instrumental drift was recorded.

Most inclusion work was done at a magnification of 40X objective by 10X optical zoom, and commonly increasing the ocular by 1.25X (12.5X ocular). Temperature of homogenization and temperature of ice melting are reported in degrees Celsius. Ice melting temperature precision on repeated analyses of fluid inclusions can be replicated to $\pm 0.2^\circ\text{C}$ below 0°C , while temperature of homogenization replicated results to $\pm 2^\circ\text{C}$ below 400°C . Salinity is calculated using equations from Bodnar (1993) for two phase and Sterner et al. (1988) for three phase fluid inclusions, respectively, and is reported in equivalent weight percent NaCl (wt. % NaCl eq.).

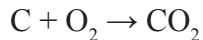
2.6 Stable Isotopes

2.6.1 Oxygen Isotopes in Quartz

Individual quartz veins were hand separated and crushed with an agate and/or steel mortar and pestle. Quartz was hand-picked under a dissection microscope to eliminate contamination by sheet-silicates and feldspars. Oxygen isotopes were measured at the University of Alberta stable isotope laboratory, by Dr. K. Muehlenbachs and his technician Olga Levner. Six samples, five plus one blank, of 20 to 30mg samples were run at a time. Oxygen isotopes were measured based on the methodology of Clayton and Mayeda (1963), using bromine pentafluoride as the oxidizing agent. The typical reaction of bromine pentafluoride with a silicate is as follows:



After collection of the oxygen, the gas is passed over hot carbon to convert it quantitatively to carbon dioxide by the reaction:



The carbon dioxide is taken to the Finnigan Mat 252 Mass Spectrometer equipped with both multi-port and continuous flow inlets in Chemistry at the University of Alberta. Isotopic accuracy is ± 0.1 to 0.2 ‰. Yield calculations were measured by weighing the samples pre and post-reaction and reactions were re-run if less than 95% yield was recovered. Values of $\delta^{18}\text{O}$ are reported in per mil and relative to the Vienna Standard Mean Ocean Water (VSMOW).

2.6.2 Carbon and Oxygen Isotopes in Calcite

Two calcite vein samples from NICO drillcore were separated, crushed, and hand-picked. Analysis of carbon isotopes were done at the University of Alberta stable isotope laboratory. Samples of 20 to 30mg of calcite were measured by Dr. K. Muehlenbachs following the extraction methodology outlined by McCrea (1950) and the collected CO_2 was measured on the Finnigan Mat 252 Mass Spectrometer. Reproducibility of the $\delta^{18}\text{O}$ values for standards and samples were generally better than ± 0.2 ‰. Oxygen and carbon isotope values are accurate to within ± 0.1 ‰. The $\delta^{13}\text{C}$ and $\delta^{18}\text{O}$ ratios are reported in per mil relative to the Vienna Peedee Belemnite (VPB) and the Vienna Standard Mean Ocean Water (VSMOW), respectively.

3 Analytical Results

3.1 Petrography, Cathodoluminescence and Trace Element Results

3.1.1 Giant Quartz Vein Zones located near Base-Metal Mineralization

Giant Quartz Vein Zone located near the NICO Deposit

The host rock near the contact with the giant quartz vein zone is extremely silicified and is comprised of quartz and iron-rich chlorite in equal proportions. The chlorite is lath-like and very fine grained, up to 0.1 x 0.3mm in length, and the quartz is 0.2 to 0.4mm in diameter with subhedral crystals. The wall rock proximal to the quartz vein zone is a potassium-feldspar altered rhyolite, and the host of the main ore zone is a dark grey to green greywacke. The greywacke, after being analysed on the electron microprobe, consisted of K-feldspar, biotite, iron- and magnesium-rich clinopyroxene, actinolite, zircon and hematite. The altered host rock is brecciated by quartz veining proximal to the main vein zone, and is comprised of monazite, Fe-Mg chlorite, and laths of K-feldspar (Plate 3A). The altered rhyolite intersected in the drill core consists of quartz, mottled-looking K-feldspar, Fe-Mg chlorite and hematite. This host rock is mineralized with pyrite and chalcopyrite; contained within these phases are small sphalerite grains and trace amounts of galena, this is interpreted to be an exsolution texture (Plate 3B).

Quartz microveinlets (0.2mm in width) cut through the altered rhyolite; these veinlets commonly contain hematite, and small (0.3 x 0.3mm) pyrite grains are disseminated through the altered host rock. The earliest phase of veining, referred to as Q1, at NICO is represented by blue to green quartz stockwork. The colour is due to entrained millimetre to centimetre sized subangular clasts of altered host rock, mainly consisting of iron-rich chlorite and muscovite and is made up of subhedral quartz crystals that are less than 0.1mm, but can be up to 3mm in length (Plate 3C). Closer to the core of the giant vein zone, this Q1 stockwork contains fine grained, 0.5 x 1mm, cloudy, fluid inclusion-rich quartz. These veins are mostly colourless but can also have a pinky hue due to hematite alteration around the vein, and exhibit fan-like extinction under cross polarized transmitted light.

Late Q2, milky white quartz veins, cross cut the stockworks, these veins contain multiple grain sizes; the majority (approximately 75%) of the quartz crystals are 2 x 2mm, with 15% up to 4 x 6mm in size, and 10% being smaller, approximately 0.5 x 1mm in crystal size. This type of quartz has a range of extinction patterns in cross polarized transmitted light, and commonly, the crystals have plumose extinction at the crystal rim. Some thin sections were cut in an orientation perpendicular to quartz growth, and euhedral hexagonal cross-sections of quartz crystals have clear cores with cloudy rims that contain numerous fluid inclusions and, locally, mineral inclusions of hematite. Four laser ablation transects attempted to identify trace element concentration fluctuations between the core and rims of these quartz crystals. Many of the elements included in the analyses had concentrations below the detection limits or do not show

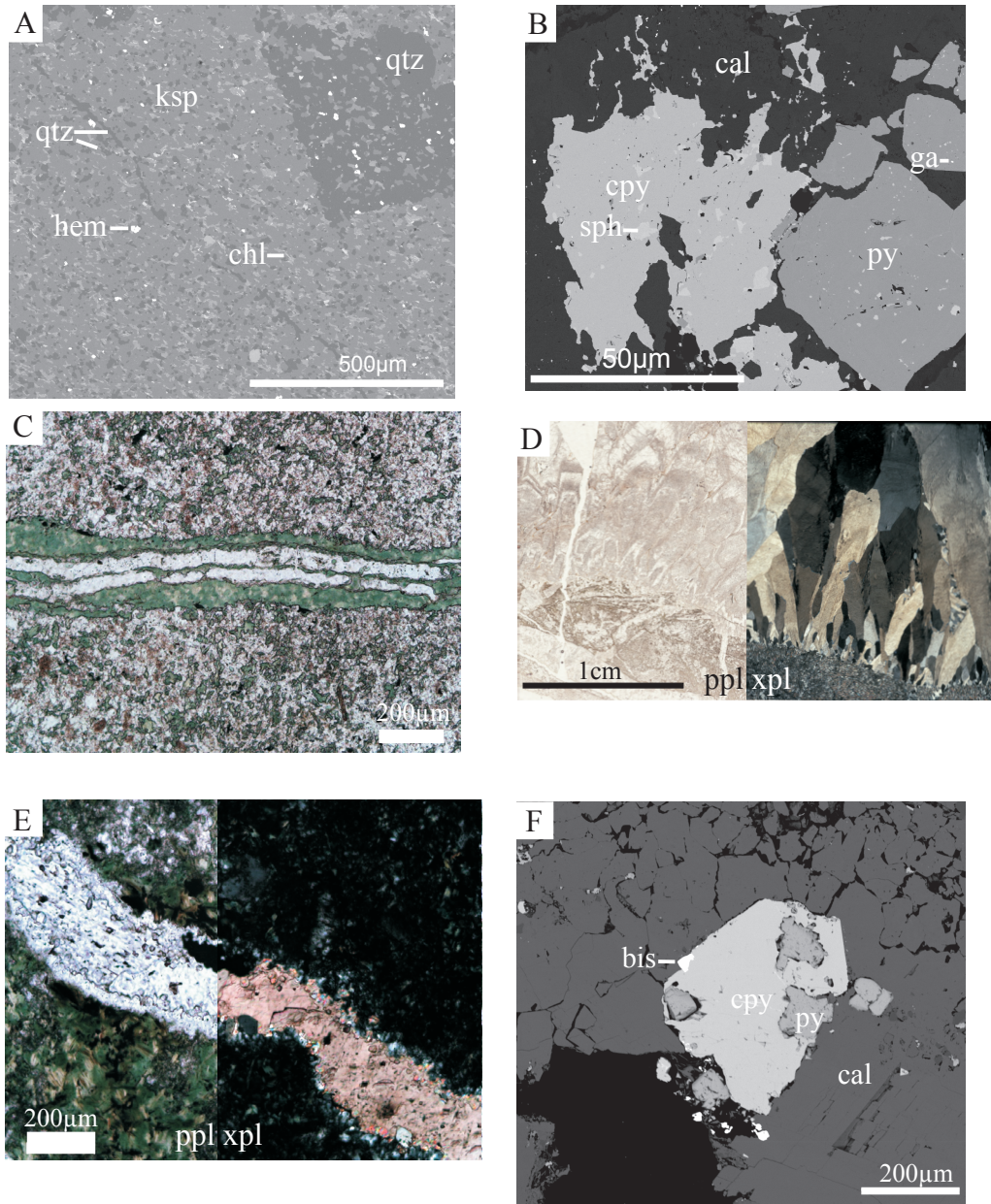


Plate 3. A) Electron microprobe image of NICO drill-core of rhyolitic host rock with K-feldspar alteration, altered angular quartz phenocryst and thin quartz veinlet, with shreddy chlorite and hematite. B) Electron microprobe image of NICO drill-core calcite vein with pyrite cubes and chalcopyrite with exsolution of sphalerite and galena. C) NICO Q1 veins rimmed by chlorite in plane transmitted light. D) NICO Q2 vein with euhedral comb quartz crystals. E) A NICO Q3 quartz vein is fractured and filled with calcite and an anhedral grain of pyrite. F) Electron microprobe image of a late calcite vein in NICO drill core with vuggy porosity, mineralized with chalcopyrite, pyrite and bismuthinite. Ksp = k-feldspar, qtz = quartz, chl = chlorite, hem = hematite, cal = calcite, cpy = chalcopyrite, sph = sphalerite, ga = galena, py = pyrite, bis = bismuthinite. Ppl = plane polarized light; xpl = crossed polarized light.

systematic changes in concentration across the crystal (e.g. La, Y, Ge, Be, Co, Ti and P). However, The LA-ICP-MS analyses from the inclusion-poor core to the inclusion-rich cloudy rim of a single quartz crystal shows a sharp increase in Li, Al, Na, K, Mn and Rb (Appendix D). Rubidium increases sharply from less than 4 to 28ppm; similarly, Na increases from 350 to 2900ppm at the onset of the cloudy quartz, however iron concentrations remain at an average of 50ppm across the entire laser ablation transect.

Other Q2 veins are bladed and euhedral in shape, and usually these are coarse grained (30 x 50mm). Commonly these bladed grains are small at the contact with host rock, but widen toward the centre of the vein (Plate 3D). In SEM-CL, some NICO veins contain euhedral quartz crystals with dark grey to black cores with light grey to bright white rims. When imaged in SEM-CL, these euhedral crystals can contain light and dark grey zones up to 0.75mm in width. These crystals are also commonly rimmed with hematite that fills the thin space between grain zone boundaries. Locally, these late Q2 veins show plumose extinction and ghost textures, where previous crystal grain boundaries appear when viewed in polarized transmitted light.

Some Q2 veins show banding that contains crystals that are up to 4 x 10mm. These commonly contain quartz with fluid inclusion rich and poor zones. One Q2 vein zone contains a thin layer of carbonaceous material located between layers of banded quartz. The bands include both bladed euhedral crystals and feathery quartz, each vein approximately 1cm in width.

Quartz microfractures, referred to as Q3, are found cross cutting all types of quartz veining. These are generally 0.1 to 0.3mm in width, although they can be up to 3mm, and are laterally extensive. Under cross polarized transmitted light, these veins commonly remain optically continuous with the veins they cross cut, but are obviously a later vein set. The Q3 veins are commonly partially filled with hematite and yellow clays (kaolinite \pm illite). Chalcopyrite and pyrite can be found within these microfractures. In SEM-CL, late quartz veinlets, 0.3mm in width, cross cut previous veins and have a dark grey luminescence with no zonation. Many of these Q3 veinlets are cross cut by bright white luminescent hematite filled-fractures that are less than 50 μ m in width. The trace element composition of quartz, which makes up a 0.25mm width microveinlet, only fluctuates in Mn, which ranges from below detection limits (less than 0.4ppm) up to 90ppm. One Q3 veinlet is cross cut by a fracture filled with hematite, this results in peak concentrations of Fe, P, K, Ca, Ti, Co, Ge, Rb, La and Y.

Giant Quartz Vein Zone within NICO Drill Core

A section of drill-core intersected the giant quartz vein zone at NICO, and these veins contain multiple generations and textures of quartz. At the contact with the host rock, the quartz crystals are fine grained, only 0.1 to 0.4mm in diameter, but within the core of the vein are much coarser and subhedral to euhedral, similar to Q2 veins. One sample contains quartz crystals with cloudy cores and clear rims, in other words, the opposite to some of the veins in the giant quartz vein. Small amounts of pyrite and hematite are contained within these veins. These veins are also cut by thin fractures that are 0.1mm wide and unfilled. The quartz veins commonly exhibit plumose extinction and ghost textures in cross polarized transmitted light. Locally, Q2 veins within drill-core are filled with bornite, chalcopyrite and small grains of a copper-bismuth mineral, wittichenite (Appendix B).

NICO drill core veins contain similar SEM-CL zoned euhedral quartz crystals with cloudy cores and clear rims. This quartz in SEM-CL has a feathery dark grey luminescence in the core of the crystal that radiates towards the rim; and from 1 to 3mm within the edge of the crystals have light and dark banded zones, each zone approximately 50 to 150µm in width.

Euhedral Q2 quartz crystals in SEM-CL imaging contained light and dark-grey zones. The light and dark grey zones appear to coincide with increasing and decreasing concentrations of Al and Li, the maximum concentration of both elements occurs in areas of light-grey to white SEM-CL zones (Appendix D). The maximum concentration of Al is 7488ppm and Li is 255ppm in this sample, while the dark-grey SEM-CL zones correspond with minimum Al and Li concentrations of less than 116 and 4ppm, respectively. Another LA-ICP-MS transect crossed similar light and dark-banded SEM-CL zones in quartz veins within the NICO drill-core. A laser ablation track passed through a feldspar mineral inclusion, which results in a spike in Rb (26ppm), Na (8531ppm) and K (3771ppm).

Some Q2 quartz veins contain hydrothermal sericite. Dating this sericite by Ar-Ar methods was considered, and samples were crushed and separated. However, x-ray diffraction on the separated samples showed that the samples contained sericite ± clinocllore ± quartz ± kaolinite and sanidine.

Late fractures are filled with chlorite and rutile laths. Calcite veining is also prevalent within the drill core. The calcite consists of 3 x 6mm euhedral grains, and vugs (less than 0.5cm in width) within the veins remain open. These veins are commonly mineralized with pyrite and chalcopyrite (Plate 3E). The calcite veins are the most mineralized vein set found on the property, and commonly contain chalcopyrite, bornite, cuprite, covellite, pyrite and hematite. The pyrite and chalcopyrite appear coeval but locally, in thin section, the chalcopyrite forms rims between 0.1 to 0.3mm thick on the pyrite grains. The drill core also intersected calcite veins that are less than 1cm in width and refractured previous quartz veins; as well, within the main mine adit a large calcite vein, 20cm thick, contained thick selvages of chalcopyrite and pyrite. Late calcite veins contain vuggy porosity, which is partially filled with pyrite enveloped by chalcopyrite, with small amounts of bismuthinite, bornite and hematite (Plate 3F).

Giant quartz vein zone located near the Sue-Dianne Deposit

The Sue-Dianne deposit is hosted in an alkali feldspar rhyolite; although it does not contain any indication of welding, it does contain a fine grained groundmass. The alkali feldspar rhyolite is made up of various abundances of quartz, K-feldspar, plagioclase and pyroxenes, and has been variably affected by alteration, resulting in variable abundances of muscovite, chlorite, hematite and clays. Hematite grains are disseminated throughout the host rock as 0.02 to 0.4mm anhedral grains.

The giant quartz vein zone at Sue-Dianne consists of two main types of quartz veins. The first, Q1, contains anhedral microcrystalline quartz (<0.05mm in length) that commonly has a sericite and chlorite selvage. The drill-core at Sue-Dianne contained many small (1 to 2mm width) quartz veins, but no sulfide mineralized quartz veins were observed.

This Q1 quartz is commonly cross cut by coarser grained (0.5 to 10cm thick) Q2 veins with euhedral medium grained clear quartz (0.25 to 1.5mm in width). These Q2 veins commonly consist of coxcomb or feathery quartz (Plate 4A/B). When analysed by SEM-CL, the feathery quartz gives a distinct speckled texture (Plate 4C). This texture is comprised of dark grey to black luminescing quartz with fine grained fragments of light grey luminescent quartz. These lighter anhedral spots are multiple shades of grey in SEM-CL, usually 10 to 150µm in diameter. Large subhedral crystals of feathery quartz contain many small fluid (<5µm) and feldspar (<50µm) inclusions. The laser ablation tracks through the feathery quartz show much higher concentrations of Al (maximum of 13 920ppm), K (5 527ppm), Fe (800ppm), Mn (maximum value of 207ppm, average of 50ppm), and Rb (50ppm) than that of the euhedral milky white quartz crystals. The feathery quartz with feldspar inclusions, on average, contained up to four times the trace element concentration of K, Mn, Rb, Al and Ca than the milky white euhedral quartz (Appendix D).

The Q2 veins, made up of euhedral quartz, consist of fluid inclusion rich and poor zones. With SEM-CL imaging the Q2 quartz contains light and dark-grey zones, the finest (~1µm thick) of these zones are located within the cores of the quartz crystals (Plate 4D). Light-grey SEM-CL zones correspond to an average high concentration of Al and Li, of 500ppm and 20ppm respectively, while dark-grey zones contain low concentrations of Al and Li, with less than 20ppm for Al and below detection limits (<4ppm) of Li, in some instances (Appendix D). The light and dark grey SEM-CL zones reflect an average variation of 100ppm and 20ppm for Al and Li, respectively.

Locally, the host rock is brecciated into subangular 0.5 to 1.0cm clasts within these Q2 veins. In polarized transmitted light, undulatory fan-like extinction is common within the quartz veins. Textures such as plumose extinction at grain boundaries as well as ghost textures were observed in two vein samples.

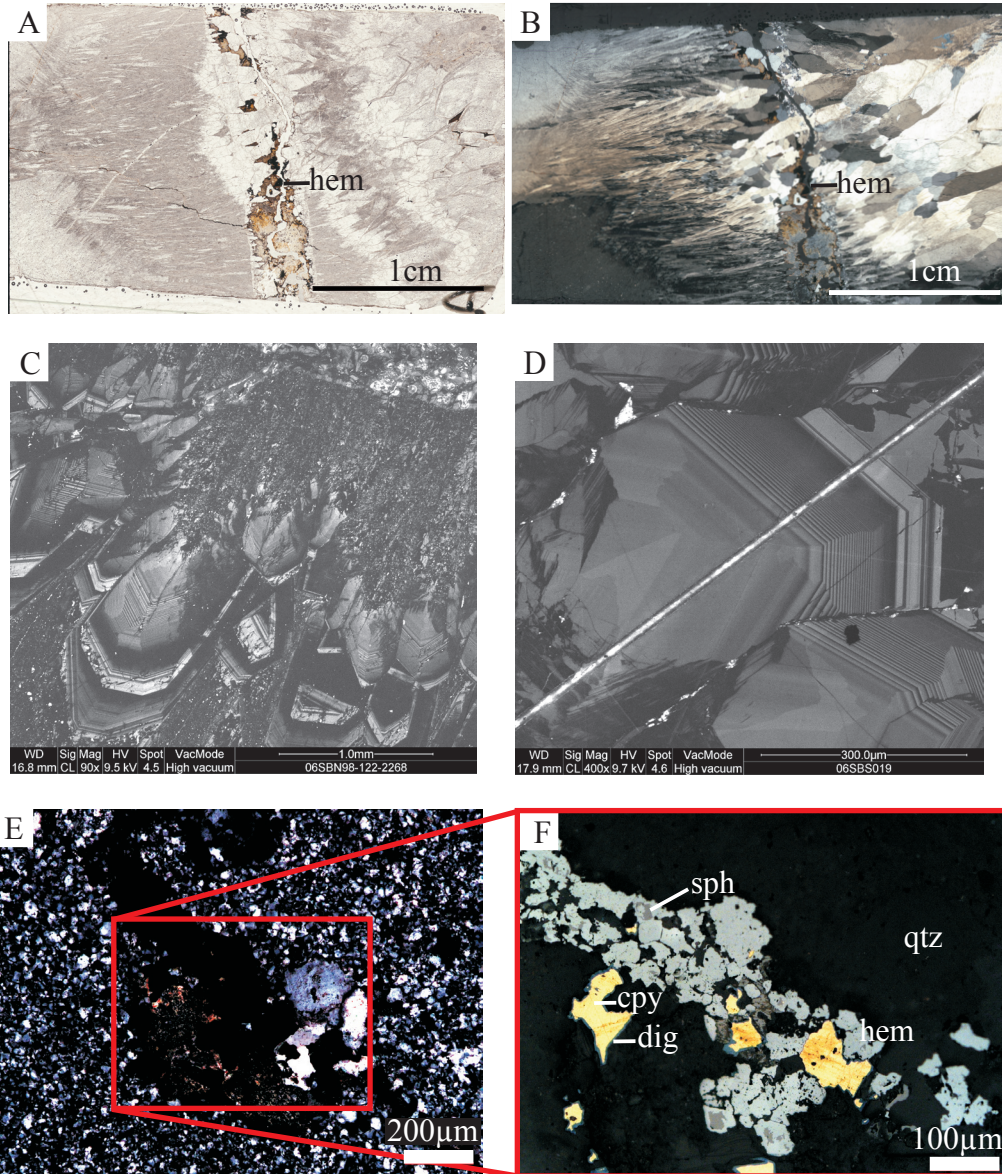


Plate 4. A) Sue-Dianne Q3 quartz veinlet with hematite cross-cuts the Q2 feathery (left) and comb (right) quartz vein in plane transmitted light. B) Same image as A in cross-polarized transmitted light. C) SEM-CL photo of Sue-Dianne Q2 vein of feathery (speckled) and comb (euhehedral zoned) quartz. D) SEM-CL photo of Sue-Dianne Q2 euhehedral finely-zoned quartz crystal. E) Sue-Dianne Q3 mosaic quartz vein with iron-oxides and copper-iron sulphides in cross-polarized transmitted light. F) Zoomed view of E, shows chalcopyrite rimmed by digenite and sphalerite surrounded by hematite in plane reflected light. Hem = hematite, cpy = chalcopyrite, dig = digenite, sph = sphalerite, qtz = quartz.

Late-stage, Q3 veins, cross cut all previous generations and commonly contain sparse amounts of hematite, copper sulfides and minor sphalerite. Subhedral grains of chalcopyrite, 0.1 to 0.2mm in diameter, are locally surrounded by a 50µm thick rim of digenite (Plate 4E/F). Coeval grains of magnetite (0.5mm in width) with hematite alteration rims are also observed. Hematite grains range from 0.1 to 1.0mm in diameter in mineralized fractures.

Northern Sloan Extension

The light pink host rocks consist of an altered monzogranite, which consists of quartz (55%), plagioclase (10%), K-feldspar (10%), sericite (20%), chlorite (5%). The phenocrysts in the granite are composed of quartz and iron oxides, pyrite, and rarely, chalcopyrite grains make up the remainder. The pyrite and chalcopyrite crystals are very small, less than 0.05mm in width, and disseminated throughout the host rock.

Similarly to the Sloan vein, the Northern Sloan Extension giant quartz vein zone is under exploration to determine if the vein zone is mineralized to appreciable economic quantities. The giant vein zone consists of similar quartz veins found in other vein zones near base-metal mineralization. The quartz veins commonly have irregular contacts with the host rock. Thin Q1 veinlets, 0.5 to 3mm thick, of anhedral quartz crystals are found at the host-rock vein zone contact. These veins split repeatedly forming a stockwork. The individual quartz crystals are 0.2 x 0.5mm. Minor pyrite mineralization is noted within these veins. This pyrite is rimmed by supergene hematite; this secondary hematite is found along microfractures that cross these thin veinlets.

Milky white, Q2, euhedral quartz veins contain bladed or growth zoned crystals (2.5 x 7mm). Other quartz crystals in these veins are more moderate in size, around 0.5mm. These veins mainly consist of coxcomb quartz but also form a cockade texture on brecciated host rock clasts. These veins can exhibit plumose extinction as well as ghost textures in polarized transmitted light (Plate 5A/B). Other similar veins contain yellow quartz, which contain clays (kaolinite and illite).

Late Q3 quartz veins cross cut the milky white veins in 0.5 to 1mm thick fractures. Q3 quartz is generally finer grained (less than 0.2mm) and subhedral. In polarized transmitted light, these veins remain optically continuous with the milky white quartz veins and contain a small amount of hematite and sericite. A texture visible only during SEM-CL analysis consists of light and dark grey zones that do not parallel the euhedral shape of individual quartz crystals (Plate 5C).

Q3 veins also contain 0.1 x 0.1mm grains of bornite, chalcopyrite, pyrite and hematite. Sulfide mineralization is found proximal to brecciated clasts of host rock; these rafts are usually a few centimetres in width. Late fractures, only 0.01mm wide, are commonly filled with microcrystalline anhedral quartz and hypogene chalcopyrite. Hypogene mineralization consists of chalcopyrite, pyrite and hematite within fractures. Mineralization can make up 3 to 7% of the sample, and chalcopyrite is the most common ore mineral.

In a small number of cases chalcopyrite is replaced by supergene covellite and 0.2mm wide layer of chalcocite (Plate 5D). Supergene hematite is found along fractures, rimming chalcocite grains, and cross cutting other fractures. At the surface the mineralization has been oxidized to malachite. In SEM-CL, late fractures are filled with bright white luminescing hematite. Some vugs, up to 3mm in width, are partially to completely filled with hematite.

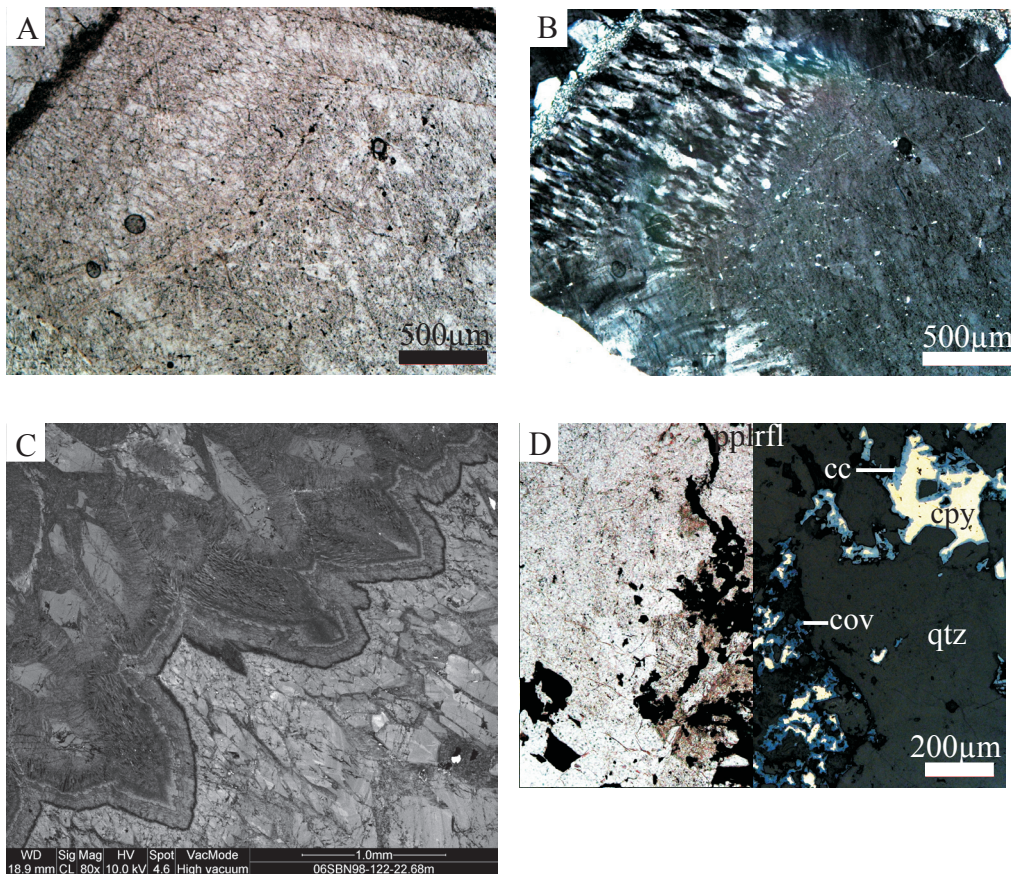


Plate 5. A) Northern Sloan Extension Q2 vein contains euhedral quartz crystals in plane transmitted light. B) Same as A, euhedral quartz crystals exhibit plumose extinction in cross-polarized transmitted light. C) Northern Sloan Extension Q2 vein, the light and dark banded zones reflect repeated quartz crystal overgrowths. D) Northern Sloan Extension Q3 quartz vein mineralized with chalcopyrite, covellite and chalcocite along a late fracture. Cpy = chalcopyrite, cov = covellite, cc = chalcocite, qtz = quartz. Ppl = plane polarized light; rfl = plane reflected light.

3.1.2 Uranium Associated Giant Quartz Vein Zones

Beaverlodge Lake

The giant quartz vein zone at Beaverlodge Lake cross cuts an altered porphyry rock. The porphyry contains 0.5 to 1.0mm phenocrysts of quartz and potassium feldspar with mottled hornblende and minor chlorite and hematite. This porphyry contains pitchblende, up to 2% in one sample. Uranium minerals are commonly located near zircons or along small fractures, and these grains were qualitatively mapped which revealed small amounts of selenium, titanium, and bismuth (Plate 6A/B). Other Beaverlodge Lake samples contain uranium minerals with equal proportions of uranium, titanium and silica, and inclusions of bismuth-selenides. The quartzite, that hosts the giant vein zone, is made up of uniform rounded quartz grains (0.2 to 0.3mm) with trace amounts of sericite.

The giant quartz vein zone at Beaverlodge Lake consists of a small number of cloudy, Q1 quartz and numerous milky white Q2 veins. The Q1 quartz has a feathery texture. In SEM-CL, this feathery-texture results in light and dark irregular lath-shapes; the matrix of the feathery quartz is dark grey to black in colour, the irregular lath-shapes, 10 to 50µm in diameter, are a variety of dark to light grey colours. This feathery quartz contained many small (<20µm) mineral and fluid inclusions, resulting in sharp spikes in concentration of Li (958ppm), Al (77 631ppm), Na (15 698ppm), K (4 917ppm) and Rb (6ppm).

The giant quartz vein consists of milky white Q2 veins, made up of subhedral to euhedral bladed quartz grains, between 0.1 to 1.5mm; veins are usually 5mm to a few centimetres thick (Plate 7A/B). Q2 veins consist of coxcomb or bladed quartz textures, the crystals, on average, are larger than 0.5cm and exhibit fan-like extinction. At Beaverlodge Lake the growth zoned crystals contain a highly regular zoned pattern. The growth zones in transmitted light microscopy are defined by fluid inclusion rich and poor zones, but under SEM-CL, many more zones are visible and they mirror the shape of the quartz crystals (Plate 7C). On average, each SEM-CL zone is a maximum of 0.75mm and minimum of 10µm in width. Euhedral growth zoned quartz crystals contain a variety of grey shades in SEM-CL that are a direct result of the abundance of Al, Li and, to a small degree, Ge within the quartz (Appendix D). Although Ge in some samples appears to reflect the increases and decreases that Li and Al, the maximum concentration for Ge in the sample is 15ppm. This milky white euhedral quartz resulted in low amounts of trace elements, but did contain an average of 2000ppm Ca, 300ppm Na, 175ppm K, 450ppm Al, and 15ppm Li.

Pyrite can be found as 0.1mm small anhedral crystals within the Q2 veins. Electron microprobe analysis shows zircon grains, usually 0.1mm in diameter, entrained in the Q2 veins are well-rounded and zoned. Chlorite contains small (less than 100µm in diameter) bismuth-tellurides, as well as, monazite and rutile grains. Small vugs, less than 10µm in diameter, are filled with native Pb.

The youngest veins, Q3, at Beaverlodge Lake are infilled with clear microcrystalline quartz and commonly parallel and refracture earlier milky white quartz veins. These thin veinlets, only 0.1 to 0.2mm wide, cross cut all the other veining and are filled with hematite, chlorite and locally muscovite.

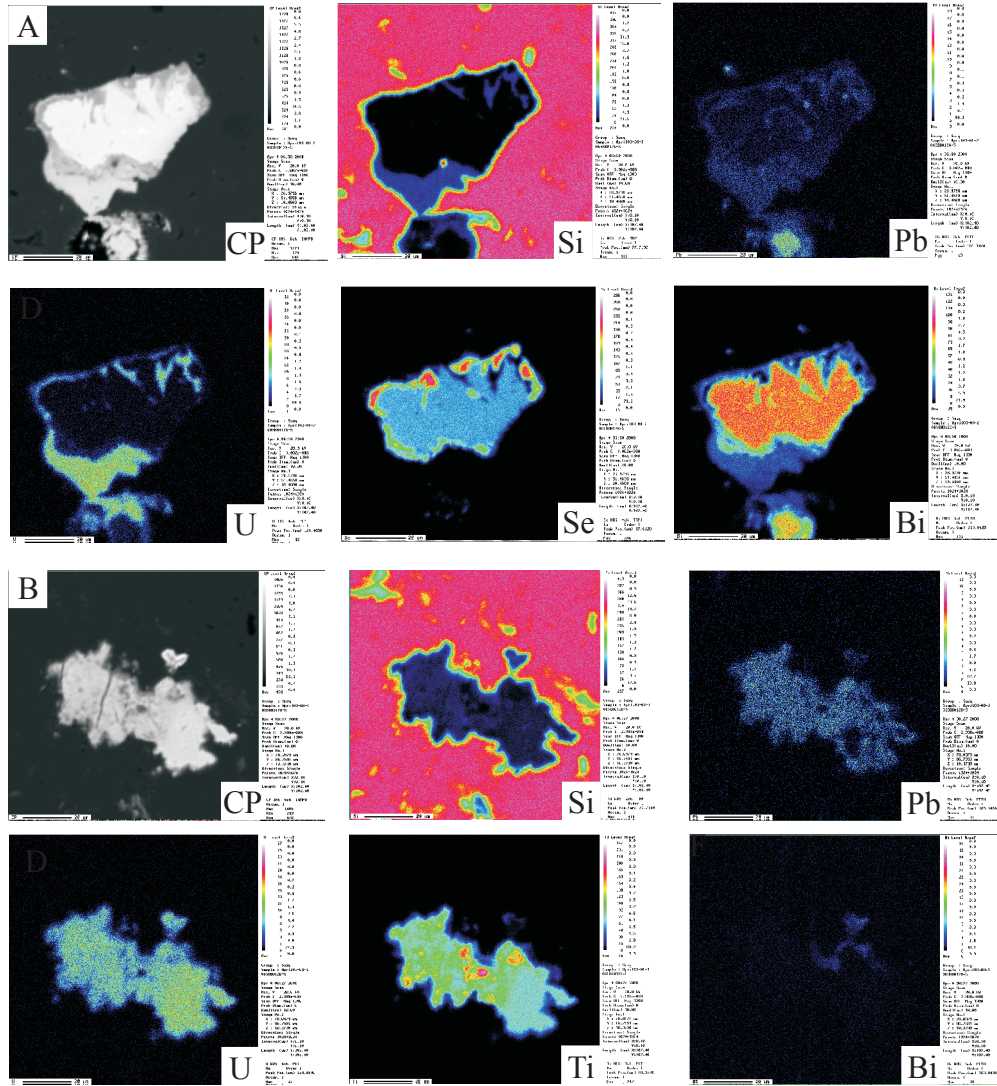


Plate 6. A) Electron microprobe analyses (EMPA) of an anhedronal grain of bismuth-selenide with micrometer pitchblende and lead overgrowths within a Beaverlodge Lake Q2 vein sample. The scale bar is 20 μ m. B) EMPA image of a small grain of rutile which contains high uranium and lead and minor bismuth concentrations, within a similar Beaverlodge Lake sample. The scale bar is 20 μ m. The specific element mapped is displayed in the lower-right corner. CP = composite image, Si = silica, Pb = lead, U = uranium, Se = selenium, Bi = bismuth, Ti = titanium.

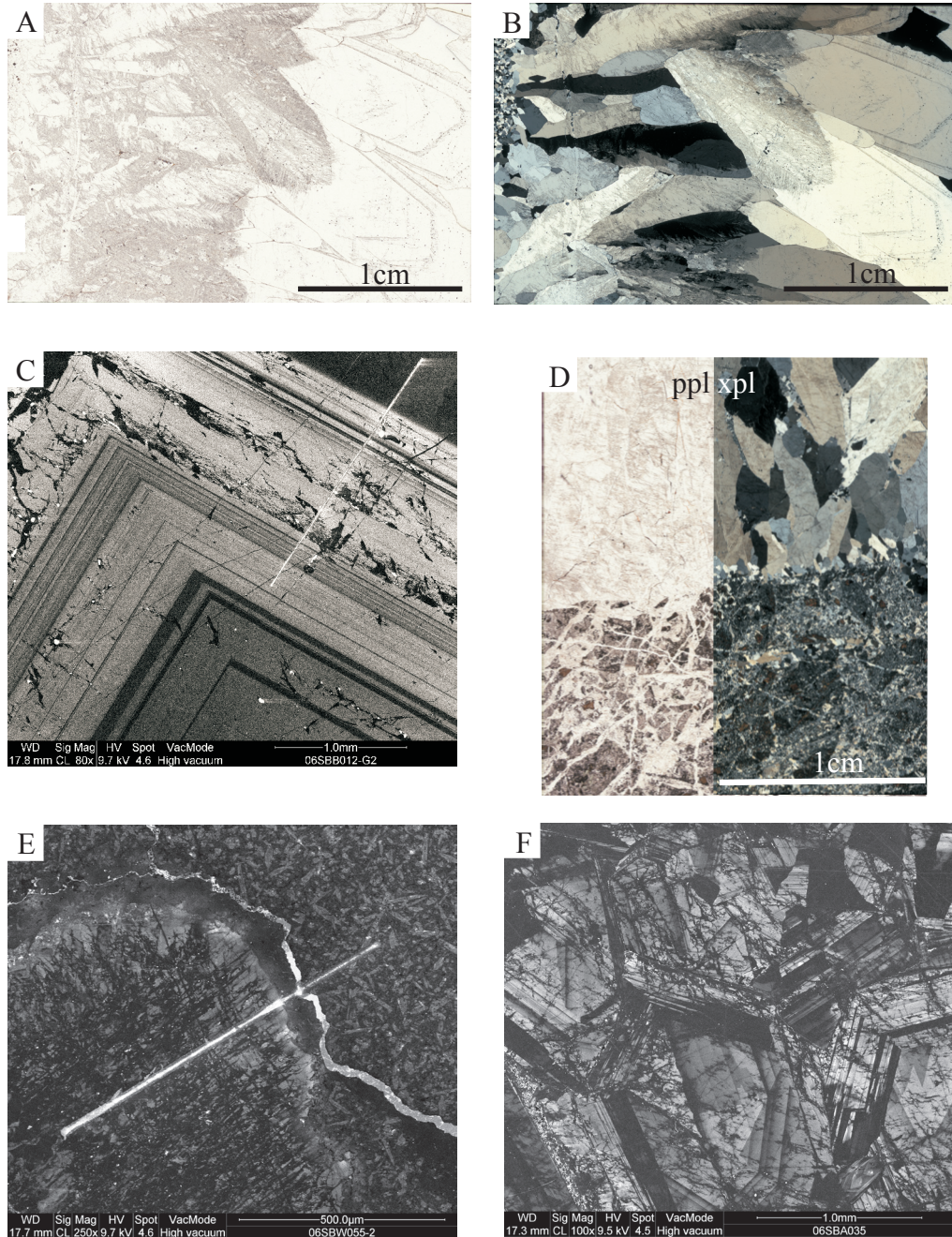


Plate 7. A) Beaverlodge Lake Q2 quartz vein of feathery and euhedral comb quartz in plane transmitted light. B) Same as A, in cross-polarized transmitted light. C) SEM-CL image of a Beaverlodge Lake Q2 vein showing light and dark zones. White laser ablation track in upper-right corner. D) Fab Lake Q1 stockwork vein, lower half of image, crosscut by Q2 vein of euhedral quartz. E) SEM-CL image of a Wopmay Q2 quartz vein with network-like luminescence. White laser ablation track cuts through a Q2 quartz vein (left), a hematite veinlet and altered feldspars of granitic hostrock (right). F) SEM-CL image of “Arm” Lake Q2 quartz vein showing network-like or cross-hatched texture of dark luminescing quartz overprinting light and dark grey zones of euhedral quartz.

Fab Lake

The earliest Q1 quartz vein development is made up of multi-directional stockwork veining (Plate 7D). This phase of quartz is cloudy, microcrystalline (less than 0.05mm) with subhedral to anhedral crystals, although larger grains (up to 1 x 4mm) make up approximately 5% of these veins. Minor amounts of sericite are coeval with this phase of veining but no sulfide mineralization is apparent. Rarely, late fractures can be seen within the larger quartz grains; however, the quartz in these fractures has grown in optical continuity with the quartz crystals they cut.

The Q2 veins at Fab consist of euhedral quartz of an average crystal length to width ratio of 1:4, with an average size of 0.5 x 2mm, with a few larger grains at 1 x 4mm (Plate 7D). Late Q3 fractures are common and are filled with fine grained anhedral quartz. Where these veins are in contact with the host rock, the contact can be lined with hematite; some vugs also locally contain hematite.

The host rock the giant quartz vein zone cross cuts is a dacite, and is comprised of plagioclase (40%), quartz (35%), K-feldspar (10%), hornblende (<15%), and chlorite and sericite alteration with a minor amount of hematite and pyrite. Locally, welding of the grains was observed and suggests that this unit is extrusive in origin. Phenocrysts of quartz and feldspar are on average 0.5 to 0.6mm in length, within a fine grained groundmass of chlorite, sericite, and feldspar. Hydrothermal alteration of this host rock has resulted in the replacement of the plagioclase phenocrysts, by muscovite and sericite, and proximal to the giant vein zone the dacite is heavily epidotized.

Northern Wopmay Fault

The giant quartz vein zone at the Northern Wopmay fault is made up of Q1 and Q2 veins over a small area between two host rock types. Q1 veins at this location are made of cloudy and bladed feathery quartz and are generally fine grained (up to 0.5 x 1mm). Bladed fan-like quartz had a bright white luminescence in SEM-CL and contains much higher Al and Li than the other light and dark-grey SEM-CL zoned quartz from the Wopmay fault. The maximum value for Al is 20 982ppm and Li is 325ppm. This quartz contained peaks in concentration of Rb, Y and La together with K. This area contained the highest concentration of Y and La, averaging 10ppm for each element.

Later Q2 veins are coarser grained (1 x 2mm or larger) and the quartz is milky white to clear in colour. Some coarse grained euhedral Q2 veins have brecciated Q1 veins. The Q1 breccia fragments luminesce with fine zoned light and dark grey zones, while the younger quartz vein consists of homogenous light grey luminescent quartz in SEM-CL. Euhedral quartz crystals from Q2 veins contain light and dark grey zones in SEM-CL, have low concentrations of La, Y, Ge, Co, Ti, Fe, Be and P. Bright luminescent zones have an increased concentration of Al, up to 6 258ppm, and Li, up to 86ppm. Q2 subhedral coarse grained quartz crystals contain dark-grey to black luminescence in SEM-CL images. These quartz crystals have very few inclusions within them. Dark grey zones have concentrations as low as 51ppm for Al and below detection limits

(<5ppm) for Li (Appendix D). On average, most trace element concentrations are very low for this type of non-luminescing quartz.

Some Q2 veins have the appearance of a network of overlapping laths of dark-grey quartz in SEM-CL, similar to the networks visible within samples from “Arm” Lake (Plate 7E). This black cross-hatched network is multidirectional; however, it is concentrated in the core of the quartz crystals and radiates to the rim, and it does not appear to be associated with fluid inclusion abundance or fractures within the quartz. These veins were analysed for trace elements, and resulted in variation in K, Na, Al, Li, Rb, Ti and Mn, but these elements do not vary in unison with the network texture. At this time, there is no clear trace element association with this black cross-hatched network SEM-CL texture. Plumose extinction is visible in this type of quartz in cross polarized transmitted light.

Late Q3 veins are space filling and can contain large (2 to 4cm) vugs. Some veins exhibit colloform banding. The quartz crystals of these veins are euhedral and commonly have a 2:1 length to width ratio, with grains that are 2 x 4mm.

The Northern Wopmay fault zone consists of two host rocks, the first, a foliated mylonitic granodiorite, and the second, a fine grained metasediment. The granodiorite comprises quartz (45%), plagioclase (20%), K-feldspar (10%) and amphibole/chlorite (25%). The quartz and feldspar grains are elongated into a 4:1 length to width ratio; the quartz crystals are either 0.1mm anhedral with an interlocking mosaic “jigsaw” texture (Dong et al. 1995) or large subhedral crystals that are 1.5 x 4mm. Chlorite and white mica abundances are variable and make up 25% of the mylonite. The greywacke is extremely fine grained; the fresh rock is dark green in colour and consists of hornblende, quartz and hematite. In SEM-CL analysis, K-feldspar and plagioclase, from brecciated host rock, results in dark and light grey laths that are 0.1mm in width and 0.3 to 0.5mm in length.

3.1.3 Giant Quartz Vein Zones Isolated from Mineralization

“Arm” Lake

The quartz veins at “Arm” Lake are milky white with a large grain size, making them most similar to Q2 veins of other vein zones. Many Q2 vein quartz crystals are 0.75 x 0.75mm and some can be up to 2cm in length. The crystals are subhedral to euhedral and most veins are monomineralic. In SEM-CL, this euhedral quartz contained numerous light and dark colour banded zones, up to 0.25mm in width. Other Q2 vein quartz crystals contain a dark grey to black cross-hatched network that cross cuts the light and dark grey zones in SEM-CL. This cross-hatched network has no preferred orientation, and appears to radiate from fractures within the quartz (Plate 7F).

Late Q3 veins filled with fine grained (0.1 to 0.5mm) anhedral quartz cut these milky white veins. In SEM-CL, late quartz veins have a dark-grey luminescence and are not zoned; locally some small bright grains are visible at the vein and host rock contact; these are likely hematite. All quartz generations cross

cut by late fractures (100µm thick) filled with hematite, which shows up in SEM-CL as bright continuous veinlets.

The host rock at “Arm” Lake is dominated by 45% plagioclase (average grain size is 1 x 2mm) and 10% K-feldspar (1 x 2mm) and 25% quartz (0.5 x 1mm), with the remainder made up of hornblende (1 x 2mm), hematite and chlorite (approximately 1% of the rock), pyrite (associated with hematite) and zircon. The felsic grains are subhedral to euhedral, while the softer mafic minerals are anhedral. Sericitic alteration of the host rock results in small sericite inclusions within large plagioclase grains.

Hardisty Lake

The oldest generation of veining, Q1, at Hardisty Lake consists of cloudy microcrystalline (0.02 to 0.1mm diameter) quartz crystals. Minor amounts of sericite infill space between quartz crystals. En echelon microfractures, each a few millimetres to centimetres long, cross cut the stockworks but do not offset them.

Milky white, Q2, veins contain 3.5 to 5mm blocky subhedral quartz crystals, with an average size of 1 to 2mm. These veins sometimes contain vugs within the veins, which are 0.3 to 1.0mm in length. Most vugs contain a minor amount of hematite and specularite coating prismatic quartz.

Late fractures, 0.1 to 0.2mm wide, cross cut all vein types and host rock. Generally, these fractures are filled with quartz, forming Q3 veinlets, or hematite.

The monzogranite host rock at this location consists of K-feldspar (35%), plagioclase (30%), quartz (25%) and hornblende (10%). Small grains of hematite are disseminated throughout the monzogranite, and hematite is concentrated near subhedral hornblende grains.

Margaret Lake

Q1 veins consist of fine grained (0.2mm) interlocking quartz crystals. Near the core of euhedral Q2 veins the quartz crystals are 0.5 to 3mm in diameter and within the centre of the vein can be up to 6 x 8mm. These Q2 vein quartz crystals are euhedral and prismatic and can be found lining vugs.

Both generations of veining are cross cut by Q3, microcrystalline quartz in veinlets, which are less than 0.2mm in diameter. These veinlets commonly offset other veins. Under cross polarized transmitted light the late stage veinlets are optically continuous with previous vein sets.

Most of the granite to monzogranite host rock is made up of subhedral plagioclase and quartz (0.05 to 0.1mm in length) phenocrysts in a matrix of anhedral fine-grained chlorite and sericite that occur in patches (less than 1 x 1mm) between the plagioclase and quartz crystals.

3.2 Fluid Inclusions from Giant Quartz Vein Zones

Microthermometry is a non-destructive analytical technique for fluid inclusion analysis to provide the temperature and chemistry of the original fluids that formed the veins (e.g. Roedder 1984 and references therein). The giant quartz vein zones examined contain one to three types of fluid inclusions defined at room temperature; Type I, II and III. These types of fluid inclusions are described here, and these descriptions apply to fluid inclusions found within the veins from all the giant quartz vein zones studied.

Type I fluid inclusions contain two phases, with an aqueous liquid and vapour bubble and usually contain a degree of fill, which is defined as a ratio of liquid to vapour within the fluid inclusion, of 0.9. On average, they are 2 to 8 μm in width, and generally less than 10 μm in length (Plate 8A). Many Type I inclusions have a negative-crystal shape, although some are subrounded or oblong in shape. These inclusions are commonly found in growth zones of euhedral quartz crystals and within subhedral cloudy quartz. Pseudo-secondary trails of these inclusions occur along arrays that run from the crystal edge towards the core. Locally, small (<5 μm) Type I fluid inclusions form densely clustered arrays.

Type II fluid inclusions contain three phases; an aqueous liquid, vapour phase and a daughter mineral (Plate 8B). This daughter phase is commonly <1 μm in diameter, or slightly smaller than the vapour phase, and appears euhedral and cubic in shape, and is commonly attached to the wall of the fluid inclusion. This phase is interpreted to be halite, based on its cubic form and heating characteristics (see below). These fluid inclusions are 8 to 20 μm in diameter and subhedral in shape. This is the rarest type of primary fluid inclusion and is not present in most giant quartz veins.

Other fluid inclusion types commonly found in the quartz veins include monophasic liquid inclusions (Type III), and Type I pseudo-secondary inclusions, which are found along trails. Monophasic fluid inclusions are commonly trapped along secondary trails. These trails are generally 0.5 to 2mm in length, and the fluid inclusions are usually less than 3 μm in size and oblong in shape or pinched at one end. Some primary inclusions are necked such as an anhedral inclusion with two to three monophasic inclusions making a 'tail'.

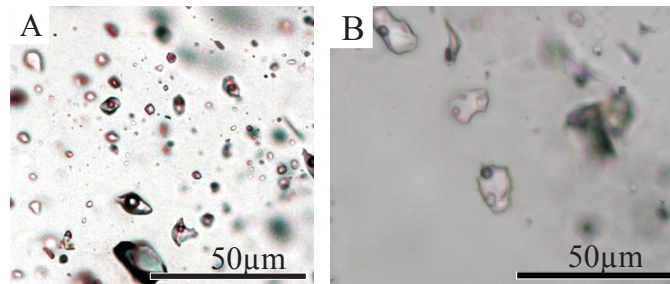


Plate 8. A) Type I fluid inclusions. The liquid-vapour inclusions have a small vapour bubble and degree of fill of 0.8 or more. B) Type II fluid inclusions. These inclusions consist of a liquid and vapour phase and a halite cube.

Microthermometry was carried out on two and three phase fluid inclusions from each vein zone studied. Analysis of each fluid inclusion was complicated by the presence of multiple generations of inclusions (primary and secondary) within the quartz veins. Petrography of fluid inclusions within quartz veins were used to group specific fluid inclusion assemblages to solve the complexity of multiple fluid inclusion generations. Eutectic temperatures recorded from fluid inclusions are generally $-21.2 \pm 0.5^{\circ}\text{C}$, corresponding to the $\text{H}_2\text{O}-\text{NaCl}$ system (Brown 1985).

Results are reported from all giant vein zones with respect to the first order standard deviation, and are tabulated in Table 1, located at the end of this section. The results of the microthermometry study are graphically displayed defined by quartz vein type (Q1, Q2, Q3) and individual fluid inclusions are displayed, fluid inclusion assemblages are reflected by different symbols. Individual fluid inclusion assemblage results are located in Appendix E.

3.2.1 Giant Quartz Vein Zones Located near Base-Metal Mineralization

Giant Quartz Vein Zone located near the NICO Deposit

The Q1 veins of the giant quartz vein zone near NICO are made up of bladed quartz grains which contain many monophasic fluid inclusions. This paragenetic phase rarely contained Type I inclusions, but most were too small ($<2\mu\text{m}$) to use for microthermometry. Although most veins have no evidence of recrystallization, as discussed by Sander and Black (1988), some quartz crystals contained plumose extinction, ghost-textures, or extinction that did not match quartz crystal shape. Areas where quartz has plumose extinction under cross polarized transmitted light, or quartz crystals in which the core and rim would go into extinction at different times were avoided for microthermometry, as this may indicate recrystallized quartz (e.g. Plate 5A-C; Sander and Black 1988).

A growth zoned Q2 vein from the NICO giant quartz vein zone was cut perpendicular to the c-axis of the dominant quartz crystals. Each euhedral quartz crystal contains a fluid inclusion-rich zone that is 50 to $250\mu\text{m}$ thick that consists

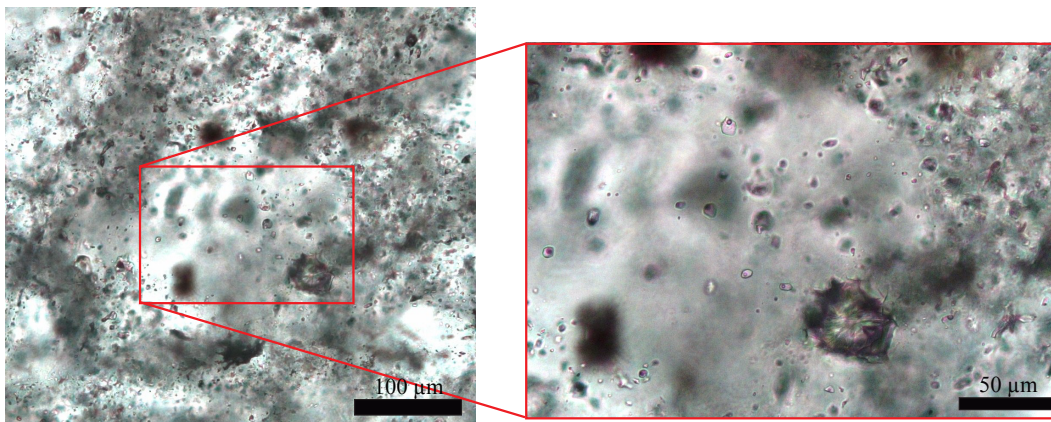


Plate 9. NICO giant quartz vein sample of a fluid inclusion poor core and fluid inclusion rich rim quartz crystal in plane polarized transmitted light. Inset image (in red) displays the Type I fluid inclusions used for microthermometry.

of Type I fluid inclusions (Plate 9). Most of the fluid inclusions are concentrated in the rims of the quartz crystal, although fluid inclusions are also located within the crystal core (Plate 9). Q2 quartz contains Type I fluid inclusions with an average salinity of 20.6 ± 2.1 wt. % NaCl eq. (n = 31) Q2 quartz fluid inclusions contain a Th range from 110° to 183°C , with an average of $135 \pm 18^\circ\text{C}$ (n = 31; Fig. 12).

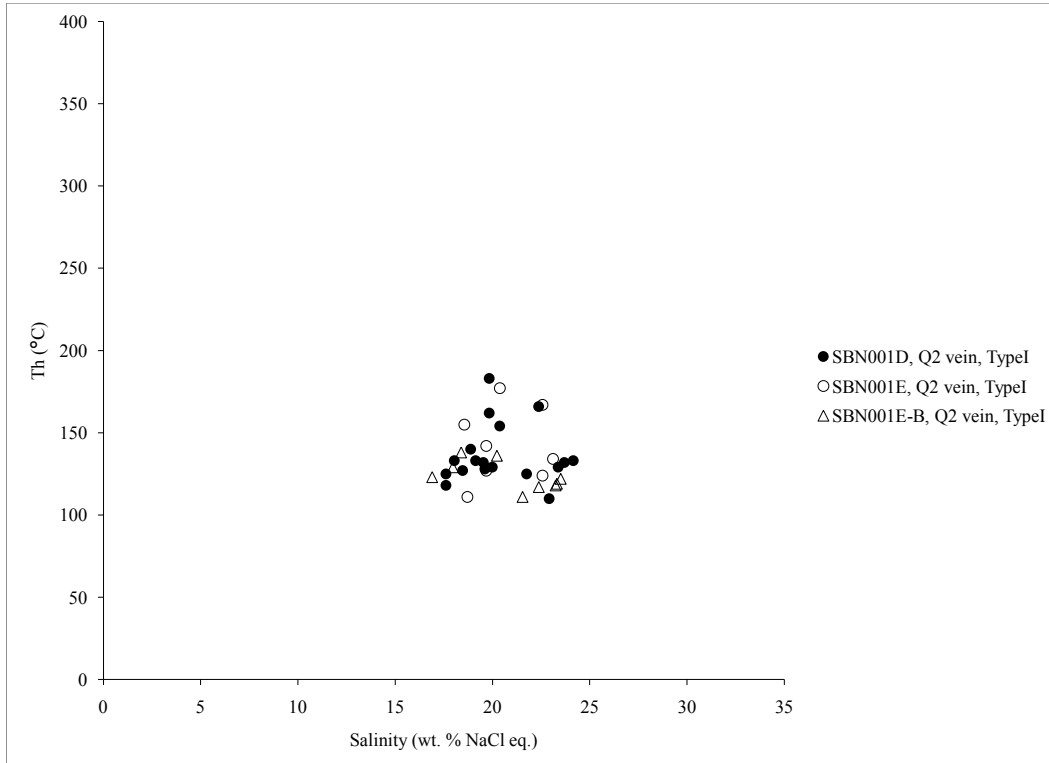


Figure 12. Temperature of homogenization versus salinity from primary fluid inclusions from Q2 quartz from the NICO giant vein zone. Each data point represents a single fluid inclusion analysed, each symbol represents a specific fluid inclusion assemblage.

Giant Quartz Vein Zone intersected by NICO Drill-Core

The drill-core from NICO intersected a section of the giant quartz vein zone, and contains abundant Type I inclusions. These fluid inclusions are generally $5\mu\text{m}$ in diameter and are concentrated within growth zones in bladed quartz crystals. Fluids from NICO drill-core Q2 veins are similar in salinity to the NICO giant quartz vein zones, with an average salinity of 18.9 ± 2.4 wt. % NaCl eq. (n = 11). Fluid inclusion homogenization temperatures range from 107° to 168°C , with an average of $144 \pm 22^\circ\text{C}$ (n = 11), which is very similar to the veins sampled at surface (Fig. 13).

The vein samples from the drill-core commonly contain late fractures filled with calcite; these late calcite veins are coeval with bornite, chalcopyrite and pyrite. Fluid inclusion microthermometry was not done on the fluid inclusions from the calcite veins, since most inclusions were less than $2\mu\text{m}$ in diameter.

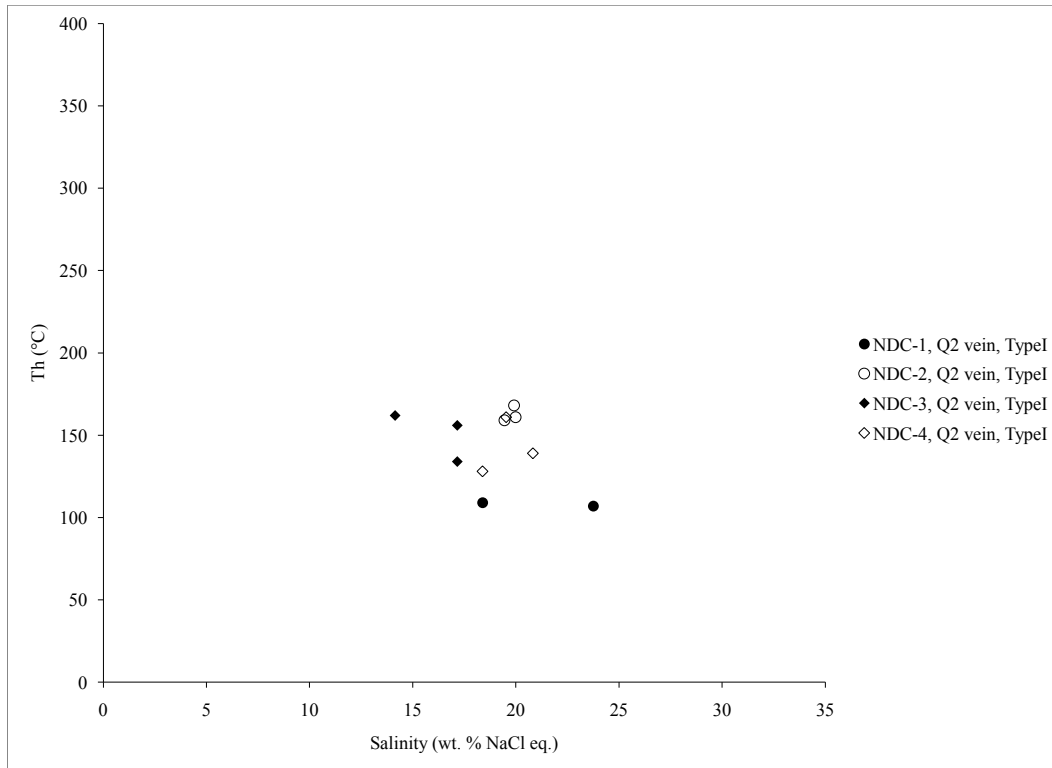


Figure 13. Temperature of homogenization versus salinity from primary fluid inclusions from Q2 quartz from the NICO drill-core (NDC) which has intersected the giant quartz vein zone. Each data point represents a single fluid inclusion analysed, each symbol represents a specific fluid inclusion assemblage.

Giant Quartz Vein Zone located near the Sue-Dianne Deposit

The oldest veins within Sue-Dianne are comprised of feathery, cloudy, quartz crystals. Fluid inclusions suitable for microthermometric analyses were rare; however, a small number of primary Type I inclusions, 8 to 10 μ m in diameter, were analysed. Inclusions within the feathery cloudy Q1 veins contain hundreds of very small (<2 μ m) inclusions and were very hard to measure; therefore the inclusion-poor cores of the feathery crystals were the main target for microthermometry (Plate 10). The Q1 feathery veins at Sue-Dianne have an average fluid inclusion salinity of 18.2 ± 4.9 wt. % NaCl eq. (n = 12) and temperature of homogenization of $180 \pm 25^\circ\text{C}$ (n = 12; Fig. 14). The calculated salinities of fluid inclusions in veins from the giant quartz vein located near Sue-Dianne are similar to those from the giant quartz vein zone near NICO (Table 1).

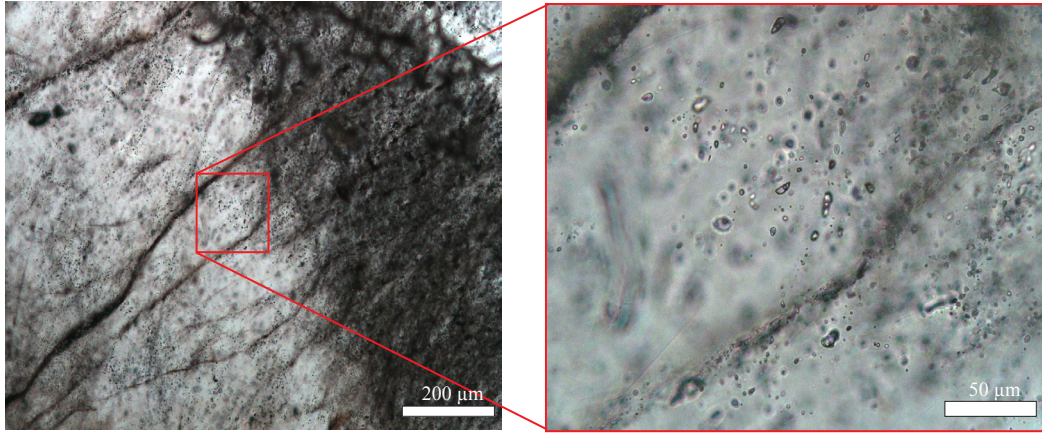


Plate 10. Sue-Dianne sample of a feathery quartz crystal in plane polarized transmitted light. Inset image (in red) displays the Type I fluid inclusions used for microthermometry.

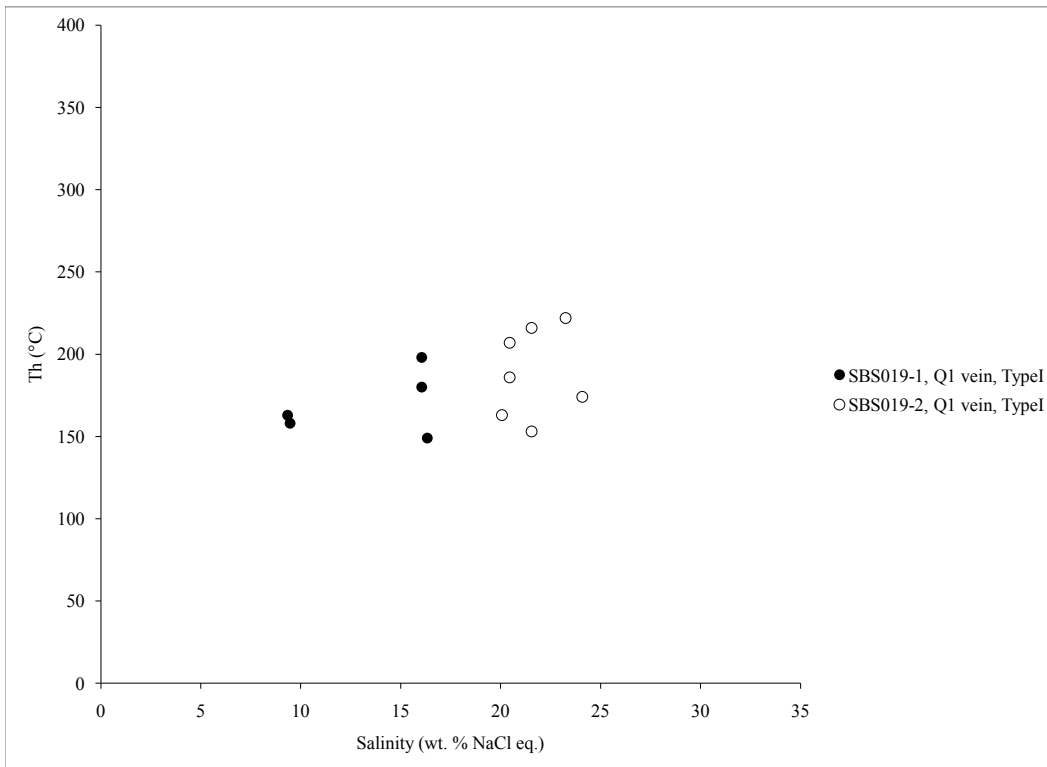


Figure 14. Temperature of homogenization versus salinity from primary Type I fluid inclusions from Q1 quartz veins from the Sue-Dianne giant vein zone. Each data point represents a single fluid inclusion analysed, each symbol represents a specific fluid inclusion assemblage.

The Q2 veins commonly contain growth-zones, defined by fluid inclusion-rich and poor zones. Generally, each zone is between 50 to 300 μ m thick. Most of these zones contain Type I inclusions, with an average diameter of 8 μ m, although they range from 2 to 10 μ m. These inclusions are subangular and oblong or round, although some inclusions have negative-crystal shapes. The Q2 veins have primary fluid inclusions with a range of variable salinities and temperatures.

Some Q2 veins have fluid inclusions with a low salinity of 1.4 ± 1.3 wt. % NaCl eq. ($n = 5$) and a Th from 250° to 318°C ($n = 5$; Fig. 15). However, most Q2 veins have fluid inclusions with an average salinity of 19.4 ± 4.0 wt. % NaCl eq. ($n = 32$) and an average Th of $172 \pm 26^\circ\text{C}$ ($n = 32$; Fig. 16 and 17).

Heating of Type II inclusions resulted in the dissolution of the halite-cube followed by, generally within 20°C , homogenization of the vapour bubble. Type II fluid inclusions from Q2 quartz have an average salinity of 29.8 ± 1.5 wt. % NaCl eq. ($n = 8$) and average Th of $178 \pm 28^\circ\text{C}$ ($n = 8$; Fig. 16 and 17). The Sue-Dianne Q2 veins range in fluid inclusion salinity and Th.

The Q3 veins contain a small amount of chalcopyrite and hematite. These mineralized veins are filled with colourless quartz with Type I inclusions. The late-stage veins contain primary Type I inclusions that have a high salinity. Type I fluid inclusions from mineralized Q3 veins had an average salinity of 22.3 ± 3.2 wt. % NaCl eq. ($n = 11$) and the highest average Th, of $293 \pm 50^\circ\text{C}$ ($n = 11$), from all fluid inclusions associated quartz vein zones proximal to base-metal mineralization (Fig. 18).

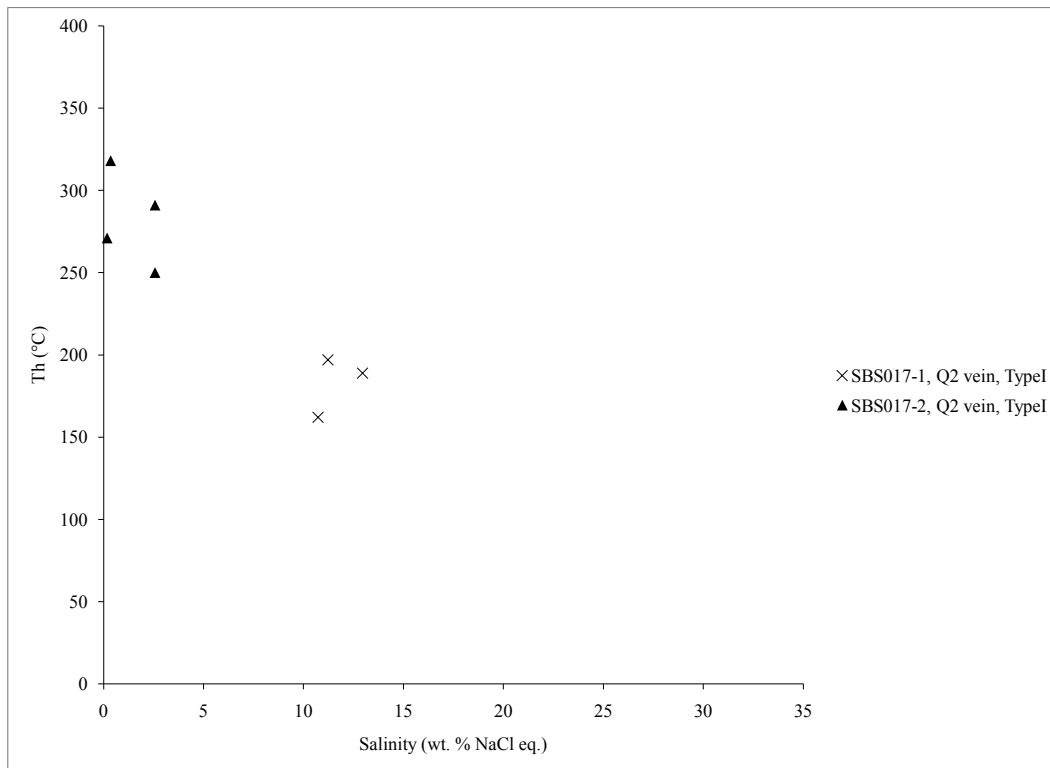


Figure 15. Temperature of homogenization versus salinity from primary Type I fluid inclusions from Q2 quartz veins from the Sue-Dianne giant vein zone sample 06SBS017. Each data point represents a single fluid inclusion analysed, each symbol represents a specific fluid inclusion assemblage.

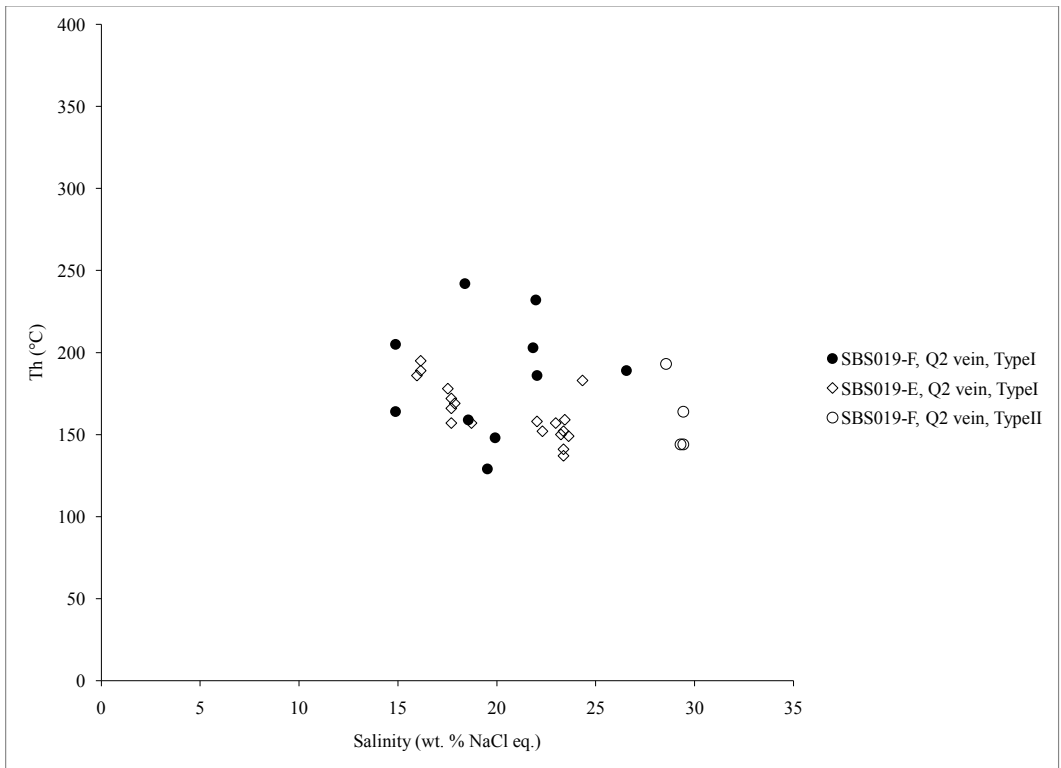


Figure 16. Temperature of homogenization versus salinity from primary Type I and Type II fluid inclusions from Q2 quartz from the Sue-Dianne giant vein zone sample 06SBS019. Each data point represents a single fluid inclusion analysed, each symbol represents a specific fluid inclusion assemblage.

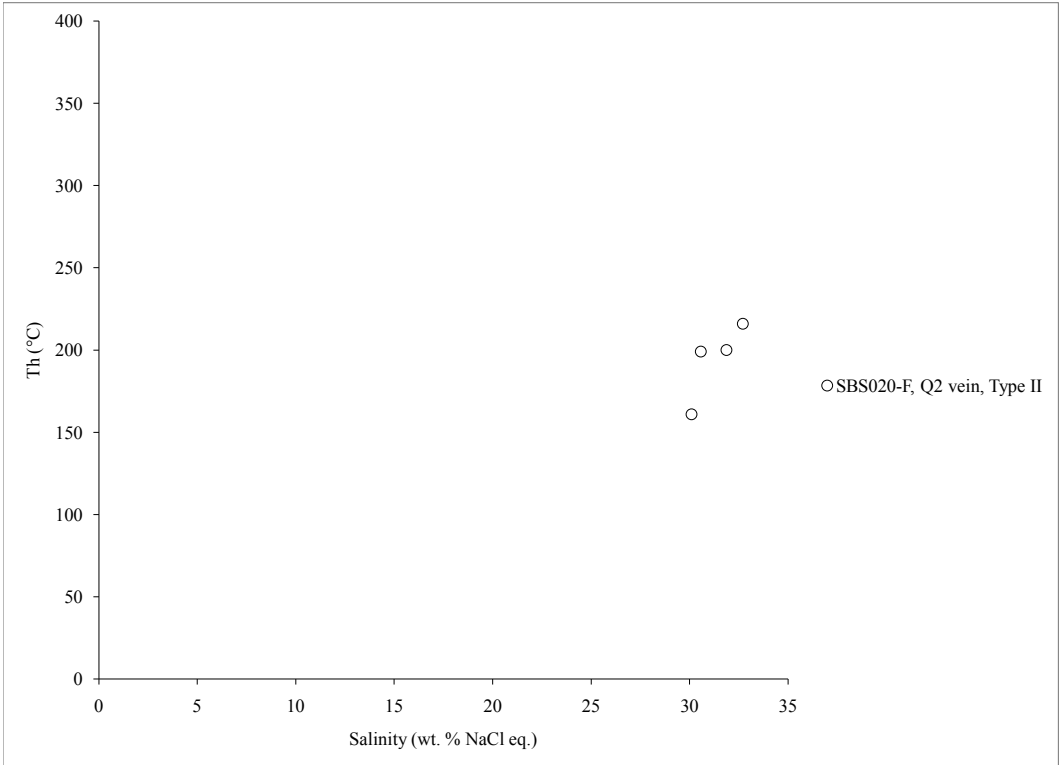


Figure 17. Temperature of homogenization versus salinity from primary Type II fluid inclusions from Q2 quartz from the Sue-Dianne giant vein zone sample 06SBS020-F. Each data point represents a single fluid inclusion analysed from a single fluid inclusion assemblage.

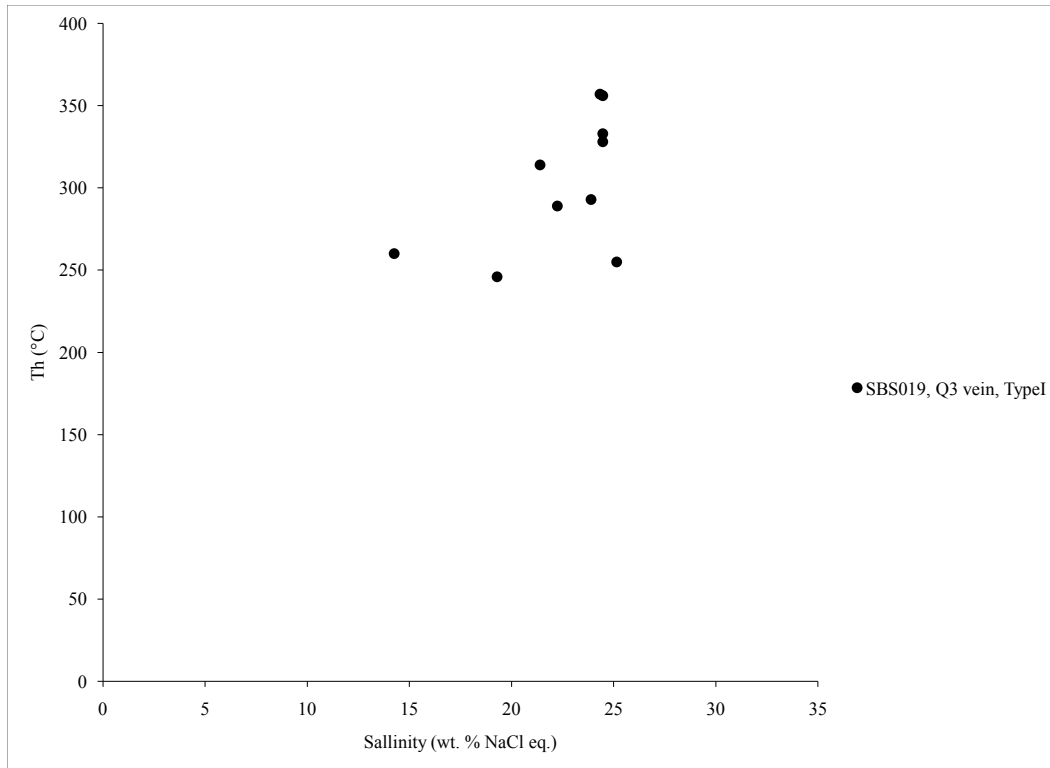


Figure 18. Temperature of homogenization versus salinity from primary Type I fluid inclusions from mineralized Q3 quartz from the Sue-Dianne giant vein zone sample 06SBS019. Each data point represents a single fluid inclusion analysed from a single fluid inclusion assemblage.

Northern Sloan Extension

The Northern Sloan Extension giant quartz vein contains many different textures and styles of quartz. Early Q1 veins contain anhedral quartz with fluid inclusions too small ($\leq 1\mu\text{m}$) to analyse.

Within Q2 late-stage veins, quartz crystals are commonly zoned into fluid inclusion-rich and -poor zones. However, these zones do not mirror quartz crystal shape, but cross quartz crystal boundaries. Type I fluid inclusions are common, although many are along trails and others appear necked down. They have an average size of $10\mu\text{m}$ and a degree of fill of 0.8 or 0.9. Similarly, necked down Type III fluid inclusions are present within late-stage quartz crystals, so no analyses were carried out from the Northern Sloan Extension vein.

3.2.2 Uranium Associated Giant Quartz Vein Zones

Beaverlodge Lake

Many Q1 stockwork veins from Beaverlodge Lake contain small ($<1\mu\text{m}$) primary and secondary monophasic fluid inclusions, which were not suitable for microthermometry. However, some Q1 quartz contains primary Type I fluid inclusions, with an average salinity of 23.1 ± 2.1 wt. % NaCl eq. ($n = 10$) with an average Th of $129 \pm 27^\circ\text{C}$ ($n = 10$; Fig. 19).

Feathery Q1 quartz and bladed quartz of Beaverlodge Lake contain fluid inclusions different to Q1 stockworks. Primary fluid inclusions within feathery quartz have an average salinity of 10.7 ± 0.8 wt. % NaCl eq. ($n = 8$) with an average Th of $144 \pm 22^\circ\text{C}$ ($n = 8$; Fig. 19).

Late Q2 veins consist of euhedral quartz containing fluid inclusion-rich and poor zones, 100 to $300\mu\text{m}$ thick. These zoned quartz crystals contain an average of 4 to 6 fluid inclusion rich-zones, and generally, the remainder of the quartz crystal is inclusion free. Type I fluid inclusions from milky white Beaverlodge Lake quartz veins have an average salinity of 21.7 ± 3.6 wt. % NaCl eq. ($n = 9$) and a range of Th between 151° to 218°C , with an average of $185 \pm 26^\circ\text{C}$ ($n = 9$; Fig. 20). The Q2 veins contain fluid inclusions with the highest average salinity and the highest average Th from Beaverlodge Lake.

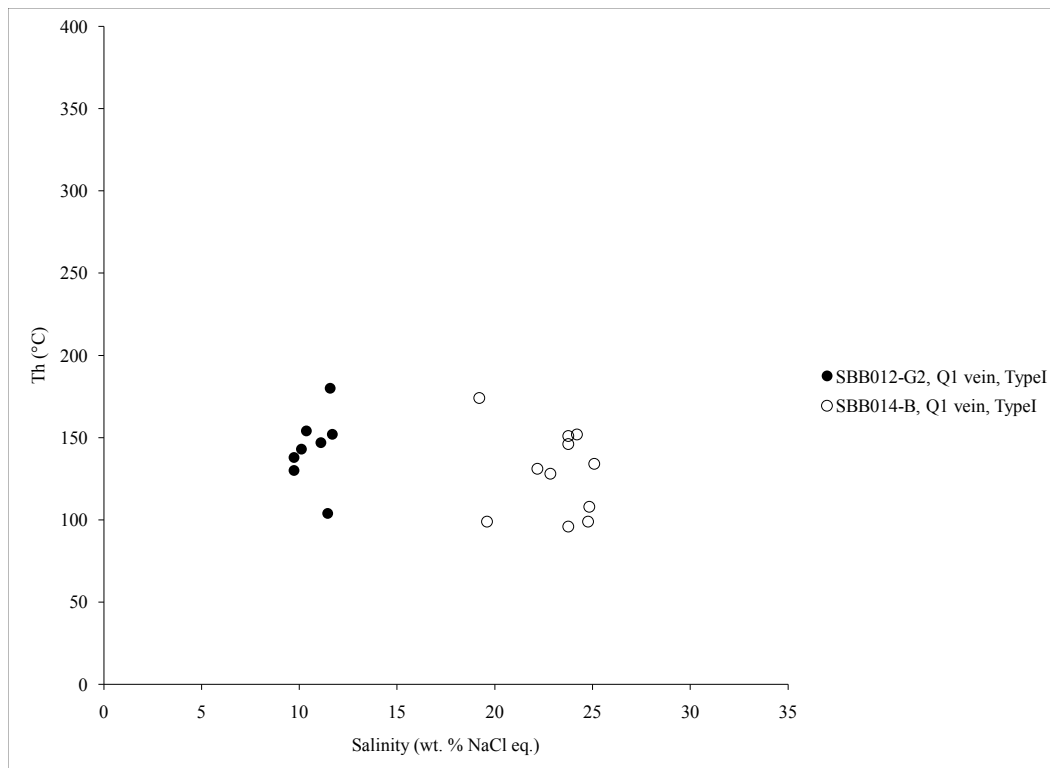


Figure 19. Temperature of homogenization versus salinity from primary Type I fluid inclusions from Q1 quartz from two samples from the Beaverlodge Lake giant vein zone. Each data point represents a single fluid inclusion analysed, each symbol represents a specific fluid inclusion assemblage.

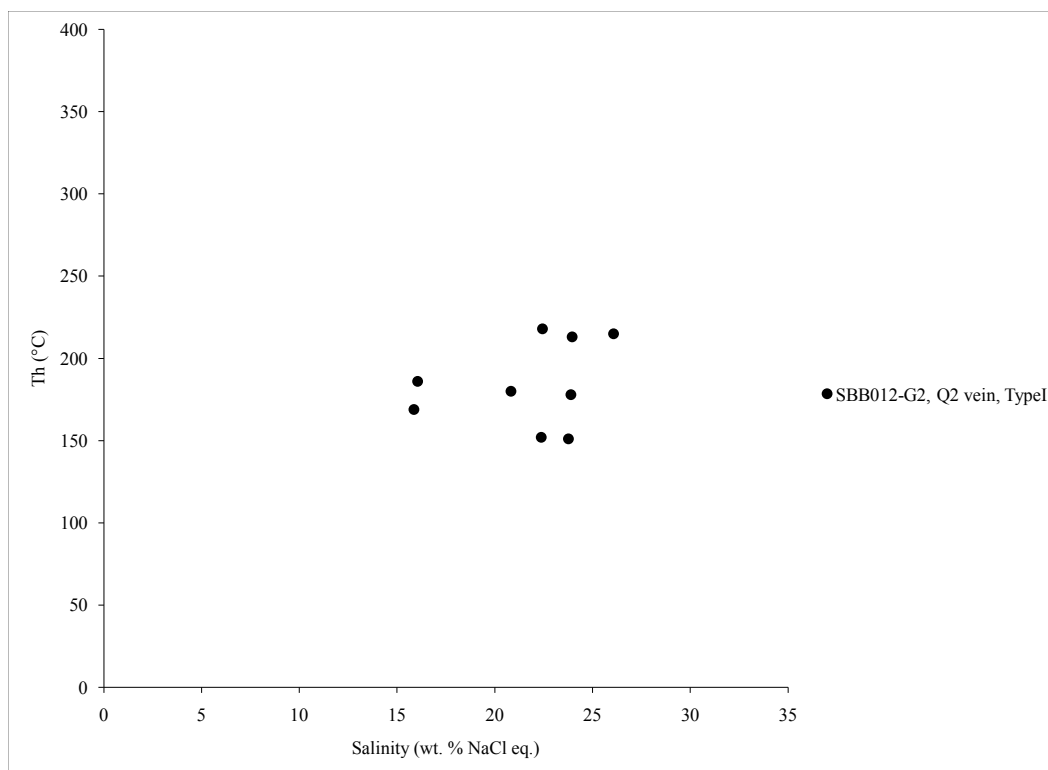


Figure 20. Temperature of homogenization versus salinity from primary Type I fluid inclusions from Q2 quartz from the Beaverlodge Lake giant vein zone. Each data point represents a single fluid inclusion analysed from a single fluid inclusion assemblage.

Fab Lake

Fluid inclusions from Fab Lake are evenly distributed throughout the quartz crystals, and the majority are subhedral to euhedral in shape. Q1 stockworks contain subhedral subrounded primary Type I fluid inclusions. Fluid inclusions from Q1 stockworks, for the most part, are moderately saline, with an average salinity of 14.9 ± 2.8 wt. % NaCl eq. and an average Th of $150 \pm 36^\circ\text{C}$ ($n = 6$; Fig. 21). One Q1 stockwork vein contained very few workable fluid inclusions, but three inclusions contained an average salinity of 0.35 ± 0.0 wt. % NaCl eq. and Th of $180 \pm 2^\circ\text{C}$ (Fig. 21).

Late Q2 veins from Fab Lake contain many large (4 to $8\mu\text{m}$) primary Type I fluid inclusions. Fluid inclusions from Q2 veins at Fab Lake have a bimodal distribution, with fluid inclusion assemblages trapping high salinity fluids, 19.6 ± 3.9 wt. % NaCl eq. that have a lower average Th of $127 \pm 21^\circ\text{C}$ ($n = 15$), and other fluid inclusion assemblages with a low salinity fluid of 0.7 ± 0.6 wt. % NaCl eq. and average Th of $197 \pm 33^\circ\text{C}$ ($n = 15$; Fig. 22).

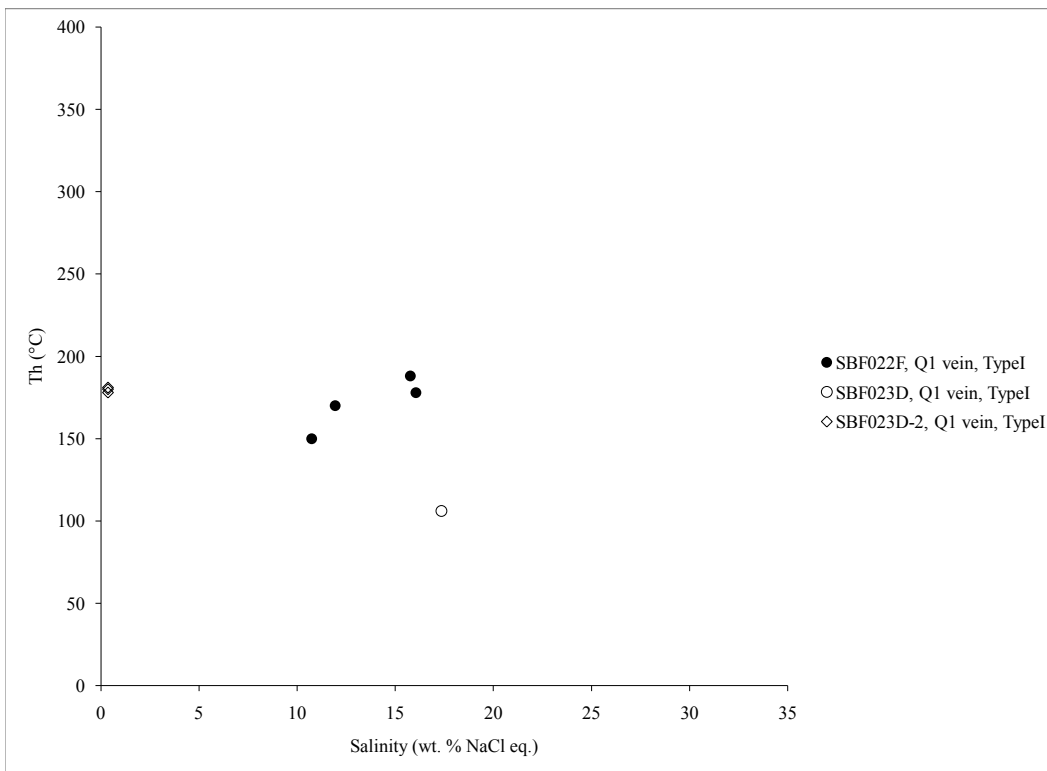


Figure 21. Temperature of homogenization versus salinity from primary Type I fluid inclusions from Q1 quartz from the Fab Lake giant vein zone. Each data point represents a single fluid inclusion analysed, each symbol represents a specific fluid inclusion assemblage.

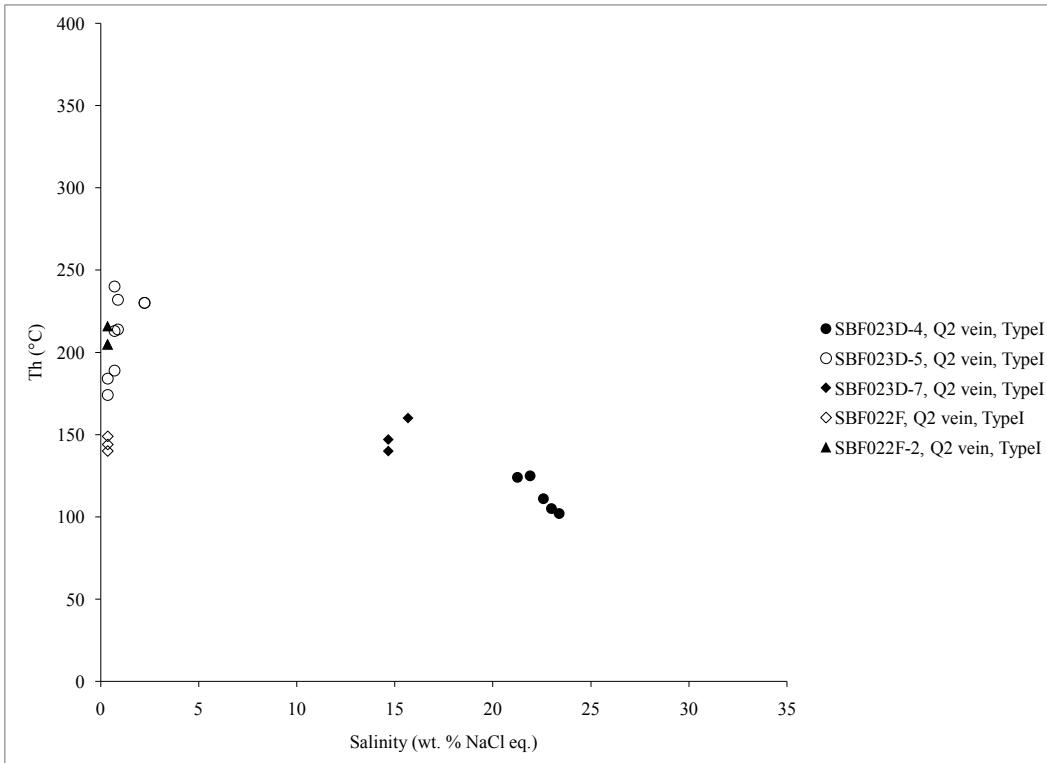


Figure 22. Temperature of homogenization versus salinity from primary Type I fluid inclusions from Q2 quartz from the Fab Lake giant vein zone. Each data point represents a single fluid inclusion analysed, each symbol represents a specific fluid inclusion assemblage.

Northern Wopmay fault

The quartz within veins from the Northern Wopmay fault zone contains primary Type I fluid inclusions, and most of these inclusions are trapped along trails. Many inclusions showed evidence of post entrapment modification (necking or leakage), and were not analysed during microthermometry.

Q1 veins and stockworks consisted of cloudy feathery quartz; however, many round Type I fluid inclusions occur near the cores and edges of these bladed feathery crystals. Some cloudy veins consist of inclusion-defined growth zones, these zones also contain many Type I inclusions (Plate 11A). The fluid inclusions hosted by quartz veins on the Northern Wopmay fault zone vary in salinity, stockwork vein fluid inclusions with an average salinity of 0.39 ± 0.1 wt. % NaCl eq. ($n = 11$) have an average Th of $212 \pm 36^\circ\text{C}$ ($n = 11$), whereas inclusions with a moderate salinity of 18.9 ± 2.6 wt. % NaCl eq. ($n = 11$) have an average Th of $153 \pm 16^\circ\text{C}$ ($n = 11$; Fig. 23).

Younger Q2 veins consist of colourless quartz and contain small Type I inclusions (Plate 11B). Northern Wopmay fault zone a Q2 vein of euhedral quartz formed from fluids with an average salinity of 20.1 ± 2.3 wt. % NaCl eq. ($n = 11$) and Th of $239 \pm 26^\circ\text{C}$ ($n = 11$; Fig. 24).

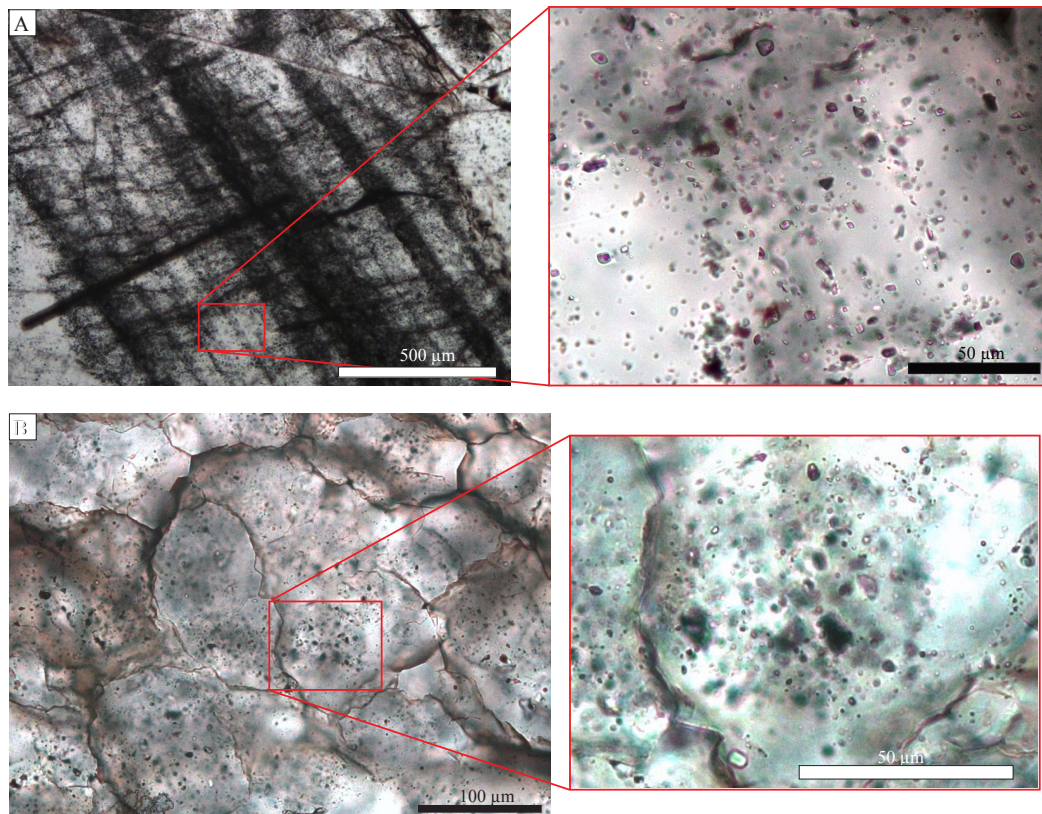


Plate 11. A) Wopmay fault sample of Q1 growth zoned quartz vein in plane polarized transmitted light; a laser ablation track line cross cuts vein growth zones. Inset image (in red) displays the Type I fluid inclusions used for microthermometry. B) Wopmay fault sample of Q2 quartz in plane polarized transmitted light. Inset image (in red) displays the Type I fluid inclusions used for microthermometry.

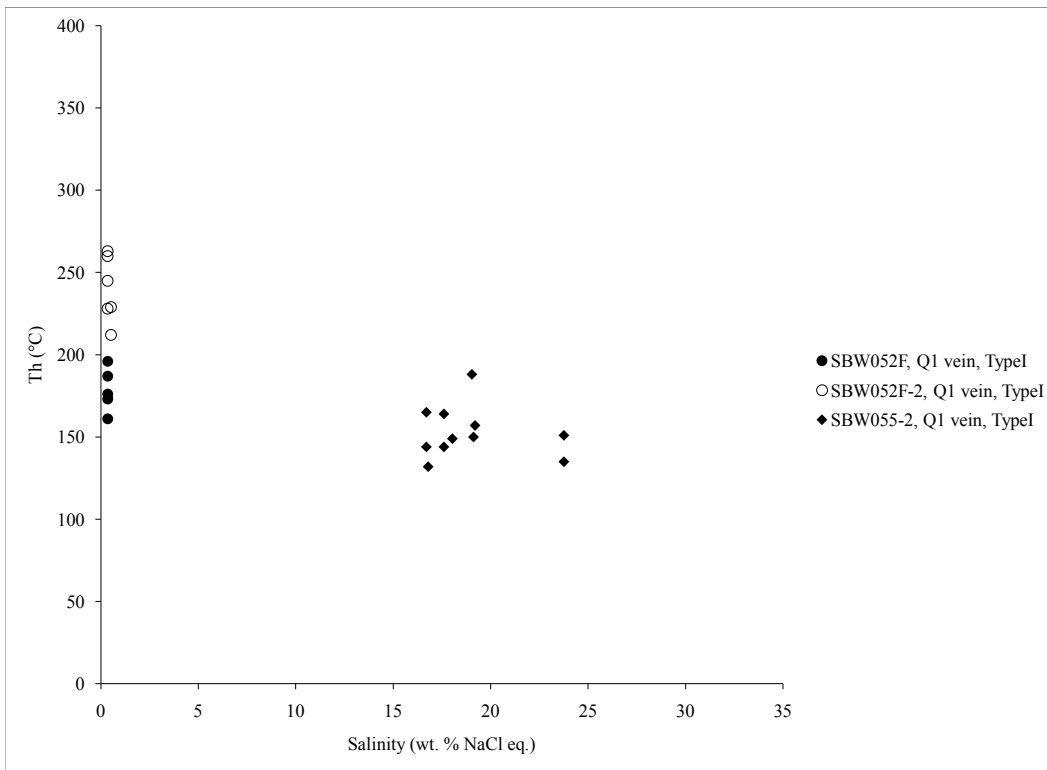


Figure 23. Temperature of homogenization versus salinity from primary Type I fluid inclusions from Q1 quartz from the Wopmay fault giant vein zone. Each data point represents a single fluid inclusion analysed, each symbol represents a specific fluid inclusion assemblage.

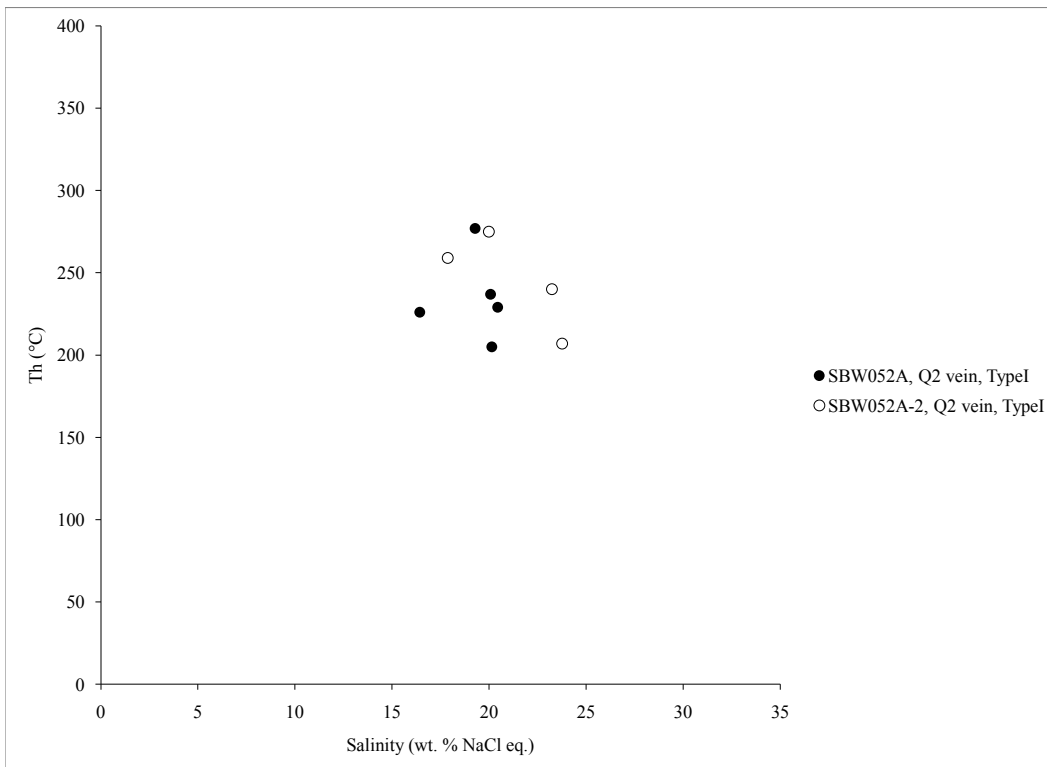


Figure 24. Temperature of homogenization versus salinity from primary Type I fluid inclusions from Q2 quartz from the Wopmay fault giant vein zone. Each data point represents a single fluid inclusion analysed, each symbol represents a specific fluid inclusion assemblage.

3.2.3 Giant Quartz Vein Zones Isolated from Mineralization

“Arm” Lake

The giant quartz vein from “Arm” Lake consists of Q1 and Q2 veins that do not contain fractures or evidence of recrystallization. Some Q1 stockwork quartz contained many small ($<1\mu\text{m}$) fluid inclusions that could not be properly identified or measured. Q2 veins contain many primary euhedral Type I inclusions.

Fluid inclusions from “Arm” Lake Q2 veins consistently contain low salinity fluids, with an average of 0.6 ± 0.8 wt. % NaCl eq. ($n = 35$) from all primary fluid inclusions measured. On the whole, “Arm” Lake inclusions contain less than 3.2 wt. % NaCl eq. and the “Arm” Lake fluid inclusions have an average Th of $216 \pm 33^\circ\text{C}$ ($n = 35$; Fig. 25 and 26).

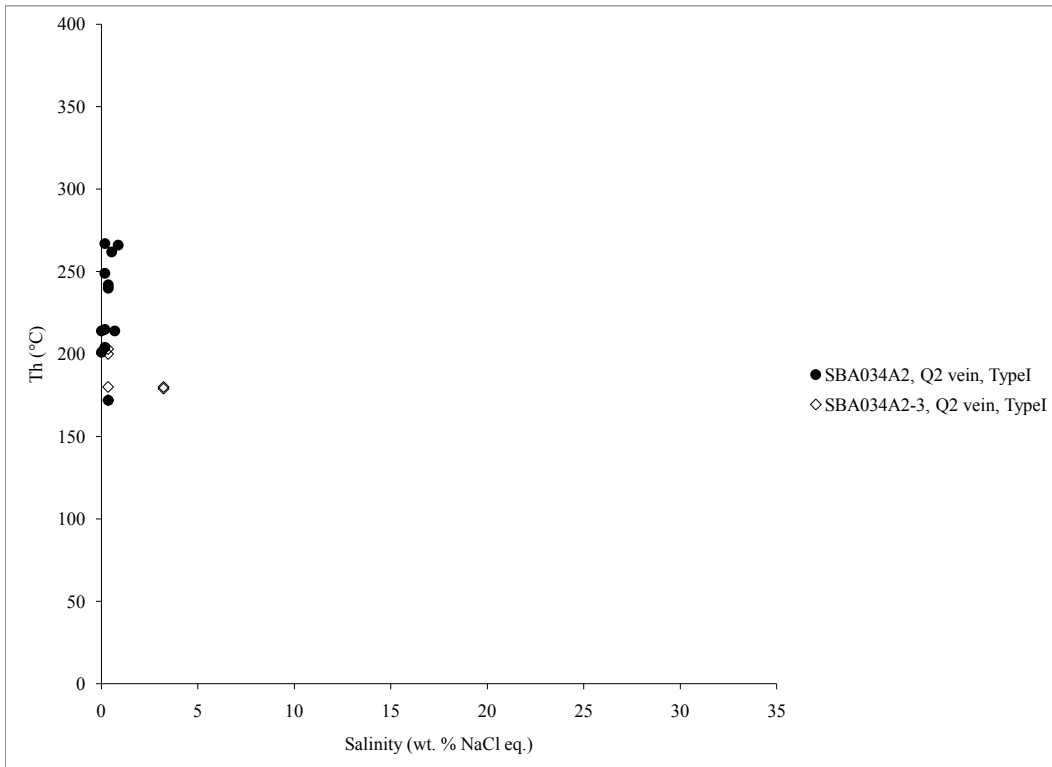


Figure 25. Temperature of homogenization versus salinity from primary Type I fluid inclusions from Q2 quartz (sample SBA034-A2) from the “Arm” Lake giant vein zone. Each data point represents a single fluid inclusion analysed, each symbol represents a specific fluid inclusion assemblage.

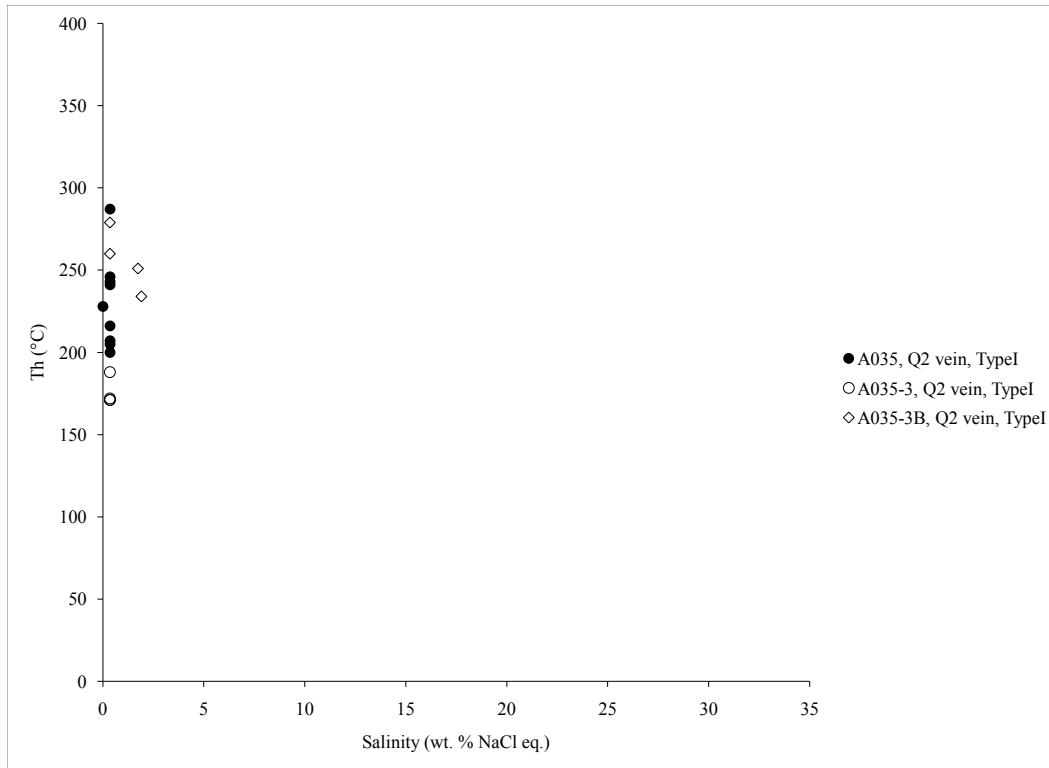


Figure 26. Temperature of homogenization versus salinity from primary Type I fluid inclusions from Q2 quartz (sample SBA035) from the “Arm” Lake giant vein zone. Each data point represents a single fluid inclusion analysed, each symbol represents a specific fluid inclusion assemblage.

Hardisty Lake

Hardisty Lake giant quartz vein zone is made up of Q1, Q2 and Q3 veins containing primary Type I, and occasionally primary Type II fluid inclusions. Type I inclusions are subhedral, subrounded and locally have a negative-crystal shape. There are small amounts of pseudo-secondary inclusions which are necked and stretched along fractures. Generally, Hardisty Lake quartz veins contain fluid inclusions with low to moderate salinities. Fluid inclusions from two Hardisty Lake Q1 vein quartz samples contain average salinities of 0.6 ± 0.2 wt. % NaCl eq. ($n = 16$) and an average Th of $234 \pm 50^\circ\text{C}$ ($n = 16$; Fig. 27).

Three Type I fluid inclusions within a growth zone within a Q2 Hardisty Lake quartz vein, have an average salinity of 21.8 ± 0.1 wt. % NaCl eq. ($n = 3$). Within a different fluid inclusion assemblage of the same Q2 vein, consists of Type II inclusions. The Type II inclusions are subhedral and 8 to $13\mu\text{m}$ in diameter. Nearby Type I inclusions do not appear to be stretched, but some Type II inclusions are anhedral and stretched. The halite daughter minerals are cubic in shape, although some have subrounded corners. Three Type II fluid inclusions within this Q2 vein’s growth zone have an average salinity of 29.8 ± 2.2 wt. % NaCl eq. with a range of Th from 215° to 310°C ($n = 3$; Fig. 28).

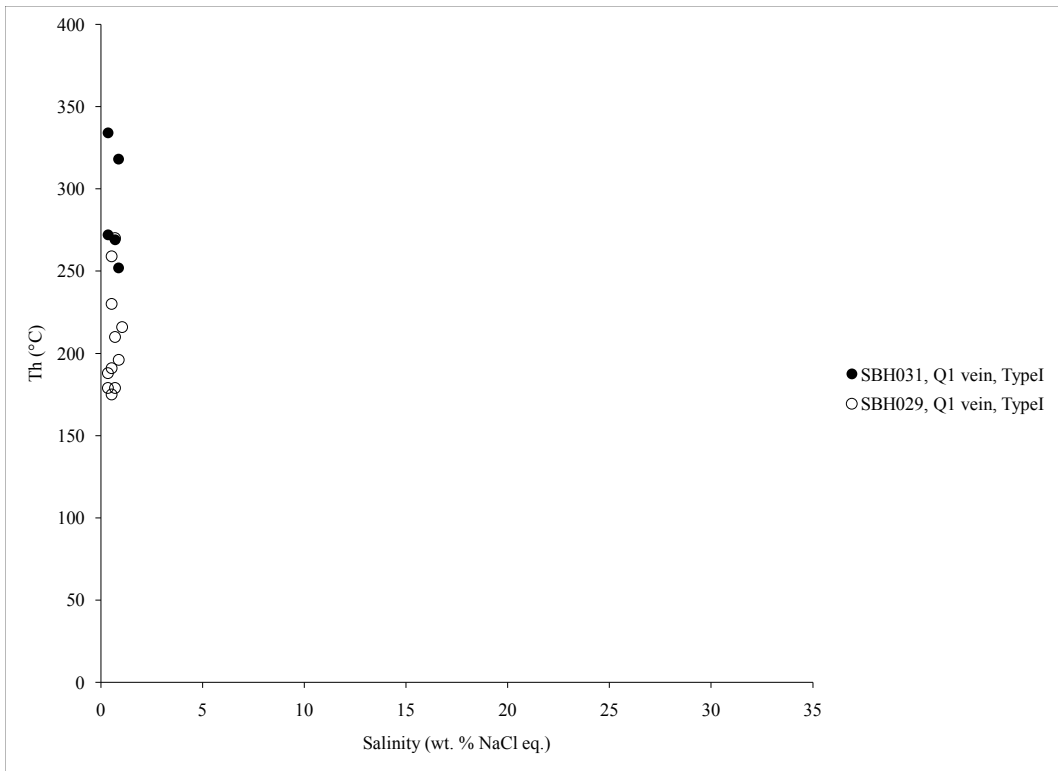


Figure 27. Temperature of homogenization versus salinity from primary Type I fluid inclusions from Q1 quartz from the Hardisty Lake giant vein zone. Each data point represents a single fluid inclusion analysed, each symbol represents a specific fluid inclusion assemblage.

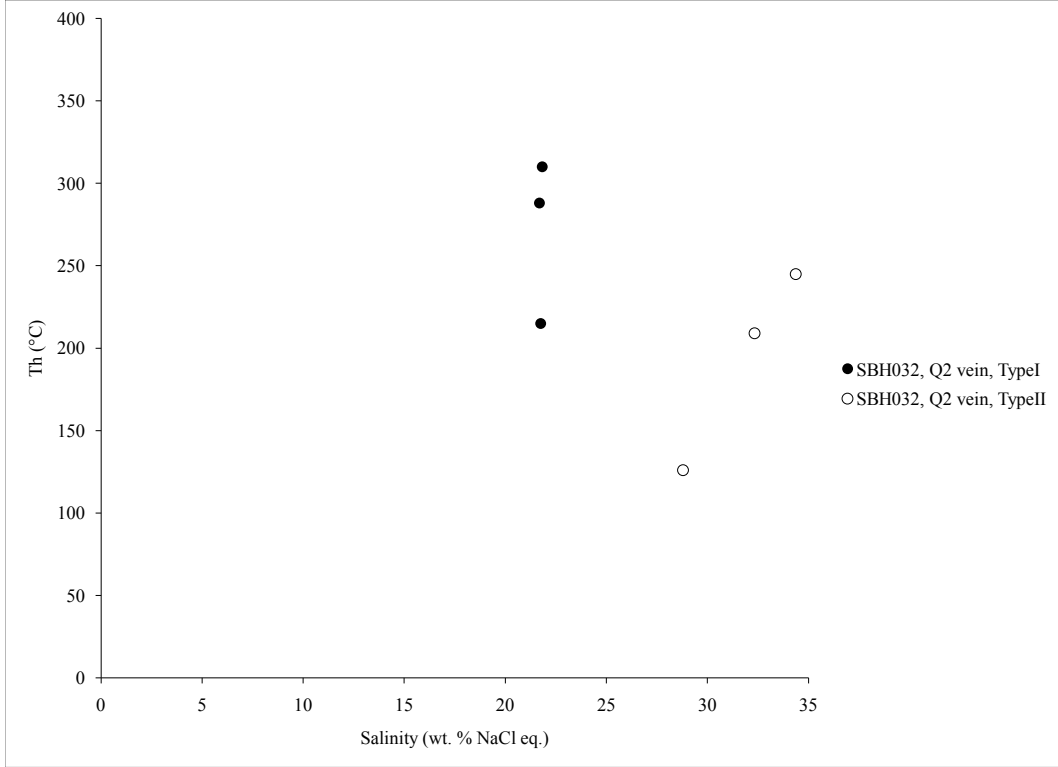


Figure 28. Temperature of homogenization versus salinity from primary Type I and II fluid inclusions from Q2 quartz from the Hardisty Lake giant vein zone. Each data point represents a single fluid inclusion analysed, each symbol represents a specific fluid inclusion assemblage.

A Q3 quartz microveinlet, which cross cuts a Q2 vein, contains Type I fluid inclusions that have an average salinity of 0.35 ± 0.1 wt. % NaCl eq. ($n = 8$) and an average Th of $190 \pm 41^\circ\text{C}$ ($n = 8$; Fig. 29). Another Q3 vein consists of Type I fluid inclusions that have an average salinity of 23.2 wt. % NaCl eq. ($n = 5$) and an average Th of $166 \pm 28^\circ\text{C}$ ($n = 5$; Fig. 29).

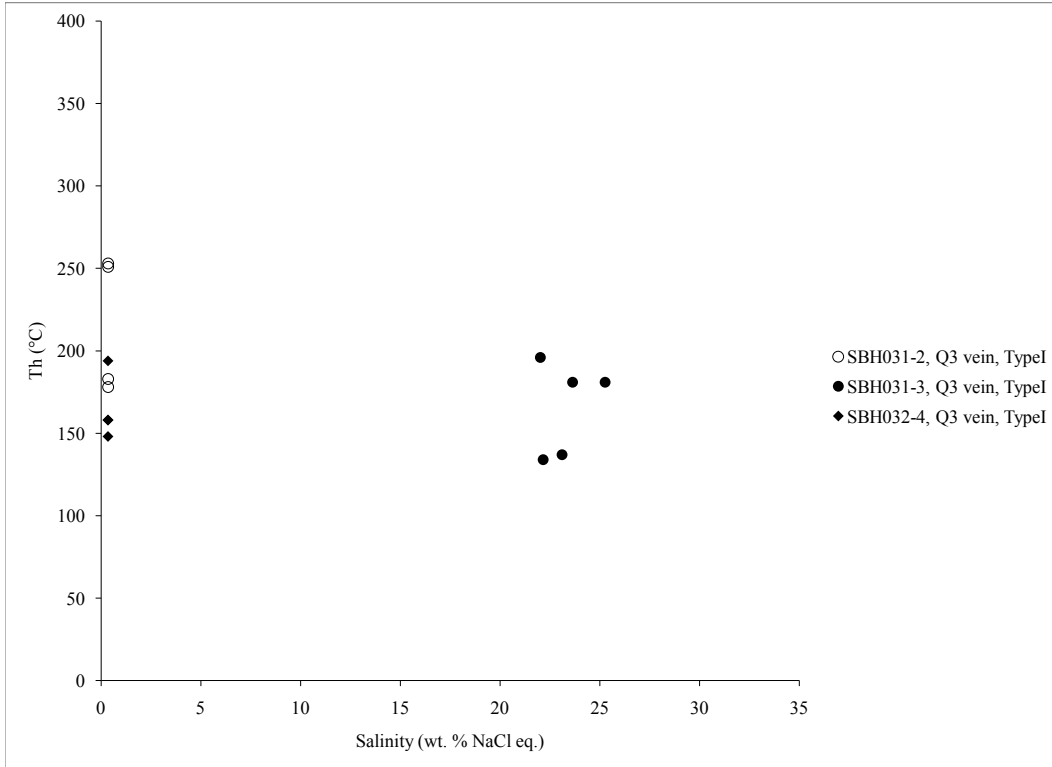


Figure 29. Temperature of homogenization versus salinity from primary Type I fluid inclusions from Q3 quartz from the Hardisty Lake giant vein zone. Each data point represents a single fluid inclusion analysed, each symbol represents a specific fluid inclusion assemblage.

Margaret Lake

Margaret Lake Q1 stockwork quartz contains many small ($<6\mu\text{m}$ diameter) fluid inclusions. The primary fluid inclusions within the Q1 stockworks are low in salinity, with one vein with fluid inclusions that have an average salinity of 0.8 ± 1.2 wt. % NaCl eq. ($n = 13$) and Th average at $344 \pm 21^\circ\text{C}$ ($n = 13$) and another vein with fluid inclusions which have an average salinity of 0.6 ± 0.7 wt. % NaCl eq. ($n = 9$) and an average Th at $224 \pm 33^\circ\text{C}$ ($n = 9$; Fig. 30).

Margaret Lake contains many Q2 veins, some that have growth zoned quartz crystals. These quartz crystals generally contain a clear core, a cloudy inclusion-rich zone and a clear inclusion-poor rim. Inclusions from the Q2 vein quartz consist of large (15 to $20\mu\text{m}$ diameter) Type I fluid inclusions. Primary fluid inclusions within these veins are similar to fluid inclusions from Q1 stockwork quartz, containing an average fluid salinity of 2.8 ± 2.5 wt. % NaCl eq. ($n = 10$) with an average Th of $195 \pm 18^\circ\text{C}$ ($n = 10$; Fig. 31).

Many secondary fluid inclusion trails exist within the Margaret Lake Q2 milky white quartz veins. Trails of monophasic and two-phase inclusions are commonly along fractures and irregularly shaped. Other inclusions are fractured; these inclusions have leaked and were not analysed.

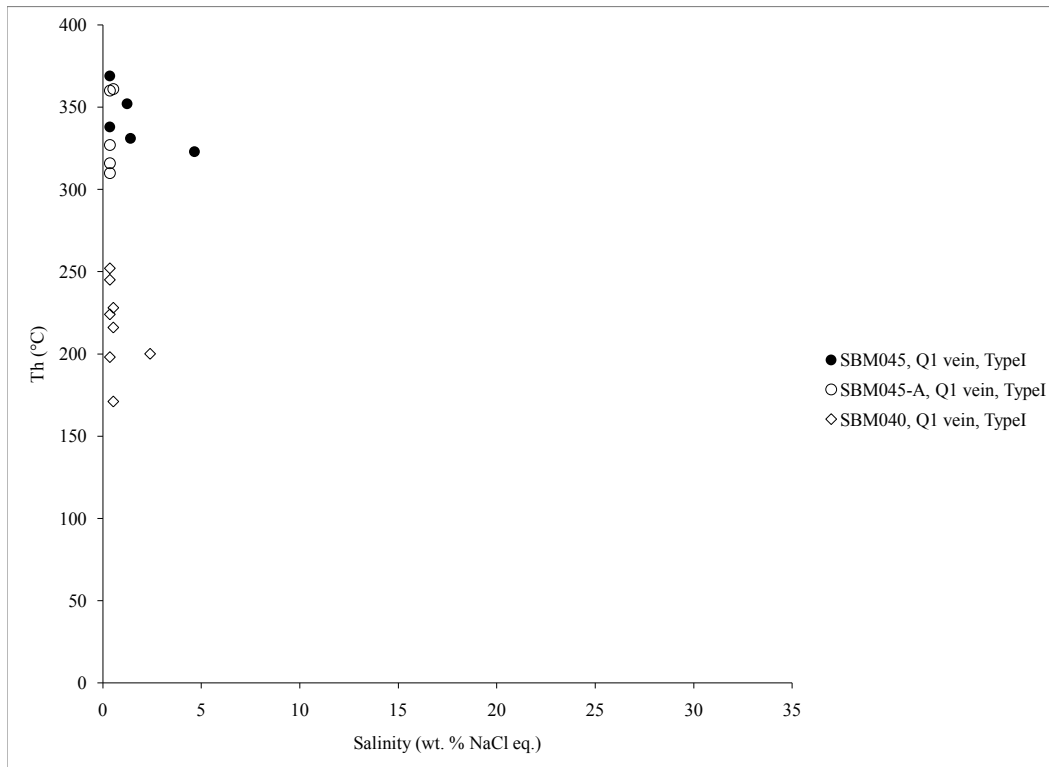


Figure 30. Temperature of homogenization versus salinity from primary Type I fluid inclusions from Q1 quartz from the Margaret Lake giant vein zone. Each data point represents a single fluid inclusion analysed, each symbol represents a specific fluid inclusion assemblage.

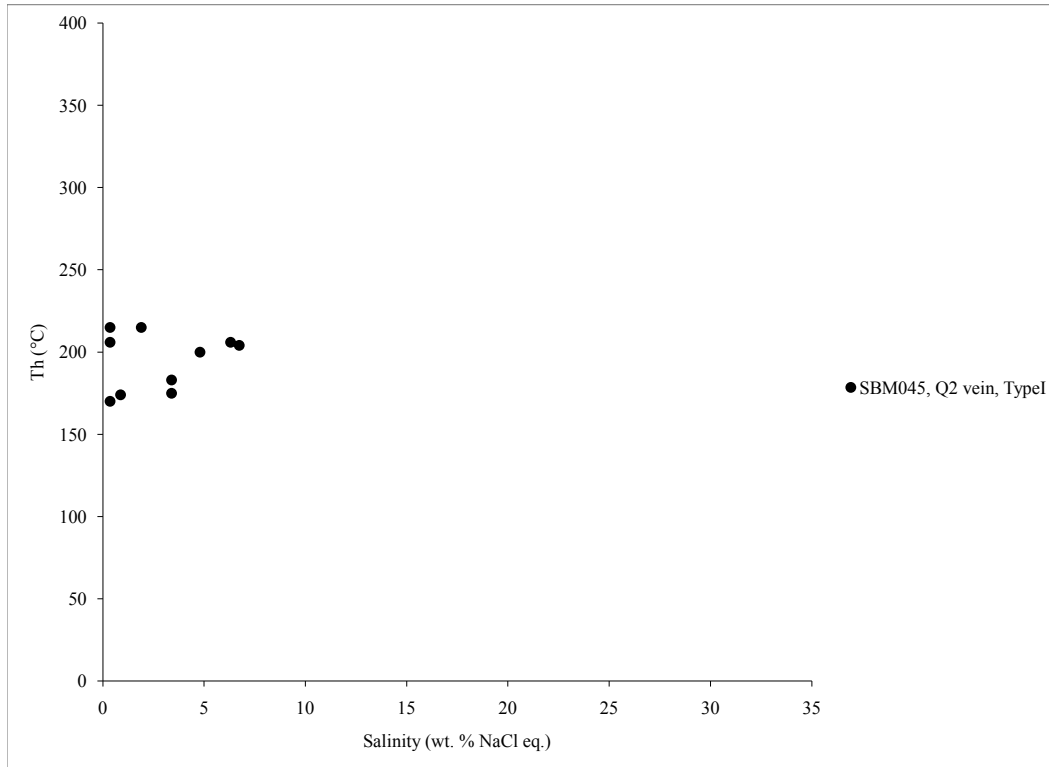


Figure 31. Temperature of homogenization versus salinity from primary Type I fluid inclusions from Q2 quartz from the Margaret Lake giant vein zone. Each data point represents a single fluid inclusion analysed from a single fluid inclusion assemblage.

3.2.4 Fluid Inclusion Summary

Fluid inclusion Th and salinity from the giant quartz vein zones were clarified by defining distinct fluid inclusion assemblages. Figures 32 to 34 display summary diagrams of the average Th and salinity to one standard deviation, taken from fluid inclusion assemblages from Q1, Q2 and Q3 veins within giant quartz vein zones located near areas of base-metal mineralization, giant quartz vein zones associated with uranium mineralization, and giant quartz vein zones isolated from mineralization, respectively.

Most fluid inclusions from the giant quartz vein zones are identified as belonging to two general fluid types, a low salinity and a moderate salinity fluid. The low salinity fluid is trapped as Type I fluid inclusions, whereas the higher salinity fluid contains a range in salinity from 12 to 30 wt. % NaCl eq. and is therefore trapped as both Type I (lower end of the salinity range) and Type II (higher end of salinity range) fluid inclusions. This occurs in all giant quartz vein zones.

Giant quartz vein zones proximal to base-metal mineralization consist of fluid inclusions with moderate Th and salinity (Fig. 32); although this may be the result of a sampling bias since many Q1 veins had fluid inclusions that were not suitable for microthermometry. One Q2 vein from the giant quartz vein zone near Sue-Dianne contains fluid inclusions that are low in salinity, while another Q2 vein with Type II fluid inclusions with high salinity and moderate Th (Fig. 32). The Q3 mineralized vein from the giant quartz vein zone at Sue-Dianne contains fluid inclusions with the highest Th and a high salinity than all other fluid inclusion assemblages (Fig. 32).

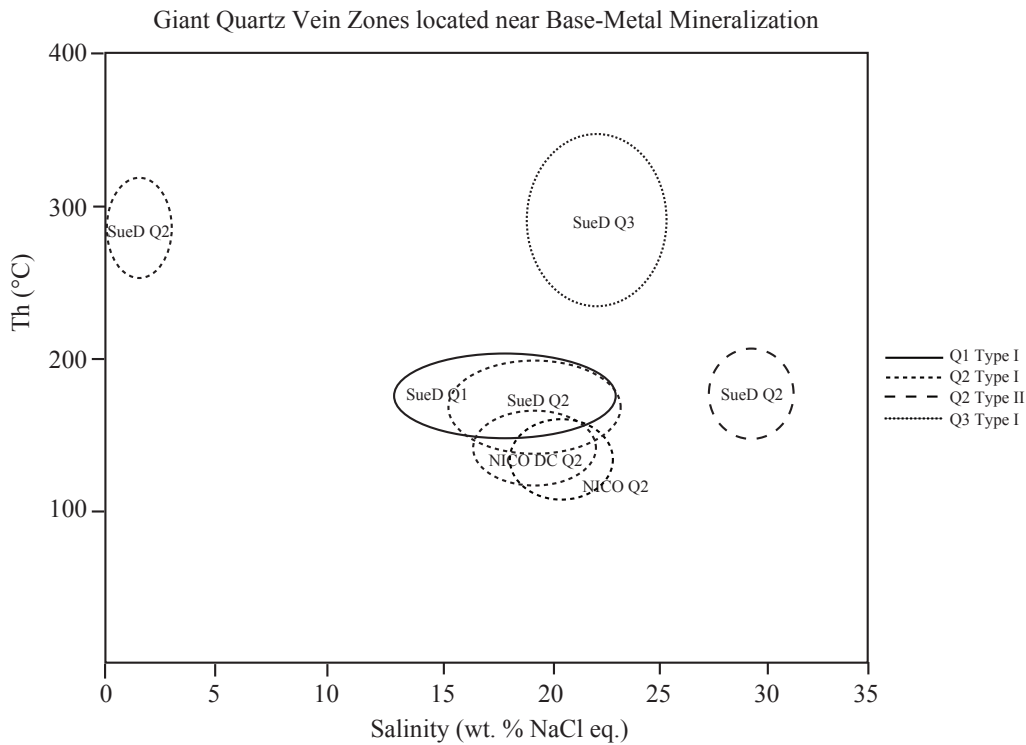


Figure 32. Summary diagram of the temperature of homogenization versus salinity from primary Type I and Type II fluid inclusion assemblages from giant vein zones located proximal to mineralized deposits. SueD = giant quartz vein zone near the Sue-Dianne deposit, NICO = giant quartz vein zone near the NICO deposit, NICO DC = giant quartz vein zone found within NICO drill core for Q1, Q2 and Q3 quartz veins. Size of fluid inclusion assemblage circle is equal to the average Th and salinity to one standard deviation.

Giant quartz vein zones associated with uranium mineralization contain fluid inclusions with average Th and salinities similar to fluid inclusions from giant quartz vein zones proximal to base-metal mineralization. Most fluid inclusion assemblages from the giant quartz vein zones at Beaverlodge Lake, Fab Lake and Northern Wopmay fault contain moderate salinities and temperatures, although a few Q1 and Q2 veins from Fab Lake and Northern Wopmay fault contain fluid inclusions with a low salinity fluid (Fig. 33).

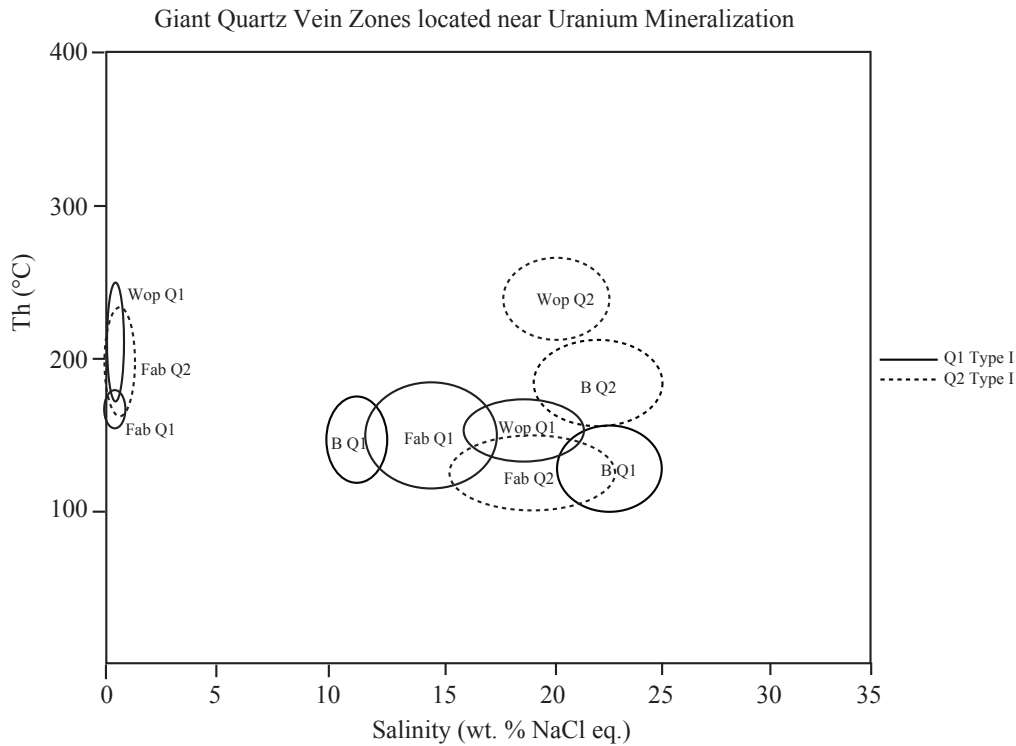


Figure 33. Summary diagram of the temperature of homogenization versus salinity from primary Type I fluid inclusion assemblages from giant vein zones associated with uranium mineralization. Wop = giant quartz vein at the Northern Wopmay fault, Fab = giant quartz vein zone at Fab Lake, B = giant quartz vein zone at Beaverlodge Lake for Q1 and Q2 quartz veins. Size of fluid inclusion assemblage circle is equal to the average Th and salinity to one standard deviation.

The majority of fluid inclusions from giant quartz vein zones isolated from mineralization contain dilute fluids with moderate Th from Q1, Q2 and Q3 veins (Fig. 34). The giant quartz vein zone at Hardisty Lake also contains a Q2 vein at high salinity and moderate Th, as well as another fluid inclusion assemblage from a Q2 vein with Type II halite-bearing fluid inclusions. It is also noted that most fluid inclusion assemblages from Q1 veins appear to contain a higher average Th than fluid inclusion assemblages from Q2 veins (Fig. 34).

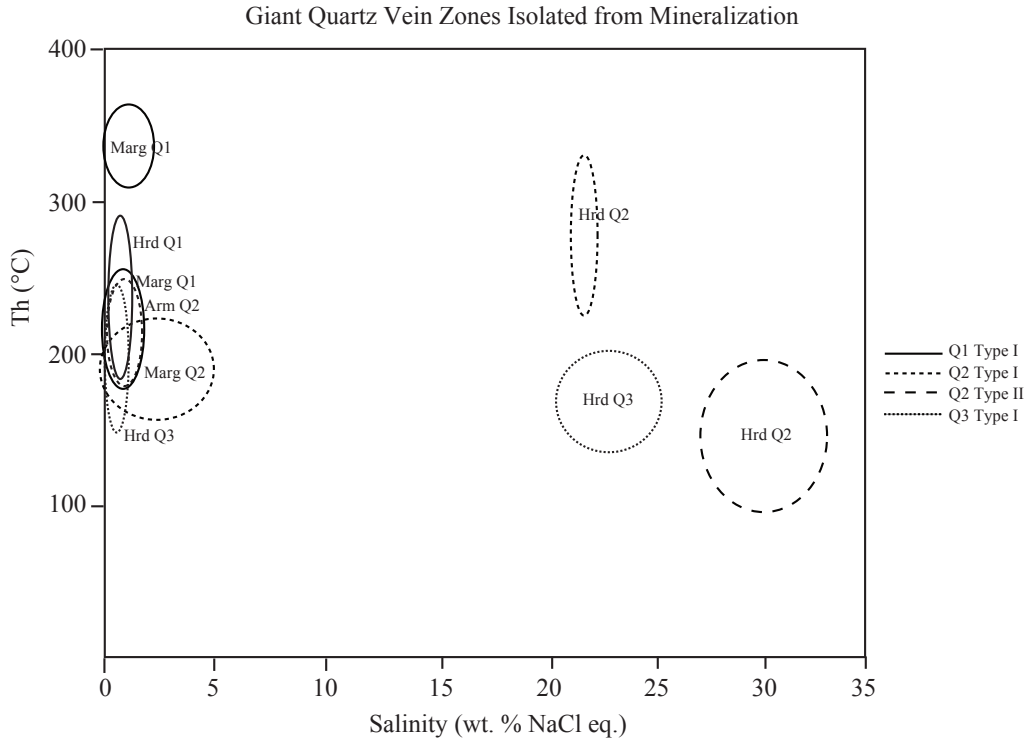


Figure 34. Summary diagram of the temperature of homogenization versus salinity from primary Type I and Type II fluid inclusion assemblages from giant vein zones isolated from mineralization. Arm = giant quartz vein zone at Arm Lake, Hrd = giant quartz vein zone at Hardisty Lake, Marg = giant quartz vein zone at Margaret Lake for Q1, Q2 and Q3 quartz veins. Size of fluid inclusion assemblage circle is equal to the average Th and salinity to one standard deviation.

Table 1. Summary of fluid inclusion and stable isotope data for all vein zones

Location	Sample	Vein Type		Inclusion	Inclusion Type	Count		Th			T _{m,ice}			Salinity		Salinity mode
		Q1,2,3	P ₁ ,P ₂ ,S			max °C	min °C	avg °C	std-dev 1σ	mode °C	avg °C	std-dev 1σ	avg wt. % NaCl _{eq}	std-dev 1σ	rt. % NaCl _{eq}	
NICO	06SBN001E	Q2	P	I	I	8	177	111	142	23	NM	-17.5	20.7	1.8	19.7	
NICO	06SBN001E-2	Q2	P	I	I	6	136	111	195	31	NM	-18.1	21.1	2.0	NM	
NICO	06SBN001D	Q2	P	I	I	17	137	110	183	18	133	-17.1	20.4	2.1	17.6	
NICO Drill-Core	06SBN98-122-122.1m-1	Q2	P	I	I	2	109	107	108	1	NM	-18.2	21.1	3.8	NM	
NICO Drill-Core	06SBN98-122-122.1m-2	Q2	P	I	I	3	168	159	163	5	NM	-16.2	19.8	0.3	NM	
NICO Drill-Core	06SBN98-122-122.1m-3	Q2	P	I	I	3	162	134	151	15	NM	-12.1	16.2	1.7	17.2	
NICO Drill-Core	06SBN98-122-122.1m-4	Q2	P	I	I	3	161	128	143	17	NM	-16	19.6	1.2	NM	
Sue-Dianne	06SBS019	Q1	P	I	I	12	222	149	181	25	163	-14.6	18.2	4.9	16.1	
Sue-Dianne	06SBS019	Q2	P	I	I	19	195	147	164	16	157	-17.6	20.4	3.1	17.7	
Sue-Dianne	06SBS019	Q2	P	II	II	4	161	144	193	23	144		29.2	0.4	29.4	
Sue-Dianne	06SBS017-A1	Q2	P	I	I	4	318	250	283	29	NM	-0.8	1.4	1.3	2.6	
Sue-Dianne	06SBS017-A2	Q2	P	I	I	3	297	162	183	18	NM	-8	11.6	1.2	NM	
Sue-Dianne	06SBS020-F	Q2	P	II	II	4	216	161	194	23	NM		31.3	1.2	NM	
Sue-Dianne	06SBS019	Q3	P	I	I	11	357	194	293	51	NM	-19.8	22.3	3.2	24.5	
Beaverlodge Lake	06SBB012-G2	Q1	P	I	I	8	180	104	144	22	NM	-7.2	10.7	0.8	9.7	
Beaverlodge Lake	06SBB014-B	Q1	P	I	I	10	174	96	129	27	99	-21.2	23.1	2.1	23.8	
Beaverlodge Lake	06SBB012-G2	Q2	P	I	I	9	218	151	185	26	NM	-19.3	21.7	3.6	NM	
Fab Lake	06SBF022-F	Q1	P	I	I	6	188	106	150	36	106	-11	14.9	2.8	17.3	
Fab Lake	06SBF023-D	Q1	P	I	I	3	181	178	180	2	NM	-0.2	0.4	0.0	0.4	
Fab Lake	06SBF023-D4	Q2	P	I	I	6	143	102	118	15	NM	-19.2	21.7	1.8	NM	
Fab Lake	06SBF023-D5	Q2	P	I	I	6	240	170	210	26	NM	-0.4	0.6	0.1	0.7	
Fab Lake	06SBF023-D7	Q2	P	I	I	3	160	140	149	10	NM	-11	15.0	0.6	14.7	
Fab Lake	06SBF022-F	Q2	P	I	I	3	149	140	144	5	NM	-0.2	0.4	0.0	0.4	
Fab Lake	06SBF022-F2	Q2	P	I	I	3	216	205	209	6	205	-0.2	0.4	0.0	0.4	

Table 1 Continued.

Location	Sample	Vein Type	Inclusion	Inclusion Type	Inclusions measured	Th			T _{m,ice}			Salinity		
						max °C	min °C	avg °C	std-dev °C	mode °C	avg °C	std-dev °C	mode °C	avg wt. % NaCl eq.
Wopmay fault zone	06SBW052-F	Q1,2,3	P,PS,S	I,II	5	196	161	179	13	NM	-0.2	0.4	0.0	0.4
Wopmay fault zone	06SBW052-F2	Q1	P,PS	I	6	263	212	140	20	NM	-0.2	0.4	0.1	0.4
Wopmay fault zone	06SBW055-2	Q1	P	I	11	188	132	153	16	144	-15.6	18.9	2.6	16.7
Wopmay fault zone	06SBW052-A	Q2	P	I	6	277	129	217	49	NM	-16.1	19.5	1.6	NM
Wopmay fault zone	06SBW052-A2	Q2	P	I	5	275	165	229	44	NM	-18.2	21.0	2.5	20.0
"Arm" Lake	06SBA034-A2	Q2	P	I	18	267	172	214	33	214	-0.4	0.7	1.0	0.4
"Arm" Lake	06SBA035	Q2	P	I	8	246	200	223	19	NM	-0.2	0.3	0.1	0.4
"Arm" Lake	06SBA035-3	Q2	P	I	5	188	171	178	9	171	-0.2	0.4	0.0	0.4
"Arm" Lake	06SBA035-3B	Q2	P	I	4	279	234	256	19	NM	-0.6	1.1	0.8	0.4
Hardisty Lake	06SBH031	Q1	P,PS	I	5	334	252	289	35	NM	-0.4	0.6	0.3	0.9
Hardisty Lake	06SBH029	Q1	P	I	11	270	175	208	33	179	-0.4	0.6	0.2	0.5
Hardisty Lake	06SBH032	Q2	P	I	3	310	215	271	50	NM	-19.1	21.8	0.1	NM
Hardisty Lake	06SBH032	Q2	P	II	3	209	107	147	54	NM		29.8	2.2	NM
Hardisty Lake	06SBH031-2	Q3	P	I	4	253	178	216	41	NM	-0.2	0.4	0.0	0.4
Hardisty Lake	06SBH031-3	Q3	P	I	5	196	134	166	28	181	-21.1	23.2	1.3	NM
Hardisty Lake	06SBH032-4	Q3	P	I	4	194	148	165	20	158	-0.2	0.4	0.0	0.4
Margaret Lake	06SBM045	Q1	P,PS	I	5	369	323	343	18	NM	-0.9	1.6	1.8	0.4
Margaret Lake	06SBM045-A	Q1	P,PS	I	8	370	310	345	24	370	-0.2	0.4	0.1	0.4
Margaret Lake	06SBM040	Q1	P	I	9	281	171	224	33	NM	-0.4	0.6	0.7	0.4
Margaret Lake	06SBM045	Q2	P	I	10	215	170	195	18	215	-1.7	2.8	2.5	0.4

NM - mode value is not available

3.3 Stable Isotopes from Giant Quartz Vein Zones

Stable isotope analyses were carried out on Q1, Q2 and Q3 quartz veins from a selection of vein zones studied. Overall, the giant quartz vein zones yielded similar $\delta^{18}\text{O}_{\text{qtz}}$ values, mostly between 9 and 11‰, independent of one location or giant vein zone orientation. Analysis of $\delta^{18}\text{O}$ values from quartz and two analyses of $\delta^{13}\text{C}$ values from NICO drill-core calcite veins are tabulated in Table 2, located at the end of this section.

3.3.1 Giant Quartz Vein Zones located near Base-Metal Mineralization

Giant Quartz Vein Zone near the NICO Deposit

Quartz from Q1 and Q2 veins, from the giant vein zone and veins intersected in drill core, range in $\delta^{18}\text{O}_{\text{qtz}}$ values from +9.6 to +14.7‰ (Fig. 35 and 36). There is no significant distinction with regard to isotopic signature between the various types of quartz (e.g. Q1 versus Q2 vein quartz). Q1 quartz contained an average $\delta^{18}\text{O}_{\text{qtz}}$ value of $11.4 \pm 2.3\text{‰}$ ($n = 2$) while Q2 quartz contained a similar average $\delta^{18}\text{O}_{\text{qtz}}$ value of $11.4 \pm 1.5\text{‰}$ ($n = 10$; Table 2).

The veins from NICO contain multiple generations of quartz; for instance, sample 06SBN001-A is made up of four generations of Q2 quartz that can be characterized by different colour, texture, size or shape of quartz crystals. Each of the four phases of veining was measured and resulted in a progressive decrease of $\delta^{18}\text{O}_{\text{qtz}}$ from the vein in contact with the host rock, V1, which has a $\delta^{18}\text{O}_{\text{qtz}}$ of +11.6‰ to the vein furthest from the host rock, V4, which has a $\delta^{18}\text{O}_{\text{qtz}}$ of +10.4‰ (Fig. 37).

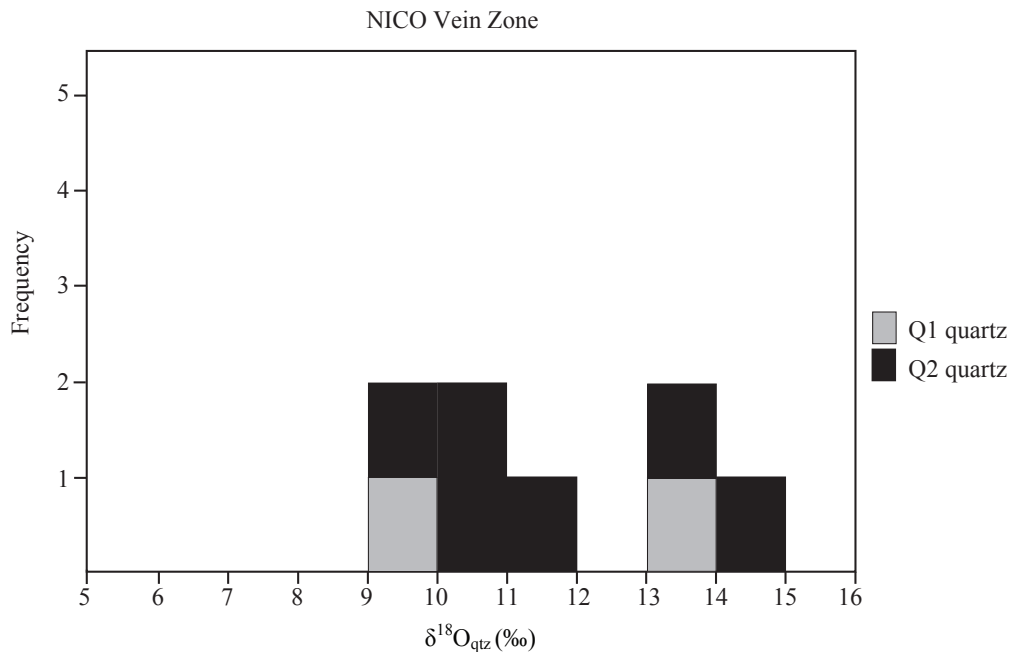


Figure 35. The $\delta^{18}\text{O}$ values from Q1 and Q2 quartz from the NICO giant quartz vein.

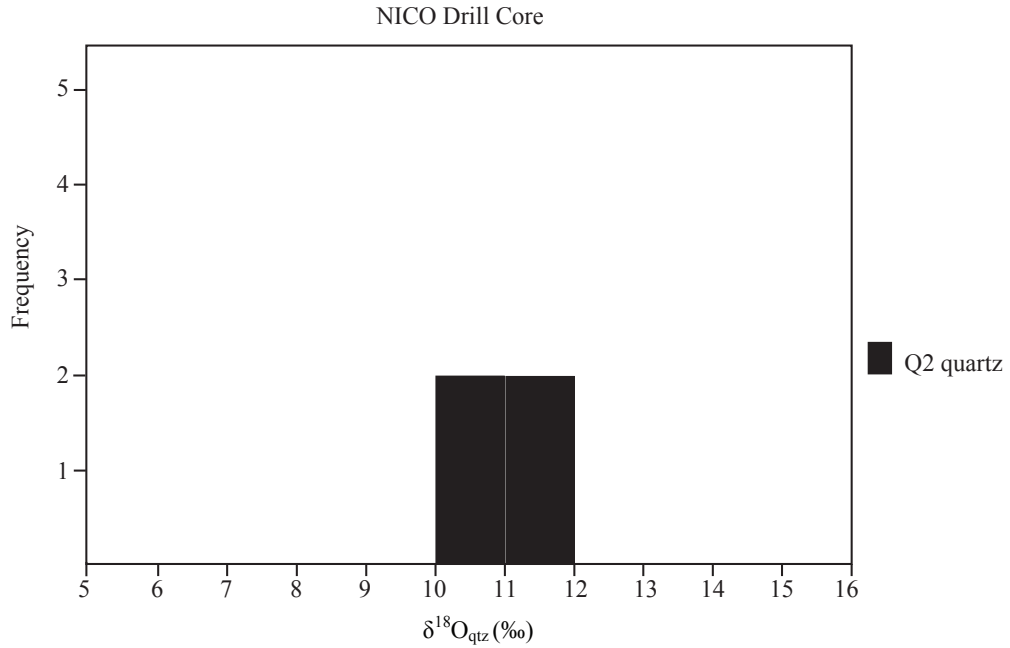


Figure 36. The $\delta^{18}\text{O}$ values from Q1 and Q2 quartz from the NICO giant quartz vein intercepted during drilling.

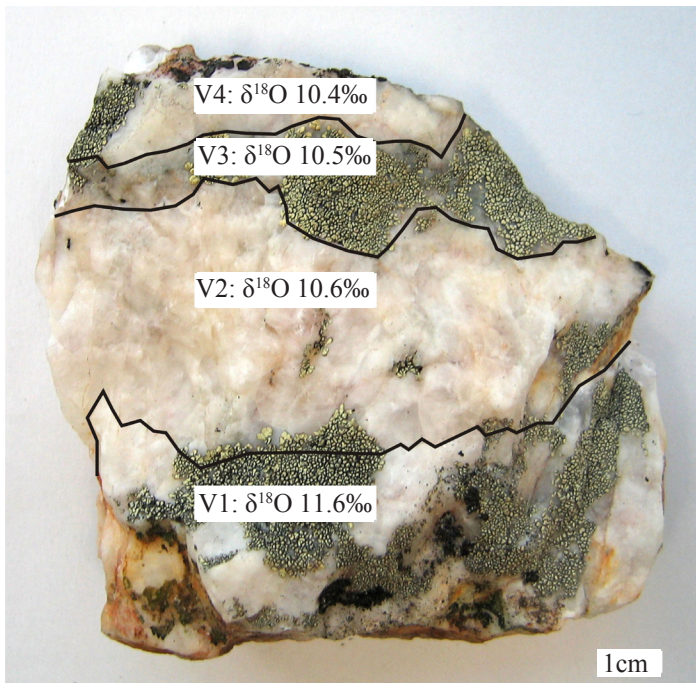


Figure 37. The $\delta^{18}\text{O}$ values from a Q2 quartz vein with four veins from the NICO giant quartz vein zone. Vein 1 (V1) is the initial vein next to the host rock, vein 4 (V4) is the last phase of veining.

The oxygen isotope results from the two drill-core calcite samples are very similar; with a $\delta^{18}\text{O}_{\text{calcite}}$ of +9.4 and +9.5‰ (Table 2). Two calcite samples from the NICO drill-core have a carbon isotope $\delta^{13}\text{C}_{\text{calcite}}$ value of -15.6‰ (Table 2).

3.3.2 Uranium Associated Giant Quartz Vein Zones

Fab Lake

Stable isotopes were analysed from Q1 and Q2 Fab Lake quartz and resulted in a small range of $\delta^{18}\text{O}_{\text{qtz}}$ values. Q1 mosaic quartz veins have an average $\delta^{18}\text{O}_{\text{qtz}}$ value of $+10.1 \pm 1.5\text{‰}$ (n = 2; Fig. 38). Similarly, Q2 late stage veins have a $\delta^{18}\text{O}_{\text{qtz}}$ average value of $+10.9 \pm 0.1\text{‰}$ (n = 2; Fig. 35).

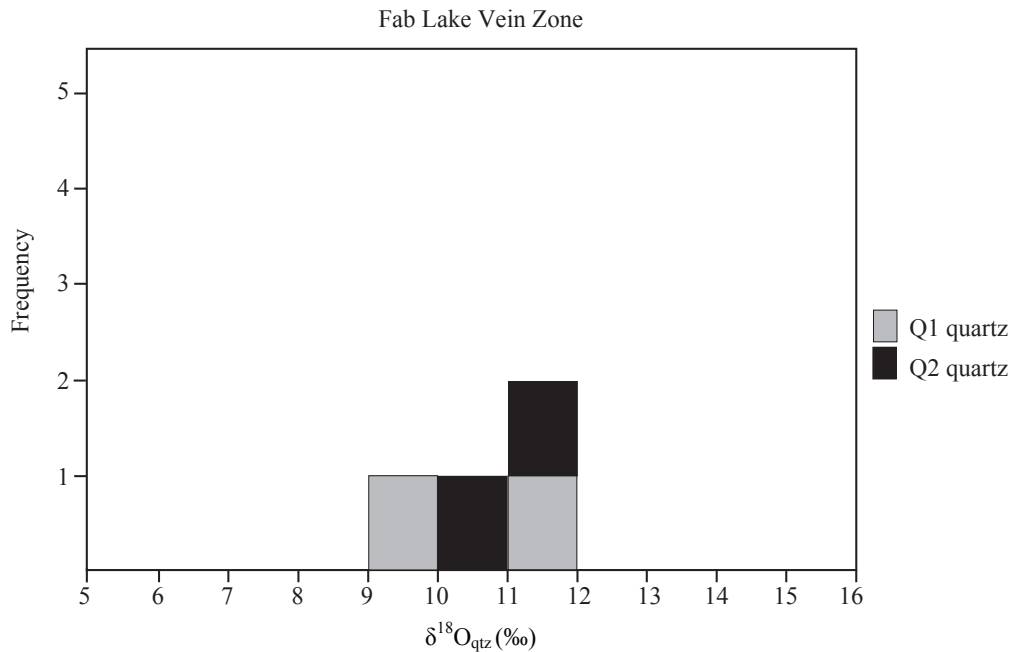


Figure 38. The $\delta^{18}\text{O}$ values from Q1 and Q2 quartz from the Fab Lake giant quartz vein zone.

Northern Wopmay fault

Two Q1 veins from the Northern Wopmay fault contain a $\delta^{18}\text{O}_{\text{qtz}}$ values of +8.1 and +8.8‰ whereas two Q2 veins have an average $\delta^{18}\text{O}_{\text{qtz}}$ value of $+9.0 \pm 0.4\text{‰}$ (Fig. 39). A Q3 vein contained a minor amount of pyrite and hematite mineralization; although unsuitable for microthermometry, the associated quartz had a $\delta^{18}\text{O}_{\text{qtz}}$ value of +9.9‰. The Northern Wopmay fault giant quartz vein zone contains the lowest average $\delta^{18}\text{O}_{\text{qtz}}$ values of all giant quartz vein zones.

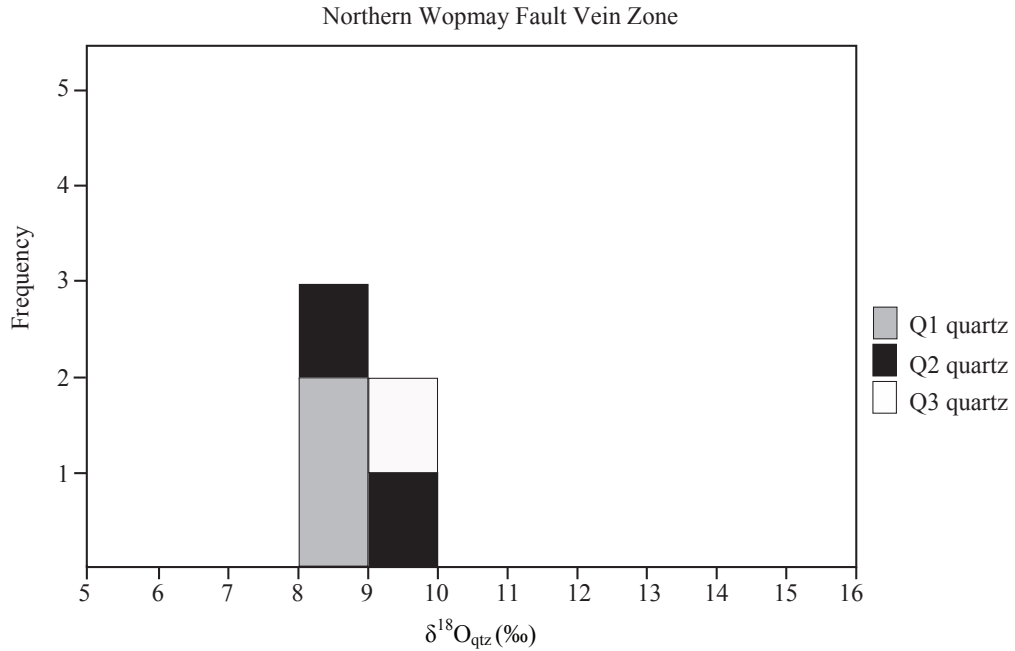


Figure 39. The $\delta^{18}\text{O}$ values from Q1, Q2 and Q3 quartz from the Northern Wopmay fault giant quartz vein zone.

3.3.3 Giant Quartz Vein Zones Isolated from Mineralization

“Arm” Lake

Oxygen isotope values were analysed on four Q2 veins from “Arm” Lake. The $\delta^{18}\text{O}_{\text{qtz}}$ values ranged from +9.3 to +11.0‰ with an average $\delta^{18}\text{O}_{\text{qtz}}$ value of $10.0 \pm 0.7\text{‰}$ (n = 4; Fig. 40).

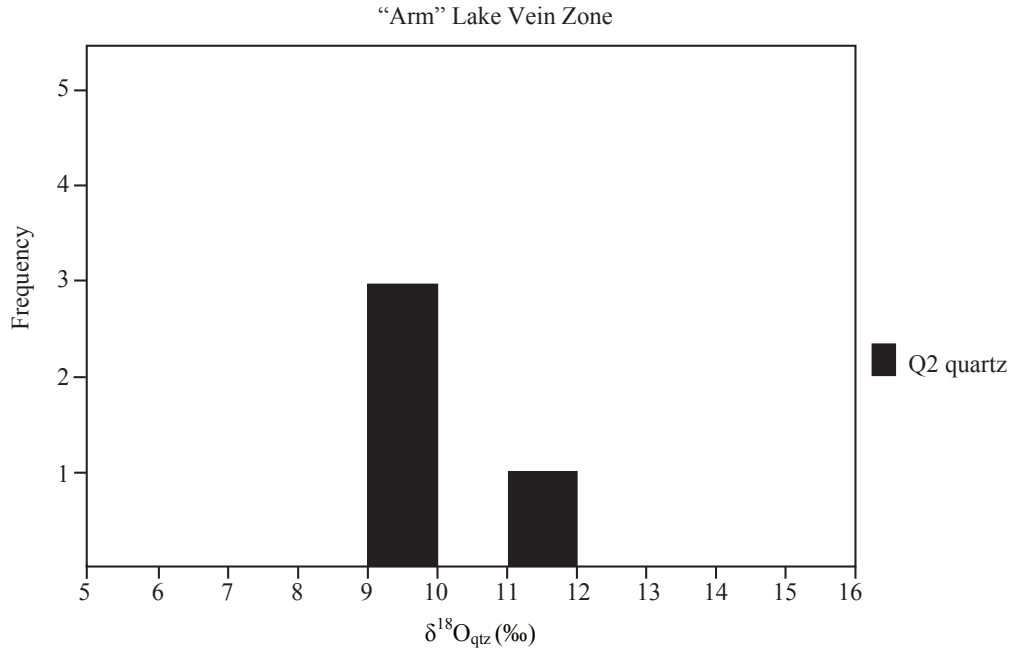


Figure 40. The $\delta^{18}\text{O}$ values from Q2 quartz from the “Arm” Lake giant quartz vein zone.

Hardisty Lake

Oxygen isotopic values from two paragenetically early Q1 vein from Hardisty Lake resulted in an average $\delta^{18}\text{O}_{\text{qtz}}$ value of $+10.9 \pm 0.6\text{‰}$ (Fig. 41). Q2 veins contained $\delta^{18}\text{O}_{\text{qtz}}$ values that ranged from $+11.2$ to $+12.2\text{‰}$ ($n = 6$; Fig. 41). A single Q3 vein resulted in a $\delta^{18}\text{O}_{\text{qtz}}$ value of 11.2‰ , similar to Q2 quartz (Fig. 41).

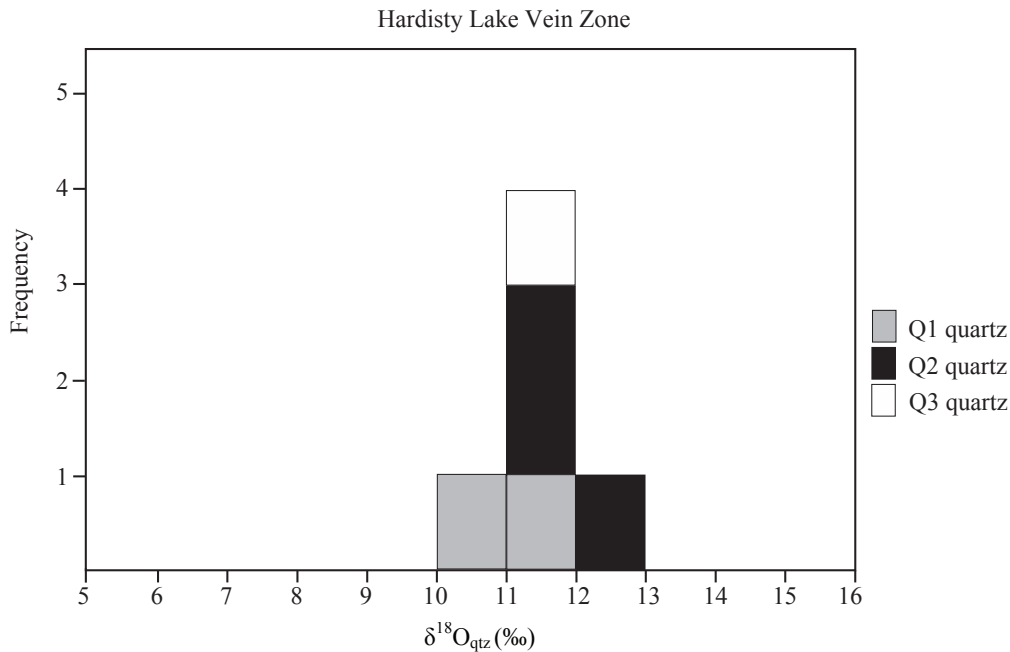


Figure 41. The $\delta^{18}\text{O}$ values from Q1, Q2 and Q3 quartz from the Hardisty Lake giant quartz vein zone.

Table 2. Summary of stable isotope data for all vein zones

Location	Sample	Vein Type	$\delta^{18}\text{O}$	$\delta^{18}\text{O}$	$\delta^{13}\text{C}$
			quartz Q1,2,3 ‰	calcite ‰	calcite ‰
NICO	06SBN003	Q1	9.7		
NICO	06SBN005B-V1	Q1	13		
NICO	06SBN001-E	Q2	9.6		
NICO	06SBN001-A	Q2	10.8		
NICO	06SBN002	Q2	11.6		
NICO	06SBN004-A	Q2	10.8		
NICO	06SBN005B-V2	Q2	14.7		
NICO	06SBN005B-V3	Q2	13.5		
NICO Drill-Core	06SBN98-31.60m-V1	Q2	11	9.5	-15.6
NICO Drill-Core	06SBN98-31.60m-V2	Q2	11	9.4	-15.6
NICO Drill-Core	06SBN98-122-41.81n	Q2	10.8		
NICO Drill-Core	06SBN98-122-81.81n	Q2	10.3		
Fab Lake	06SBF022-A	Q1	9		
Fab Lake	06SBF024-A	Q1	11.1		
Fab Lake	06SBF022-E	Q2	10.8		
Fab Lake	06SBF023-D	Q2	11		
Wopmay fault zone	06SBW053A	Q1	8.1		
Wopmay fault zone	06SBW055-2	Q1	8.8		
Wopmay fault zone	06SBW057	Q1, Q2	9.5		
Wopmay fault zone	06SBW050	Q2	8.7		
Wopmay fault zone	06SBW051A	Q2	9.2		
Wopmay fault zone	06SBW052F	Q3	9.9		
"Arm" Lake	06SBA034-A1	Q2	9.3		
"Arm" Lake	06SBA034-A2	Q2	9.6		
"Arm" Lake	06SBA035	Q2	9.9		
"Arm" Lake	06SBA032	Q2	11		
Hardisty Lake	06SBH031	Q1	10.5		
Hardisty Lake	06SBH029	Q1	11.3		
Hardisty Lake	06SBH026	Q2	11.2		
Hardisty Lake	06SBH028	Q2	11.1		
Hardisty Lake	06SBH030	Q2	9.8		
Hardisty Lake	06SBH032	Q2	12.2		
Hardisty Lake	06SBH032	Q2	12.2		
Hardisty Lake	06SBH027	Q2, Q3	11.5		
Hardisty Lake	06SBH025	Q3	11.2		

4 Discussion

4.1 Giant Quartz Vein Zones in the GBmz

4.1.1 Tectonic Control and Age of Giant Quartz Vein Zone Formation

Syntaxial veins and veins with symmetrical quartz growth from the host rock walls towards the vein centre suggest that the veins formed in an extensional environment (Ramsay and Huber 1983; Sibson et al. 1988). The hydraulic gradient in crustal fluids is influenced by permeability, porosity, and elasticity of crustal rock (Sibson 1996). The space between the walls of a vein is filled with quartz deposited more or less synchronously with progressive vein opening or incremental quartz deposition (Ramsay and Huber 1983). The thickness of each giant vein zone corresponds to the direction of strain, or maximum extension. The overall extension over the entire GBmz region due to the formation of the giant quartz veins can be calculated using Equation 4.1, which relates the length of the GBmz, including vein zones, to the length of the host rock prior to vein zone formation. For the calculation the measured thickness of each vein zone at surface or the reported thickness from previous mapping is used. If vein zone thickness is unknown, an average of 20m is used as a minimum thickness estimate. The calculation suggests that the regional extension of the GBmz, taken up by the giant quartz vein zones, is 0.0022 (Equation 4.1). This estimate is reasonable, and agrees with similar calculations carried out on other vein deposits, such as the Broken Hills gold mine in New Zealand (Nortje et al. 2006). Although these giant quartz vein zones may be some of the largest in the world, the associated regional extension is small, when compared with the entire width, over 450km, of the GBmz.

Equation 4.1 Extension Formula

$$e = S - 1 = (l - l_0)/l_0$$

Extension (e) is a one dimension ratio of the stretch (S) minus 1, which is equivalent to the length of area including the giant quartz vein zones (l) minus the original length of the host rock prior to the giant vein zones (l_0) divided by the original length of the host rock prior to the giant vein zones.

The giant quartz veins of the GBmz are emplaced along regional transcurrent faults and the regional north-east trend of most giant quartz veins along these regional faults provides evidence that all the giant vein zones across the GBmz formed at similar times. The regional transcurrent faulting of the GBmz has been estimated to have occurred between 1843 – 1810 Ma (Hildebrand et al. 1987) and provided structural permeability with extensional vein-fractures forming important conduits for large volume flow of hydrothermal fluids (Oliver 1996; Sibson 1996; Bons 2001; Pati et al. 2007). These faults are a result of brittle deformation, interpreted as part of a regionally extensive conjugate set of faults that resulted from east-west compression in the Wopmay orogen (Hildebrand et al. 1987). The east-west compression is suggested to be either a result of a

terminal collision of the Fort Simpson terrane with the Hottah terrane, after cessation of the Great Bear magmatic activity (Hildebrand et al. 1987) or docking of the Nahanni terrane to the west (Hoffman 1988). Although conclusive evidence is lacking, it has been suggested that most, if not all, strike-slip faulting existed, and/or was reactivated during the sedimentation of the ca. 1680 Ma Hornby Bay Group in the north (Gandhi and Paktunu 1989; Ross and Kerans 1989). Mapping of displaced rocks and cross cutting relationships suggest that faulting predates the 1400 ± 75 Ma Western Channel diabase (Wanless et al. 1970), the Muskox Intrusion and the Mackenzie dyke swarm (Hoffman 1980).

A maximum age of the giant vein zones is given by the veins cross cutting all the major rock units of the GBmz including a suite of granodiorite-monzogranite plutons, dated between 1858 – 1843 Ma (Hildebrand et al. 1987). The region has been tectonically stable since, except for the intrusion of diabase dykes (Gandhi et al. 2000). A minimum age estimate for the giant quartz veins comes from two vein zones that are cross cut by gabbroic dykes, termed “Hottah sheets”. These dykes have been dated by U-Pb at 780 Ma (Park et al. 1995; Gandhi et al. 2001; Harlan et al. 2003).

Gandhi et al. (2000) estimated that the giant quartz vein zones were formed ca. 1840 – 1700 Ma, but this is speculative. There have been a few attempts to date mineralization in some of the giant quartz vein zones, which provided mineralization ages younger than that of the Great Slave Supergroup evaporites. Radiometric ages have been reported for the U-Ni-Ag-Cu minerals within a giant quartz vein, and pitchblende within quartz veins resulted in a U-Pb age of 1445 ± 20 Ma (Jory 1964). Miller’s (1982) analysis of pitchblende north of Port Radium gave a mineralization age of 1500 ± 10 Ma. The Hardisty Lake and Sloan vein zone contain fault gouges through the vein zones, and this may indicate that the vein zones formed synchronously with regional faulting, and may agree with Gandhi’s (2000) estimate.

4.1.2 Quartz Textures and Mineralogy

Regionally, all the giant quartz vein zones across the GBmz contain similar quartz textures. The Q1 stockworks and quartz veins are the oldest veins at all the sampled locations; they are consistently made up of cloudy veins and multidirectional stockworks that commonly contain fine to medium grained quartz. Some cloudy stockwork veins proximal to base-metal mineralization (e.g. NICO, Sloan, and Northern Sloan Extension) are made up of massive, feathery and mosaic quartz. The fine grained nature of the quartz suggests that this quartz was deposited as metastable, amorphous silica (silica gel) or hydrous chalcedony (Fournier 1985; Sander and Black 1988; Dong et al. 1995; Hollinger and Mauk 2002). Oehler’s (1976) study of silica gels found that quartz was the only crystalline silica polymorph produced from silica gel, and there was an absence of intermediate crystalline polymorphs. This suggests either that quartz formed directly from silica gel or that any intermediate phases (e.g. cristobalite, keatite, or opal-CT) involved in the silica gel to quartz transformation were short-lived and became quartz almost immediately after they formed (Oehler 1976).

As well, experimental work by Carr and Fyfe (1958) and Bettermann and Liebau (1975) suggested that under peak P-T conditions of vein formation, conversion of amorphous silica to quartz might take a matter of tens or hundreds of hours, effectively instantaneous in geologic terms. The fluid inclusions within these veins may, therefore, adequately reflect environmental and chemistry conditions of the fluid or gel (Herrington and Wilkinson 1993). The Q1 quartz veins from the uranium-mineralized and non-mineralized vein zones do not contain evidence of a silica gel precursor or quartz recrystallization.

The second phase of veining, referred to as Q2 quartz veins, consists of a variety of quartz textures that include coxcomb, bladed and prismatic quartz. These textures result from the direct precipitation of quartz from fluids undergoing slow changes during quiescent conditions into open-space environments (Lindgren 1933; Fournier 1985; Dong et al. 1995; Hollinger and Mauk 2002).

SEM-CL images of some Q2 quartz show non-luminescing network-like quartz. This occurs in some samples from the Northern Wopmay fault and “Arm” Lake. This cross-hatched texture has also been described as dense networks of quasi-linear healed microcracks in other hydrothermal quartz SEM-CL studies (e.g. Boiron et al. 1992; Rusk and Reed 2008). This texture is indicative of quartz dissolution, resulting from corrosion of light-grey quartz along microfractures, followed by precipitation of dark-grey quartz in the corrosion cavities (Rusk and Reed 2008). Potential causes for dissolution of quartz are fluctuations in pressure, temperature and fluid composition, change in fluid pH, and fluid mixing (Rusk et al. 2008).

Zoned Q2 quartz exists within many giant vein zones, especially at Beaverlodge Lake, NICO, and Sue-Dianne. Zoned quartz crystals contain numerous bands rich in fluid inclusions, suggesting repeated periods of growth (Sander and Black 1988). Quartz that is zoned in transmitted light is usually complexly zoned when viewed with cathodoluminescence (Allan and Yardley 2007; Götze and Kempe 2008). Variations in cathodoluminescence intensity and wavelength are widely accepted to be a function of structural defects or chemical impurities (Allan and Yardley 2007), and these zones correspond directly to fluctuations in Al and Li concentration, with light-grey quartz possessing higher Al and Li concentrations within the quartz crystal lattice than dark-grey quartz. This correlation has been observed by Heaney (1994) to be “attributable to tetrahedral substitution of $[\text{SiO}_4]^0$ sites by $[\text{AlO}_4]^-$, accompanied by charge compensation by Li^+ in neighbouring interstitial sites”. As previously suggested, the SEM-CL zonation is likely derived from shifts in precipitation rate (Allan and Yardley 2007). Impurity concentrations (especially Al) in dynamic hydrothermal systems are largely influenced by variations in quartz precipitation rate, which may be a result of quartz solubility gradients (Rimstidt and Barnes 1980) driven by temperature and pressure changes during fluid ascent (Allan and Yardley 2007).

Locally, some of the Q2 veins from Sue-Dianne have feathery, milky-looking quartz, with abundant fluid and mineral (feldspar and hematite)

inclusions. This feathery quartz has been previously described as having a flamboyant-texture and may indicate crystallization from gelatinous amorphous silica (Dong et al. 1995; Hollinger and Mauk 2002). Small feldspar inclusions within feathery quartz resulted in up to four times the elemental concentrations of Al, K, Fe, Mn and Rb to that of clear quartz.

Most Q2 veins consist of primary epithermal quartz textures with primary fluid inclusions, and reflect direct precipitation from a fluid (Dong et al. 1995; Onasch and Vennemann 1995). Silica saturation fluctuations may result in zoned quartz crystals and this may be caused by decreased pressure upon fluid ascent through the fault structures (Rimstidt and Barnes 1980; Allan and Yardley 2007).

The late-stage Q3 veins are commonly made up of clear and fine grained subhedral quartz. The Q3 veins occur in all giant quartz vein zones, but mainly occur in vein zones near to base-metal mineralization. Late-stage Q3 veinlets are sporadically mineralized with copper sulfides \pm uranium, but only where the vein zone is proximal to ore-deposits or mineral showings. The formation of vein zones likely post-dates much of the mineralization found in the GBmz, and remobilization of local metals are occasionally found within late Q3 veins of the giant vein zones. For instance, the ore-zone at NICO parallels the host rock stratigraphy, and at an orientation unlike the orientation of the nearby giant quartz vein zone. These Q3 veins lack any indication of dissolution, precipitation from a silica gel, or boiling, during microscopy, SEM-CL or microthermometry. For crystals with no significant variations in SEM-CL zonation or trace element concentrations, continuous growth is suggested (Onasch and Vennemann 1995). The sporadically mineralized Q3 veins may be used as a diagnostic technique for finding mineralization within the GBmz, and this will be discussed presently.

In summary, the three phases of quartz vein paragenesis contain primary epithermal textures within each giant vein zone and contain variable textures but are similar to other giant quartz vein zones across the GBmz. It is likely that the vein zones were formed under a similar tectonic regime, with multiple fluid pulses and refracturing events that eventually formed the giant vein zones across the GBmz.

4.1.3 Pressure Estimates of Vein Formation and Isochores

The microthermometric data give a minimum estimate of the pressure and temperature conditions during quartz vein formation. Isochores are lines of specific density of fluid inclusions, and can be calculated for a range of pressure and temperature conditions from microthermometric data. In the absence of any evidence for phase separation (in which case a pressure correction is not necessary), an independent estimate of pressure or temperature is required to fix the trapping P and T of the inclusions (Roedder and Bodnar 1980). Equilibrium isotope geothermometry on NICO drill-core quartz and calcite veins could not be used to calculate temperature estimates, given that the veins did not form synchronously. There were no other mineral geothermometers available to constrain the temperature axes. The only study that offers independent pressure estimates and paleodepths of the Wopmay Orogen was recently published by

Ault et al. (2009). This study used apatite thermochronometry to assess the age and maximum burial depth of the Slave Craton and Wopmay Orogen during the Phanerozoic. Details of the analytical technique can be found in Ault et al. (2009). Their findings suggest that the Slave craton and Wopmay orogen reached a maximum burial depth of ≥ 3.3 km. This was followed by unroofing to near-surface conditions by earliest Cretaceous time, followed by a lesser episode of burial and unroofing in the Cretaceous through Early Eocene (Ault et al. 2009). The depth estimates from Ault et al. (2009) can be converted to equivalent lithostatic and hydrostatic pressure estimates, based on densities of average rock types. The average density of a sandstone, 2.15 g/cm^3 was used for the lithostatic pressure estimate, and the density of water, 1.00 g/mL , was used for the hydrostatic pressure limit (Natural Resources Canada 2008). A 3.3 km maximum burial estimate would translate to 696 bars (lithostatic) and 324 bars (hydrostatic) of pressure. However, the work by Ault et al. (2009) reflects burial during the Phanerozoic, which is most useful if the giant quartz veins were formed during the Phanerozoic; if the age of the veins is closer to ca. 1840 – 1700 Ma, as suggested by Gandhi et al. (2000), then this study may not reflect the maximum burial depths.

Isochores were constructed for each vein zone and type (e.g. Q1, Q2), especially if there was a significant difference in Th or salinity between vein-types from a single vein zone locality. The isochores constructed for each quartz vein zone are shown in Appendix F. Three isochores were constructed for each vein zone, based on the modal, maximum, and minimum Tt and the corresponding salinities. If a mode could not be established, the average Tt and salinity value were used. Pressure estimates by Ault et al. (2009) resulted in an increase of $40^\circ \pm 10^\circ \text{C}$ from the measured Th values (Appendix F). A 40°C increase in formation temperature is applied to all Th values; however, due to the inaccuracy of the estimate, it is difficult to provide a definitive conclusion about the fluid origin at this time; the fluid origins proposed in the discussion should be regarded as speculative.

4.2 Fluid Origin

4.2.1 Giant Quartz Vein Zones Spatially Associated with Mineralization

The fluid conditions and the paragenesis of vein growth and mineralization for the base-metal mineralized and uranium-associated vein zones are summarized in Figures 42 and 43, respectively. The fluid inclusion data show evidence for multiple pulses of fluids from various sources used to form the giant vein zones: a dilute fluid and a saline brine. The dilute fluid contains a salinity that is generally less than 5 wt. % NaCl eq.; however, the saline fluid can range 10 to 15 wt. % NaCl eq. within a single fluid inclusion assemblage, which is unlikely for a single fluid source. The range in fluid inclusion salinity may be the result of two (or more) fluids mixing, allowing the trapping fluid inclusions of variable salinities, as there is no evidence for boiling within the giant quartz vein zones.

Using the fluid inclusion Tt, to one standard deviation, and the pressure

estimates, using the density range between a sandstone and ice, the $\delta^{18}\text{O}$ value of the original hydrothermal fluid ($\delta^{18}\text{O}_{\text{fluid}}$) can be calculated, using the fractionation factor of Matsuhisa et al. (1979). Distinct pulses of a dilute and saline fluid likely formed the Q1 and Q2 veins near base-metal mineralization, and are similar in salinity and temperature to the quartz vein zones near uranium mineralization.

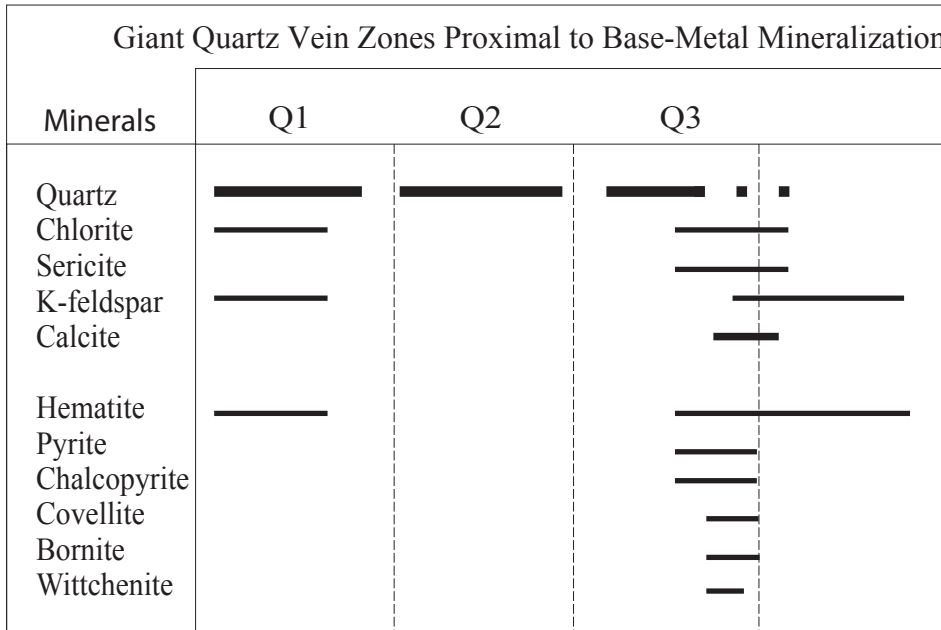


Figure 42. Paragenesis of quartz veins from vein zones associated with base-metal mineralization. Paragenesis line thickness is representative of mineral abundance.

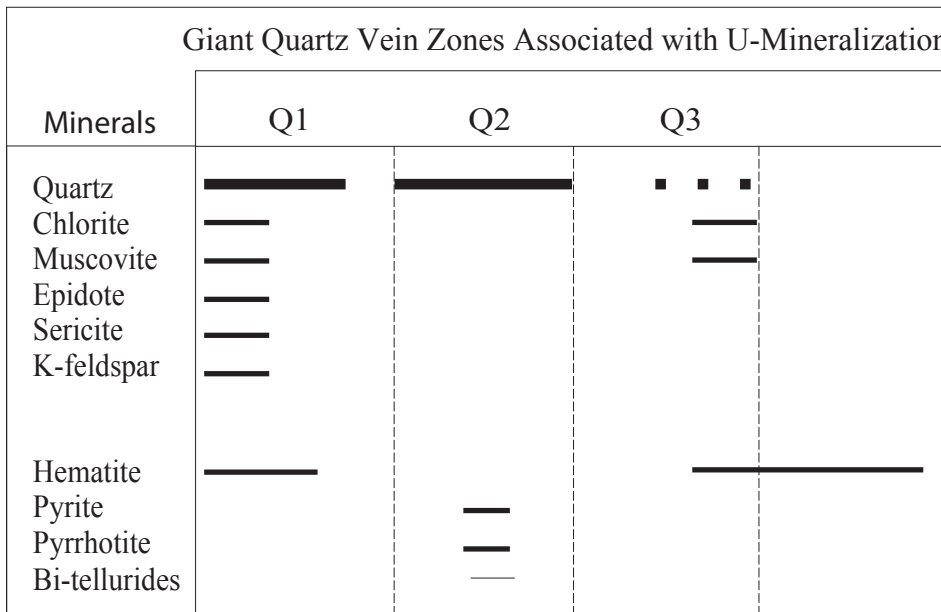


Figure 43. Paragenesis of quartz veins from vein zones associated with uranium mineralization or radioactive anomalies. Paragenesis line thickness is representative of mineral abundance.

Due to the range in salinity and temperatures calculated for the vein zones associated with base-metal mineralization or uranium mineralization, the calculated $\delta^{18}\text{O}_{\text{fluid}}$ values from Q1 quartz in mineralized (base-metal mineralized and uranium associated) vein zones are poorly constrained, and range from -16.5 to -6.0‰ (Appendix G). Similarly, the Q2 quartz veins proximal to mineralized locales have $\delta^{18}\text{O}_{\text{fluid}}$ values range from -15.5 to -5.0‰ (Appendix G).

The negative $\delta^{18}\text{O}_{\text{fluid}}$ values for the mineralized vein zones, along with the low salinity fluid inclusions (commonly less than 1.4 wt. % NaCl eq.) suggest that the dilute fluid in the veins is meteoric water which was heated to $>200^{\circ}\text{C}$. To attain these temperatures this fluid was likely circulated to depths between 5 and 8km (assuming a relatively high geothermal gradient of 30°C ; Lerner and Lerner 2003). The Tt in the uranium-associated vein zones increases from Q1 to Q2, and is likely the result of hotter, deeper-circulated meteoric fluids accessing the same fault structures that formed the Q2 veins.

Sue-Dianne, NICO and the Northern Sloan Extension contain small amounts of mineralization within late-stage Q3 quartz and calcite veins, in the form of copper sulfides. As well, there is copper sulfide mineralization within Q2 veins at Beaverlodge Lake. This late-stage mineralization within Q2 and Q3 quartz veins and late-stage calcite veins is likely the result of remobilization of ore-minerals from surrounding host rocks. Evidence for this locally derived mineralization within late-stage veins is the occurrence of sporadic mineralization from giant quartz vein zones located near to mineralized deposits. The fluid inclusions from Q3 veins proximal to base-metal mineralization and Q2 veins associated with uranium mineralization represent a fluid end-member that has high salinities and high temperatures necessary to precipitate small amounts of locally derived mineralization. The Q3 quartz veins from vein zones associated with base-metal mineralization have calculated $\delta^{18}\text{O}_{\text{fluid}}$ values that range from -4.0 to -9.0‰, based on weakly constrained pressure estimates by Ault et al. (2009) to find Tt values based on measured Th (Appendix G).

Late calcite vein samples of NICO drill-core were also often mineralized and had $\delta^{13}\text{C}_{\text{calcite}}$ values of -15.4 and -15.6‰, which are lower than average crustal carbon values (-7 to -5.5‰) and mantle values (-7 to -2‰) (Hoefs 1978; Ohmoto and Rye 1979; Deines et al. 1991). These data fall within the range expected for reduced C in sedimentary rocks, for instance, bituminous coal averages $\delta^{13}\text{C}$ of -25‰ (Faure and Mensing, 2005). Unfortunately, no other signs of biogenic carbonate have been seen within the drill core. Another potential carbon source could be metamorphic rocks (Schoell and Wellmer 1981), or Precambrian reduced carbon (Kerrick 1986); however, evidence for this interaction is absent.

Numerous veins from all locations, except for “Arm” Lake, Margaret Lake, and Q1 veins from Hardisty Lake, contain moderate salinity fluid inclusions (17 to 25 wt. % NaCl eq.). This saline fluid could be sourced from a nearby active magmatic system or derived from a sedimentary brine. Mumin et al. (2008) suggested that the giant quartz vein zones are the waning stages of a large magmatic system; if this is the case, the high salinity fluid may be the result of intermittent input from a magmatic source. However, the stable isotope

$\delta^{18}\text{O}_{\text{fluid}}$ values from this study do not suggest a magmatic fluid source, but rather, meteoric water. If magmatic fluid was not a factor in the formation of the giant quartz vein zones, the saline fluid may be derived from either a deep crustal fluid or the interaction of meteoric water with evaporites.

The giant quartz vein zones appear to have a genetic relationship with major trans-crustal structures, since most giant quartz vein zones occur, for the most part, along the western margin of the GBmz or parallel to the Wopmay fault. These terrain boundaries may have provided a conduit for a deep-seated saline fluid. Another saline fluid source may be meteoric fluids interacting with thick sequences of well-preserved unmetamorphosed sedimentary rocks of the Great Slave Supergroup, ca. 2300 – 1790 Ma along the East Arm graben of Great Slave Lake (Stanworth and Badham 1984). The Great Slave Supergroup contains abundant evidence for the former presence of evaporites in the section of sequence that was deposited within 30° of the palaeoequator (Stanworth and Badham 1984). Evidence of evaporites comes from beds containing various pseudomorphs after gypsum and halite, as well as evaporate collapse breccias, contorted laminae and salt diapirs (Stanworth and Badham 1984). Hydrothermal fluid interaction with evaporites may have resulted in the saline brine observed within fluid inclusions of quartz veins in many of the giant quartz vein zone locations. However, if such interaction with evaporitic units occurred, or if deep crustal fluids assisted in the formation of the giant quartz vein zones can only be speculated upon and further analyses are needed to clarify this issue.

Whatever the origin of the salinity, chlorine-rich solutions are capable of transporting metals in the presence of low concentrations of dissolved sulfide ions (Skinner 1979), such as within Q3 veins at Sue-Dianne. To form these intermittently mineralized Q3 veins, cooling of the saline fluid or dilution of saline fluids by meteoric waters near the surface may change the pH sufficiently to destroy these complexes and initiate deposition of base-metal sulfides (O'Neil and Silberman 1974; Hemley et al. 1991).

In summary, the giant vein zones associated with mineralization contain fluid inclusions that contain variable salinity and temperatures distinct to the vein. A 5 to 8km depth meteoric fluid may be trapped in the low salinity fluid inclusions, while other veins may be the result of a brine, which was possibly sourced from proximal evaporites. The Great Slave Supergroup evaporites are located along the Northeastern arm of Great Slave Lake, and would not be considered proximal to most giant quartz vein zone locations. However, these or other unknown evaporites nearer to the GBmz, may result in fluid inclusions trapping a moderate to high salinity fluid. Another potential brine fluid source is deep crustal fluids circulating at depth to the GBmz. The hottest saline fluids are from inclusions within mineralized Q3 quartz veins; and this fluid may have leached metals from the local ore zones at Sue-Dianne and deposited them in the giant vein zone.

4.2.1.1 Relationship to Mineralization in the GBmz

It has been previously suggested, that the giant quartz veins may be the waning phase of mineralizing hydrothermal fluid activity associated with the formation of the deposits at NICO and Sue-Dianne (Mumin et al. 2008). This study shows that the giant quartz vein zones cross-cut the host rocks and are younger than the mineralized deposits proximal to a few vein zones. The giant quartz vein zones therefore may only contain small amounts of remobilized ore from nearby proximal deposits. Although there have been a limited number of studies on other epithermal deposits in the GBmz, there have been two stable isotope studies carried out on the Great Bear Lake silver deposits (e.g. Camsell River and Echo Bay districts).

The deposits located in the Camsell River and Echo Bay districts include proximal large vein zones, and mineralization consists of native silver associated with Ni-, Co-, and Fe-arsenides and sulfides, and pitchblende (Changkakoti et al. 1986). The study by Changkakoti et al. (1986) indicated that during early stages of mineralization, magmatic water was predominant, while during late stage mineralization, the influence of meteoric water became more pronounced (Changkakoti et al. 1986). Robinson and Ohmoto (1973) examined vein-hosted ore and concluded that evolved sea water leached metals from the Echo Bay volcanic rocks and deposited them in the veins; and that later circulating meteoric water was active, as suggested by the isotopic values of calcite. Although neither study included the nearby giant vein zones, Robinson and Ohmoto (1973) suggested that the mineralized veins contain fluid inclusions that show evidence of saline fluids mixing with low temperature meteoric water.

A study by the Geological Survey of Canada investigated two giant quartz veins from the GBmz associated with uranium mineralization (Gandhi et al. 2000). The giant quartz vein zones, named Crowfoot and Ted, are located 20km north and 5km northwest, respectively, of the Rayrock mine. Rayrock is a giant quartz vein zone that consisted of uranium and copper-sulfide mineralization that produced 150t of uranium from 1956 to 1958 (Gandhi et al. 2000). This preliminary study by Gandhi et al. (2000) concluded that the proximal quartz vein zones are likely a result of two or more fluids mixing and required multistage development to produce the numerous quartz veins at Crowfoot and Ted, although they did not suggest possible fluid origins. The U-associated giant quartz vein zones of Beaverlodge Lake, Fab Lake and Northern Wopmay fault contain similar low and high salinity fluids with similar Th to the Gandhi et al. (2000) study. The giant vein zones associated with uranium mineralization at Beaverlodge Lake, Fab Lake and Northern Wopmay fault, show that these vein zones also formed by two, or more, distinct fluids with access to the same fault structures.

4.2.2 Giant Quartz Vein Zones Isolated from Mineralization

The northeast trending Hardisty Lake, Margaret Lake, and the northwest trending “Arm” Lake giant quartz vein zones have no known occurrences of mineralization or ore-mineral showings within or proximal to the veins. Three types of veins exist: Q1, Q2 and Q3, similar to vein zones associated with base-metal or uranium

mineralization, and are assumed to have formed under similar pressure constraints (Ault et al. 2009). However, these vein zones formed from fluids with a distinct chemistry from the fluids that formed the mineralized vein zones (Fig. 44)

Giant quartz vein zones isolated from mineralization are formed from fluids with low salinity and high temperature; unlike base-metal associated vein zones, some of these giant quartz vein zones, “Arm Lake, Margaret Lake and Q1 Hardisty Lake, do not show evidence for a saline fluid. The calculated $\delta^{18}\text{O}$ of the original fluid ranges from -12.0 to -4.0‰, based on pressure estimates by Ault et al. (2009; Appendix F). In comparison to giant quartz vein zones located near mineralized deposits, the non-mineralized veins are made from fluids with a higher Th and lower salinity. The temperature of this fluid suggests circulation of a meteoric fluid to 6 to 8km depth, based on Tt, weakly constrained pressure constraints by Ault et al. 2009, and assuming a geothermal gradient of 30°C/km (Lerner and Lerner 2003).

The temperatures of the non-mineralized vein zones decrease during paragenesis, with fluid inclusions from Q1 quartz having the highest average Th, followed by Q2 and Q3 quartz. The lack of mineralization within these vein zones may be the result of the fluids’ inability to leach metals from the host-rocks due to a lack of Cl⁻ ions to form base-metal chloride complexes (Skinner 1979; Barnes 1979). The findings of this study show that the fluids for giant quartz vein zones isolated from mineralization have fluid inclusions with high Th and low salinity, likely originated as a deeply circulated meteoric fluid.

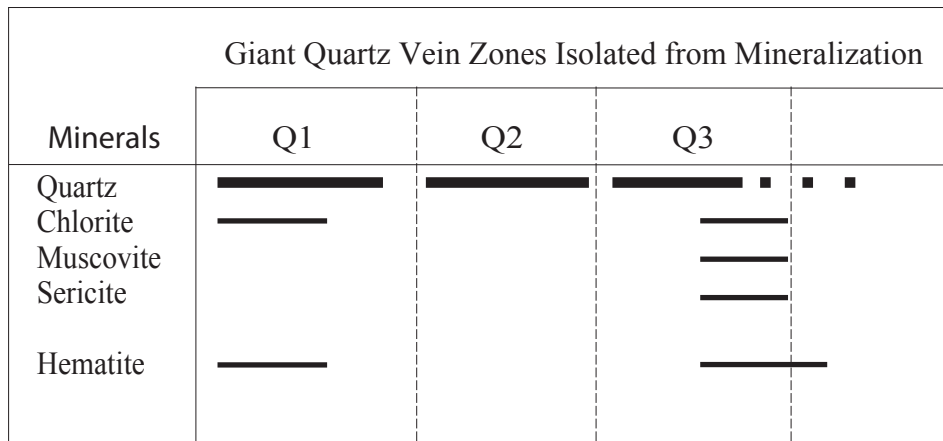


Figure 44. Paragenesis of quartz veins from vein zones not associated with mineralization or proximal mineral showings. Paragenesis line thickness is representative of mineral abundance.

4.3 Epithermal Systems

The term epithermal was initially defined by Lindgren (1933) to include a broad range of precious- and base-metal, mercury, and stibnite deposits formed from aqueous fluids at low temperatures (<200°C) and down to 2km depth. Mumin et al. (2008) suggests that the giant quartz vein zones are a late epithermal system found throughout the GBmz. In this study we consider that the veins formed in the epithermal environment, although the giant quartz vein zones were formed at hotter temperatures than most classic epithermal systems. Work done by Heald et al. (1987) divided epithermal deposits into two main types, based on ore, gangue and alteration mineral assemblages, as well as size, temperatures of mineral deposition, chemical composition of fluids, origin(s) of fluids, paleodepth estimates and regional geological setting.

High sulfidation epithermal deposits, also referred to as acid-sulfate type, form in the root zones of volcanic domes from acid waters that contain residual magmatic volatiles (Heald et al. 1987). High sulfidation deposits contain high-sulfidation-state minerals (e.g. enargite, tennantite and covellite) and advanced argillic alteration minerals (e.g. pyrophyllite and kaolinite), which Thompson et al. (1986) suggested were characteristic of magmatic fluid sources. Evidence for this type of epithermal deposit is lacking in the giant quartz vein zones of the GBmz. Fluids of many high-sulfidation deposits consist of a magmatic fluid source, with a lesser meteoric component as evidenced from fluid inclusions (Bethke et al. 2005), oxygen and hydrogen isotopes (Arribas 1995), and sulfur isotopes (Hayba et al. 1985).

Low sulfidation epithermal deposits, also called adularia-sericite type, are structurally complex and commonly associated with silicic to intermediate volcanic rocks (Hayba et al. 1985). The mineralogy of the low sulfidation deposits are characterized by the presence of vein adularia and sericite; chlorite is also common, with ore mineralogy comprised of native gold, native silver and electrum (Hayba et al. 1985). Fluid composition ranges from 0 to 13 wt. % NaCl eq.; the higher salinity fluid may be a factor in the ability to transport base-metals (Skinner 1979; Henley 1985). Heald et al. (1987) shows examples of low sulfidation deposits that form when “surficial waters mix with deeper, heated, saline waters in a lateral flow regime”. Two categories of low sulfidation deposits exist; Type I consists of very low salinity (0.2 - 0.5 wt. %) fluids from geothermal systems, such as neutral-pH hot springs and mud pools, the second type, Type II, consists of moderate salinity (10 - 20 wt %) fluids (Hedenquist and Lowenstern 1994). Although the giant quartz vein zones are often not mineralized, they share many structural, host rock and fluid characteristics of low sulfidation epithermal deposits.

The giant quartz vein zones of the GBmz demonstrate characteristics of both Type I and Type II low sulfidation epithermal deposits as defined by Hedenquist and Lowenstern (1994). The alteration mineralogy of the giant quartz veins relates to the low sulfidation type due to the presence of hematite, chlorite and sericite within the veins, and K-feldspar, silicic and chloritic alteration of the host rocks. Textures of quartz, especially Q2 quartz, are described as primary

epithermal textures by Dong et al. (1995). The majority of previous stable isotope studies carried out on epithermal deposits result in relatively low $\delta^{18}\text{O}$ values, indicating a meteoric water component to the ore fluid (O'Neil and Silberman 1974), similar to the giant quartz vein zones of the GBmz. Mineralized vein zones contain fluid inclusions of low salinity meteoric fluids (Type I) as well as moderate salinity fluids (Type II) forming low sulfidation epithermal systems across the GBmz.

The giant quartz vein zones are a late regional fluid event that likely occurred shortly after regional faulting. It has been suggested that the giant quartz veins are a low-temperature end-member of a larger hydrothermal continuum (which includes IOCG and porphyry Cu-like systems) in the GBmz (Mumin et al. 2007; Mumin et al. 2008). Most of the veins within this study were formed from either meteoric water or a saline brine in intermittent pulses during multiple periods of quartz vein formation based on cross-cutting relationships. Although the saline fluid source is unknown, it is found mostly in vein zones proximal to mineralization. A hot saline fluid appears to be a requirement to mobilize ore from the proximal mineralization (e.g. NICO and Sue-Dianne), and this is evidenced by late-stage Q3 base-metal mineralized veinlets within the giant vein zones. Without better age constraints, it is not possible to assess if some or any of the giant quartz vein zones are genetically related in any way to the IOCG deposits within the GBmz as described by Mumin et al. (2007; 2008).

5 Conclusions

- Numerous giant quartz vein zones are located along regional transcurrent NE, NW, and N trending transcurrent faults that occur across the entire GBmz.
- The giant quartz vein zones contain characteristics of Type I and II low sulfidation epithermal deposits, based on alteration, quartz morphology and chemistry.
- Most quartz vein textures consist of primary epithermal textures. Some Q1 stockworks and rare Q2 quartz veins contain textural evidence for recrystallization and precipitation as a silica gel; this mainly occurs with giant quartz vein zones spatially located near areas of mineralization.
- Base-metal sulfides are present within Q3 veins; these veins contain fluid inclusions with the highest Tt of all fluid inclusions measure, with a high salinity.
- Sporadic mineralization of Q3 veins are likely remobilized from local deposits nearby.
- Brines as well as meteoric waters formed the giant quartz vein zones proximal to base-metal or uranium mineralization. Variation in fluid inclusion salinity may be a result of fluid mixing.
- Giant quartz vein zones isolated from mineralization, excluding a Q2 Hardisty Lake vein, contains fluid inclusions with low salinity and high Th, and likely formed from deeply circulated meteoric water. The low salinity and related lack of chloride metal complexing agents may result in the barren nature of these veins.
- All giant quartz vein zones contain similar $\delta^{18}\text{O}_{\text{qtz}}$ values that result in a meteoric water signature.

6 Future Research and Implications for Exploration

Future research on the giant quartz vein zones should attempt to constrain the age of vein zone formation. As well, an investigation of halogens and chlorine isotopes within the moderate to high salinity fluid inclusions of base-metal and uranium-associated vein zones may help determine the Cl^- origin, and whether the salinity in the fluids that formed the giant vein zones was in fact derived from sediments (e.g. interacted with evaporites within the Great Slave Supergroup), or perhaps of a magmatic origin (Yardley et al. 2000).

The giant quartz vein zones could aid exploration by mining companies. The late-stage Q3 veins that are sporadically mineralized with base-metal sulfides (pyrite, chalcopyrite, hematite) often are proximal to ore-bearing deposits (e.g. NICO, Sue-Dianne, Rayrock). Mining companies may use the giant quartz vein zones, more specifically, quartz veins with sporadically mineralized Q3 veins, as a 'first-pass' exploration. Finding small amounts of locally remobilized ore within Q3 veins should alert mining companies to the necessity for more detailed exploration in that area. Although the giant quartz vein zones themselves are not significantly mineralized, the late-stage Q3 veins may indicate potential mineralization in close proximity to the giant quartz vein zones.

7 References

- Ault AK, Flowers RM, Bowring SA (2009) Phanerozoic burial and unroofing history of the western Slave craton and Wopmay orogen from apatite (U-Th)/He thermochronometry. *Earth and Planetary Science Letters* 284:1-11
- Allan MM, Yardley BWD (2007) Tracking meteoric infiltration into a magmatic-hydrothermal system: A cathodoluminescence, oxygen isotope and trace element study of quartz from Mt. Leyshon, Australia. *Chemical Geology* 240:343-360
- Arribas A Jr (1995) Characteristics of high-sulfidation epithermal deposits, and their relation to magmatic fluid. Mineralogical Association of Canada, Short Course Series 23:419-454
- Barnes HL (1979) Solubility of ore minerals. In Barnes HL, ed.2, *Geochemistry of Hydrothermal Ore Deposits*: New York, Wiley Interscience Publication:404-460
- Badham JPN, Stanworth CW (1977) Evaporites from the lower Proterozoic of the East Arm, Great Slave Lake. *Nature* 268:516-158
- Belkin HE (1994) Microthermometric Investigation: Th and Tm. Practical and theoretical aspects. In: De Vivo B, Frezzotti MI (Eds.) *Fluid inclusions in minerals: methods and applications*. Pontignano (Siena): Short course of the IMA working group "Inclusions in minerals". Virginia Polytechnic Institute and State Univ. Press, Blacksburg, VA:7-25
- Bethke PM, Rye RO, Stoffregen RE, Vikre PG (2005) Evolution of the magmatic-hydrothermal acid-sulfate system at Summitville, Colorado: integration of geological, stable-isotope, and fluid-inclusion evidence. *Chemical Geology* 215:281-315
- Bettermann P, Liebau F (1975) The transformation of amorphous silica to crystalline silica under hydrothermal conditions. *Contributions to Mineralogy and Petrology* 53:23-36
- Bodnar RJ (1992) Revised equation and table for determining the freezing point depression of H₂O-NaCl solutions. *Geochimica et Cosmochimica Acta* 57:683-684
- Bodnar RJ (1993) Revised equation and table for determining the freezing point depression of H₂O-NaCl solutions. *Geochimica et Cosmochimica Acta* 57:683-684
- Bodnar RJ (1994) Synthetic fluid inclusions; XII, The system H₂O-NaCl.

- Experimental determination of the halite liquidus and isochores for a 40 wt% NaCl solution. *Geochimica et Cosmochimica Acta* 58(3):1053-1063
- Bons PD (2001) The formation of large quartz veins by rapid ascent of fluids in mobile hydrofractures. *Tectonophysics* 336(1-4):1-17
- Borrok DM, Kesler SE, Boeh RH (1998) The Vergenoeg magnetite-fluorite deposit, South Africa: Support for a hydrothermal model for massive iron oxide deposits. *Economic Geology* 93:564-586
- Brown PE (1985) Chapter 7: Fluid inclusion modeling for hydrothermal systems. In: *A Practical Guide to Fluid Inclusions Studies* (eds) Blackie, Glasgow 7:151-171
- Carr RM, Fyfe WS (1958) Some observations on the crystallization of amorphous silica. *The American Mineralogist* 43:908-916
- Cook FA, van der Velden AJ, Hall KW, Roberts BJ (1999) Frozen subduction in Canada's Northwest Territories: Lithoprobe Deep Lithospheric Reflection Profiling of the Western Canadian Shield. *Tectonics* 18(1):1-24
- Changkakoti A, Morton RD, Gray J, Yonge CJ (1986) Oxygen, hydrogen, and carbon isotopic studies of the Great Bear Lake silver deposits, Northwest Territories. *Canadian Journal of Earth Sciences* 23:1463-1469
- Clayton RN, Epstein S (1958) The relationship between O^{18}/O^{16} ratios in coexisting quartz, carbonate, and iron oxides from various geological deposits. *Journal of Geology* 66(4):352-373
- Clayton RN, Mayeda TK (1963) The use of bromine pentafluoride in the extraction of oxygen from oxides and silicates for isotopic analysis. *Geochimica et Cosmochimica Acta* 27(1):43-52
- Deines P, Harris JW, Gurney JJ (1991) The carbon isotopic composition and nitrogen content of lithospheric and asthenospheric diamonds from the Jagersfontein and Koffiefontein kimberlites, South Africa. *Geochimica et Cosmochimica Acta* 53:2615-2626
- Dong G, Morrison G, Jaireth S (1995) Quartz textures in epithermal veins, Queensland: classification, origin and implication. *Economic Geology* 90:1841-1856
- Easton RM (1981) Stratigraphy of the Akaitcho Group and the development of an early Proterozoic continental margin, Wopmay orogen, Northwest Territories, Canada. *Geological Survey of Canada* 81-10:79-95

- Faure G, Mensing TM (2005) Chapter 26: Hydrogen and Oxygen. Isotopes – Principles and Applications. Third Edition. John Wiley & Sons, Inc. Hoboken, New Jersey:716-718
- Fitch TJ (1972) Plate convergence, transcurrent faults, and internal deformation adjacent to southeast Asia and the western Pacific. *Journal of Geophysical Research* 77(23):4432-4460
- Fournier RO (1985) Chapter 3: The Behavior of Silica in Hydrothermal Solutions. *Reviews in Economic Geology*:45-61
- Furnival GM (1935) The large quartz veins of Great Bear Lake, Canada. *Economic Geology* 30(8):843-859
- Gandhi SS (1988) Volcano-plutonic setting of U-Cu bearing magnetite veins of FAB claims, southern Great Bear magmatic zone, Northwest Territories. In *Current Research, Geological Survey of Canada* 88-1C:177–187
- Gandhi SS (1994) Geological setting and genetic aspects of mineral occurrences in the southern Great Bear magmatic zone, Northwest Territories. *Geological Survey of Canada Bulletin, Report* 475:63-96
- Gandhi SS, Carriere JJ, Prasad N (2000) Implications of a preliminary fluid-inclusion study of giant quartz veins of the southern Great Bear magmatic zone, Northwest Territories. *Geological Survey of Canada* 2000-C1(13):1-13
- Gandhi SS, Mortensen JK, Prasad N, van Breemen O (2001) Magmatic evolution of the southern Great Bear continental arc, northwestern Canadian Shield: geochronological constraints. *Canadian Journal of Earth Sciences* 38(5):767-785
- Gandhi SS, Paktunc AD (1989) Au, Pt and Pd in pitchblende and copper sulphide veins at the Rah, Far and Jaciar prospects, northern Bear Province, Northwest Territories. *Geological Survey of Canada Current Research, Part C*:147-158
- Gandhi SS, Prasad N, Charbonneau BW (1996) Metallogenic evolution of the southern Great Bear magmatic zone. *Exploration Overview* 1995: 3.14-3.16
- Goad RE, Mumin AH, Duke NA, Neale KL, Mulligan DL (2000a) Geology of the Proterozoic iron oxide-hosted NICO cobalt-gold-bismuth and Sue-Dianne copper-silver deposits, southern Great Bear magmatic zone, Northwest Territories, Canada. In: Porter TM (eds) *Hydrothermal Iron Oxide Copper-Gold & Related Deposits: A Global Perspective*. PGC Publishing, Adelaide 1:249-267
- Goad RE, Mumin AH, Duke NA, Neale KL, Mulligan DL, Camier, WJ (2000b)

The NICO and Sue-Dianne Proterozoic, iron oxide-hosted, polymetallic deposits, Northwest Territories; application of the Olympic Dam model in exploration. *Exploration and Mining Geology*, Canadian Institute of Mining, Metallurgy and Petroleum 9(2):123-140

Götze J, Kempe U (2008) A comparison of optical microscope- and scanning electron microscope-based cathodoluminescence (CL) imaging and spectroscopy applied to geosciences. *Mineralogical Magazine* 74(4):909-924

Harlan SS, Heaman L, LeCheminant AN, Premo WR (2003) Gunbarrel mafic magmatic event: A key 780 Ma time marker for Rodinia plate reconstructions. *Geology* 31(12):1053-1056

Hayba DO, Bethke PM, Heald P, Foley NK (1985) Geologic, mineralogic, and geochemical characteristics of volcanic-hosted epithermal precious-metal deposits. In Berger BR, Bethke PM (1985) *Geology & Geochemistry of Epithermal Systems*. *Reviews in Economic Geology* 2:129-167

Heald P, Foley NK, Hayba DO (1987) Comparative Anatomy of Volcanic-Hosted Epithermal Deposits: Acid-Sulfate and Adularia-Sericite Types. *Economic Geology* 82(1):1-26

Heaney PJ (1994) Structure and chemistry of the low-pressure silica polymorphs. *Reviews in Mineralogy* 29:1-40

Hedenquist JW, Lowenstern JB (1994) The role of magmas in the formation of hydrothermal ore deposits. *Review Article Nature* 370:519-527

Heinrich CA (2007) Fluid-fluid interactions in magmatic-hydrothermal ore formation. *Reviews in Mineralogy & Geochemistry* 65:363-387.

Hemley JJ, Cygan GL, Robinson GR, D'Angelo WM (1991) Hydrothermal ore-forming processes in the light of studies in rock-buffered systems: I. Iron-copper-zinc-lead sulphide solubility relations. *Economic Geology* 87:1-22

Henley RW (1985) The geothermal framework of epithermal deposits. *Reviews in Economic Geology* 2:1-24.

Herrington RJ, Wilkinson JJ (1993) Colloidal gold and silica in mesothermal vein systems. *Geology* 21:539-542

Hildebrand RS (1981) Early Proterozoic Labine Group of Wopmay Orogen; remnant of a continental volcanic arc developed during oblique convergence. *Geological Survey of Canada* 81-10:133-156

- Hildebrand RS (1983) Early Proterozoic folded cauldrons of the Great Bear magmatic zone, Wopmay Orogen, Canada. *American Geophysical Union* 64(45):873
- Hildebrand RS (1986) Kiruna-type deposits; their origin and relationship to intermediate subvolcanic plutons in the Great Bear magmatic zone, Northwest Canada. *Economic Geology* 81:640-659
- Hildebrand RS, Bowring SA (1984) Continental intra-arc depressions: A nonextensional model for their origin, with a Proterozoic example from Wopmay orogen. *Geology* 12(2):73-77
- Hildebrand RS, Bowring SA, Housh T (1990) The medial zone of Wopmay Orogen, District of Mackenzie. *Geological Survey of Canada, Report 90-1C*:167-176
- Hildebrand RS, Hoffman PF, Bowring SA (1987) Tectono-magmatic evolution of the 1.9-Ga Great Bear magmatic zone, Wopmay orogen, northwestern Canada; tectonic controls on magma chemistry. *Journal of Volcanology and Geothermal Research* 32(1-3):99-118
- Hildebrand RS, Roots CF (1985) Geology of the Riviere Grandin map area (Hottah Terrane and western Great Bear magmatic zone), District of Mackenzie. *Geological Survey of Canada* 85-1A:373-383
- Hoffman P (1973) Evolution of an early Proterozoic continental margin; the Coronation Geosyncline and associated aulacogens of the northwestern Canadian Shield. *Philosophical Transactions of the Royal Society of London, Series A: Mathematical and Physical Sciences* 273(1235):547-581
- Hoffman PF (1980) Conjugate transcurrent faults in north-central Wopmay orogen (early Proterozoic) and their dip-slip reactivation during post-orogenic extension, Hepburn Lake Map Area, District of Mackenzie. *Geological Survey of Canada* 80-1A:183-185
- Hoffman PF (1988) United plates of America, the birth of a craton: early Proterozoic assembly and growth of Laurentia. *Annual Review of Earth and Planetary Sciences* 16:543-603
- Hoffman PF, McGlynn JC (1977) Great Bear batholiths; a volcanic-plutonic depression. *Geological Association of Canada* 16:169-192
- Hoefs J (1978) Some peculiarities in the carbon isotope composition of "juvenile" carbon. *DSIR Bulletin* 220:181-184

Hollinger E, Mauk JJ (2002) Textures, mineralogy and geochemistry of low-sulfidation Au-Ag epithermal veins at the Favona Deposit, Waihi, New Zealand. 150 Years of Mining: Publication Series – Australasian Institute of Mining and Metallurgy 6/2002:223-228

INAC (2009) Indian and Northern Affairs Website. <http://www.ainc-inac.gc.ca/index-eng.asp>. Last modified 28/01/2009. Last visited 01/01/2009.

Jackson VA (2007) Preliminary geologic map of part of the Southern Wopmay Orogen (parts of NTS 86B and 86C; 2006 updates). Northwest Territories Geoscience Office, NWT Open Report 2007-005 Map, scale 1:100,000:1

Jolliffe AW (1935) Pitchblende in a giant quartz vein, Beaverlodge Lake, Northwest Territories. Doctoral Thesis, Princeton University, Princeton, NJ, United States.

Jory LT (1964) Mineralogical and isotopic relations in the Port Radium pitchblende deposits, Great Bear Lake, Canada. Thesis Doctoral: California Institute of Technology, Pasadena, CA. Within Robinson BW, Badham JPN (1974) Stable Isotope Geochemistry and the Origin of the Great Bear Lake Silver Deposits, Northwest Territories, Canada. Canadian Journal of Earth Sciences 11:698-711

Kerrick R (1986) Fluid infiltration into fault zones: chemical, isotopic, and mechanical effects. Pure and Applied Geophysics 124(1-2):225-268

Kidd DF (1933) Great Bear Lake, McTavish Arm between Richardson Island and Hornby Bay, District of Mackenzie, NWT. Geological Survey of Canada, "A" Series Map 286A:1

Landtwing MR, Pettke T (2005) Relationships between SEM-cathodoluminescence response and trace-element composition of hydrothermal vein quartz. American Mineralogist 90:122-131

Lee J (2009) Personal Communication. University of Queens, Kingston, Ontario.

Lerner KL, Lerner BW. (2003) Geothermal Gradient: World of Earth Science. Gale Cengage, eNotes.com 2006. <http://www.enotes.com/earth-science/geothermal-gradient>. Last updated 2006. Last visited 03/2010.

Lindgren W (1933) Mineral Deposits. 4th Edition. New York and London, McGraw-Hill Book Co. Inc:1-930

Longerich HP, Jackson SE, Gunther D (1996) Laser ablation inductively

coupled plasma mass spectrometric transient signal data acquisition and analyte concentration calculation. *Journal of Analytical Atomic Spectrometry* 11(9):899-904

Mark G, Oliver NHS, Williams PJ, Valenta RK, Crookes RA (2000) The evolution of the Ernest Henry Fe-oxide-(Cu-Au) hydrothermal system. In Porter TM (ed.) *Hydrothermal Iron Oxide Copper-Gold & Related Deposits: A Global Perspective*. PGC Publishing Adelaide 1:123-136

Marschik R, Leveille RA, Martin W (2000) La Candelaria and the Punta del Cobre district, Chile: Early Cretaceous iron oxide Cu-Au(-Zn-Ag) mineralization. In Porter TM (Ed.) *Hydrothermal Iron-Oxide Copper Gold & Related Deposits: A Global Perspective*. PGC Publishing, Adelaide 1:163-175

Marshall DJ (1988) *Cathodoluminescence of geological materials*. Unwin Hyman, Boston:1-146

Matsuhisa Y, Goldsmith JR, Clayton RN (1979) Oxygen isotopic fractionation in the system quartz-albite-anorthite-water. *Geochimica et Cosmochimica Acta* 43:1131-1140

McCrea JM (1950) On the isotopic chemistry of carbonates and a paleotemperature scale. *The Journal of Chemical Physics* 18(6):849-857

McGlynn (1979) Geology of the Precambrian rocks of the Riviere Grandin and in part of the Marian River map areas, District of Mackenzie. *Geological Survey of Canada* 79-1A:127-131

Miller RG (1982) The geochronology of uranium deposits in the Great bear Batholith, Northwest Territories. *Canadian Journal of Earth Sciences* 19(7):1428-1448

Mumin AH, Corriveau L, Somarin AK, Ootes L (2007) Iron oxide copper-gold-type polymetallic mineralization in the Contact Lake belt, Great Bear magmatic zone, Northwest Territories, Canada. *Exploration and Mining Geology* 16(3-4):187-208

Mumin AH, Somarin AK, Jones B, Corriveau L, Ootes L, Camier C (2008) The IOCG-Porphyry-Epithermal Continuum in the Great Bear Magmatic Zone, Northwest Territories, Canada. In: Corriveau L, Mumin H (eds) *Exploring for Iron Oxide Copper-Gold Deposits: Canada and Global Analogues*. Geological Association of Canada, Short Course Notes:57-75

Natural Resources Canada (2008) Gravity Field Measurements. http://gsc.nrcan.gc.ca/gravity/index_e.php. Earth Sciences Sector, Priorities, Geological Survey of

Canada, Gravity. Last visited 2009-10-17, last modified 2008-01-17

Nortje GS, Rowland JV, Spörli KB, Blenkinsop TG, Rabone SDC (2006) Vein deflections and thickness variations of epithermal quartz veins as indicators of fracture coalescence. *Journal of Structural Geology* 28:1396-1405

Normin (2009) Northwest Territories: Geoscience Web site. <<http://www.nwtgeoscience.ca/normin>>. Last updated: 2009. Last visited: 01/01/2010.

Oehler JH (1976) Hydrothermal crystallization of silica gel. *Geological Society of America Bulletin* 87:1143-1152

Ohmoto H, Rye RO (1979) Isotopes of sulfur and carbon. In Barnes HL (1979) *Geochemistry of hydrothermal ore deposits*. Edition 2, John Wiley & Sons, New York, NY:509-569

Oliver NHS (1995) Hydrothermal history of the Mary Kathleen fold belt, Mt Isa Block, Queensland. *Australian Journal of Earth Sciences* 42(3):267-279

Oliver NHS (1996) Review and classification of structural controls on fluid flow during regional metamorphism. *Journal of Metamorphic Geology* 14:477-492

Oliver NHS, Cleverley GM, Pollard PJ, Fu B, Marshall LJ, Rubenach MJ, Williams PJ, Baker T (2004) Modeling the Role of Sodic Alteration in the Genesis of Iron Oxide-Copper-Gold Deposits, Eastern Mount Isa Block, Australia. *Economic Geology* 99:1145-1176

Onasch CM, Vennemann TW (1995) Disequilibrium partitioning of oxygen isotopes associated with sector zoning in quartz. *Geology* 23(12):1103-1106

O'Neil JR, Silberman ML (1974) Stable Isotope Relations in Epithermal Au-Ag Deposits. *Economic Geology* 69:902-909

Park JK, Buchan KL, Harlan SS (1995) A proposed giant radiating dyke swarm fragmented by the separation of Laurentia and Australia based on Paleomagnetism of ca. 780 Ma mafic intrusions in western North America. *Earth and Planetary Science Letters* 132(1-4):129-139

Pati JK, Patel SC, Pruseth KL, Malviya VP, Arima M, Raju S, Pati P, Prakash K (2007) Geology and geochemistry of giant quartz veins from the Bundelkhand Craton, central India and their applications. *Journal of Earth System Science* 116:497-510

Pierce KL, Turner WA (2004) GIS compilation of the Southern Wopmay orogen (south of 65°N). Northwest Territories Geoscience Office, Open Report 2004-

005:1 CD ROM.

Puritch E, Brown F (2010) Reserve estimate for NICO deposit. P&E Mining Consultants Inc. for Fortune Minerals Limited. <http://www.fortuneminerals.com/>. Last updated: 2010. Last visited: 30/03/2010

Puritch E, Hennessey T (2010) Reserve estimate for Sue-Dianne deposit. Miicon International Limited and P&E Mining Consultants Inc. for Fortune Minerals Limited. <http://www.fortuneminerals.com/>. Last updated: 2010. Last visited: 30/03/2010

Ramsay JG, Huber MI (1983) *The Techniques of Modern Structural Geology: Strain Analysis*. Academic Press, Measurement of Progressive Deformation: Extension veins 13:235-265

Ramseyer K, Mullis J (2000) Geologic application of cathodoluminescence of silicates. *Cathodoluminescence in geosciences*. Springer:177-191

Richards JP (2009) Personal Communication. University of Alberta, Edmonton, Alberta.

Rimstidt JD, Barnes HL (1980) The kinetics of silica-water reactions. *Geochimica et Cosmochimica Acta* 44:1683-1699

Robinson BW, Ohmoto H (1973) Mineralogy, fluid inclusions, and stable isotopes of the Echo Bay U-Ni-Ag-Cu deposits, Northwest Territories, Canada. *Economic Geology* 68(5):635-656

Roedder E, Bodnar RJ (1980) Geologic pressure determinations from fluid inclusion studies. *Annual Review of Earth and Planetary Sciences* 8:263-301

Roedder E (1984) Fluid inclusions. *Reviews in Mineralogy* 12:644

Ross GM, Kerans C (1989) Geology, Hornby Bay and Dismal Lakes groups, Coppermine Homocline, District of Mackenzie, Northwest Territories. Geological Survey of Canada, "A" Series Map, Report 1663A:1 Sheet

Rusk BG, Lowers HA, Reed MH (2008) Trace elements in hydrothermal quartz: relationships to cathodoluminescent textures and insights into vein formation. *Geology* 36:547-550

Rusk BG, Reed MH, Dilled JH, Kent AJR (2006) Intensity of quartz cathodoluminescence and trace-element content in quartz from the porphyry copper deposit at Butte, Montana. *American Mineralogist* 91:1300-1312

- Sander MV, Black JE (1988) Crystallization and Recrystallization of Growth-Zoned Vein Quartz Crystals from Epithermal Systems – Implications for Fluid Inclusion Studies. *Economic Geology* 83:1052-1060
- Schoell M, Wellmer FW (1981) Anomalous (super 13)C depletion in early Precambrian graphites from Superior Province, Canada. *Nature* 290 (5808):696-699
- Shaheen M, Gagnon JE, Yang Z, Fryer BJ (2008) Evaluation of the analytical performance of femtosecond laser ablation inductively coupled plasma mass spectrometry at 785nm with glass reference materials. *Journal of Analytical Atomic Spectrometry* 23:1610-1621
- Shepherd TJ, Rankin AH, Alderton DHM (1985) Chapter 6: Fluid inclusion techniques of analysis. In: *A Practical Guide to Fluid Inclusions Studies* (eds) Blackie, Glasgow 6:125-149
- Sibson RH (1996) Structural permeability of fluid-driven fault-fracture meshes. *Journal of Structural Geology* 18(8):1031-1042
- Sibson RH, Robert F, Poulsen KH (1988) High-angle reverse faults, fluid-pressure cycling, and mesothermal gold-quartz deposits. *Geology* 16:551-555
- Skinner BJ (1979) The many origins of hydrothermal mineral deposits. In Barnes HL, ed.2, *Geochemistry of Hydrothermal Ore Deposits*: New York, Wiley Interscience Publication:1-21
- Stanworth CW, Badham JPN (1984) Lower Proterozoic red beds, evaporates and secondary sedimentary uranium deposits from the East Arm, Great Slave Lake, Canada. *Journal of Geological Society of London* 141:235-242
- Sterner SM, Hall DL, Bodnar RJ (1988) Synthetic fluid inclusions; V, Solubility relations in the system NaCl-KCl-H₂O under vapour-saturated conditions. *Geochimica et Cosmochimica Acta* 52(5):989-1005
- Storz M (1928) Die sekundäre authigene Kieselsäure in ihrer petrogenetisch-geologischen Bedeutung. *Monographien zur Geologie und Palaeontologie* 2(4):28-32 within Herrington RJ, Wilkinson JJ (1993) Colloidal gold and silica in mesothermal vein systems. *Geology* 21:539-542
- Tirrul R (1983) Structure cross-sections across Asiatic Foreland thrust and fold belt, Wopmay orogen, district of Mackenzie. *Geological Survey of Canada* 83-1B:253-260
- Thompson JFH, Lessman J, Thompson AJB (1986) The Temora gold-silver

deposit; a newly recognized style of high sulphur mineralization in the lower Paleozoic of Australia. *Economic Geology* 81(3):732-738

Walker E (1999) Mineralogy report, unpublished company report for SNC Lavalin Engineers & Constructors Inc. 136p. In: Goad RE, Mumin AH, Duke NA, Neale KL, Mulligan DL (2000a) Geology of the Proterozoic iron oxide-hosted NICO cobalt-gold-bismuth and Sue-Dianne Copper-Silver Deposits, Southern Great Bear Magmatic Zone, Northwest Territories, Canada.

Wanless RK, Stevens RD, Lachance GR, Delabio RN (1970) Age Determinations and Geological Studies, K-Ar Isotopic Ages; Report 9. Geological Survey of Canada 69-2A:1-78

Yang Z (2009) Personal Communication. Great Lakes Institute for Environmental Research, University of Windsor, Windsor, Ontario.

Yardley BWD, Banks DA, Barnicoat AC (2000) The chemistry of crustal brines: tracking their origins. In Porter, TM (Ed.) *Hydrothermal Iron Oxide Copper-Gold & Related Deposits: A Global Perspective*. PGC Publishing, Adelaide 1:61-70

Appendix A

Location and analyses performed for each sample.

<i>Petrography Sample</i>	<i>Location</i>		<i>Microprobe</i>	<i>SEM-CL</i>	<i>LA-ICP-MS</i>	<i>Microthermometry</i>	<i>Stable Isotopes</i>
	UTM NAD83 Zone 11W						
	Easting (m)	Northing (m)					
NICO							
06SBN001-A	512151	7047478		X			X
06SBN001-C	512151	7047478					
06SBN001-D	512151	7047478		X	X	X	
06SBN001-E	512151	7047478				X	X
06SBN001-G	512151	7047478					
06SBN002	512163	7047475					X
06SBN003	512160	7047472					X
06SBN004	512163	7047479					X
06SBN005-B	512147	7047484	X	X	X		X
06SBN005-E	512147	7047484					X
06SBN006	512145	7047474					
06SBN007-B1	512923	7047472					
06SBN007-B2	512923	7047472					
06SBN008-B1	513032	7046618					
06SBN009-B	513032	7046618					
NICO Drill Core							
06SBN98-122-22.27m	511605	7047422					
06SBN98-122-22.68m	511605	7047422		X	X		
06SBN98-122-27.60m	511605	7047422					
06SBN98-122-31.60m	511605	7047422		X			X
06SBN98-122-41.11m	511605	7047422					
06SBN98-122-41.81m	511605	7047422					X
06SBN98-122-75.36m	511605	7047422					
06SBN98-122-81.81m	511605	7047422					X
06SBN98-122-82.98m	511605	7047422					
06SBN98-122-108.0mA-E	511605	7047422	X				
06SBN98-122-122.10m	511605	7047422				X	
Sue-Dianne							
06SBS017-A	504411	7070374				X	
06SBS017-E	504411	7070374					
06SBS018-A	504319	7070410					
06SBS019	504145	7070497		X	X	X	
06SBS020-A	504217	7070489				X	
06SBS020-E	504217	7070489					
06SBS020-F	504217	7070489					

<i>Petrography Sample</i>	<i>Location</i>		<i>Microprobe</i>	<i>SEM-CL</i>	<i>LA-ICP-MS</i>	<i>Microthermometry</i>	<i>Stable Isotopes</i>
	UTM NAD83 Zone 11W						
	Easting (m)	Northing (m)					
Northern Sloan Extension							
07SBHAR001-B	481035	7375088					
07SBHAR003	481035	7375088					
07SBHAR004	481035	7375088					
07SBHAR005-B	481035	7375088					
07SBHAR006	481035	7375088					
07SBHAR007-B	481159	7375333					
07SBHAR008	481159	7375333		X			
07SBHAR009-B	481159	7375333					
07SBHAR010-A/B	481156	7375288		X			
07SBHAR011-B	481218	7375432					
07SBHAR012	481218	7375432					
07SBHAR014-A	481218	7375432					
07SBHAR015	481218	7375432					
07SBHAR016	481218	7375432					
Beaverlodge Lake							
06SBB012-A	443574	7179358					
06SBB012-B	443578	7179363					
06SBB012-C	443578	7179363					
06SBB012-D	443578	7179363	X				
06SBB012-E	443578	7179363					
06SBB012-F	443578	7179363					
06SBB012-G	443578	7179363	X	X	X	X	
06SBB013-A	443583	7179356					
06SBB014-A	442607	7179337					
06SBB014-B	442607	7179337				X	
06SBB014-C	442607	7179337				X	
06SBB015-A	443613	7179399					
06SBB015-B	443613	7179399					
06SBB015-C1	443613	7179399					
06SBB015-C2	443613	7179399					
06SBB015-D	443613	7179399	X				
06SBB015-E	443613	7179399	X				
06SBB015-F	443613	7179399					
06SBB016	443416	7179234					
Fab Lake							
06SBF022-A	492923	7410847					X
06SBF022-B	492923	7410847					
06SBF022-E	492925	7410847				X	X
06SBF022-F	492925	7410847				X	
06SBF022-G	492916	7410847					
06SBF023	492913	7110876					
06SBF023-D	492913	7110876				X	X
06SBF024	492907	7110911					X

<i>Petrography Sample</i>	<i>Location</i>		<i>Microprobe</i>	<i>SEM-CL</i>	<i>LA-ICP-MS</i>	<i>Microthermometry</i>	<i>Stable Isotopes</i>
	UTM NAD83 Zone 11W Easting (m)	UTM NAD83 Zone 11W Northing (m)					
Wopmay fault							
06SBW047-A	515412	7153625					
06SBW047-B	515412	7153625					
06SBW049-A	575499	7153612					
06SBW049-B	575499	7153612					
06SBW050	515545	7153578					X
06SBW051	515545	7153578					X
06SBW052-A	515584	7153567				X	
06SBW052-E	515584	7153567					X
06SBW052-F	515584	7153567				X	X
06SBW053	515619	7153644					X
06SBW055	515619	7153644		X	X	X	X
06SBW057-A	515571	7153879					X
06SBW058	515488	7154305					
"Arm" Lake							
06SBA032	521791	7131869					X
06SBA034-A1	521789	7131871				X	X
06SBA034-A2	521789	7131871				X	X
06SBA034-A3	521789	7131871					
06SBA034-B	521789	7131871					X
06SBA034-C	521789	7131871					
06SBA035	521789	7131973		X		X	X
06SBA036	521789	7131857					
Hardisty Lake							
06SBH025	469127	7160093					X
06SBH026	469127	7160093					X
06SBH027	469127	7160093					X
06SBH028	469127	7160093					X
06SBH029	469769	7160733				X	X
06SBH030	469738	7160689					X
06SBH031	469708	7160653				X	X
06SBH032	469133	7160181				X	X
06SBH032-B	469133	7160181					
Margaret Lake							
06SBM037-B	490363	7145851					
06SBM038	490361	7145853					
06SBM039	490376	7145854					
06SBM040	490376	7145854				X	
06SBM042	490338	7145831					
06SBM043	490344	7145838					
06SBM044-A	477087	7130602					
06SBM044-B	477087	7130602					
06SBM045	477128	7130613				X	
06SBM046	477128	7130613					

Appendix B

Electron microprobe chemistry from NICO drill-core samples 06SBN98-122-109.8m, results are in weight percent.

Electron Microprobe samples, results in weight percent.													
Sample	S	Fe	Bi	As	Ni	Sb	Pb	Cu	Au	Co	Total	Mineral	Formula
109.8A-2-Fe-rich	34.71	29.2	0.063	0.039	<0.0089	<0.0210	<0.0366	34.63	0.065	0.054	98.761	chalcopyrite	CuFeS ₂
109.8A-2-Fe-rich	34.99	29.04	0.254	0.055	<0.0088	<0.0212	<0.0366	34.97	<0.0553	0.053	99.362	chalcopyrite	CuFeS ₂
109.8A-2-Fe-rich	34.66	29.05	0.109	0.016	<0.0087	<0.0212	0.041	34.85	0.09	0.053	98.87	chalcopyrite	CuFeS ₂
109.8A-2-Cu-1	26.49	11.04	0.225	0.023	<0.0093	<0.0206	0.112	62.32	0.101	0.027	100.338	bornite	Cu ₅ FeS ₄
109.8A-2-Cu-2	26.96	11.28	0.317	<0.0147	0.014	<0.0216	<0.0363	61.84	<0.0552	0.019	100.43	bornite	Cu ₃ FeS ₄
109.8A-2-Cu-3	26.3	11.27	0.3	0.06	<0.0094	<0.0206	<0.0365	62.35	<0.0549	0.019	100.298	bornite	Cu ₃ FeS ₄
109.8A-2-Cu-4	26.14	11.03	0.282	0.021	<0.0094	<0.0207	0.034	62.87	<0.0554	0.013	100.391	bornite	Cu ₃ FeS ₄
109.8A-2-Cu-5	26.23	11.08	0.302	0.069	<0.0093	<0.0217	0.037	62.62	0.031	0.027	100.396	bornite	Cu ₃ FeS ₄
109.8A-2-Cu-frac-1	28.05	11.41	0.2	0.023	0.017	<0.0217	<0.0362	60.22	<0.0529	0.012	99.932	bornite	Cu ₃ FeS ₄
109.8A-2-Cu-frac-2	28.75	11.67	0.248	0.006	0.008	<0.0210	<0.0362	58.75	<0.0560	0.022	99.454	bornite	Cu ₃ FeS ₄
109.8A-2-Cu-frac-3	28.17	11.45	0.288	0.016	0.009	<0.0214	<0.0375	60.54	<0.0546	0.028	100.501	bornite	Cu ₃ FeS ₄
109.8A-2-Cu-frac-4	28.78	11.94	0.365	0.019	<0.0093	<0.0210	0.015	58.58	<0.0554	0.008	99.707	bornite	Cu ₃ FeS ₄
109.8A-2-Bi-1	19.32	0.39	44.36	0.078	<0.0119	0.087	<0.0446	38.96	0.133	<0.0112	103.328	wittchenite	Cu ₃ BiS ₃
109.8A-2-Bi-2	19.34	0.586	44.02	0.014	<0.0118	0.079	<0.0428	39.04	<0.0675	<0.0112	103.08	wittchenite	Cu ₃ BiS ₃
109.8A-2-Bi-3	19.3	0.743	43.8	<0.0195	<0.0117	<0.0240	<0.0437	37.68	<0.0648	<0.0111	101.523	wittchenite	Cu ₃ BiS ₃
109.8A-2-Bi-4	19.67	0.331	44.52	<0.0194	<0.0118	<0.244	<0.0448	37.18	0.047	<0.0111	101.747	wittchenite	Cu ₃ BiS ₃
109.8A-2-Bi-5	19.62	0.24	44.91	<0.0185	<0.0118	0.041	<0.0466	37.25	<0.0664	0.005	102.065	wittchenite	Cu ₃ BiS ₃
109.8A-2-Bi-6	19.44	0.637	44.96	<0.0195	<0.0118	<0.0236	<0.0440	39.35	<0.0663	<0.0111	104.387	wittchenite	Cu ₃ BiS ₃
109.8A-2-Bi-7	17.96	2.07	42.17	<0.0203	<0.0117	<0.0240	0.009	37.16	0.04	<0.0108	99.409	wittchenite	Cu ₃ BiS ₃
109.8A-2-outeredge-1	24.71	10.41	0.171	0.006	<0.0091	<0.0206	<0.0362	61.36	0.047	0.019	96.723	bornite	Cu ₃ FeS ₄
109.8A-2-outeredge-2	26.12	10.82	0.195	0.03	<0.0094	<0.0203	<0.0359	62.88	<0.0544	0.022	100.067	bornite	Cu ₃ FeS ₄
109.8A-2-outeredge-3	26.27	10.89	0.198	<0.0143	<0.0093	<0.0217	<0.0354	62.88	0.019	0.015	100.272	bornite	Cu ₃ FeS ₄
109.8A-2-outeredge-4	25.92	11.07	0.289	0.005	<0.0095	<0.0201	0.124	62.97	0.109	0.024	100.511	bornite	Cu ₃ FeS ₄
109.8A-2-outerdarkhalo-1	33.35	27.28	0.29	<0.0150	<0.0089	0.036	0.074	35.19	0.051	0.052	96.323	chalcopyrite	CuFeS ₂
109.8A-2-outerdarkhalo-2	34.33	27.76	0.274	<0.0147	<0.0088	<0.0218	0.08	34.28	<0.0536	0.061	96.785	chalcopyrite	CuFeS ₂
109.8A-2-outerdarkhalo-3	31.63	26.01	0.305	<0.0151	<0.0086	<0.0196	0.067	32.32	0.007	0.038	90.378	chalcopyrite	CuFeS ₂

Electron Microprobe samples (continued).													
Sample	S	Fe	Bi	As	Ni	Sb	Pb	Cu	Au	Co	Total	Mineral	Formula
109.8A-2-outerdarkhalo-4	5.99	43.88	0.124	0.008	0.006	<0.0242	<0.0327	18.41	0.126	0.098	68.642	cuprospinel	CuFeO ₄
109.8A-2-outerdarkhalo-5	34.74	28.06	0.182	<0.0141	<0.0089	<0.0210	0.118	35.52	<0.0514	0.058	98.678	chalcopyrite	CuFeS ₂
109.8A-2-outerdarkhalo-6	34.5	27.08	0.176	<0.0141	0.012	<0.0207	0.028	36.52	0.054	0.039	98.409	chalcopyrite	CuFeS ₂
109.8A-4-Fe-1	4.24	51.56	0.139	0.06	0.017	<0.0223	0.035	10.2	0.121	0.105	66.477	hematite	Fe ₂ O ₃
109.8A-4-Fe-2	0.576	59.4	0.05	0.036	<0.0081	<0.0216	0.033	1.9	0.184	0.109	62.289	hematite	Fe ₂ O ₃
109.8A-4-Fe-3	26.73	11.15	0.226	0.012	<0.0094	<0.0216	0.052	60.92	0.012	0.019	99.12	bornite	Cu ₅ FeS ₄
109.8A-4-Fe-4	14.6	29.61	0.156	0.033	0.033	<0.0215	0.017	42.6	0.02	0.05	87.12	low total	
109.8A-4-Fe-5	9.12	42.94	0.113	0.054	<0.0087	<0.0218	<0.0286	25.56	<0.0471	0.062	77.849	low total	
109.8A-4-Cu-1	26.4	12.88	0.277	0.043	0.007	0.007	0.107	61.57	0.073	0.015	101.38	bornite	Cu ₅ FeS ₄
109.8A-4-Cu-2	26.83	12	0.299	0.076	0.03	<0.0218	0.012	61.89	0.066	0.019	101.221	bornite	Cu ₅ FeS ₄
109.8A-4-Cu-3	26.49	11.71	0.343	0.08	<0.0097	0.006	0.014	62.31	0.008	0.02	100.98	bornite	Cu ₅ FeS ₄
109.8A-4-Cu-4	25.89	13.31	0.209	0.017	<0.0096	0.006	0.09	58.46	<0.0533	0.028	98.011	bornite	Cu ₅ FeS ₄
109.8A-4-Cu-5	26.36	11.77	0.255	<0.0143	<0.0098	<0.0214	0.062	59.76	<0.0510	0.019	98.227	bornite	Cu ₅ FeS ₄
109.8A-4-brightspot	25.65	7.07	0.342	0.032	0.016	<0.0203	0.134	59.08	0.054	0.022	92.4	bornite	Cu ₅ FeS ₄
109.8A-4-brightspot	0.026	0.252	1.9	0.052	0.022	<0.0290	<0.0318	0.052	0.31	<0.0095	2.615	low total	Au-anomaly
109.8A-4-brightspot	27.34	10.77	0.285	0.125	<0.0095	<0.0215	0.102	60.68	0.035	0.021	99.358	idaite	Cu ₃ FeS ₆
109.8A-3-bright-1	19.28	0.093	44.6	<0.0198	0.011	0.03	<0.0476	38.62	<0.0681	<0.0111	102.634	wittchenite	Cu ₃ BiS ₃
109.8A-3-bright-2	19.32	0.135	44.52	<0.0196	<0.0117	0.014	<0.0449	38.45	<0.0689	<0.0112	102.439	wittchenite	Cu ₃ BiS ₃
109.8A-3-bright-3	18.97	0.112	44.99	<0.0192	<0.0118	0.085	<0.0438	38.5	0.01	<0.0111	102.667	wittchenite	Cu ₃ BiS ₃
109.8A-3-bright-4	19.07	0.212	44.58	<0.0192	<0.0117	0.014	<0.0469	38.32	<0.0657	<0.0110	102.196	wittchenite	Cu ₃ BiS ₃
109.8A-3-bright-3	19.08	0.312	44.68	<0.0205	<0.0118	<0.0240	0.012	37.39	0.079	<0.0113	101.553	wittchenite	Cu ₃ BiS ₃
109.8A-3-dark-1	25.92	10.82	0.192	0.058	<0.0095	<0.0216	0.036	62.9	<0.0560	0.026	99.953	bornite	Cu ₅ FeS ₄
109.8A-3-dark-2	26.18	10.81	0.441	<0.0145	<0.0094	<0.0220	<0.0362	62.84	0.062	0.011	100.344	bornite	Cu ₅ FeS ₄
109.8A-3-fracture-1	1.03	59.13	0.0318	0.009	0.007	<0.0225	<0.0301	2.98	<0.0531	0.122	63.277	hematite	Fe ₂ O ₃
109.8A-3-fracture-2	0.531	60.2	0.017	0.054	<0.0078	<0.0213	<0.0322	2.2	<0.0520	0.099	63.101	hematite	Fe ₂ O ₃
109.8A-3-fracture-3	0.054	58.98	0.009	0.018	<0.0078	<0.0217	<0.0315	1.44	0.196	0.122	60.819	hematite	Fe ₂ O ₃

Appendix C

The detection limits for LA-ICP-MS analysis of each of the six vein samples, results are in parts per million.

NICO Vein																	
Vein	Sample	Li	Be	Na	Al	Si	P	K	Ca	Ti	Mn	Fe	Co	Ge	Rb	Y	La
SBN001-D	3	3.33	0.31	46.97	26.94	1033.97	28.84	22.09	290.75	5.49	0.47	29.42	0.26	0.46	0.23	0.05	0.01
SBN001-D	4	3.01	0.33	37.78	23.07	892.95	22.62	19.48	243.67	4.70	0.49	24.97	0.23	0.40	0.21	0.05	0.01
SBN001-D	5	2.95	0.30	41.24	22.35	846.91	17.75	19.14	250.74	4.57	0.44	22.89	0.21	0.39	0.21	0.05	0.01
SBN001-D	6	3.50	0.37	46.26	23.14	920.50	17.38	21.52	270.89	5.77	0.48	25.80	0.22	0.43	0.23	0.05	0.01

NICO Vein																	
Vein	Sample	Li	Be	Na	Al	Si	P	K	Ca	Ti	Mn	Fe	Co	Ge	Rb	Y	La
SBN005-B	3	3.12	0.29	40.82	15.37	773.58	22.96	19.92	225.01	3.86	0.36	23.41	0.24	0.40	0.27	0.03	0.01
SBN005-B	4	4.22	0.32	57.59	20.76	946.04	26.05	23.25	270.38	4.35	0.49	28.31	0.27	0.51	0.29	0.04	0.01
SBN005-B	5	3.35	0.31	49.85	17.43	858.58	20.08	22.05	240.98	4.57	0.41	25.03	0.23	0.45	0.26	0.03	0.01
SBN005-B	6	4.35	0.31	61.72	18.17	867.46	23.32	22.52	261.60	4.22	0.44	29.74	0.27	0.55	0.31	0.04	0.01
SBN005-B	7	4.22	0.31	51.92	17.03	829.78	18.09	19.27	248.76	4.44	0.46	26.36	0.21	0.50	0.27	0.04	0.01

NICO Drill-Core																	
Vein	Sample	Li	Be	Na	Al	Si	P	K	Ca	Ti	Mn	Fe	Co	Ge	Rb	Y	La
SBN98-122-22.68m	3	3.40	0.41	52.75	23.11	941.78	22.88	23.49	288.36	4.84	0.46	27.67	0.27	0.54	0.28	0.05	0.01
SBN98-122-22.68m	4	3.68	0.31	57.24	21.11	1070.05	21.14	23.19	291.09	5.03	0.54	27.40	0.27	0.53	0.24	0.04	0.01
SBN98-122-22.68m	5	4.00	0.49	55.68	25.43	1101.60	23.23	24.96	333.47	6.13	0.55	32.25	0.26	0.52	0.28	0.05	0.01
SBN98-122-22.68m	6	3.84	0.17	57.50	22.38	1070.05	19.23	23.37	288.72	5.36	0.50	29.27	0.24	0.49	0.22	0.04	0.01
SBN98-122-22.68m	7	4.52	0.41	57.96	20.96	1158.86	21.68	23.46	323.43	5.33	0.53	32.81	0.25	0.54	0.24	0.05	0.01

Sue-Dianne																	
Vein	Sample	Li	Be	Na	Al	Si	P	K	Ca	Ti	Mn	Fe	Co	Ge	Rb	Y	La
SBS019-A	3	2.49	0.19	44.60	17.84	682.63	13.42	18.71	230.43	4.13	0.43	20.36	0.18	0.49	0.21	0.04	0.01
SBS019-A	4	3.31	0.33	125.30	17.38	908.29	14.17	19.57	225.03	3.62	0.39	21.98	0.20	0.47	0.23	0.05	0.01
SBS019-A	5	2.84	0.21	50.64	19.30	704.54	17.16	18.38	254.04	3.94	0.42	23.20	0.17	0.46	0.21	0.04	0.01
SBS019-A	6	3.79	0.25	52.44	19.17	882.29	16.18	21.39	265.91	4.49	0.46	24.15	0.23	0.49	0.28	0.04	0.01
SBS019-A	7	3.45	0.12	96.16	21.55	783.07	14.03	17.62	257.11	4.39	0.41	23.71	0.19	0.42	0.25	0.05	0.01

Beaverlodge Lake																	
Vein	Sample	Li	Be	Na	Al	Si	P	K	Ca	Ti	Mn	Fe	Co	Ge	Rb	Y	La
SBB012-G2	3	2.46	0.38	58.18	27.98	1301.61	26.69	30.39	350.73	6.40	0.68	32.67	0.29	0.65	0.23	0.06	0.01
SBB012-G2	4	2.95	0.12	58.96	26.49	1342.80	25.85	27.84	349.23	6.50	0.55	32.61	0.30	0.54	0.25	0.06	0.01
SBB012-G2	5	3.53	0.39	78.50	34.12	1514.80	31.27	24.95	377.49	6.41	0.62	38.84	0.32	0.63	0.29	0.06	0.02
SBB012-G2	6	2.71	0.36	55.10	24.16	951.62	19.17	21.23	302.84	4.90	0.55	30.64	0.26	0.48	0.19	0.04	0.01

Wopmay Vein																	
Vein	Sample	Li	Be	Na	Al	Si	P	K	Ca	Ti	Mn	Fe	Co	Ge	Rb	Y	La
SBW055-2	3	3.95	0.37	46.82	15.78	901.71	22.81	19.60	253.18	4.34	0.41	24.90	0.24	0.51	0.30	0.04	0.01
SBW055-2	4	4.74	0.43	58.67	19.02	849.54	25.32	20.86	287.21	4.82	0.51	31.81	0.23	0.51	0.32	0.05	0.01
SBW055-2	5	5.11	0.29	66.30	24.74	947.51	24.66	23.36	273.81	5.22	0.49	36.71	0.26	0.55	0.34	0.04	0.01
SBW055-2	6	4.93	0.40	60.31	20.43	972.26	22.52	26.27	255.09	4.72	0.47	29.54	0.27	0.57	0.31	0.04	0.01

Sample	Track	Li	Be	Na	Al	P	K	Ca	Ti	Mn	Fe	Co	Ge	Rb	Y	La
06SBN001-D	3	3.34	3.33	94.58	32.19	28.86	25.47	291.49	5.53	0.48	29.57	0.27	0.46	0.27	0.07	0.04
06SBN001-D	4	3.03	2.59	39.18	23.4	22.73	19.94	244.59	4.73	0.49	25.05	0.23	0.43	0.21	0.06	0.03
06SBN001-D	5	3.01	2.46	41.28	22.8	17.8	21.64	254.02	4.58	0.45	23.11	0.21	0.39	0.21	0.05	0.03
06SBN001-D	6	3.5	3.21	47.79	23.77	17.42	21.74	288.82	5.94	0.5	26.76	0.22	0.44	0.23	0.09	0.04
06SBN005-B	3	bdl	1.93	58.19	29.52	26.73	30.51	359.93	6.46	0.68	32.82	0.3	0.66	bdl	0.06	0.02
06SBN005-B	4	bdl	2.48	60.1	169.74	bdl	29.04	375.03	6.5	0.55	32.65	0.3	0.55	bdl	0.06	0.02
06SBN005-B	5	3.96	2.75	82.76	66.05	31.69	25.17	407.99	6.51	0.63	39.43	0.32	0.63	0.29	0.07	0.03
06SBN005-B	6	2.74	1.9	57.53	28.65	19.23	21.66	340.39	4.91	0.55	30.76	0.26	0.51	0.19	0.04	0.02
06SBN005-B	7	3.55	2.99	53.23	24.83	23.1	23.57	297.54	5.47	0.49	27.92	0.28	0.29	0.28	0.05	0.04
06SBN-22.68m	3	3.74	2.37	58.97	36.53	bdl	24.44	306.66	5.05	0.54	27.74	0.27	bdl	0.24	bdl	0.02
06SBN-22.68m	4	4.06	2.59	bdl	116.14	23.25	27.49	334.31	6.17	0.55	32.28	bdl	bdl	0.28	0.06	0.03
06SBN-22.68m	5	4.12	2.84	57.99	27.72	bdl	bdl	bdl	5.39	bdl	29.91	bdl	0.51	bdl	0.06	0.04
06SBN-22.68m	6	4.61	2.05	58.3	91.52	21.79	23.57	333.84	bdl	0.53	33.04	0.25	0.54	0.24	0.05	0.03
06SBN-22.68m	7	bdl	1.48	bdl	bdl	bdl	bdl	bdl	bdl	bdl	bdl	bdl	bdl	bdl	bdl	0.02
06SBS019-A	3	3.31	1.35	126.24	17.78	14.2	19.69	231.03	bdl	bdl	22.09	0.2	bdl	bdl	0.05	0.02
06SBS019-A	4	bdl	2.15	bdl	34.95	17.2	27.76	264.71	4	0.44	23.58	bdl	0.48	bdl	0.06	0.03
06SBS019-A	5	3.8	2.19	52.49	99.17	16.27	21.4	266.12	4.51	0.46	24.43	0.23	0.49	0.28	0.05	0.04
06SBS019-A	6	bdl	2.89	97.19	21.72	bdl	bdl	278.87	4.49	bdl	bdl	bdl	bdl	0.25	0.05	0.04
06SBS019-A	7	bdl	1.69	bdl	bdl	23.46	20.8	bdl	bdl	bdl	23.79	0.24	bdl	0.28	bdl	0.03
06SBB012-G2	3	4.22	2.42	58.52	269.82	bdl	bdl	bdl	bdl	bdl	bdl	bdl	bdl	0.29	0.06	0.03
06SBB012-G2	4	4.34	2.07	bdl	538.65	bdl	39.49	bdl	bdl	bdl	bdl	bdl	bdl	0.27	bdl	0.03
06SBB012-G2	5	4.36	3	bdl	bdl	bdl	bdl	bdl	bdl	bdl	bdl	bdl	bdl	0.31	bdl	0.04
06SBB012-G2	6	4.68	3.12	bdl	bdl	bdl	bdl	bdl	bdl	bdl	bdl	bdl	0.53	0.27	0.04	0.03
06SBW055-2	3	3.99	2.56	bdl	19.28	1039.5	24.96	270.23	4.38	0.44	26.62	0.25	0.52	0.3	0.07	0.04
06SBW055-2	4	4.77	2.12	58.9	19.18	25.38	22.05	287.7	4.83	0.51	31.99	0.23	0.53	0.32	0.07	0.03
06SBW055-2	5	5.12	3.23	66.45	51.18	24.74	23.6	275.18	5.28	0.5	37	0.26	0.55	0.35	0.04	0.04
06SBW055-2	6	5.07	2.18	77.03	432.21	22.58	101.7	263.38	4.73	0.52	29.54	0.27	0.57	0.31	0.04	0.03

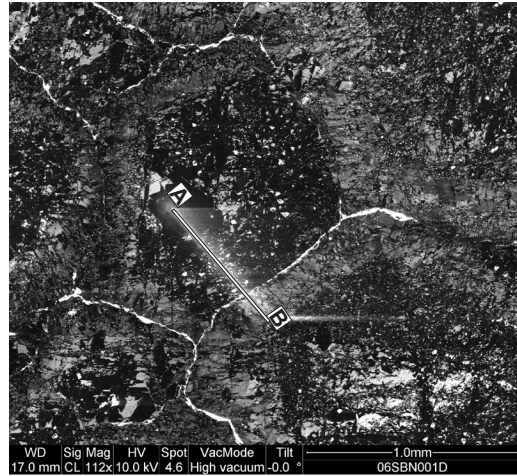
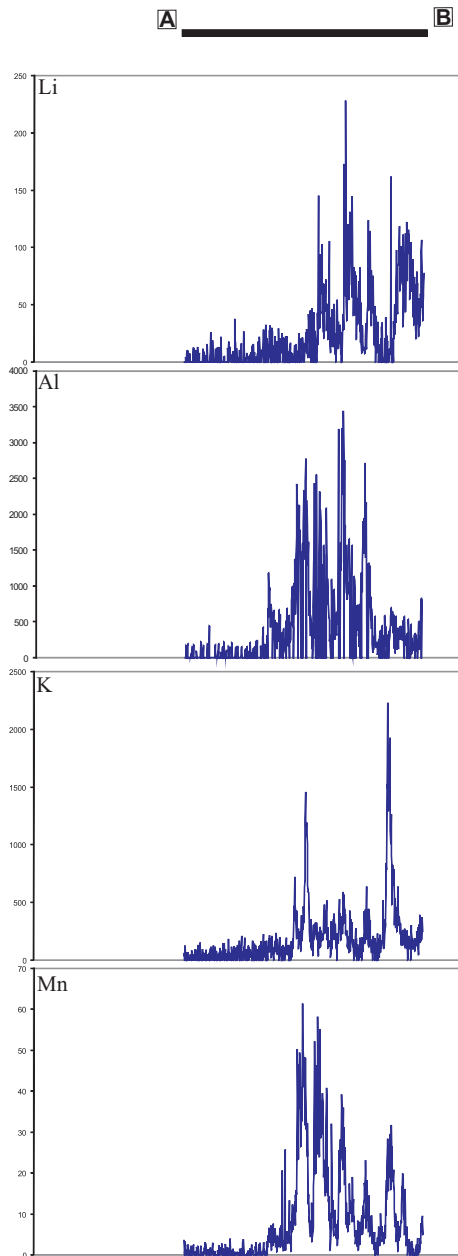
Bdl – below detection limit, refer to previous table for specific detection limits per sample.

Maximum LA-ICP-MS trace element concentration from each quartz vein sample (results in ppm).																
Sample	#	Li	Be	Na	Al	P	K	Ca	Ti	Mn	Fe	Co	Ge	Rb	Y	La
06SBN001-D	3	447.8	20.8	7611.6	26416	291.6	13739	10825	72.4	341.6	64480	4.9	6.8	148.1	0.7	0.2
06SBN001-D	4	186.2	11.7	2901.9	22146	287	4156.6	5254.5	455.9	117.9	453.5	2.2	8.5	28.5	0.6	0.2
06SBN001-D	5	3836.3	199.9	219537	144009	33042	96304	860831	12167	157.9	20031	191.5	358.8	501.2	68.6	13.1
06SBN001-D	6	227.9	12.5	3433.9	60657	765	2224	7080.8	64.8	61.3	38792	2.2	8	24.4	1	0.2
06SBN005-B	3	1232	7.6	3703.1	42637	3608.5	10918	11974	184.8	39.4	75444	2.6	25.7	48.5	0.7	2.2
06SBN005-B	4	169.1	8.1	1573.7	7507.9	274.3	2964.9	4003.9	52.7	24.5	383.9	2.7	17.3	14.9	0.5	0.2
06SBN005-B	5	226.3	7.1	1663.1	8537.8	264	3300.6	6498.3	58.2	25.7	4586.9	2.8	20.5	20.7	0.6	0.3
06SBN005-B	6	123.6	8.7	1219.2	4174	334.3	1624	5169.4	70.4	67.4	385	3.7	9.1	3.7	0.5	0.2
06SBN005-B	7	286.7	11.2	2221.3	6946.6	284.4	1669.6	12352	827.2	52.1	2271.6	2.6	20.8	11	9.2	24.7
06SBN-22.68m	3	86.1	6.9	410.6	1255.7	277.9	264.8	6190.3	50.2	5.7	588.6	1.9	4.6	2.6	0.4	0.3
06SBN-22.68m	4	130.4	11.2	2794.4	6176.2	193.6	3026.5	3986.2	65.4	612.1	2062.9	3.1	4.1	20.5	0.5	2
06SBN-22.68m	5	255.3	9.1	1202.3	7488	253.5	1569.5	4159.5	85.5	47.7	1324.2	3	7.8	4.6	0.6	4
06SBN-22.68m	6	88.1	8.8	1475.6	1967.3	219.6	793.9	7499	56.3	17.1	382.8	2.4	8.7	4.8	0.7	0.2
06SBN-22.68m	7	178.9	9.1	8531.1	8377	280.3	3771.2	9209.4	62.2	501	518.7	11.6	5.7	26.4	0.7	2.1
06SBS019-A	3	149.4	8.2	1666.6	2342.5	131.6	264.7	3374.3	36.6	29	559.1	2	3.7	2.6	0.3	0.2
06SBS019-A	4	87.3	7.5	23534	6841.7	221.6	5556.2	26534	99.4	448.4	5190.5	3.8	4.5	38.3	1.9	1.2
06SBS019-A	5	61.6	9.2	3651.7	20474	134.1	7681.8	22855	192.1	141	6915.5	6.8	3.9	75.3	0.9	1.4
06SBS019-A	6	241.5	23.9	4406.8	13920	239.6	5527.7	10165	59.7	207.3	1691.5	2.2	6.5	50	0.6	0.2
06SBS019-A	7	111.8	51.8	3236.6	304256	932.1	170747	62663	809.2	402.9	165613	15.4	20.9	992.7	7.5	5.8
06SBB012-G2	3	732.3	9.1	5593	57114	518.9	3053.5	12139	348	55.1	807.1	7.9	17.4	14.9	59.1	3.6
06SBB012-G2	4	957.5	14.4	15698	77631	372.9	4916.5	13365	339.8	101	485.2	3.8	16.2	6	522.2	4.4
06SBB012-G2	5	50.5	5.5	1187.9	936.3	345.5	455.9	18358	77.3	6.4	219.5	3.3	11.4	3.4	0.7	0.2
06SBB012-G2	6	226.9	7.6	1585.9	15374	325.2	526.8	6576.9	361.7	7.7	4397.9	2.9	15.3	3	84.2	0.3
06SBW055-2	3	179.4	26.9	2350.9	60879	125115	10630	7339.2	1715.1	1474.8	161136	25.5	1439.6	98.7	152977	183638
06SBW055-2	4	58.4	8.2	1026.4	286.5	229.4	394.8	6956.5	58.7	17.6	894.2	1.8	4.7	2.7	0.3	0.3
06SBW055-2	5	86.8	7.6	965.4	6258.7	254.9	1698.7	3751.7	59.9	13.5	2546.9	1.8	5	10.5	0.5	0.4
06SBW055-2	6	325.6	43.9	2996.8	20982	3957.1	12114	6482.1	2089.7	683	66396	15	6.8	105	2432.1	21.9

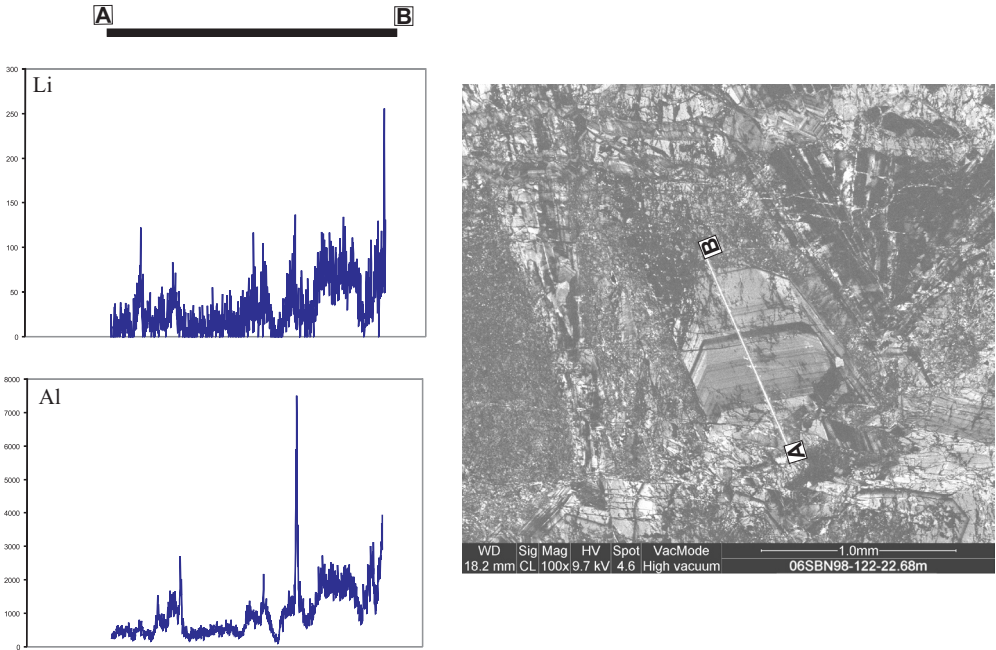
Appendix D

LA-ICP-MS trace element study. Quantities of specific elements (Li, Al, Ge, K, Na, Ca, Mn and Rb), are graphed from A to B of a laser ablation track, image in SEM-CL.

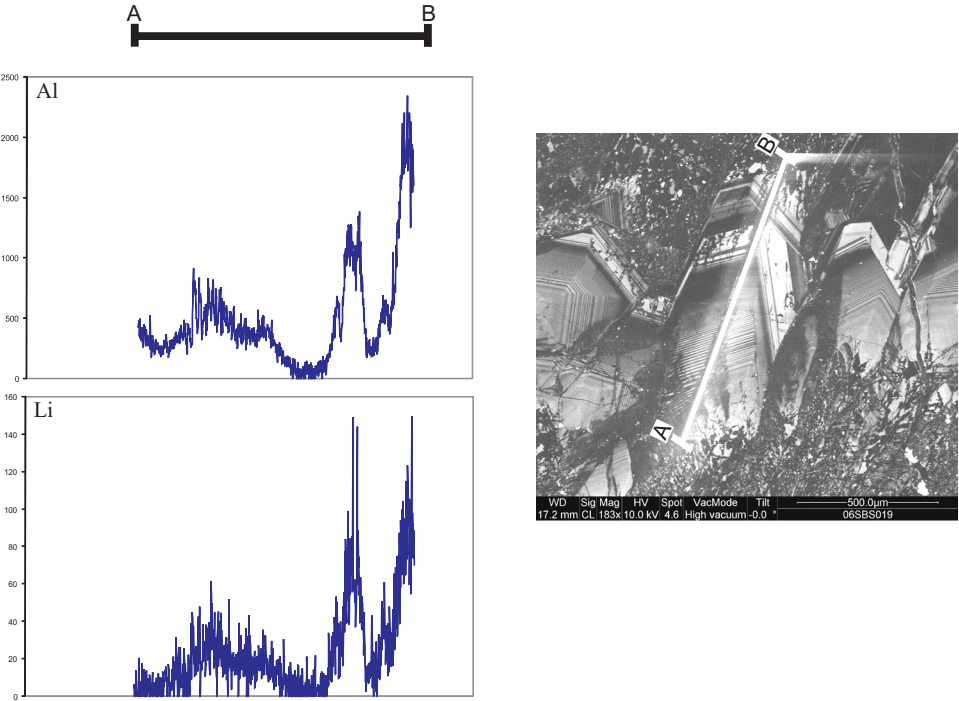
Trace element data for NICO sample 06SBN001-D. Laser ablation track section line from A to B, shown in SEM-CL image of quartz with clear core and cloudy rim, on right.



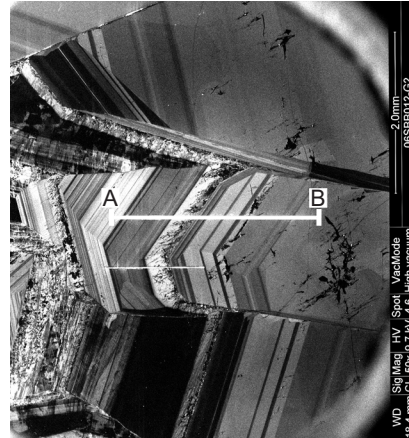
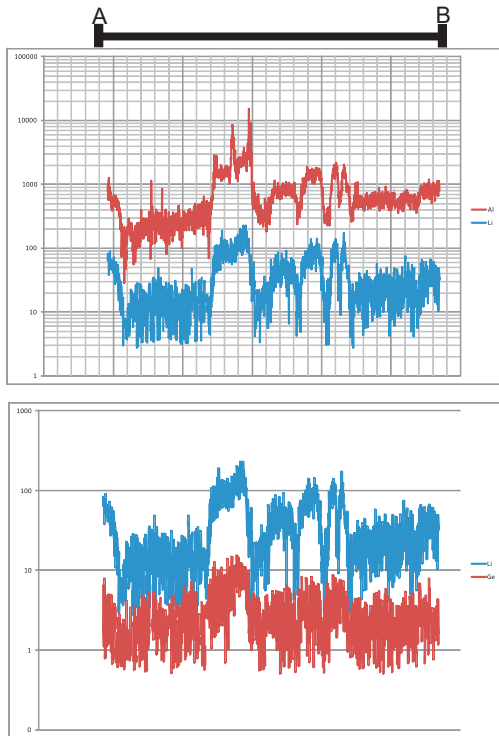
NICO drill-core Q2 sample 06SBN98-122-22.68m. Laser ablation track section line from A to B, shown in SEM-CL image of zoned quartz crystal on right. Li and Al concentration on y-axis in ppm.



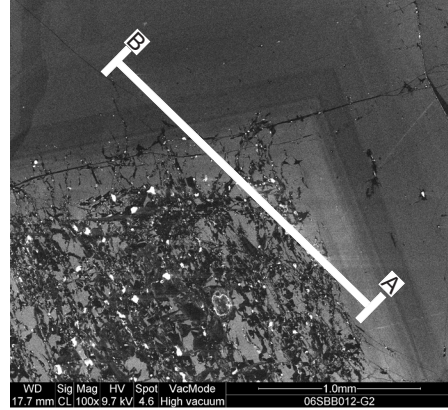
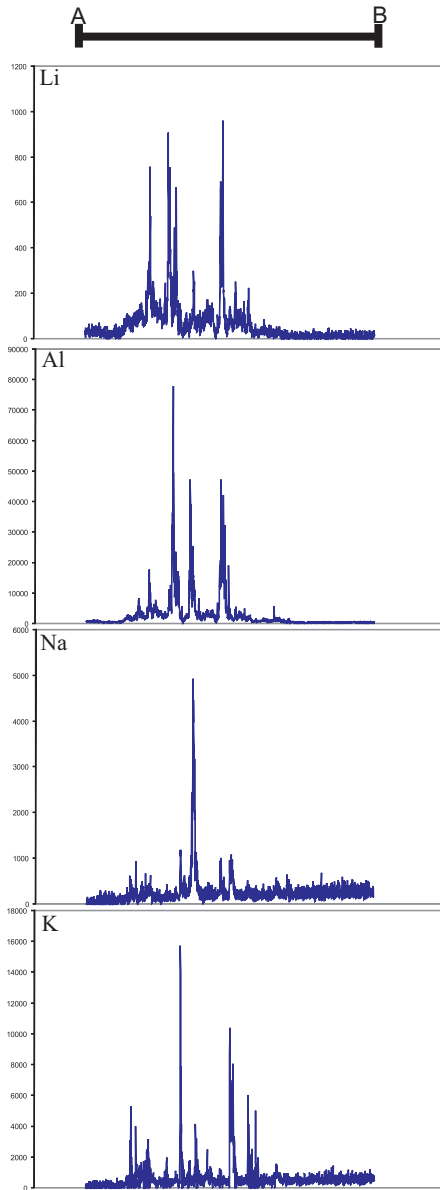
Zoned Q2 quartz vein from Sue-Dianne, sample 06SBS019. Trace element data for Al and Li from laser ablation track along section line A to B. Scale bar in photo 0.5mm. Note: the vertical scales on the trace element plots change according to what element is being analysed.



Beaverlodge Lake Q2 quartz vein, sample 06SBB012-G-A06. Trace element data for Al, Li and Li, Ge from laser ablation track along section line A to B in SEM-CL image. Scale bar in photo 2mm. Note: the vertical scales are log scales, and the increase and decrease of trace element concentration varies with light- and dark-grey zones in SEM-CL image.



Beaverlodge Lake Q2 quartz vein, sample 06SBB012-G-A04. Trace element data for Li, Al and K from laser ablation track along section line A to B in SEM-CL image. Scale bar in photo 1mm. Note: the vertical scales on the trace element plots change according to what element is being analysed.



Appendix E

Microthermometry data for all fluid inclusions analysed for eight giant quartz vein zones, grouped by fluid inclusion assemblage. Abbreviations used in the tables include: FIA – fluid inclusion assemblage, FPD – freezing point depression, $T_{m_{ice}}$ – fluid inclusion ice melting temperature, T_h – homogenization temperature.

Location	Sample	Vein Type	FI Chip	FIA	Inclusion No.	Inclusion Type	Tm _{ice} (°C)	FPD (°C)	Salinity wt. % NaCl eq.	Th (°C)	Halite dissolution (°C)
NICO	06SBN001E	Q2	A	1	1	I	-16.3	16.3	19.7	142	
NICO	06SBN001E	Q2	A	1	2	I	-14.9	14.9	18.6	155	
NICO	06SBN001E	Q2	A	1	3	I	-16.3	16.3	19.7	127	
NICO	06SBN001E	Q2	A	1	4	I	-21.1	21.1	23.1	134	
NICO	06SBN001E	Q2	A	1	5	I	-15.1	15.1	18.7	111	
NICO	06SBN001E	Q2	A	1	7	I	-17.2	17.2	20.4	177	
NICO	06SBN001E	Q2	A	2	1	I	-20.3	20.3	22.6	124	
NICO	06SBN001E	Q2	A	2	2	I	-20.3	20.3	22.6	167	
NICO	06SBN001E	Q2	B	1	1	I	-21.4	21.4	23.3	119	
NICO	06SBN001E	Q2	B	1	2	I	-21.3	21.3	23.2	118	
NICO	06SBN001E	Q2	B	1	3	I	-18.8	18.8	21.5	111	
NICO	06SBN001E	Q2	B	2	1	I	-17.0	17.0	20.2	136	
NICO	06SBN001E	Q2	B	2	2	I	-14.7	14.7	18.4	138	
NICO	06SBN001E	Q2	B	3	1	I	-21.7	21.7	23.5	122	
NICO	06SBN001E	Q2	B	3	2	I	-20.0	20.0	22.4	117	
NICO	06SBN001E	Q2	B	3	3	I	-14.2	14.2	18.0	129	
NICO	06SBN001E	Q2	B	3	4	I	-13.0	13.0	16.9	123	
NICO	06SBN001D	Q2	X	1	1	I	-19.1	19.1	21.8	125	
NICO	06SBN001D	Q2	X	1	2	I	-13.8	13.8	17.6	125	
NICO	06SBN001D	Q2	X	1	3	I	-14.8	14.8	18.5	127	
NICO	06SBN001D	Q2	X	1	4	I	-13.8	13.8	17.6	118	
NICO	06SBN001D	Q2	X	2	1	I	-22.7	22.7	24.1	133	
NICO	06SBN001D	Q2	X	2	2	I	-21.5	21.5	23.4	129	
NICO	06SBN001D	Q2	X	2	3	I	-20.8	20.8	22.9	110	
NICO	06SBN001D	Q2	X	2	4	I	-17.2	17.2	20.4	154	
NICO	06SBN001D	Q2	X	2	5	I	-16.2	16.2	19.6	128	
NICO	06SBN001D	Q2	X	2	6	I	-14.3	14.3	18.0	133	
NICO	06SBN001D	Q2	X	2	7	I	-15.3	15.3	18.9	140	

Location	Sample	Vein Type Q1,2,3	FI Chip	FIA Inclusion	No Inclusion	Type	T _{m,ce} (°C)	FPD (°C)	Salinity wt. % NaCl eq.	Th (°C)	Halite dissolution (°C)
NICO	06SBN001D	Q2	X	3	1	I	-22.0	22.0	23.7	132	
NICO	06SBN001D	Q2	X	3	2	I	-16.5	16.5	19.8	162	
NICO	06SBN001D	Q2	X	3	3	I	-16.5	16.5	19.8	183	
NICO	06SBN001D	Q2	X	3	4	I	-16.7	16.7	20.0	129	
NICO	06SBN001D	Q2	X	3	5	I	-15.6	15.6	19.1	133	
NICO	06SBN001D	Q2	X	3	6	I	-16.1	16.1	19.5	132	
NICO	06SBN001D	Q2	X	3	7	I	-20.0	20.0	22.4	166	
NICO Drill-Core	06SBN98-122-122.1m	Q2	A	1	1	I	-22.1	22.1	23.8	107	
NICO Drill-Core	06SBN98-122-122.1m	Q2	A	1	2	I	-14.7	14.7	18.4	109	
NICO Drill-Core	06SBN98-122-122.1m	Q2	D	2	1	I	-16.0	16.0	19.4	159	
NICO Drill-Core	06SBN98-122-122.1m	Q2	D	2	2	I	-16.7	16.7	20.0	161	
NICO Drill-Core	06SBN98-122-122.1m	Q2	D	2	3	I	-16.6	16.6	19.9	168	
NICO Drill-Core	06SBN98-122-122.1m	Q2	D	3	1	I	-13.3	13.3	17.2	134	
NICO Drill-Core	06SBN98-122-122.1m	Q2	D	3	2	I	-13.3	13.3	17.2	156	
NICO Drill-Core	06SBN98-122-122.1m	Q2	D	3	3	I	-10.2	10.2	14.1	162	
NICO Drill-Core	06SBN98-122-122.1m	Q2	E	4	1	I	-17.8	17.8	20.8	139	
NICO Drill-Core	06SBN98-122-122.1m	Q2	E	4	2	I	-14.7	14.7	18.4	128	
NICO Drill-Core	06SBN98-122-122.1m	Q2	E	4	3	I	-16.1	16.1	19.5	161	

Location	Sample	Vein Type	FI Chip	FIA	Inclusion No.	Inclusion Type	Tm _{ice} (°C)	FPD (°C)	Salinity wt. % NaCl eq.	Th (°C)	Halite dissolution (°C)
Sue-Dianne	06SBS019	Q1	SC	1	1	I	-12.4	12.4	16.3	149	
Sue-Dianne	06SBS019	Q1	SC	1	2	I	-12.1	12.1	16.1	180	
Sue-Dianne	06SBS019	Q1	SC	1	3	I	-12.1	12.1	16.1	198	
Sue-Dianne	06SBS019	Q1	SC	1	4	I	-6.1	6.1	9.3	163	
Sue-Dianne	06SBS019	Q1	SC	1	5	I	-6.2	6.2	9.5	158	
Sue-Dianne	06SBS019	Q1	SC	4	1	I	-18.8	18.8	21.5	216	
Sue-Dianne	06SBS019	Q1	SC	4	2	I	-18.8	18.8	21.5	153	
Sue-Dianne	06SBS019	Q1	SC	4	3	I	-17.3	17.3	20.4	207	
Sue-Dianne	06SBS019	Q1	SC	4	4	I	-17.3	17.3	20.4	186	
Sue-Dianne	06SBS019	Q1	SC	4	5	I	-16.8	16.8	20.1	163	
Sue-Dianne	06SBS019	Q1	SC	4	6	I	-22.6	22.6	24.1	174	
Sue-Dianne	06SBS019	Q1	SC	4	7	I	-21.3	21.3	23.2	222	
Sue-Dianne	06SBS020F	Q2	S1	1	1	II	2.2	2.2	32.7	216	210
Sue-Dianne	06SBS020F	Q2	S1	1	2	II	2.0	2.0	31.9	200	190
Sue-Dianne	06SBS020F	Q2	S1	2	1	II	1.6	1.6	30.1	161	161
Sue-Dianne	06SBS020F	Q2	S1	2	2	II	1.7	1.7	30.6	199	172
Sue-Dianne	06SBS017-A	Q2	SA	1	1	I	-7.2	7.2	10.7	162	
Sue-Dianne	06SBS017-A	Q2	SA	1	2	I	-9.1	9.1	13.0	189	
Sue-Dianne	06SBS017-A	Q2	SA	1	3	I	-7.6	7.6	11.2	197	
Sue-Dianne	06SBS017-A	Q2	SA	3	1	I	-1.5	1.5	2.6	291	
Sue-Dianne	06SBS017-A	Q2	SA	3	2	I	-1.5	1.5	2.6	250	
Sue-Dianne	06SBS017-A	Q2	SA	3	3	I	-0.2	0.2	0.4	318	
Sue-Dianne	06SBS017-A	Q2	SA	3	4	I	-0.1	0.1	0.2	271	
Sue-Dianne	06SBS019	Q2	SF	2	1	I	-19.2	19.2	21.8	203	
Sue-Dianne	06SBS019	Q2	SF	2	2	I	-14.9	14.9	18.6	159	
Sue-Dianne	06SBS019	Q2	SF	2	3	I	-19.4	19.4	22.0	232	
Sue-Dianne	06SBS019	Q2	SF	2	4	I	-10.9	10.9	14.9	164	
Sue-Dianne	06SBS019	Q2	SF	3	1	I	-26.6	26.6	26.6	189	
Sue-Dianne	06SBS019	Q2	SF	3	2	I	-16.1	16.1	19.5	129	
Sue-Dianne	06SBS019	Q2	SF	3	3	I	-16.6	16.6	19.9	148	
Sue-Dianne	06SBS019	Q2	SE	1	1	I	-13.9	13.9	17.7	172	
Sue-Dianne	06SBS019	Q2	SE	1	2	I	-12.0	12.0	16.0	186	

Location	Sample	Vein Type	FI Chip	FIA	Inclusion No.	Inclusion Type	Tm _{ice} (°C)	FPD (°C)	Salinity wt. % NaCl _{eq.}	Th (°C)	Halite dissolution (°C)
		Q1,2,3									
Sue-Dianne	06SBS019	Q2	SE	1	3	I	-21.5	21.5	23.4	141	
Sue-Dianne	06SBS019	Q2	SE	1	4	I	-21.5	21.5	23.4	137	
Sue-Dianne	06SBS019	Q2	SE	1	5	I	-20.9	20.9	23.0	157	
Sue-Dianne	06SBS019	Q2	SE	1	6	I	-12.2	12.2	16.1	189	
Sue-Dianne	06SBS019	Q2	SE	1	7	I	-13.7	13.7	17.5	178	
Sue-Dianne	06SBS019	Q2	SE	1	8	I	-21.9	21.9	23.6	149	
Sue-Dianne	06SBS019	Q2	SE	1	9	I	-21.6	21.6	23.4	159	
Sue-Dianne	06SBS019	Q2	SE	1	10	I	-12.2	12.2	16.1	195	
Sue-Dianne	06SBS019	Q2	SE	2	1	I	-13.9	13.9	17.7	166	
Sue-Dianne	06SBS019	Q2	SE	2	2	I	-14.1	14.1	17.9	169	
Sue-Dianne	06SBS019	Q2	SE	2	3	I	-21.3	21.3	23.2	150	
Sue-Dianne	06SBS019	Q2	SE	2	4	I	-13.9	13.9	17.7	157	
Sue-Dianne	06SBS019	Q2	SE	2	5	I	-15.1	15.1	18.7	157	
Sue-Dianne	06SBS019	Q2	SE	2	6	I	-21.5	21.5	23.4	152	
Sue-Dianne	06SBS019	Q2	SE	2	7	I	-19.9	19.9	22.3	152	
Sue-Dianne	06SBS019	Q2	SE	2	8	I	-23.0	23.0	24.3	183	
Sue-Dianne	06SBS019	Q2	SE	2	9	I	-19.5	19.5	22.0	158	
Sue-Dianne	06SBS019	Q2	SF	3	1	II			29.4	144	140
Sue-Dianne	06SBS019	Q2	SF	3	2	II			29.3	144	140
Sue-Dianne	06SBS019	Q2	SF	3	3	II			29.4	164	144
Sue-Dianne	06SBS019	Q2	SF	3	4	II			28.6	193	119
Sue-Dianne	06SBS019	Q3	SB	2	1	I	-19.8	19.8	22.2	289	
Sue-Dianne	06SBS019	Q3	SB	3	1	I	-14.0	14.0	17.8	338	
Sue-Dianne	06SBS019	Q3	SB	3	2	I	-10.3	10.3	14.3	260	
Sue-Dianne	06SBS019	Q3	SB	3	3	I	-15.8	15.8	19.3	246	
Sue-Dianne	06SBS019	Q3	SB	3	4	I	-22.3	22.3	23.9	293	
Sue-Dianne	06SBS019	Q3	SB	3	5	I	-24.3	24.3	25.1	255	
Sue-Dianne	06SBS019	Q3	SB	4	1	I	-23.2	23.2	24.5	356	
Sue-Dianne	06SBS019	Q3	SB	4	2	I	-23.2	23.2	24.5	333	
Sue-Dianne	06SBS019	Q3	SB	4	3	I	-18.6	18.6	21.4	314	
Sue-Dianne	06SBS019	Q3	SB	4	4	I	-23.2	23.2	24.5	328	
Sue-Dianne	06SBS019	Q3	SB	4	5	I	-23.0	23.0	24.3	357	

Location	Sample	Vein Type	FI Chip	FIA	Inclusion No.	Inclusion Type	T _{ice} (°C)	FPD (°C)	Salinity wt. % NaCl eq.	Th (°C)
Beaverlodge Lake	06SBB012G2	Q1	S1-CI	1	1	I	-6.7	6.7	10.1	143
Beaverlodge Lake	06SBB012G2	Q1	S1-CI	1	2	I	-6.9	6.9	10.4	154
Beaverlodge Lake	06SBB012G2	Q1	S1-CI	1	3	I	-8.0	8.0	11.7	152
Beaverlodge Lake	06SBB012G2	Q1	S1-CI	1	4	I	-6.4	6.4	9.7	138
Beaverlodge Lake	06SBB012G2	Q1	S1-CI	1	5	I	-6.4	6.4	9.7	130
Beaverlodge Lake	06SBB012G2	Q1	S1-CI	1	6	I	-7.8	7.8	11.5	104
Beaverlodge Lake	06SBB012G2	Q1	S1-CI	2	1	I	-7.9	7.9	11.6	180
Beaverlodge Lake	06SBB012G2	Q1	S1-CI	2	2	I	-7.5	7.5	11.1	147
Beaverlodge Lake	06SBB014B	Q1	A	1	1	I	-22.1	22.1	23.8	96
Beaverlodge Lake	06SBB014B	Q1	A	1	2	I	-19.7	19.7	22.2	131
Beaverlodge Lake	06SBB014B	Q1	A	1	3	I	-15.7	15.7	19.2	174
Beaverlodge Lake	06SBB014B	Q1	A	2	1	I	-23.7	23.7	24.8	99
Beaverlodge Lake	06SBB014B	Q1	A	2	2	I	-24.2	24.2	25.1	134
Beaverlodge Lake	06SBB014B	Q1	A	2	3	I	-16.2	16.2	19.6	99
Beaverlodge Lake	06SBB014B	Q1	A	2	3	I	-23.8	23.8	24.8	108
Beaverlodge Lake	06SBB014B	Q1	B	1	1	I	-22.8	22.8	24.2	152
Beaverlodge Lake	06SBB014B	Q1	B	2	1	I	-22.1	22.1	23.8	151
Beaverlodge Lake	06SBB014B	Q1	B	2	2	I	-22.1	22.1	23.8	146
Beaverlodge Lake	06SBB014B	Q1	B	3	1	I	-20.7	20.7	22.8	128
Beaverlodge Lake	06SBB012G2	Q2	S2	1	1	I	-25.8	25.8	26.1	215
Beaverlodge Lake	06SBB012G2	Q2	S2	1	2	I	-12.1	12.1	16.1	186
Beaverlodge Lake	06SBB012G2	Q2	S2	1	3	I	-22.4	22.4	24.0	213
Beaverlodge Lake	06SBB012G2	Q2	S2	1	4	I	-22.1	22.1	23.8	151
Beaverlodge Lake	06SBB012G2	Q2	S2	2	1	I	-20.0	20.0	22.4	152
Beaverlodge Lake	06SBB012G2	Q2	S2	3	1	I	-22.3	22.3	23.9	178
Beaverlodge Lake	06SBB012G2	Q2	S2	3	2	I	-20.1	20.1	22.4	218
Beaverlodge Lake	06SBB012G2	Q2	SA	1	1	I	-17.8	17.8	20.8	180
Beaverlodge Lake	06SBB012G2	Q2	SA	1	2	I	-11.9	11.9	15.9	169

Location	Sample	Vein Type	FI Chip	FIA	Inclusion No.	Inclusion Type	Tm _{ice}	FPD	Salinity	Th
		Q1,2,3				I,II	(°C)	(°C)	wt. % NaCl eq.	(°C)
Fab Lake	06SBF022-F	Q1	S1	1	1	I	-11.8	11.8	15.8	188
Fab Lake	06SBF022-F	Q1	S1	1	2	I	-12.1	12.1	16.1	178
Fab Lake	06SBF022-F	Q1	S1	2	1	I	-8.2	8.2	11.9	170
Fab Lake	06SBF022-F	Q1	S1	2	2	I	-7.2	7.2	10.7	150
Fab Lake	06SBF023D	Q1	1	1	1	I	-13.5	13.5	17.3	106
Fab Lake	06SBF023D	Q1	1	1	2	I	-13.5	13.5	17.3	106
Fab Lake	06SBF023D	Q1	2	1	1	I	-0.2	0.2	0.4	180
Fab Lake	06SBF023D	Q1	2	1	2	I	-0.2	0.2	0.4	181
Fab Lake	06SBF023D	Q1	2	1	3	I	-0.2	0.2	0.4	178
Fab Lake	06SBF023D	Q2	4	1	1	I	-21.5	21.5	23.4	102
Fab Lake	06SBF023D	Q2	4	1	2	I	-18.4	18.4	21.3	124
Fab Lake	06SBF023D	Q2	4	1	3	I	-20.9	20.9	23.0	105
Fab Lake	06SBF023D	Q2	4	1	4	I	-19.3	19.3	21.9	125
Fab Lake	06SBF023D	Q2	4	2	5	I	-20.3	20.3	22.6	111
Fab Lake	06SBF023D	Q2	5	1	1	I	-0.4	0.4	0.7	240
Fab Lake	06SBF023D	Q2	5	1	2	I	-0.4	0.4	0.7	213
Fab Lake	06SBF023D	Q2	5	1	3	I	-0.5	0.5	0.9	214
Fab Lake	06SBF023D	Q2	5	1	4	I	-0.5	0.5	0.9	232
Fab Lake	06SBF023D	Q2	5	3	1	I	-0.2	0.2	0.4	184
Fab Lake	06SBF023D	Q2	5	3	2	I	-0.2	0.2	0.4	174
Fab Lake	06SBF023D	Q2	7	1	1	I	-1.3	1.3	2.2	230
Fab Lake	06SBF023D	Q2	7	1	2	I	-0.4	0.4	0.7	189
Fab Lake	06SBF023D	Q2	7	1	3	I	-1.3	1.3	2.2	230
Fab Lake	06SBF023D	Q2	7	2	1	I	-11.7	11.7	15.7	160
Fab Lake	06SBF023D	Q2	7	2	2	I	-10.7	10.7	14.7	140
Fab Lake	06SBF023D	Q2	7	2	3	I	-10.7	10.7	14.7	147
Fab Lake	06SBF022-F	Q2	S1	1	1	I	-11.8	11.8	15.8	188
Fab Lake	06SBF022-F	Q2	S1	1	2	I	-12.1	12.1	16.1	178
Fab Lake	06SBF022-F	Q2	S1	2	1	I	-8.2	8.2	11.9	170
Fab Lake	06SBF022-F	Q2	S1	2	2	I	-7.2	7.2	10.7	150

Location	Sample	Vein Type Q1,2,3	FI Chip	FIA	Inclusion No.	Inclusion Type I,II	Tm _{ice} (°C)	FPD (°C)	Salinity wt. % NaCl eq.	Th (°C)
N. Wopmay fault zone	06SBW052F	Q1	1	1	1	I	-0.2	0.2	0.4	187
N. Wopmay fault zone	06SBW052F	Q1	1	1	2	I	-0.2	0.2	0.4	173
N. Wopmay fault zone	06SBW052F	Q1	1	1	4	I	-0.2	0.2	0.4	161
N. Wopmay fault zone	06SBW052F	Q1	1	1	5	I	-0.2	0.2	0.4	176
N. Wopmay fault zone	06SBW052F	Q1	1	1	6	I	-0.2	0.2	0.4	196
N. Wopmay fault zone	06SBW052F	Q1	1	2	1	I	-0.3	0.3	0.5	212
N. Wopmay fault zone	06SBW052F	Q1	1	2	2	I	-0.2	0.2	0.4	263
N. Wopmay fault zone	06SBW052F	Q1	4	2	1	I	-0.2	0.2	0.4	260
N. Wopmay fault zone	06SBW052F	Q1	4	2	2	I	-0.3	0.3	0.5	229
N. Wopmay fault zone	06SBW052F	Q1	4	2	3	I	-0.2	0.2	0.4	228
N. Wopmay fault zone	06SBW052F	Q1	4	3	4	I	-0.2	0.2	0.4	245
N. Wopmay fault zone	06SBW055-2	Q1	SD	1	1	I	-12.9	12.9	16.8	144
N. Wopmay fault zone	06SBW055-2	Q1	SD	2	1	I	-12.8	12.8	16.7	149
N. Wopmay fault zone	06SBW055-2	Q1	SD	2	2	I	-14.3	14.3	18.0	165
N. Wopmay fault zone	06SBW055-2	Q1	SD	2	3	I	-12.8	12.8	16.7	132
N. Wopmay fault zone	06SBW055-2	Q1	SD	3	1	I	-15.6	15.6	19.1	150
N. Wopmay fault zone	06SBW055-2	Q1	SD	3	2	I	-22.1	22.1	23.8	135
N. Wopmay fault zone	06SBW055-2	Q1	SD	3	3	I	-22.1	22.1	23.8	151
N. Wopmay fault zone	06SBW055-2	Q1	SD	3	4	I	-13.8	13.8	17.6	144
N. Wopmay fault zone	06SBW055-2	Q1	SD	3	5	I	-13.8	13.8	17.6	164
N. Wopmay fault zone	06SBW055-2	Q1	SD	4	1	I	-15.7	15.7	19.2	157
N. Wopmay fault zone	06SBW055-2	Q1	SD	4	2	I	-15.5	15.5	19.0	188
N. Wopmay fault zone	06SBW052A	Q2	1	1	1	I	-16.8	16.8	20.1	237
N. Wopmay fault zone	06SBW052A	Q2	1	1	2	I	-16.9	16.9	20.1	205
N. Wopmay fault zone	06SBW052A	Q2	1	2	3	I	-17.3	17.3	20.4	229
N. Wopmay fault zone	06SBW052A	Q2	1	2	4	I	-12.5	12.5	16.4	226
N. Wopmay fault zone	06SBW052A	Q2	1	2	5	I	-15.8	15.8	19.3	277
N. Wopmay fault zone	06SBW052A	Q2	2	2	1	I	-16.7	16.7	20.0	275
N. Wopmay fault zone	06SBW052A	Q2	2	2	2	I	-14.1	14.1	17.9	259
N. Wopmay fault zone	06SBW052A	Q2	2	3	1	I	-22.1	22.1	23.8	207
N. Wopmay fault zone	06SBW052A	Q2	2	4	1	I	-21.3	21.3	23.2	240

Location	Sample	Vein Type	FI Chip	FIA	Inclusion No.	Inclusion Type	T _{m,ice} (°C)	FPD (°C)	Salinity	Th (°C)
		Q1,2,3				I,II				
"Arm" Lake	06SBA034A2	Q2	2	S2	1	I	-0.1	0.1	0.2	215
"Arm" Lake	06SBA034A2	Q2	2	S2	2	I	-0.2	0.2	0.4	242
"Arm" Lake	06SBA034A2	Q2	2	S2	3	I	-10.4	10.4	14.4	208
"Arm" Lake	06SBA034A2	Q2	2	S2	4	I	-0.1	0.1	0.2	249
"Arm" Lake	06SBA034A2	Q2	2	S2	5	I	-0.2	0.2	0.4	240
"Arm" Lake	06SBA034A2	Q2	2	S2	6	I	-0.1	0.1	0.2	204
"Arm" Lake	06SBA034A2	Q2	2	S2	7	I	-0.1	0.1	0.2	267
"Arm" Lake	06SBA034A2	Q2	2	S3	1	I	-0.2	0.2	0.4	203
"Arm" Lake	06SBA034A2	Q2	2	S3	2	I	-0.2	0.2	0.4	200
"Arm" Lake	06SBA034A2	Q2	2	S3	3	I	-1.9	1.9	3.2	180
"Arm" Lake	06SBA034A2	Q2	2	S3	4	I	-0.2	0.2	0.4	180
"Arm" Lake	06SBA034A2	Q2	2	S3	5	I	-0.2	0.2	0.4	172
"Arm" Lake	06SBA034A2	Q2	2	S3	6	I	-1.9	1.9	3.2	179
"Arm" Lake	06SBA035	Q2	2	1	1	I	-0.2	0.2	0.4	246
"Arm" Lake	06SBA035	Q2	2	2	1	I	0.0	0.0	0.0	228
"Arm" Lake	06SBA035	Q2	2	2	2	I	-0.2	0.2	0.4	216
"Arm" Lake	06SBA035	Q2	2	3	1	I	-0.2	0.2	0.4	205
"Arm" Lake	06SBA035	Q2	2	3	2	I	-0.2	0.2	0.4	243
"Arm" Lake	06SBA035	Q2	2	3	3	I	-0.2	0.2	0.4	200
"Arm" Lake	06SBA035	Q2	2	3	4	I	-0.2	0.2	0.4	207
"Arm" Lake	06SBA035	Q2	2	3	5	I	-0.2	0.2	0.4	241
"Arm" Lake	06SBA035	Q2	3	1	1	I	-0.2	0.2	0.4	171
"Arm" Lake	06SBA035	Q2	3	1	2	I	-0.2	0.2	0.4	188
"Arm" Lake	06SBA035	Q2	3	1	3	I	-0.2	0.2	0.4	188
"Arm" Lake	06SBA035	Q2	3	1	4	I	-0.2	0.2	0.4	172
"Arm" Lake	06SBA035	Q2	3	1	5	I	-0.2	0.2	0.4	171
"Arm" Lake	06SBA035	Q2	3	2	1	I	-1.1	1.1	1.9	234
"Arm" Lake	06SBA035	Q2	3	2	2	I	-1.0	1.0	1.7	251
"Arm" Lake	06SBA035	Q2	3	2	3	I	-0.2	0.2	0.4	279
"Arm" Lake	06SBA035	Q2	3	2	4	I	-0.2	0.2	0.4	260

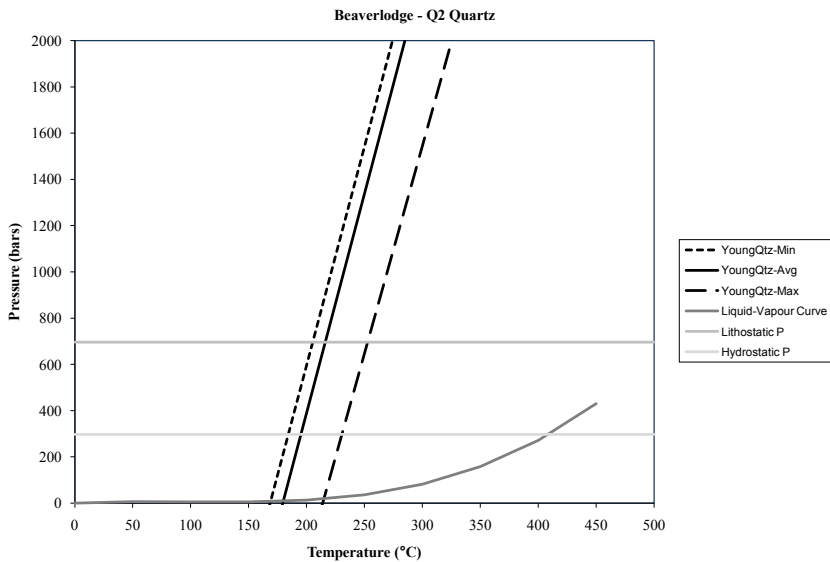
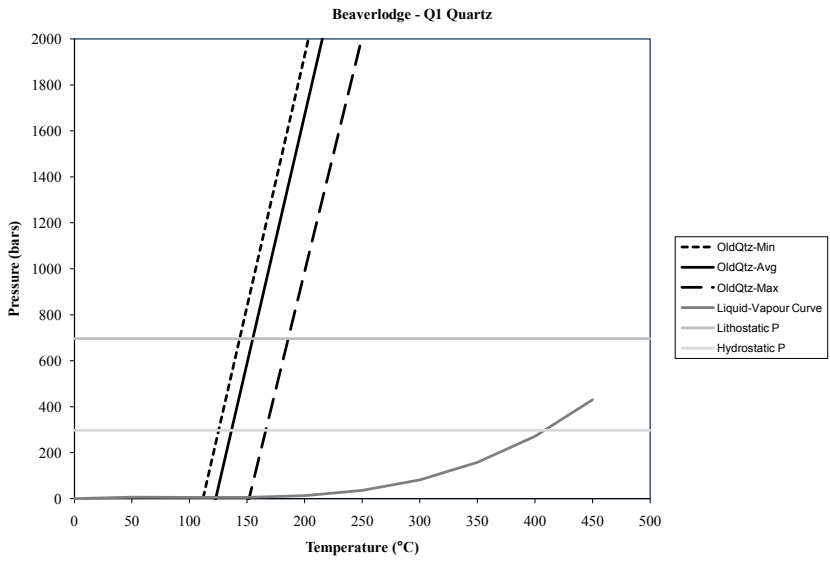
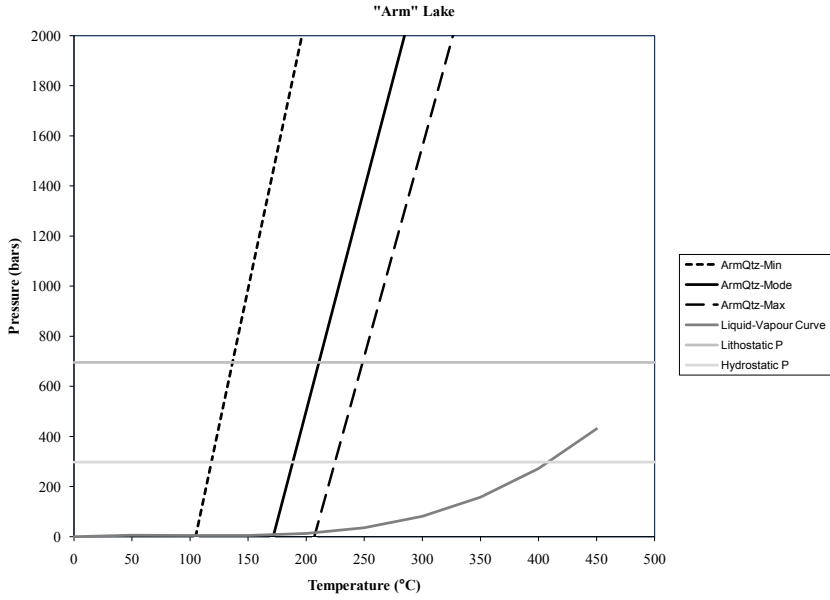
Location	Sample	Vein Type	FI Chip	FIA	Inclusion No.	Inclusion Type	T _{m,ice} (°C)	FPD (°C)	Salinity wt. % NaCl eq.	Th	Halite dissolution (°C)
Hardisty Lake	06SBH031	Q1	3	3	1	I	-0.4	0.4	0.7	269	
Hardisty Lake	06SBH031	Q1	3	3	2	I	-0.5	0.5	0.9	318	
Hardisty Lake	06SBH031	Q1	3	3	3	I	-0.5	0.5	0.9	252	
Hardisty Lake	06SBH031	Q1	3	3	4	I	-0.2	0.2	0.4	334	
Hardisty Lake	06SBH031	Q1	3	3	5	I	-0.2	0.2	0.4	272	
Hardisty Lake	06SBH029	Q1	1	1	1	I	-0.2	0.2	0.4	179	
Hardisty Lake	06SBH029	Q1	1	1	2	I	-0.4	0.4	0.7	179	
Hardisty Lake	06SBH029	Q1	1	1	3	I	-0.2	0.2	0.4	188	
Hardisty Lake	06SBH029	Q1	1	1	4	I	-0.3	0.3	0.5	230	
Hardisty Lake	06SBH029	Q1	1	2	1	I	-0.6	0.6	1.1	216	
Hardisty Lake	06SBH029	Q1	1	2	2	I	-0.4	0.4	0.7	270	
Hardisty Lake	06SBH029	Q1	1	2	3	I	-0.5	0.5	0.9	196	
Hardisty Lake	06SBH029	Q1	1	3	1	I	-0.3	0.3	0.5	175	
Hardisty Lake	06SBH029	Q1	1	3	2	I	-0.3	0.3	0.5	259	
Hardisty Lake	06SBH029	Q1	1	3	3	I	-0.4	0.4	0.7	210	
Hardisty Lake	06SBH029	Q1	1	3	4	I	-0.3	0.3	0.5	191	
Hardisty Lake	06SBH032	Q2	1	1	1	I	-19.1	19.1	21.8	215	
Hardisty Lake	06SBH032	Q2	1	1	2	I	-19.2	19.2	21.8	310	
Hardisty Lake	06SBH032	Q2	1	2	1	I	-19.0	19.0	21.7	288	
Hardisty Lake	06SBH032	Q2	2	1	1	II			28.8	126	120
Hardisty Lake	06SBH032	Q2	2	1	2	II			34.4	245	245
Hardisty Lake	06SBH032	Q2	2	1	3	II			32.3	209	209
Hardisty Lake	06SBH031	Q3	2	3	1	I	-0.2	0.2	0.4	341	
Hardisty Lake	06SBH031	Q3	2	3	2	I	-0.2	0.2	0.4	183	
Hardisty Lake	06SBH031	Q3	2	3	3	I	-0.2	0.2	0.4	178	
Hardisty Lake	06SBH031	Q3	2	3	4	I	-0.2	0.2	0.4	253	
Hardisty Lake	06SBH031	Q3	2	3	5	I	-0.2	0.2	0.4	251	

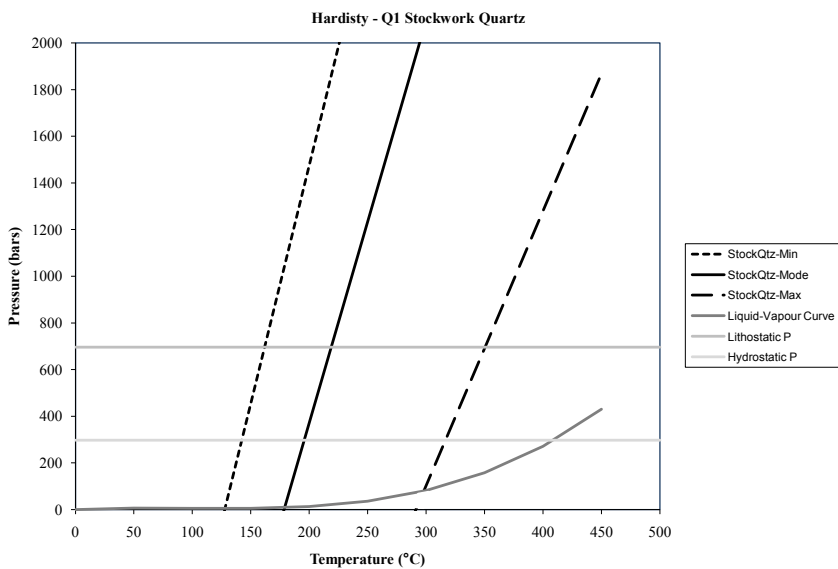
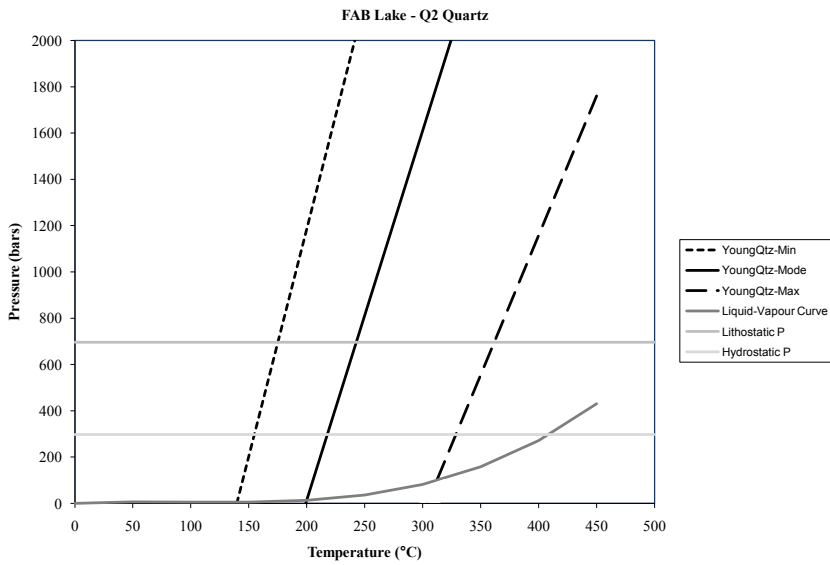
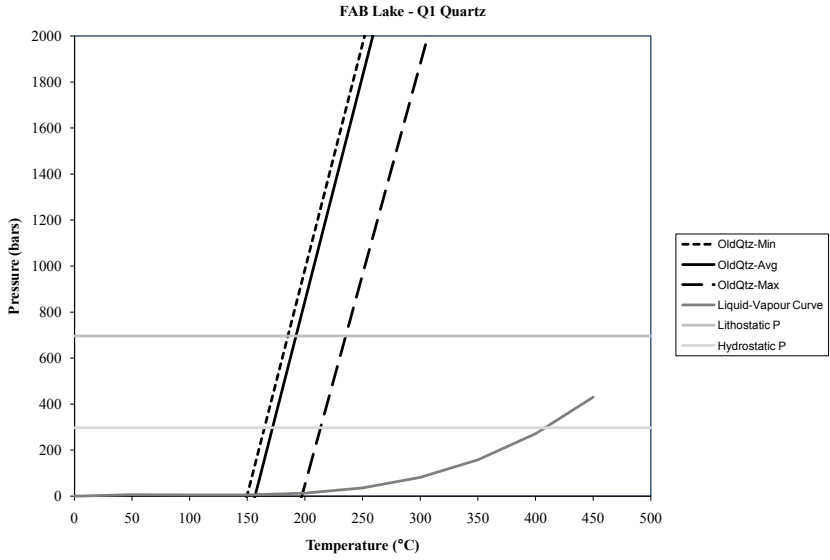
Location	Sample	Vein Type	FI Chip	FIA	Inclusion No.	Inclusion Type	T _{m,ice} (°C)	FPD (°C)	Salinity wt. % NaCl eq.	Th (°C)	Halite dissolution (°C)
Hardisty Lake	06SBH031	Q3	2	4	1	I	-21.1	21.1	23.1	137	
Hardisty Lake	06SBH031	Q3	2	4	2	I	-21.9	21.9	23.6	181	
Hardisty Lake	06SBH031	Q3	2	4	3	I	-19.5	19.5	22.0	196	
Hardisty Lake	06SBH031	Q3	2	4	4	I	-19.7	19.7	22.2	134	
Hardisty Lake	06SBH031	Q3	2	4	5	I	-24.5	24.5	25.3	181	
Hardisty Lake	06SBH032	Q3	4	2	1	I	-0.2	0.2	0.4	158	
Hardisty Lake	06SBH032	Q3	4	2	2	I	-0.2	0.2	0.4	158	
Hardisty Lake	06SBH032	Q3	4	2	3	I	-0.2	0.2	0.4	194	
Hardisty Lake	06SBH032	Q3	4	2	4	I	-0.2	0.2	0.4	148	

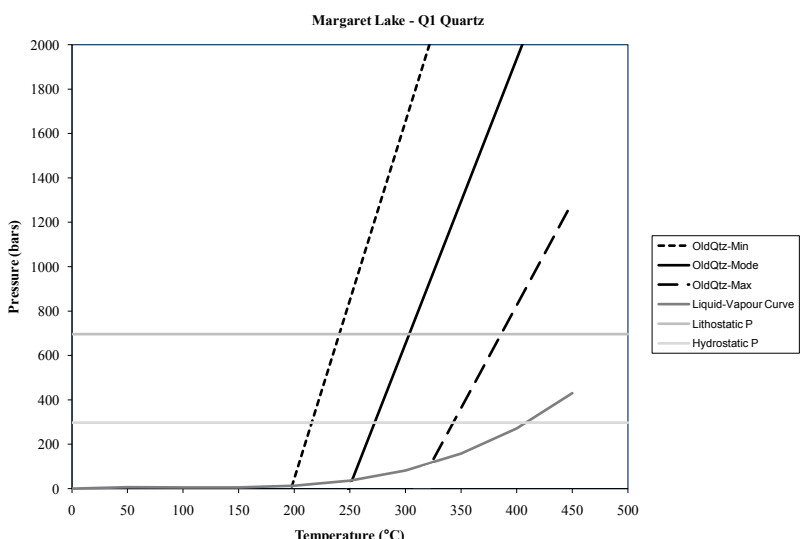
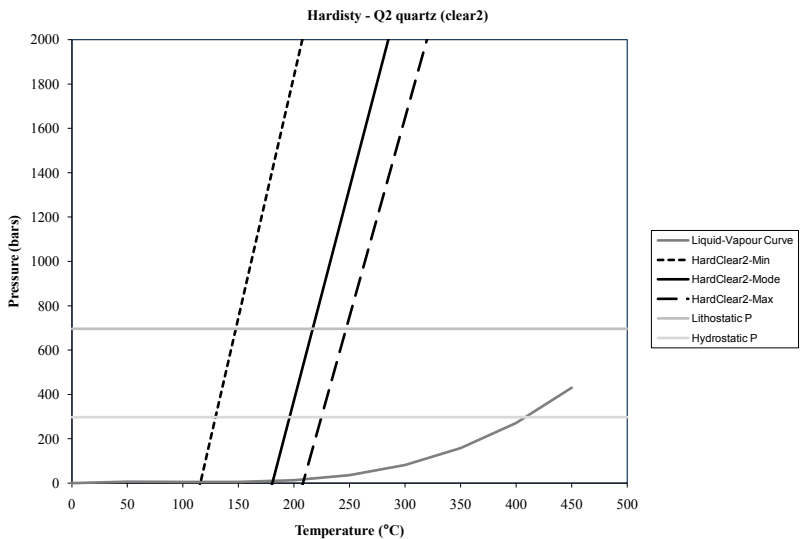
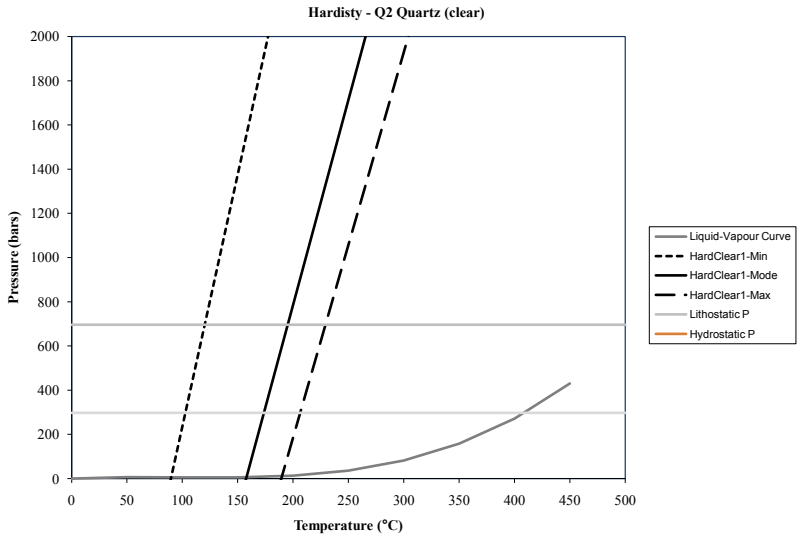
Location	Sample	Vein Type	FI Chip	FIA	Inclusion No.	Inclusion Type	T _{m,ice} (°C)	FPD (°C)	Salinity wt. % NaCl eq.
Margaret Lake	06SBM045	Q1	A	4	1	I	-0.2	0.2	0.4
Margaret Lake	06SBM045	Q1	A	4	2	I	-0.2	0.2	0.4
Margaret Lake	06SBM045	Q1	A	4	3	I	-0.2	0.2	0.4
Margaret Lake	06SBM045	Q1	A	4	4	I	-0.2	0.2	0.4
Margaret Lake	06SBM045	Q1	A	4	5	I	-0.2	0.2	0.4
Margaret Lake	06SBM045	Q1	A	5	1	I	-0.2	0.2	0.4
Margaret Lake	06SBM045	Q1	A	5	2	I	-0.2	0.2	0.4
Margaret Lake	06SBM045	Q1	A	5	3	I	-0.2	0.2	0.4
Margaret Lake	06SBM040	Q1	C	S1	1	I	-0.2	0.2	0.4
Margaret Lake	06SBM040	Q1	C	S1	2	I	-0.2	0.2	0.4
Margaret Lake	06SBM040	Q1	C	S1	3	I	-0.2	0.2	0.4
Margaret Lake	06SBM040	Q1	C	S2	1	I	-0.2	0.2	0.4
Margaret Lake	06SBM040	Q1	D	S1	1	I	-0.2	0.2	0.4
Margaret Lake	06SBM040	Q1	D	S1	2	I	-0.2	0.2	0.4
Margaret Lake	06SBM040	Q1	D	S1	3	I	-0.2	0.2	0.4
Margaret Lake	06SBM040	Q1	D	S1	4	I	-0.2	0.2	0.4
Margaret Lake	06SBM045	Q2	SC1	S1	1	I	-4.2	4.2	6.7
Margaret Lake	06SBM045	Q2	SC1	S1	2	I	-1.1	1.1	1.9
Margaret Lake	06SBM045	Q2	SC1	S1	3	I	-0.5	0.5	0.9
Margaret Lake	06SBM045	Q2	SC1	S2	1	I	-2.0	2.0	3.4
Margaret Lake	06SBM045	Q2	SC1	S2	2	I	-0.2	0.2	0.4
Margaret Lake	06SBM045	Q2	SC1	S2	3	I	-2.0	2.0	3.4
Margaret Lake	06SBM045	Q2	D1	S1	1	I	-0.2	0.2	0.4
Margaret Lake	06SBM045	Q2	D1	S2	2	I	-3.9	3.9	6.3
Margaret Lake	06SBM045	Q2	A	S2	1	I	-2.9	2.9	4.8
Margaret Lake	06SBM045	Q2	A	S2	2	I	-0.2	0.2	0.4

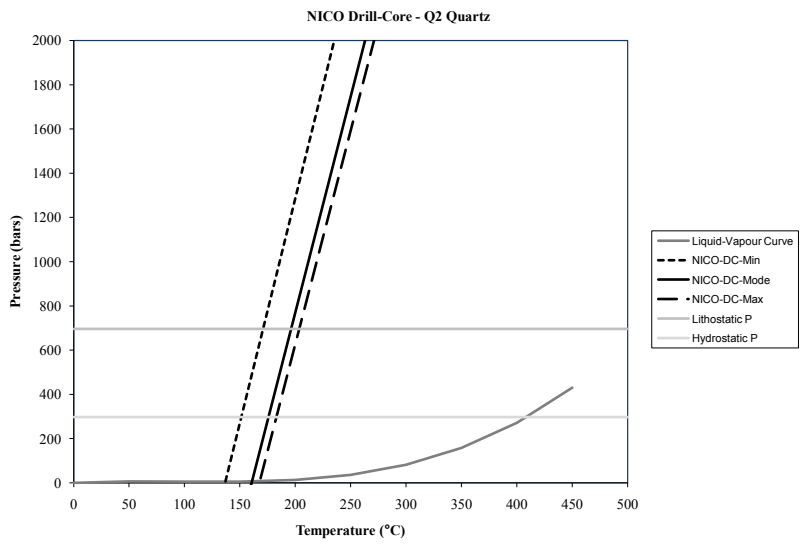
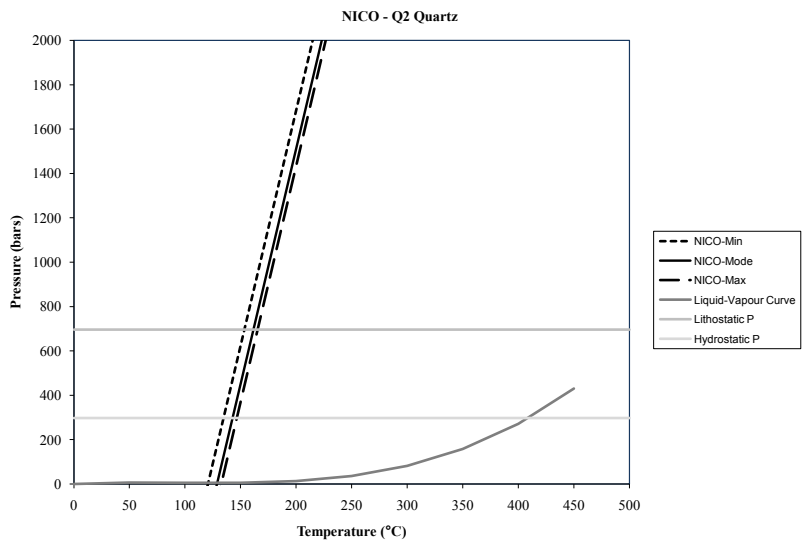
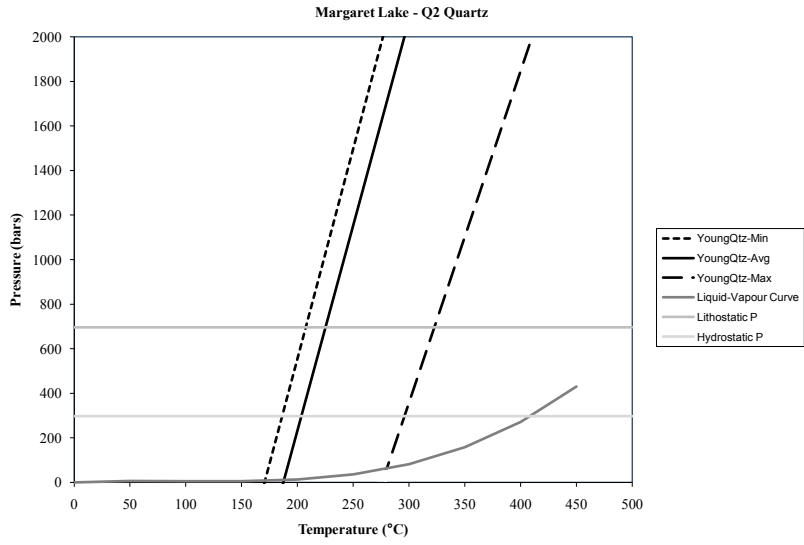
Appendix F

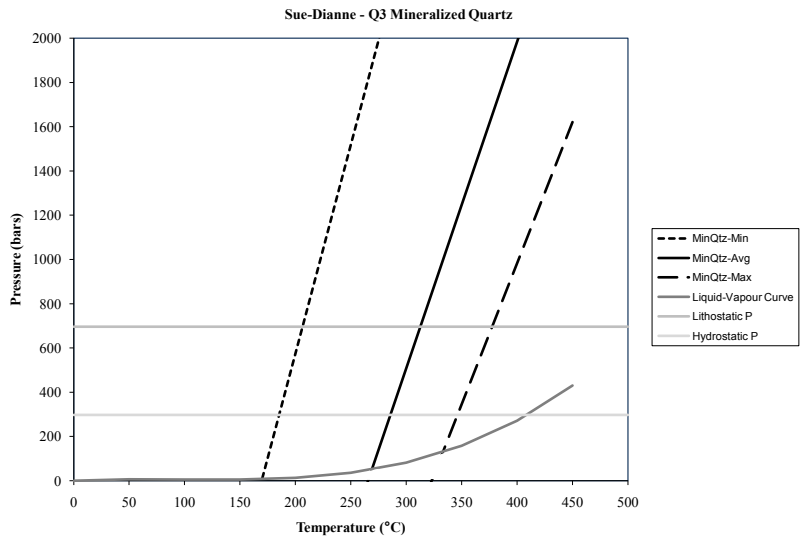
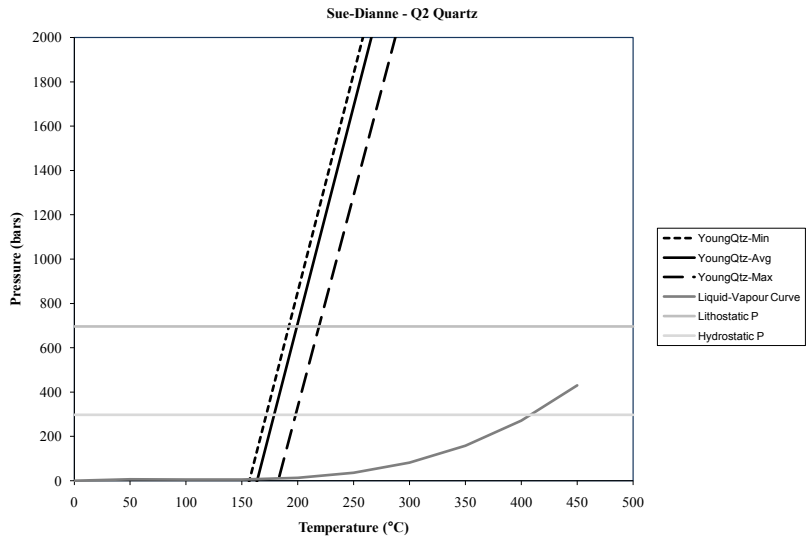
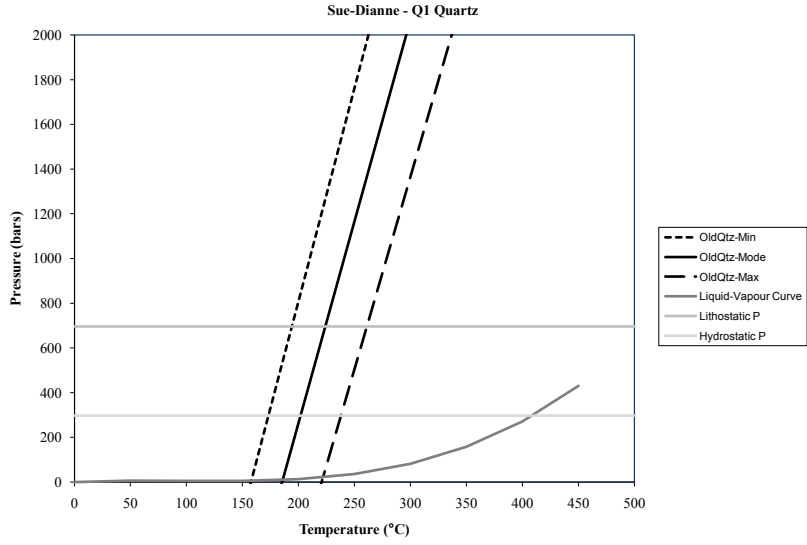
Isochores from each vein zone. Three isochores were constructed for each vein zone, based on paleodepth estimates made by Ault et al. (2009), using the modal Th, maximum Th, minimum Th and their corresponding salinities. If a mode could not be established, the average Th/salinity replaced the mode isochore, and this is indicated in the legend.

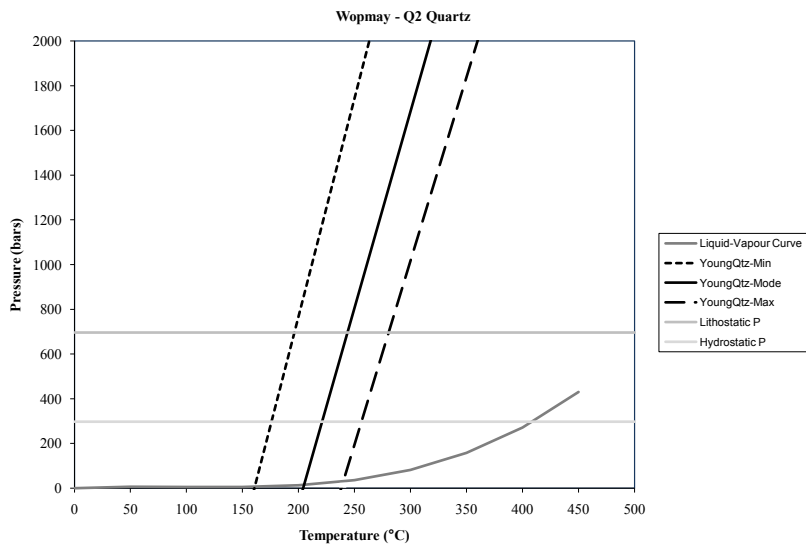
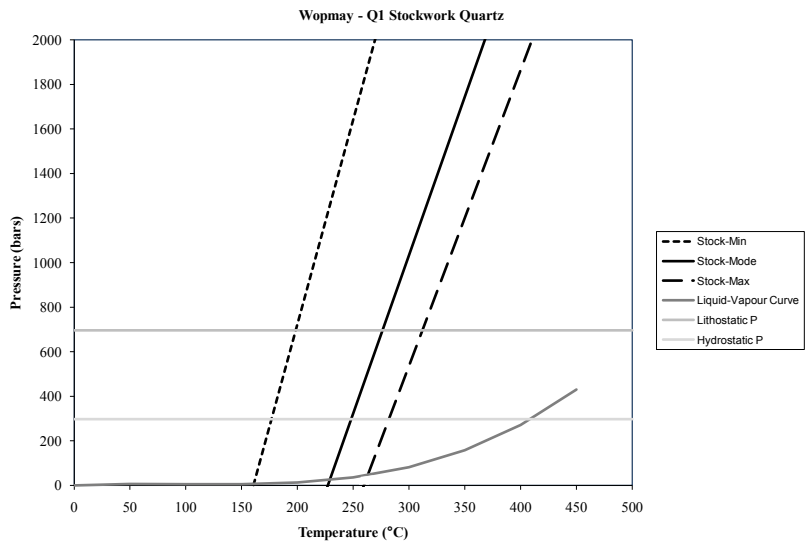










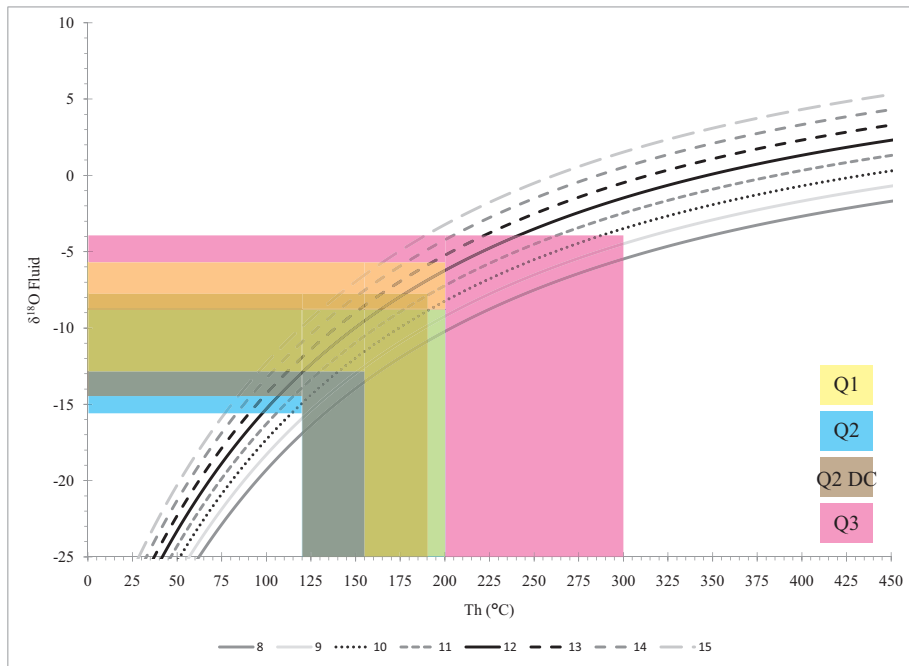


Appendix G

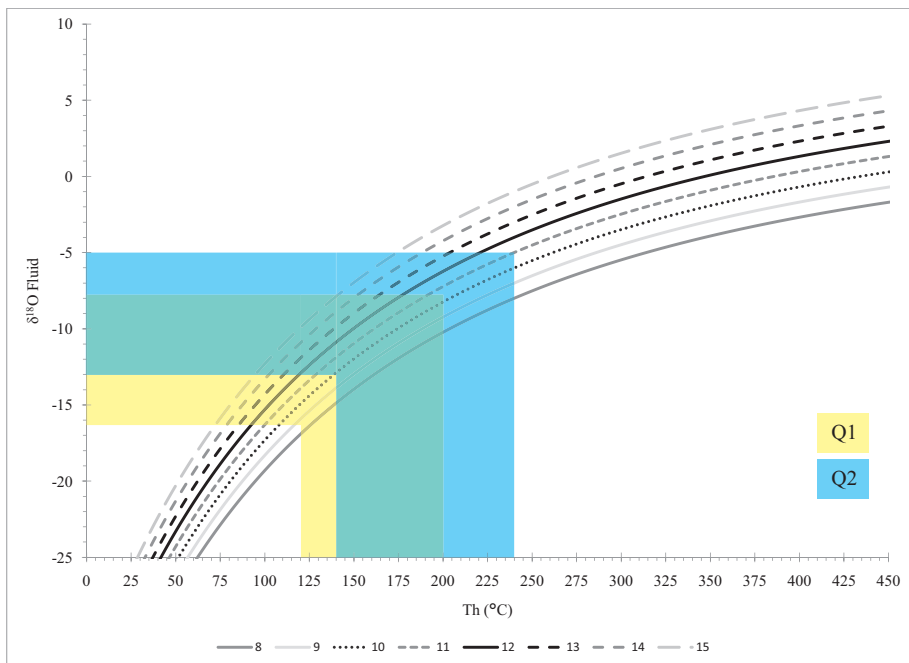
Oxygen isotopic values for the original hydrothermal fluid ($\delta^{18}\text{O}_{\text{fluid}}$) for base-metal mineralized, uranium-associated and non-mineralized giant quartz vein zones. The $\delta^{18}\text{O}_{\text{fluid}}$ values are based on $\delta^{18}\text{O}_{\text{qtz}}$ fractionation factors by Matsuhisa et al. (1979) using the equation:

$$\delta^{18}\text{O}_{\text{fluid}} = \delta^{18}\text{O}_{\text{qtz}} - ((3.34 * (10^6 / (Tt^2))) + 3.31)$$

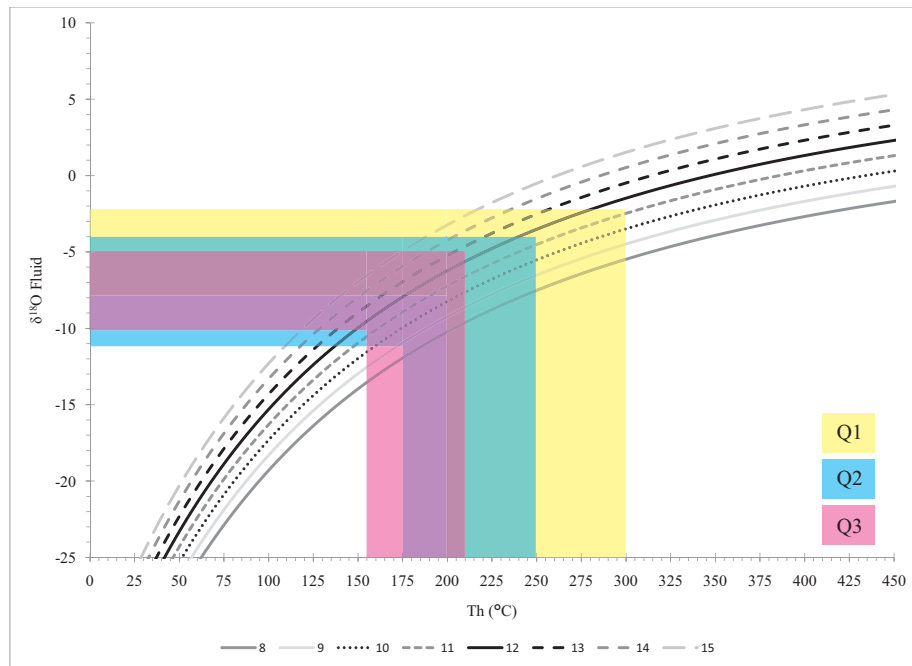
Where Tt is the measured average Tt (± 1 standard deviation), and $\delta^{18}\text{O}_{\text{qtz}}$ is the measured average $\delta^{18}\text{O}_{\text{qtz}}$ (± 1 standard deviation) value from a single vein.



Oxygen isotopic values for the original fluid ($\delta^{18}\text{O}_{\text{fluid}}$) that formed the giant quartz vein zones near base-metal mineralization.



Oxygen isotopic values for the original fluid ($\delta^{18}\text{O}_{\text{fluid}}$) that formed the uranium-associated giant quartz vein zones.



Oxygen isotopic values for the original fluid ($\delta^{18}\text{O}_{\text{fluid}}$) that formed the giant quartz vein zones isolated from mineralization.